

**Stabilizing Monopedal Robot Running:
Reduction-by-Feedback and Compliant Hybrid Zero Dynamics**

by

Ioannis Poulakakis

A dissertation submitted in partial fulfillment
of the requirements for the degree of
Doctor of Philosophy
(Electrical Engineering: Systems)
in The University of Michigan
2009

Doctoral Committee:

Professor Jessy W. Grizzle, Chair
Professor Antony M. Bloch
Professor Arthur D. Kuo
Professor N. Harris McClamroch
Assistant Professor Domitilla Del Vecchio

© Ioannis Poulakakis 2009
All Rights Reserved

To my parents, Markos and Maria, for their endless support and patience

ACKNOWLEDGEMENTS

This thesis represents the close of my (rather long) time as a graduate student. At this point, I would like to thank a number of individuals without whom the work of this thesis could not have been completed. First and foremost, I owe a great debt of gratitude to my advisor, Jessy Grizzle, for his constant encouragement and intellectual support throughout the course of this research. His superb knowledge of nonlinear control theory and practice has been an irreplaceable resource for deepening my understanding of the research problems this thesis deals with. I would also like to thank my dissertation committee members, Tony Bloch, Harris McClamroch, Arthur Kuo and Domitilla Del Vecchio, for their help. I regret not availing myself more fully to their expertise. Even so, I profited much from their diverse perspectives. Furthermore, Harris McClamroch and Tony Bloch provided their valuable advice on difficult decisions that I had to make at the beginning and end of my career as a graduate student at the University of Michigan. I would like to extend my gratitude to Demos Teneketzis, for his selfless interest and support through the many conversations we had. In my time as a graduate student at the University of Michigan, I have had the opportunity to meet with exceptional people, to whom I would like to express my deepest appreciation. First of all, I am indebted to Ben Morris, a valuable friend and colleague, whose contributions to the theory of hybrid zero dynamics enabled the work presented in this thesis. Deep gratitude is expressed to Jonathan Hurst for designing and constructing Thumper and for providing his invaluable insight into the dynamics of the robot. I would also like to thank Koushil Sreenath and Hae-Won Park, my other two team members in the project, whose help has been great during the last year. Lastly, on a personal note, I would like to thank my parents and close friends for their undying support and constant encouragement during this endeavor.

Ioannis Poulakakis
Ann Arbor, December 2008

TABLE OF CONTENTS

DEDICATION	ii
ACKNOWLEDGEMENTS	iii
LIST OF FIGURES	vii
LIST OF TABLES	xii
LIST OF APPENDICES	xiii
ABSTRACT	xiv
CHAPTER	
I. Introduction	1
1.1 Thumper and MABEL	3
1.2 Towards the Control of Thumper: The Asymmetric Spring Loaded Inverted Pendulum	6
1.3 The Control of Thumper	8
1.4 Organization of the Thesis	10
II. Literature Survey	12
2.1 Walking versus Running and the Role of Compliance	13
2.2 Simple Mechanisms for Studying Walking and Running	16
2.2.1 Walking and the Inverted Pendulum	17
2.2.2 Running and the Spring Loaded Inverted Pendulum	20
2.3 Walking and Running Robots	23
2.3.1 Passive Dynamic Walking Robots	23
2.3.2 Dynamically Stable Running Robots	25
2.4 On the Control of Hopping and Running	27
III. Approximating Thumper: The Asymmetric Spring Loaded Inverted Pendulum	31
3.1 Terminology, modeling hypotheses, and notation	32

3.2	ASLIP Flight Dynamics	34
3.3	ASLIP Stance Dynamics	35
3.4	ASLIP Flight-to-stance Transition Map	38
3.5	ASLIP Stance-to-flight Transition Map	39
3.6	ASLIP Hybrid Dynamics of Running	40
IV.	Controlling the ASLIP:	
	SLIP-embedding and Rigid Target Model Controllers	43
4.1	Overview of the Control Law	44
4.1.1	In-stride Continuous Control	45
4.1.2	Event-based Discrete Control	47
4.2	Target Model: The Energy-Stabilized SLIP	48
4.3	Main Result: The SLIP Embedding Controller	51
4.4	Proof of the SLIP Embedding Theorem	54
4.4.1	In-stride Continuous Control	54
4.4.2	Event-Based Discrete Control	61
4.4.3	Proof of Theorem 4.3	63
4.5	One DOF Hybrid Zero Dynamics: The Rigid Target Model	63
4.5.1	In-stride Continuous Control	63
4.5.2	Event-Based Discrete Control	64
4.6	Controller Evaluation via Simulation	65
4.6.1	Implementation Issues and Nominal Orbit Design	65
4.6.2	Steady-State Behavior	67
4.6.3	Transient Behavior and Performance Evaluation	67
4.6.4	Qualitative Discussion	71
V.	The Monopedal Robot Thumper	73
5.1	Terminology, modeling hypotheses, and notation	74
5.2	Transmission Dynamics	77
5.3	Dynamics of Thumper in Running	82
5.3.1	Thumper's Unconstrained Dynamics	83
5.3.2	Thumper Flight Dynamics	85
5.3.3	Thumper Stance Dynamics	91
5.3.4	Thumper Flight-to-Stance Transition Model	98
5.3.5	Thumper Stance-to-Flight Transition Model	105
5.3.6	Thumper Hybrid Dynamics of Running	110
VI.	Controlling Thumper:	
	A Compliant Hybrid Zero Dynamics Controller	112
6.1	Overview of the Control Method	113
6.2	Feedback Objectives: Designing Virtual Holonomic Constraints	115
6.2.1	Stance Phase Virtual Holonomic Constraints	115
6.2.2	Flight Phase Virtual Holonomic Constraints	120
6.3	Continuous-time Control of Thumper	122
6.3.1	Continuous-time Phases in the Closed-loop Thumper	122

6.3.2	Enforcing the Virtual Holonomic Constraints	124
6.4	Event-based Control of Thumper: General Considerations	126
6.4.1	Inner-loop Event-based Control for Invariance	129
6.4.2	Outer-loop Event-based Control for Stability	134
6.5	Event-based Control of Thumper: Details	137
6.5.1	Inner-loop Event-based Control for Invariance	137
6.5.2	Outer-loop Event-based Control for Stability	143
6.6	Nominal Running Orbits through Optimization	145
6.7	Evaluation of the Controller in Simulation	150
VII. Concluding Remarks and Future Work		154
7.1	Summary of New Contributions	154
7.2	Perspectives on Future Work	157
APPENDICES		159
BIBLIOGRAPHY		166

LIST OF FIGURES

Figure

1.1	(a) Thumper (courtesy of J. W. Hurst), and (b) MABEL. The leg consists of two links –the thigh and the shin– connected together with a knee joint. The torso contains the transmission mechanism and is attached to the leg via the hip joint. Note that the hip joint does <i>not</i> coincide with the torso’s center of mass.	4
1.2	Modeling and control hierarchy. Bridging the gap between the Spring Loaded Inverted Pendulum (SLIP) and Thumper calls for a new model: the Asymmetric Spring Loaded Inverted Pendulum (ASLIP).	6
1.3	Left: The morphology of Thumper’s leg (courtesy of J. W. Hurst). The spring in the transmission acts along the leg direction (the virtual line connecting the toe with the hip). Right: The Asymmetric Spring Loaded Inverted Pendulum (ASLIP). The leg force will be modeled as a spring in parallel with a prismatic force source. The ASLIP is a more faithful representation of the robot on the left than a SLIP model.	7
2.1	The inverted pendulum analogy of walking (adapted from [67]). The figure shows the single support phase, in which no active force is necessary to hold the weight, and the double support phase, in which the velocity of the center of mass is reoriented. Note that the hip is at its highest point at midstance.	17
2.2	The Spring Loaded Inverted Pendulum analogy of running. In the first part of the stance phase the leg is compressing and energy is stored in the spring, which is returned in the second part of the stance when the body is lifted and accelerated. Note that the hip is at its lowest point at midstance.	21
3.1	Left: The morphology of Thumper’s leg; see [52], [51] for design principles and hardware details. The knee has a revolute series compliant actuator. Right: The Asymmetric Spring Loaded Inverted Pendulum (ASLIP). The leg force u_1 will be modeled as a spring in parallel with a prismatic force source. The ASLIP is a more faithful representation of the robot on the left than a SLIP model.	32

3.2	Representation of ASLIP’s model in running as a hybrid system.	41
3.3	Representation of ASLIP’s model as a system with “impulse” effects. . . .	42
4.1	Feedback diagram presenting the basic structure of the ASLIP controllers.	45
4.2	The Energy-Stabilized SLIP (ES-SLIP), with a prismatic actuator (force source) in parallel with the spring.	48
4.3	A diagram summarizing the control procedure through which the ASLIP restriction dynamics is rendered diffeomorphic to the ES-SLIP closed-loop dynamics. Vertical arrows correspond to control actions; horizontal arrows relate diffeomorphic dynamics. The dashed box includes the ES-SLIP closed-loop target dynamics. Equation numbers refer to the text.	55
4.4	The controller (4.59) makes the actual total leg force u_1 equal to the projection of the virtual leg force $F_{ES-SLIP}$ along the direction of the ASLIP (actual) leg.	61
4.5	Nominal orbits in physical space (a), and corresponding hip torques (b), total leg forces (c), and leg actuator forces (d) computed by (4.79), for the rigid target model controller (dashed lines) and the SLIP embedding controller (solid lines).	68
4.6	Ten strides showing convergence from $\delta\theta = -6$ deg, for the the SLIP embedding controller (a), (c), and the rigid target model controller (b),(d). Dashed lines show desired values; the circles correspond to the instant when the perturbation occurs (liftoff of the second stride).	69
4.7	Leg forces for the SLIP embedding controller (left), and the rigid target model controller (right), and for the first four steps of Fig. 4.6. Upper plots show total leg forces; bottom plots show leg actuator forces computed by (4.79). The dashed lines in the upper plots show spring forces.	70
5.1	Left: Basic robot configuration. The dashed line connecting the toe with the hip corresponds to the “leg direction;” its length l and angle q_{LA} are the virtual “leg length” and “leg angle,” respectively. The leg length l is uniquely determined by the “leg shape” angle, q_{LS} . Right: Thumper’s powertrain system (courtesy of Hae-Won Park). The motors and spring are connected to the hip and knee joints via three differentials connected so that the actuated variables are the leg and leg-shape angles, q_{LA} and q_{LS} , respectively; see Fig. 5.1(a). The spring is <i>in series</i> with the leg-shape motor: one end is connected to the torso and the other to the B_{spring} pulley via a cable, which makes the spring <i>unilateral</i> . When the spring reaches its rest position, the B_{spring} pulley hits a hard stop, as shown in the detail. When this happens, the leg-shape motor is, for all intents and purposes, rigidly connected to leg shape through a gear ratio. Design details of the transmission can be found in [51].	78

5.2	A schematic of Thumper used to model running. The transmission system is not shown. Left: “Official” generalized coordinates $(q_{LA}; q_{LS}; q_{Tor}; x_{cm}; y_{cm})$ describing linkage configuration, and other important quantities. Right: Mechanical properties of Thumper. The COM of each link is placed outside from the corresponding link to emphasize asymmetry. The moment of inertia of each link is with respect to its COM.	82
5.3	A commutative diagram showing mappings between the flight and unconstrained state spaces, TQ_f and TQ_e , respectively.	88
5.4	A commutative diagram showing mappings between the stance and unconstrained model state spaces, TQ_s and TQ_e , respectively.	93
5.5	A commutative diagram showing the construction of the flight-to-stance transition map $\Delta_{f \rightarrow s}$. The coordinate representations of the various maps appearing in this figure are provided in the text. The bottom part corresponds to the construction of the base component $\Delta_{f \rightarrow s}^q$ and the upper part to the construction of the fiber component $\Delta_{f \rightarrow s}^{\dot{q}}$, which is <i>not</i> the differential of $\Delta_{f \rightarrow s}^q$ as in the ASLIP. Note that the “lift” to TQ_e is necessary for including the effects of compliance in the impact model.	100
5.6	A commutative diagram showing the construction of the stance-to-flight transition map $\Delta_{s \rightarrow f}$. The bottom part corresponds to the base component $\Delta_{s \rightarrow f}^q$ and the upper part to the fiber component $\Delta_{s \rightarrow f}^{\dot{q}}$. The coordinate representations of the various maps appearing in this figure are provided in the text. Notice that the fiber component $\Delta_{s \rightarrow f}^{\dot{q}}$ of $\Delta_{s \rightarrow f}$ is not the differential of its base component $\Delta_{s \rightarrow f}^q$ as was in the ASLIP.	106
5.7	Representation of Thumper’s model in running as a hybrid system.	110
6.1	Feedback diagram presenting the basic structure of the controller. Continuous lines represent signals in continuous time; dashed lines represent signals in discrete time. The control laws Γ_μ^c and Γ_μ^α are intended to create a well defined hybrid zero dynamics (HZD), while the controller Γ^β ensures that the resulting HZD is exponentially stable.	114
6.2	The general shape of the stance phase commanded constraints. Note that $\theta_{Tor}^{\max} = \theta_{mLS}^{\max} = \beta_{s, \text{set}}$ to avoid the introduction of an additional stance subphase.	117
6.3	Controlled variables in the flight phase. The horizontal position of the toe relative to the COM, $(p_{toe}^h - x_{cm})$, corresponds to Raibert’s touchdown angle controller. The leg-shape angle, q_{LS} determines leg length.	121

6.4	Succession of the phases $\mathcal{M} = \{\text{sc}, \text{si}, \text{sd}, \text{f}\}$ of the dynamics of Thumper in closed loop with the continuous-time controllers during running, and the correspondence with the cyclic group $\mathbb{Z}_4 \cong \{0, 1, 2, 3\}$	123
6.5	Inner-loop event-based control laws $\Gamma_{\nu(\kappa)}^\alpha$ for achieving invariance of the surfaces $\mathcal{Z}_{(\alpha_{\nu(\kappa)}, \beta_{\nu(\kappa)})}$, $\nu(\kappa) \in \mathcal{M}$. These controllers, in combination with the continuous-time control action (6.28), result in a well defined hybrid zero dynamics, which will be rendered exponentially stable via the outer-loop controller of Section 6.4.2; see Fig. 6.6. The symbols α_{sc}^+ , α_{si}^+ , α_{sd}^+ represent updated values of the parameter arrays α_{sc} , α_{si} , α_{sd} , respectively, at the beginning of the corresponding stance subphases.	131
6.6	Thumper's dynamics represented as a system with impulse effects. The outer-loop event-based control achieves stability of the system.	135
6.7	Virtual constraints during nominal motion. Top: Stance phase torso angle, (a), and leg-shape motor position, (b), constraints given by (6.4) and (6.7), respectively. Compare with Fig. 6.2. Bottom: Flight phase toe horizontal position relative to the COM, (c), and leg-shape angle uniquely determining virtual leg length, (d).	147
6.8	Evolution of the independent parameters s_{Tor} in (a), and s_{mLS} in (b), corresponding to the constraints of the stance phase.	148
6.9	Spring deflection, (a), and spring force versus spring deflection, (b).	148
6.10	Vertical component of the ground reaction force, (a), and minimum required friction coefficient computed by $ F_{\text{toe}}^{\text{T}} /F_{\text{toe}}^{\text{N}}$, (b).	149
6.11	Actuator inputs corresponding to the nominal gait presented in Fig. 6.7. Dashed lines correspond to flight phase inputs. Both torques are well within the capabilities of the actuators.	149
6.12	Discrete errors in pitch angle and forward speed showing convergence to zero. The norm of the maximum eigenvalue is 0.79; see (6.80).	151
6.13	Stance phase virtual constraints during recovery from a perturbation: torso angle, (a), and leg-shape motor position, (b). Dashed line represents nominal liftoff values: The outer-loop controller adjusts the liftoff values for the torso angle and the motor position (corresponding to energy input) to ensure convergence to the nominal orbit.	151
6.14	Torso pitch angle, (a), and spring deflection, (b), during convergence to the nominal orbit. Note that no excessive pitching is observed.	152
6.15	Vertical component of the ground reaction force, (a), and minimum required friction coefficient computed by $ F_{\text{toe}}^{\text{T}} /F_{\text{toe}}^{\text{N}}$, (b).	152

6.16	Actuator torques: Leg-angle, (a), and leg-shape, (b), motors, showing that the required input torques are within the capabilities of the motors.	153
B.1	Left: Basic robot configuration. Right: Conceptual diagram showing the placement of the three differentials (solid black lines) in the transmission system with the names of each pulley. The “-1” means that direction is inverted. B	163

LIST OF TABLES

Table

4.1	ASLIP Mechanical Parameters	65
4.2	Control Effort: SLIP Embedding and RTM Controllers	71
B.1	Transmission system nomenclature.	163

LIST OF APPENDICES

Appendix

A.	Details on The Rigid Target Controller	160
B.	Details on the Transmission Mechanism	162

ABSTRACT

Stabilizing Monopedal Robot Running:
Reduction-by-Feedback and Compliant Hybrid Zero Dynamics

by

Ioannis Poulakakis

Chair: Jessy W. Grizzle

As an alternative to traditional wheeled and tracked ground vehicles, biologically-inspired legged systems are becoming increasingly common. On a macroscopic level, locomotion on land can be understood through the introduction of archetypical reductive models, capable of capturing the salient characteristics of the task-level behavior, e.g., walking or running. Unfortunately, these reductive models provide no information of the control mechanisms, through which the multiple joints and limbs of the high-degree-of-freedom plant are coordinated to produce the observed behavior. The coordinated recruitment of the plant into a low-degree-of-freedom target model constitutes the central problem addressed in this dissertation, which aims at offering a mathematically precise feedback control solution to this problem for the particular setting of monopedal robot running. The robotic monopod Thumper, recently constructed in a collaborative effort between the University of Michigan and Carnegie Mellon University, offers a unique platform for exploring advanced feedback control strategies for running on compliant monopedal robots. The control law proposed for Thumper grows out of rigorous nonlinear controller synthesis ideas, and it coordinates the actuated degrees of freedom of the robot so that a lower-dimensional hybrid subsystem, i.e., a reductive model that encodes running, emerges from the closed-loop dynamics. This subsystem effectively governs the behavior of the robot.

CHAPTER I

Introduction

At its most fundamental level, locomotion appears to be deceptively simple: an organism (or a robot) exerts a force to its environment and through Newton's laws it accelerates in the opposite direction. Yet, studies of the basic locomotion mechanisms indicate that force application is not as simple as it might first appear.

In a strict engineering sense, animals appear to be "over-designed" for the task of locomotion alone. Complexity is a direct consequence of the multitude of joints, muscles, sensors, neurons, and the numerous neuronal connections that are engaged in order to produce the observed locomotion behavior, [29]. In fact, animals exhibit kinematic, actuator, and neuronal redundancy. They exhibit kinematic redundancy, for they have far more joint degrees of freedom than those required for placing their body in the three-dimensional task space. They exhibit actuator redundancy, for often at least two muscles are employed to actuate each joint degree of freedom. Finally, they exhibit neuronal redundancy, because more interneurons than necessary participate in generating the required motor neuron signals. The fundamental intractability of any elaborate model attempting to capture the details of the mechanisms by which limbs, joints, muscles and neurons coordinate to produce locomotion in animals could hardly be more apparent.

Fortunately, despite the complexity of the spatiotemporal mechanics associated with the coordination of the mechanical and neural systems, legged locomotion may be understood on a macroscopic level based on a few common principles, including common mechanisms of energy exchange, stability, maneuverability, and in general the use of force for propulsion. Central to this approach is the introduction of archetypical reductive mod-

els, whose purpose is to capture the salient characteristics of the task-level behavior by resolving redundancy through the use of symmetries and synergies¹, [33]. Such models not only provide a description of the motion of the body in pursuit of a task, but, more importantly, they advance hypotheses regarding the high-level control strategy underlying the achievement of this task without delving into the morphological details of body structure.

This modeling hierarchy inspired by the biologically motivated “collapse of dimension” hypothesis, produced a variety of models suitable for studying the mechanics of body movement in walking and running gaits, [49]. Notwithstanding their apparent simplicity, these models have been invaluable in uncovering basic principles of running in animals, and in synthesizing empirical control laws for running robots. Among them, the Spring Loaded Inverted Pendulum (SLIP) has been proposed as a canonical model (a template) of the center-of-mass dynamics of running animals and robots. In the relevant literature, the SLIP is not perceived merely as a model that encodes running. It is construed as a model that implies specific high-level control hypotheses underlying the achievement of the task.

Such an approach, namely the introduction of reductive models, has the advantage of capturing the dynamics of the behavior, walking or running, without explicitly relying on the morphological details of the mechanisms by which this behavior is achieved. However, by their very purpose, reductive models of the sort of the SLIP have just enough complexity to encode the task of moving the body center of mass and no more. They provide no information on the *control mechanisms* governing the coordination of the multiple joints and limbs of the high-degree-of-freedom plant in producing the observed behavior. The coordinated recruitment of the plant into a low-degree-of-freedom target model constitutes the central problem addressed in this dissertation, which aims at offering a rigorous feedback control solution to this problem for the particular setting of robotic monopodal running.

¹By “synergies” it is meant parts working together in combined action or operation.

1.1 Thumper and MABEL

The monopedal robot Thumper and the bipedal robot MABEL, shown in Fig. 1.1, are two novel robots that have been designed and constructed in a collaborative effort between The University of Michigan and Carnegie Mellon University²; see [47] for an overview and [52], [53], and [51] for details relevant to the underlying design philosophy. One of the purposes of the robots is to explore a novel powertrain design that incorporates compliance, with the objective of improving power efficiency, both in steady-state operation and in responding to disturbances. A second purpose of Thumper and MABEL is to inspire the development of advanced feedback control algorithms for running on level surfaces and walking on rough terrain and to provide reliable platforms for their experimental validation. In that respect, they represent the outgrowth of RABBIT, the French biped studied extensively by Grizzle, Westervelt, Chevallereau, and their collaborators; see [24] and [109] for an integrative view.

In this work, the focus will be on the feedback control of monopedal running; hence, Thumper will be at the center of the development. In order to motivate the developments of the following chapters, this section presents some of the challenges introduced by the design of Thumper and highlights important differences with respect to existing legged robots and the corresponding feedback solutions. It is anticipated that the rigorous understanding of feedback structures suitable for stabilizing running on the one-legged Thumper will shed light on the control of machines composed of more than one leg, and, in particular, MABEL.

Roughly speaking, Thumper has been designed so that its dynamic behavior resembles, in part, that of a SLIP; see [52], [53], and [51]. This requirement has given rise to non-traditional mechanical design solutions, which, in turn, pose new challenges in developing control laws that are suitable for inducing stable hopping motions to Thumper.

In particular, Thumper features a novel powertrain that incorporates compliance, and is capable of transmitting motor torques to the linkage in a way that the developed forces are applied to directions that do not correspond directly to isolated physical joints. A

²J. W. Hurst, then at The Robotics Institute, Carnegie Mellon University.



(a)



(b)

Figure 1.1: (a) Thumper (courtesy of J. W. Hurst), and (b) MABEL. The leg consists of two links –the thigh and the shin– connected together with a knee joint. The torso contains the transmission mechanism and is attached to the leg via the hip joint. Note that the hip joint does *not* coincide with the torso’s center of mass.

collection of differentials is used to connect two motors to the leg so that one motor controls the angle of a *virtual leg*, consisting of the line connecting the hip to the toe, and the second motor is connected—in *series* with a spring—to control the length of the virtual leg. In essence, this transmission ensures—mechanically, not by software—that the thigh and shin are coordinated, so that the leg behaves as if it were prismatic, despite the existence of a revolute knee. As a result, the spring embedded in the transmission acts along the “virtual leg” direction in much the same way as the springy leg of the SLIP: it stores energy in the compression part of the stance phase, when the support leg decelerates the downward motion of the center of mass; the energy stored in the spring can then be used to redirect the center of mass upwards in anticipation of the ensuing flight phase.

On the other hand, the design of the transmission mechanism introduces dynamic effects that have significant implications to controller synthesis in at least two ways.

First, an immediate consequence of the presence of compliance in series with the leg motor is the increase of the degree of underactuation of the system, i.e., the difference be-

tween the number of degrees of freedom the system possesses and the number of actuators available for control. In fact, during the stance phase, Thumper has two degrees of underactuation—one more than the previously studied biped RABBIT, [24]—because it has four degrees of freedom and only two actuators. A less apparent, but equally important, issue related to the compliant nature of the transmission is that feedback control should work *in concert* with the spring. Stated simply, in the pursuit of achieving closed-loop stability, the actuators should not be trying to “cancel” the spring. In the closed-loop system, compliance should still be a dominant feature. This issue calls for nontrivial modification of existent feedback structures, such as those proposed in [109].

Second, Thumper exhibits significant torso dynamics that cannot be captured by any point-mass approximations, such as the SLIP. Moreover, contrary to most of the existing monopedal robots, Thumper’s leg is attached to the torso so that the hip joint does not coincide with the torso’s center of mass, resulting in *nontrivial coupling* between the torso and leg dynamics. This particular morphology is not addressed by the vast majority of the control laws available in the relevant literature for one-legged robot models; most of these controllers are derived based on the assumption that the torso center of mass coincides with the hip joint. As a final remark, note that the torso houses the transmission system, which includes the pulleys that are associated with the differentials imposing the geometric relations constraining the revolute knee leg to act like a virtual prismatic leg. The dynamic effect of these rotating pulleys is significant—especially during the flight phase, where the robot’s angular momentum is conserved in the absence of external forcing—and should be included in the model which will be used for controlling Thumper.

Compounding these challenges, common features of legged locomotion systems, namely the highly-nonlinear, hybrid structure of the system combined with a multitude of constraints —e.g., actuator limitations, friction cone limitations, unilateral ground reaction forces, to name a few— significantly complicate the feedback design problem. It is the subject of this work to identify these challenges and to propose efficient control algorithms with provable stability properties that work together with compliance to induce stable, periodic, natural, dynamic running motions on Thumper.

1.2 Towards the Control of Thumper:

The Asymmetric Spring Loaded Inverted Pendulum

While the resort to simple physical models, such as the SLIP, may be quite revealing for the properties of running, the morphology of Thumper and its unique design characteristics make such an approach seem unrealistic. The development of more elaborate models that enjoy a more faithful correspondence to the structure and morphology of Thumper, and possess prescriptive—as opposed to just descriptive—power is necessary for the construction of feedback control strategies suitable for stabilizing Thumper.

Up to this point, much of the research relevant to running has been concentrated on the SLIP itself. However, in a locomotion modeling hierarchy, the distance separating the SLIP from Thumper is large; see Fig. 1.2. In particular, it still remains unclear how stability conclusions obtained in the context of the SLIP can predict the behavior of more complete models, such as those required to capture the dynamics of Thumper.

The first step toward the control of Thumper is the introduction of an intermediate model intended to bridge the gap between Thumper and the SLIP. This model is termed

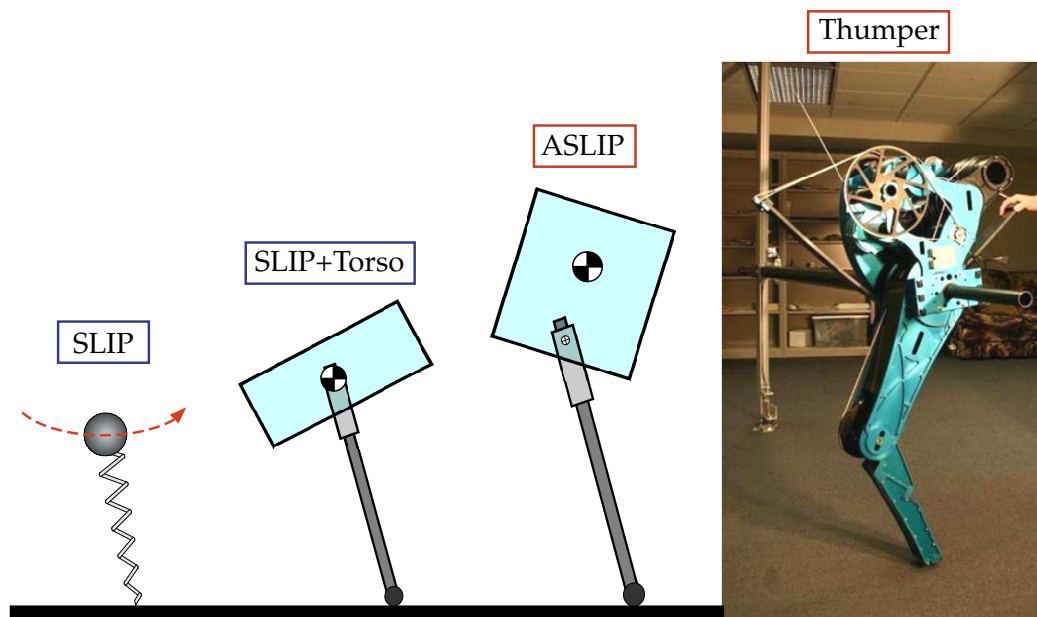


Figure 1.2: Modeling and control hierarchy. Bridging the gap between the Spring Loaded Inverted Pendulum (SLIP) and Thumper calls for a new model: the Asymmetric Spring Loaded Inverted Pendulum (ASLIP).

the *Asymmetric Spring Loaded Inverted Pendulum (ASLIP)*³; see Figs. 1.2 and 1.3. Aiming to reflect a broader purpose, the ASLIP includes torso pitch dynamics nontrivially coupled to the leg motion, an issue not addressed in the widely studied SLIP or in its straightforward extensions, in which the torso COM coincides with the hip joint; see Fig. 1.2. The ASLIP can be envisioned as a “building block” toward the design of controllers for more elaborate models that constitute more accurate representations of legged robots such as Thumper.

Part of this thesis deals with the development of a method that combines established nonlinear control synthesis tools, such as the Hybrid Zero Dynamics (HZD) originally proposed in [110], with controllers obtained in the context of the SLIP, e.g., those proposed by Raibert in [91], to induce exponentially stable running motions on the ASLIP. A second aspect addressed in this work regards the performance benefits of embedding the SLIP as the hybrid zero dynamics of the ASLIP. A SLIP embedding control law is compared with a controller that achieves a one degree-of-freedom (DOF), non-compliant hybrid zero dy-

³The ASLIP corresponds to a Spring Loaded Double Inverted Pendulum. Thanks to Harris McClamroch for pointing this out as an alternative term for the model.

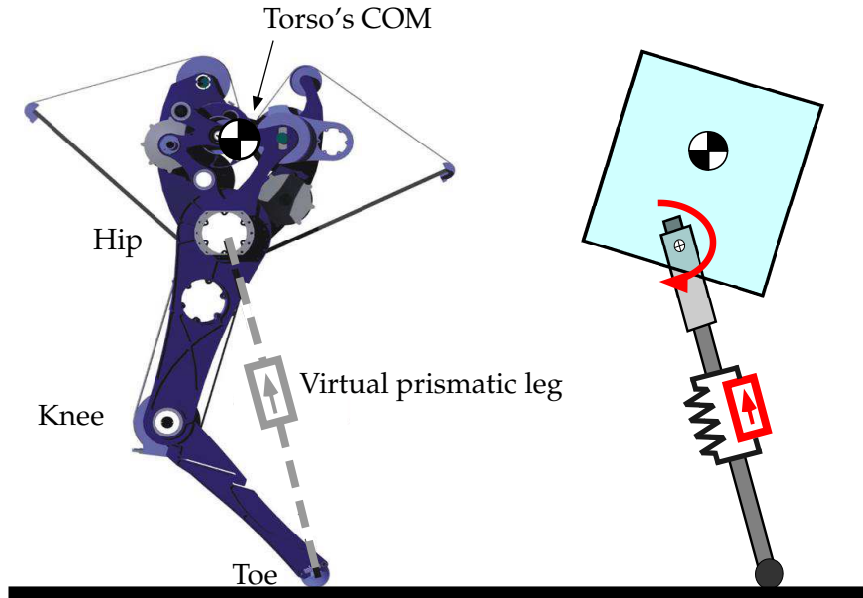


Figure 1.3: **Left:** The morphology of Thumper’s leg (courtesy of J. W. Hurst). The spring in the transmission acts along the leg direction (the virtual line connecting the toe with the hip). **Right:** The Asymmetric Spring Loaded Inverted Pendulum (ASLIP). The leg force will be modeled as a spring in parallel with a prismatic force source. The ASLIP is a more faithful representation of the robot on the left than a SLIP model.

namics. The two controllers induce identical steady-state behaviors. Under transient conditions, however, the underlying compliant nature of the SLIP allows significantly larger disturbances to be rejected, with less actuator effort, and without violation of the unilateral constraints between the toe and the ground.

These results lay the foundation for the development of a general framework for the design of control laws that induce elegant, provably stable, running motions in legged robots, by combining the practical advantages of compliance with the analytical tractability offered by the hybrid zero dynamics method. In fact, this approach will be used to derive feedback control laws that are successful in simulation in inducing efficient, natural running motions in Thumper. Proposing and formally analyzing such control laws for the stabilization of Thumper constitute the primary goal of this work.

1.3 The Control of Thumper

The capstone result of the research efforts in this thesis is the development of a hybrid controller that induces, in simulation, provably stable running gaits on the monopedal robot Thumper. Preliminary experiments at Carnegie Mellon University conducted by J. W. Hurst used extensions of Raibert's basic control procedure; see [91]. After extensive trial and error, with the robot failing over a hundred times, a non-falling⁴ running gait was implemented. In fact, this running gait was the result of a drift motion of a controller designed for hopping in place.

During a short visit at Carnegie Mellon University, the author was given the opportunity to participate in the final part of the experiments, in which the structure of robot had to be modified to make Thumper similar to a typical Raibert hopper⁵ so that Raibert's controller could be applied more successfully. In particular, a large bar had to be added to Thumper's torso with the purpose of increasing the rotational inertia of the body, thereby making it relatively insensitive to leg motions during the flight phase; see [51, Chapter

⁴The term "non-falling" is used to emphasize that the resulting motion does not correspond to a stable periodic orbit, at least in the rigorous sense.

⁵In Raibert's planar hopper, the prismatic (light-weight) leg is mounted on the torso so that the hip joint *coincides* with the torso's center of mass. Thumper's anthropomorphic morphology deviates significantly from this design.

6]. Furthermore, the distribution of the torso mass had to be modified⁶, so that its center of mass became closer to the hip joint. Even after these modifications, a stable gait—in the rigorous sense of the term—was not achieved as a result of the commanded control action. This fact, in the opinion of the author, confirms the importance of developing rigorous control-theoretic feedback solutions for compliant robots with nontrivial torso pitch dynamics.

The final chapter of this thesis, Chapter VI, undertakes the task of developing such a feedback solution for Thumper. The feedback law proposed there builds upon control ideas developed for the ASLIP. Nevertheless, extending these ideas to an elaborate model that constitutes an accurate representation of Thumper’s dynamics is far from trivial. Indeed, the ASLIP differs from Thumper in at least two important ways. First, the presence of leg mass in Thumper leads to energy loss at touchdown and, through conservation of angular momentum during flight, in torso rotation when the leg is positioned to its desired touchdown position. Second, in transmitting the actuator torques to the robot’s joints, Thumper’s powertrain introduces dynamic effects not present in the ASLIP. To be successful in producing stable natural running motions on Thumper, the controller must confront these challenges, and, in addition, it must guarantee that the compliance present in the open-loop Thumper dominates the behavior of the closed-loop system.

The proposed feedback control law is developed within the hybrid zero dynamics framework, and it acts on two levels. On the first level, continuous within-stride control asymptotically imposes (virtual) holonomic constraints that respect the compliance present in the open-loop system and reduce the dynamics of the robot to a low-degree-of-freedom hybrid subsystem. On the second level, event-based control stabilizes the resulting hybrid subsystem. Viewed from the standpoint of the modeling and control hierarchy described at the beginning of this chapter, this low-degree-of-freedom hybrid subsystem corresponds to the target dynamics for the desired behavior, namely, running, and it governs the high-level control underlying the achievement of this task. The coordination of the joints and limbs of the high-degree-of-freedom plant, i.e., Thumper, in order to realize the target dynamics, is achieved through enforcing via feedback a set of suitable virtual

⁶This was achieved by mounting Thumper’s computer below its torso.

constraints, which restrict the system's motion to a low-dimensional subset of its state space. This *reduction-by-feedback* procedure can be interpreted as an instantiation of the reductionist approach described at the beginning of this chapter.

The control law development for Thumper is systematic and the resulting controller achieves the dual objectives of working harmoniously with the system's natural dynamics and inducing provably exponentially stable running motions, while all relevant physical constraints are respected. It is anticipated that these properties will render this controller an attractive alternative to traditional heuristic approaches by avoiding laborious trial-and-error procedures during experimental implementation.

1.4 Organization of the Thesis

The remainder of this dissertation is organized into six chapters.

Chapter II provides a brief description of the related literature, and puts the work presented in this thesis into perspective by highlighting the main contributions of this research.

Chapter III introduces the Asymmetric Spring Loaded Inverted Pendulum and develops a model that describes its dynamics in running. The ASLIP is modeled as a hybrid dynamic system with two charts. The dynamic equations for the in-phase motion of flight and stance are generated using the method of Lagrange. Finally, in preparation for control law design, the model is brought into a convenient mathematical form, which affords the direct application of tools from the theory of systems with impulse effects, in particular, from the hybrid zero dynamics control synthesis framework.

Chapter IV, proposes a controller for stabilizing the ASLIP and rigorously proves its stability properties. The proposed control law acts on two levels. On the first level, continuous in-stride control asymptotically stabilizes the torso pitch, and creates an invariant surface on which the closed-loop ASLIP dynamics is *diffeomorphic* to the target SLIP dynamics. On the second level, an event-based SLIP controller is used to stabilize the system about a desired periodic orbit. An immediate practical consequence of this method is that it affords the direct use of a large body of controller results that are available in the

literature for the SLIP. Furthermore, it is deduced through comparisons of the SLIP embedding controller with a rigid target model controller creating a one-degree-of-freedom *non-compliant* subsystem, that the underlying compliant nature of the SLIP enhances performance in terms of significantly improving the transient response and reducing actuator effort.

Chapter V introduces Thumper, and provides details on the geometry of the mechanism and on the transmission system. These details are crucial for understanding the behavior of the robot and the challenges associated with its control. Moreover, they are used to develop a model of the dynamics of Thumper, which is more complete than the ASLIP in that it captures the dynamics of the transmission and of the segmented leg, which is no longer considered to be massless. The development of the equations of motion for the in-phase dynamics of flight and stance is based on the method of Lagrange. Transitions between phases are assumed to be instantaneous and are modeled using standard techniques. The procedure results in a nonlinear hybrid dynamic model of Thumper in running, which will be used for control.

Chapter VI focuses on control law design. As was mentioned above, the majority of control laws suitable for monopods with non-trivial torsos are derived under the assumption that the torso COM *coincides* with the hip joint. However, the COM of Thumper's torso is located high above the hip, as in a human, thereby requiring novel control solutions. The feedback law presented in Chapter VI builds upon control ideas developed in Chapter IV for the Asymmetric Spring Loaded Inverted Pendulum (ASLIP). Thumper's controller is developed within the framework of hybrid zero dynamics and it works in concert with compliance in inducing provably exponentially stable running motions, while all relevant physical constraints are respected.

Finally, conclusions and remarks on future directions relevant to this work are provided in Chapter VII.

CHAPTER II

Literature Survey

In this chapter, results in the relevant literature that motivate and support the work presented in this thesis are provided. Section 2.1 briefly describes the differences between walking and running, and adopts a criterion for distinguishing the two gaits based on the location—highest in walking, lowest in running—of the body center of mass at midstance. This criterion, which is based on experimental evidence and reflects the underlying energy transformations that occur in walking and running, was adopted in order to highlight the fact that, in running, elastic energy storage in compliant elements is a dominant characteristic. This observation suggests that including compliant elements in legged machines designed to run may not just be a luxury; it is a necessity, without which running may be hard, or even impossible, to realize.

In an effort to explain the remarkable similarity in the ground reaction force profiles measured in experiments with diverse animals, which in turn suggests common underlying energy-saving mechanisms despite the apparent diversity, biologists and engineers proposed simple pendulum-based models. These models are briefly described in Section 2.2, with the purpose of illustrating the meaning of “natural,” or “passive” dynamics in walking and running. Effective use of the natural dynamics is crucial to the development of dynamic walking and running robots, as the literature presented in Section 2.3 suggests. As illustrated in the short survey of Section 2.4, where controller results for monopedal running are discussed, the majority of control laws suitable for dynamic running robots are largely based on empirical observations. Analytical results are obtained mostly through simplified models, which, in general, do not correspond to faithful repre-

sentations of the robots under consideration. On the other hand, formal control methods, e.g. passivity-based or feedback linearization controllers, which could be used in the context of more realistic models, primarily focus on obtaining analytically tractable stability criteria, without incorporating conditions for the effective use of the passive dynamics.

These results show that there is space for the development of a methodology that combines analytically tractable stability statements with realistic models to design control laws that work in concert with the natural dynamics of the system in inducing agile running motions on monopedal machines, such as Thumper.

2.1 Walking versus Running and the Role of Compliance

Two of the most common patterns of locomotion are walking and running. At first glance, the difference between walking and running would appear obvious. Generally, in running there is a period of the gait cycle where all feet are in the air, whereas in walking there is always one foot on the ground. This distinction is appropriate for most animals; however, there are cases where it fails. For instance, it has been observed that, when humans run along a circular path, the aerial phase of the motion decreases and eventually disappears if the turn has a sufficiently small radius, [73, pp. 217-219]. This is similar to what would have been observed in running under conditions of enhanced gravity¹. Furthermore, other perturbations to running, including running on very compliant surfaces, [73, pp. 219-228], and running with increased knee flexion —or, “Groucho running”— [76], may result in the reduction, or even elimination, of the aerial phase. However, in all these cases, the assertion that running has been converted in walking is not entirely correct. We will need to be clear about the differences between walking and running.

As mentioned in [4], in walking, while a foot is in contact with the ground, the corresponding leg is kept fairly straight, so that the torso appears to be traveling (more or less) along a series of arcs of circles. As a result, in walking, the torso is at its *highest* point at midstance. On the other hand, in running, the supporting leg is flexed during the contact

¹The equivalence between running on a circular path and running under enhanced gravity can be understood by the effective “gravity enhancement” offered by the centripetal acceleration developed when running in circles, which adds vectorially to the gravitational acceleration to produce higher ground reaction forces at the foot, see [73, pp. 217-219].

phase, so that the torso is at its *lowest* point at midstance. It was suggested by Cavagna et al. in [21] and by McMahon in [74], that this criterion for distinguishing walking from running is more suitable, for it is not merely based on the phenomenology of the gait, but, most importantly, it reflects more profound interactions between the body and the ground, responsible for the energy changes accompanying walking and running.

More specifically, force-plate records have been used to estimate the mechanical energy of the center of mass during walking and running of a diverse assortment of animals, including bipeds and quadrupeds, at various “constant” speeds; see for example [21], [68, pp. 84–87], [22], and [73, p. 192]. These data reveal that, in walking, changes in the gravitational potential and forward kinetic energies are substantially *out of phase*, so that the net mechanical energy change of the body appears to be relatively small. In particular, the increase in the gravitational potential energy in the first phase of the step, where the body is lifted, takes place at the expense of the forward kinetic energy, and the body is decelerated. The increased potential energy the body acquires this way may in turn be utilized in the second phase of the step to increase the kinetic energy, and thus directly contribute to the forward displacement as the body is falling forward. This energy transfer mechanism is dominant at slow and moderate walking speeds, and can account for up to 65% of the total energy changes during each stride in humans, leaving only 35% to be supplied through the work performed by the muscles²; see [21] and [22].

On the other hand, similar estimates of the mechanical energy show that running is substantially different from moderate walking; [21], [68, pp. 89–92], and [73, p. 192]. Running is characterized by changes in the gravitational potential energy which appear to be substantially *in phase* with changes in the kinetic energy; both energies reach a minimum at midstance and both go through a maximum at liftoff, thus resulting in very large fluctuations of their sum during the contact phase. Intuitively, during the first half of the stance phase, the body’s center of mass decelerates and falls, and the leg, which is shortening, acts like a brake. During the second half of the stance phase, however, the center of

²Note that the phase relationship between the kinetic and gravitational potential energies is only one of the factors determining energy economy in walking. The relative magnitude of the two forms of energy, as well as how closely they approximate mirror images of each other also affect the work performed by the muscles to maintain walking. The energy recovery, computed as a percentage of the total power required to maintain walking without the energy transfer mechanism, e.g. 65% in humans, captures the effect of all these factors.

mass accelerates and rises because the leg, which is extending, performs work on the body. Therefore, it seems that in running kinetic energy cannot be exchanged with gravitational potential energy and vice versa, as in walking, yielding the energy saving mechanism of walking largely irrelevant.

Nevertheless, as mentioned in [4], human running uses much less energy than what might be expected. Suppose for a moment that the mechanical energy removed during the first half of the stance phase, where the body falls and decelerates, were degraded into heat. Then, the work required to replace it would have to be supplied by metabolic activity in the muscles. The corresponding metabolic energy has been estimated in humans, including the known efficiency of the muscle, and was found to be approximately twice the actual energy consumption in slow running, and three times the actual energy consumption in fast running; see [20]. Furthermore, it was observed in [22], that, in hopping kangaroos, the ratio of the rate of external work³, i.e. the power required to move the center of mass of the body, over the chemical power input to the muscles is much larger than the efficiency of the muscles, even in the optimal conditions of contraction: it reaches 76% at hopping speeds about $30 \text{ km} \cdot \text{h}^{-1}$ while the maximum efficiency with which the muscles convert chemical energy to positive work is approximately 25%. Similar conclusions have been obtained in other animals as well, such as turkeys, dogs, and monkeys, to name a few.

The inexplicably large efficiency of running, together with the observation that the mechanism for minimizing energy expenditure in walking, i.e. transforming kinetic to gravitational potential energy and vice versa, is not plausible in running, has led physiologists to put forward the hypothesis that part of the mechanical energy absorbed in decelerating and lowering the body in the first half of the step is stored in the muscles and tendons in the form of *elastic* energy, which is then released to lift and accelerate the body in the second half of the step; see [4] and for a brief overview and [68, pp. 96–100], [20], [22], [73, pp. 204–208], [5], for details. Perhaps, it would be interesting to note that, despite the fact that physiologists have observed the large efficiency of running as

³The term *external work* is used to refer to work performed to move the center of mass of the body through the application of forces on the ground, as opposed to the term *internal work*, which corresponds to work that does not cause any displacement of the center of mass of the body, e.g. work performed to change the kinetic energy of the limbs relative to the center of mass; [68, p. 83].

early as the 1930's, it was not until recently that elastic energy storage has been proposed as the mechanism responsible for it; this seems to be primarily due to the fact that direct measurements of the elastic energy are hard to obtain.

From this discussion, it becomes apparent that the role of the elastic energy stored in compliant elements, such as tendons, is of central importance in explaining the mechanics of running. In fact, it may be argued that compliance is not merely a dominant characteristic of running; it is a *defining feature* of running, without which running would be hard, or even impossible, to realize. It should be clarified here though that elastic energy storage may also be present in walking, despite the fact that the forces developed in walking seem to be too small to cause sufficient stretching of the tendons. Indeed, as mentioned in [65], in human walking, the ankle push-off phase amounts for approximately 15% of a stride, while the calf muscles are active for almost double that time, allowing the Achilles tendon to store energy prior to push-off⁴. Nevertheless, in walking, elastic energy storage seems to be not as dominant as it is in running.

2.2 Simple Mechanisms for Studying Walking and Running

In the previous section, two basic mechanisms for minimizing energy expenditure in walking and running have been briefly discussed. It was described that, in walking, forward kinetic energy is transformed into gravitational potential energy and vice versa, saving energy that would otherwise have to be supplied by muscles. On the other hand, in running, energy is stored prior to midstance in compliant elements, such as muscles and tendons, and is then released after midstance to lift and accelerate the body forward. What is also remarkable about these studies is the fact that these basic energy transformation mechanisms are present in diverse species that differ in skeletal type, leg number and posture; see [22], [34], [33], [29], and references therein. For instance, in [22] the subjects included bipedal birds (turkey and rhea) that walk and run, quadrupedal mammals that walk, trot, and gallop (dog, monkey, and ram), and bipedal mammals which hop (kangaroo and springhare). In an effort to explain the underlying similarity in spite of the appar-

⁴In fact, this observation has been effectively used in the Cornell biped, a biped specifically designed for minimal energy use; [27].

ent diversity, simple reductive models, whose purpose is to capture the basic mechanics of walking and running without depending on the details of body structure and morphology, have been proposed. In this section, two families of such mechanisms will be discussed, the objective being to clarify the term “passive dynamics” in walking and running, which will be important in motivating the control structures proposed in this work.

2.2.1 Walking and the Inverted Pendulum

As suggested in [21] and [22], in walking the center of mass of the body “vaults” over a rigid stance leg in a way analogous to an *inverted pendulum*, consisting of a point mass atop a stiff rod; see Fig. 2.1. In accordance to the experimental evidence described in the previous section, the kinetic and gravitational potential energies of the pendulum are exchanged cyclically, and the center of mass reaches its highest point at midstance. Furthermore, a simple exercise based on the inverted pendulum model seems to predict reasonably well the speeds at which transition to running occurs. As noted in [4], walking is restricted to speeds somewhat less than \sqrt{gl} , where g is the gravitational acceleration and l is the leg length. The centrifugal effect “lightens” the contact force at the foot, and as the speed approaches \sqrt{gl} , the total force goes to zero. Breaking the “ \sqrt{gl} -barrier” calls for a different type of gait, namely running. Note that the inverted pendulum model was shown to be general enough to qualitatively describe walking not only in vertebrates, as in [21], [22], but also in arthropods with sprawled posture; [12], [34], [29].

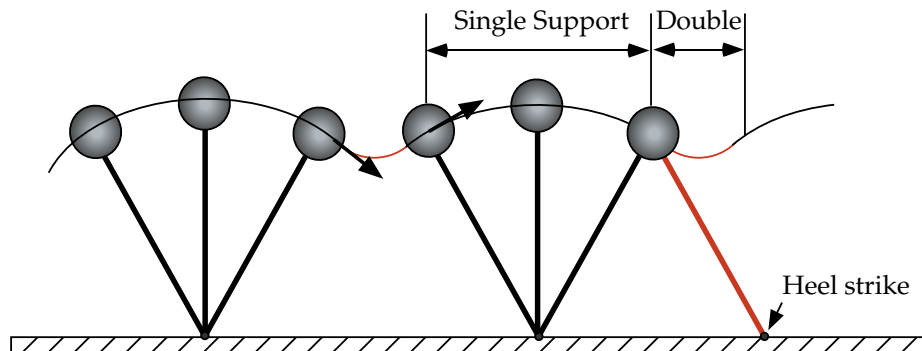


Figure 2.1: The inverted pendulum analogy of walking (adapted from [67]). The figure shows the single support phase, in which no active force is necessary to hold the weight, and the double support phase, in which the velocity of the center of mass is reoriented. Note that the hip is at its highest point at midstance.

The experimental fact that fluctuations in the total mechanical energy of the center of mass are relatively small during the single support phase in walking is captured by the inverted pendulum model adequately well. Furthermore, this observation suggests that, in bipedal walking, nearly zero muscular activity is required to move the swing leg forward in anticipation of touchdown. In fact, electromyographic records indicate very little activity in the swing leg at normal walking speeds, except at the beginning and at the end of the swing phase; [73, p. 198]. The muscles are active only during the double support period. These observations led Mochon and McMahon to introduce a more complete model for walking, comprising a second leg represented as a two-link pendulum; the two links correspond to the thigh and shank of the swing leg. This double pendulum is attached at the center of mass of the inverted pendulum representing the stiff stance leg, as shown in Fig. 2.1; see [78], [79] and [73, pp. 198–203]. This model, termed the *ballistic walking model*, shows that coupling between the swing leg (acting as a compound pendulum) and the stance leg (acting as an inverted pendulum) is important; the swing leg alone cannot predict the swing duration observed in walking experiments. Moreover, the ballistic walking model illustrates that gravity is a dominant factor in determining the dynamics of walking: despite the absence of any equivalent of muscle activity during the swing phase, the model can reproduce walking adequately well.

Other models based on the pendulum analogy of walking have been proposed; see [70], [40], and [39], for example. These models usually assume that the mass of the body is concentrated at the hip, and exhibit various assumptions concerning the distribution of inertia along the limbs, the shape of the foot, the actuation pattern etc. A multitude of interesting questions regarding walking can be addressed using these models, which, other than efficiency, [39], [30], [64], [67], they can be used to study stability [70], [40], speed/step-length relationship, [63], and to make comparisons of the pendulum analogy with other theories of human walking, [66].

The pendulum analogy is certainly very useful for explaining the energy saving mechanisms present in walking, but, as mentioned in [67], it leads to a paradox, for it does not explain why walking is so much more costly than other modes of transport such as wheeled locomotion. This paradox may be resolved by considering the double support

phase as the transition from one energy-conservative, single-support phase to the next; see [30], [64], [67]. In particular, at the end of each single-support phase, the velocity of the center of mass is directed downwards, and it needs to be redirected upwards in order to maintain forward progression; see Fig. 2.1. Changing the direction of the velocity of the center of mass requires the leading leg to perform negative work, which must be counteracted by positive work that can be supplied anytime throughout the step. The performance of negative and positive work entails a metabolic cost, which is inevitable in the pendulum representation of walking. The walking models used in [64] and [30] suggest that it is advantageous to perform positive work by applying ankle push-off at the trailing leg at the same time with, or immediately before, heel-strike, instead of employing torque on the stance leg.

As may be expected, the basic inverted pendulum model has limitations in describing walking. These are attributed mostly to the phenomena associated with the double support phase. In fact, the work in [30], [64], and [67] suggests that the degree to which potential and kinetic energy are exchanged according to the pendulum analogy should be reevaluated, mainly due to the fact that traditional methods for estimating external work —i.e., the “combined limbs method” used in [21], [22], [34] for example— tend to overestimate the energy savings in walking. This is associated with the positive and negative work performed during the double stance phase. Moreover, as pointed in [33], the assumption of a rigid stance leg does not explain the relatively small vertical excursions of the center of mass measured in experiments, and, as a result, the model cannot faithfully reproduce the observed ground reaction force profiles. To address these (and other) shortcomings, Alexander first proposed a model for walking, which includes compliance in the legs in [6]. More recently, a similar walking model with massless compliant legs has been proposed in [41], and it was found to capture the ground reaction force profiles in walking, which are characteristically “M-shaped”. The authors of this work argued that walking efficiency primarily depends on how much of the stride energy can be stored in elastic elements when redirecting the velocity of the center of mass during the double stance phase.

2.2.2 Running and the Spring Loaded Inverted Pendulum

While there is some ambiguity in quantifying the role of elastic energy storage in walking, its dominance in running admits no doubt. In running, the leg acts as a spring, storing energy by compressing during the braking phase, and then returning this energy in the propulsive phase as it decompresses. This energy saving mechanism seems to be present in a variety of animals, leading biologists to conjecture that diverse species run in a stable manner by tuning their musculoskeletal system so that their center of mass appears to be moving as if it were riding on a pogo-stick; [33], [29].

In one of the earliest works, McMahon introduced a somewhat non-physical spring-mass system for the purpose of investigating gait transitions in bipeds and quadrupeds; see [74]. The associated analysis was not based on the dynamical equations of the model, but the importance of using such a simple spring-mass system to study the properties of the gait has been clearly illustrated. A more detailed investigation of the dynamics of a spring-mass system as a canonical model for hopping and running has been undertaken by Blickhan in [11]. In this work, Blickhan introduced a model comprised of a point-mass body attached to a massless, undamped, prismatic spring, representing the action of a leg. This model, depicted in Fig. 2.2, corresponds to the most common configuration of the *Spring Loaded Inverted Pendulum* (SLIP), which has appeared widely in the locomotion literature; see [33], [49] and references therein. In [11] Blickhan imposed physiological constraints on the parameters of the model, and, notwithstanding its apparent simplicity, found it to be remarkably accurate in predicting the contact times, peak ground reaction forces and energetics of the center of mass observed in experiments of running in humans.

The potential prescriptive power of the SLIP was recognized by McMahon and Chen in [75]. McMahon and Chen focused on identifying the rules that couple leg-spring stiffness, gravity, and forward speed in running, and, among other things, they showed that, with appropriately chosen parameters and initial conditions, the model could accurately predict the relation between vertical acceleration and vertical displacement observed in experiments that included a running dog, a running man, and a hopping kangaroo. Through simulations on the SLIP, McMahon and Chen in [75] suggested two different strategies for

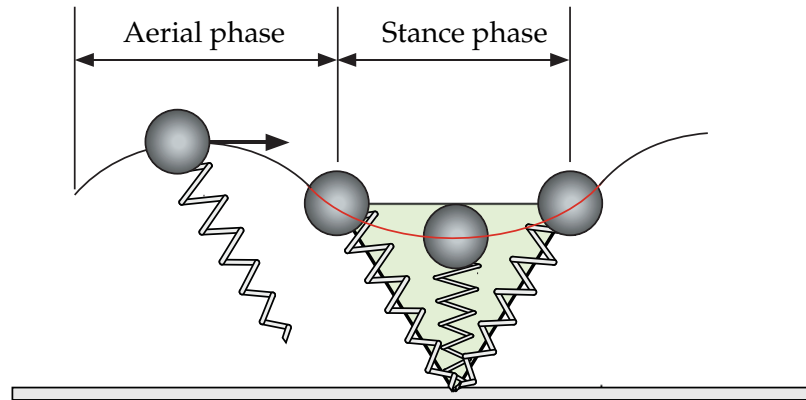


Figure 2.2: The Spring Loaded Inverted Pendulum analogy of running. In the first part of the stance phase the leg is compressing and energy is stored in the spring, which is returned in the second part of the stance when the body is lifted and accelerated. Note that the hip is at its lowest point at midstance.

maintaining periodicity in running at various forward speeds. The first strategy requires stiffening the legs in order to accommodate higher forward velocities, when the landing configuration is kept constant. The second strategy suggested that, with the spring stiffness kept constant, higher forward speeds can be accommodated by landing at less vertical configurations. This last principle was already at work in legged robotics. Raibert had already devised a foot placement feedback strategy, acting during the flight phase, to regulate forward speed in his monopedal, bipedal, and quadrupedal robots; see [90] and [92]. In fact, even though Raibert used models that were more complete than the conservative SLIP—they included actuation, energy losses, non-trivial torso etc.—simple spring-mass systems were central to the development of his control laws.

The remarkable success of the SLIP in describing and predicting the mechanics of running in a large variety of animals, ranging from humans to lizards and cockroaches, see [13], [36] and references therein, and in robots with different numbers of legs and postures as described in [91], led to the conjecture that the SLIP was not merely a descriptive model; it represents a model that could be used to advance hypotheses concerning the high-level control strategy underlying the achievement of the task; [33], [49]. For instance, Full and his collaborators observed in experiments that the cockroach *Blaberus discoidalis* runs explosively in a stable manner over rough terrain at speeds high enough to challenge the ability of proprioceptive sensing and neural reflexes to respond to perturbations within

a stride; [35]. They proposed and numerically analyzed a simple conservative model, and they argued that “mechanical feedback”⁵ (preflexes) may replace detailed neural feedback (reflexes) in rapid disturbance rejection; [62].

Such hypotheses can be made mathematically precise and tested in the context of simple mechanical models like the SLIP. In fact, Schmitt and Holmes proposed a model similar to the SLIP, termed the *Lateral Leg Spring* (LLS), suitable for studying the horizontal dynamics of sprawled insects; [98]. In agreement with [62], they arrived at the conclusion that the model exhibits asymptotically stable motions (within a constant energy level) when provided with appropriate initial conditions, and without any neural-equivalent feedback. Recently, it was discovered in [104], and, independently, in [42], that, not only the horizontal-plane LLS, but also the sagittal-plane SLIP possesses a similar behavior; namely “self-stable” running gaits. Similar results were also found in the context of quadrupedal running with a bounding gait in [87], and simple control laws operating mostly in the feed-forward regime have been proposed that enlarge the basin of attraction of “self-stable” gaits in [105]. Three-dimensional extensions of the SLIP with relevant stability analyses are also available in the literature; [103].

The inherent stability of SLIP and LLS models is a very interesting property since, as is known from mechanics, systems described by autonomous, conservative, holonomically constrained flows cannot be asymptotically stable⁶. However, Altendorfer et al. in [8] showed that the stable behavior of piecewise holonomic conservative systems is a consequence of their hybrid nature. The work in [8] offers a theoretical framework suitable for analyzing various leg placement control policies for the SLIP, by obtaining conditions that are necessary for asymptotic stability and sufficient for instability, and can be checked analytically. Analytical methods for studying the dynamics of the SLIP have been proposed in the literature before. For instance, Schwind and Koditschek introduced an iterative procedure that combined Picard-style iterates with the Mean Value Theorem for Integrals to construct closed-form approximants of the Poincaré return map associated with the run-

⁵From a rigorous control perspective, the term is somewhat vague. It refers to feedforward stabilization of an open-loop plant. More details and clarifications can be found in [37], [59] and [49].

⁶By Liouville’s theorem (see [97, p. 122]), the incompressibility of the phase fluid precludes the existence of asymptotically stable equilibria in Hamiltonian systems, for if such points existed, they would reduce a finite volume in the phase space to a single point.

ning SLIP; see [99] and [100]. Based on this approach, the authors studied conditions for existence and stability of periodic running motions in the SLIP in [101] and [102].

2.3 Walking and Running Robots

The field of legged robots has grown to the point where one can identify several schools of thought on the subject. Most visible to the general public is the part of the field focused on building humanoids, that is, robots that are inspired by human morphology. The most well known of these robots is undoubtedly Honda's ASIMO. Other robots in this vein include HRP-2 (Kawada Industries, Japan) and Johnnie (Technical University of Munich, Germany). These machines are very complicated, high-degree-of-freedom prototypes built as part of an effort to develop robots that will be able to serve humans or even directly replace humans in the operation or service of other machines. These robots involve a very broad ranging development effort that includes machine vision, portable power sources, artificial intelligence, force sensing, durability, packaging, etc. As such, upright, stable bipedal locomotion is only one piece of the overall effort, and, largely for reasons of expediency, the designers of these robots have adopted one of the simpler notions of gait stability. For the robots cited, the stabilization algorithm boils down to maintaining the center of pressure of the ground reaction forces of the stance foot strictly within the convex hull of the foot. The resulting motions are flat footed and distinctly not human like.

2.3.1 Passive Dynamic Walking Robots

At the opposite end of the complexity spectrum in terms of technology are the "minimalist" bipeds, whose designers seek the minimal assembly of links, joints, sensors and actuators to accomplish a given locomotion task. This area of bipedal locomotion was inspired by the pathbreaking work of Tad McGeer⁷, who in the late 80's and early 90's, analyzed and built planar bipedal robots which could walk stably⁸ down a slight incline with no sensing or actuation whatsoever; [69], [70], [71]. McGeer's robots are "passive"

⁷Prior to McGeer, Miura and Shimoyama demonstrated dynamic walking on a robotic biped in [77]. In contrast to McGeer's robots, however, the gait was generated by feedforward commands and was stabilized by event-based feedback.

⁸In the sense of possessing an exponentially stable periodic orbit.

because they employ no active power source; walking is purely the outcome of the interplay between gravity and the geometric and inertia properties of the robot. In accordance with biological observations, most notably the ballistic walking model proposed by Mochon and McMahon in [78], [79] and [73, pp. 198–203], the legs move freely as pendulums under the influence of gravity and, if their masses and lengths are tuned just right, they can produce stable periodic motions without any feedback control.

Further impetus to this area was provided by Collins, Wisse, and Ruina who built 3D (spatial) actively powered walkers that were able to walk on level ground through the judicious placement of actuators; [27] and [112]. In these research efforts, two different strategies for powering walking robots were employed. The Cornell team used electric motors with springs to implement ankle push-off in the trailing leg, during and after the collision of the leading leg with the ground; [27]. On the other hand, the Delft team introduced actuation at the hip by alternating the states of antagonistic pairs of McKibben’s muscles based on feedback from foot contact sensors responsible for detecting heel strike; [112]. The policy employed by the Cornell biped complies with the one suggested by Kuo in [64] and [67], and it results in a very low cost of transport—lower than that of the Delft biped, Denise, [112, Chapter 6]. This was expected based on Kuo’s analysis in [64], which suggests that employing ankle push-off is energetically advantageous, compared to employing hip torque on the stance leg. Note, however, that hip actuation offers advantages too, mainly in terms of control, by improving the robustness against falling forward, as suggested in [111]. In any case, despite the presence of actuators, the resulting motions are still dominated by passive leg dynamics; actuation is intended only to tune and shape these dynamics and not, as is commonly done in robotics, to impose prescribed motions; [65].

Dynamic walkers, passive or active, use far less—in the fully passive extreme, none—control compared to humanoid robots; yet, they exhibit remarkably human-like motions. It is at first sight surprising that an activity so apparently complex as walking can be achieved simply, without employing any feedback action. Moreover, with parsimonious actuation and minimal control action that exploit the natural dynamics of the system by accentuating the passive leg motion, energy efficiency, a critical requirement for every autonomous

legged robot, is dramatically increased. Dynamic walkers, such as the the Cornell Biped, walk at an energetic cost of transport almost identical to that of human walking. This evidence leaves no doubt of the fundamental value of dynamic walkers in uncovering the basic principles of walking, and attracted the attention of biologists and sport scientists. As noted by Alexander in [7], the message that biologists received from the success of dynamic walkers is that “walking could be generated with much less nervous control than what was originally supposed”.

Unfortunately though, it is a fact that the remarkable elegance and economy of dynamic walkers comes at the cost of poor ability in achieving tasks other than walking, e.g. climbing stairs, standing or turning. On the other hand, the impressive versatility, demonstrated by robots like ASIMO comes at the cost of increased power consumption requirements, making these robots nonviable in environments with a limited power supply. It is therefore natural to ask how feedback control methodologies can be developed to synthesize control laws that combine the efficiency and elegance of dynamic walkers with the versatility of robots like ASIMO. Currently, there are not many results on these issues, but suggestions toward this direction are outlined in [65].

2.3.2 Dynamically Stable Running Robots

In the early 80's Raibert was the first to successfully build an actively balanced legged machine, [90], [89], [91]. He and his team built a pneumatically actuated monopod that was able to run with speed of 1 m/s; [89]. The controller's task was decomposed into three subtasks dedicated to (a) forward propulsion of the robot at the desired speed, (b) regulation of the vertical rebounding motion of the body, and (c) keeping the body at a desired posture; [90], [91, Chapter 2]. To control the forward speed of the monopod, the controller places the toe at a desired position with respect to the center of mass during flight. To regulate the hopping height, the length of the leg at the bottom of the stance phase is adjusted by giving a fixed amount of thrust. Finally, to control the pitch attitude of the body, the controller employs hip torque during stance. Based on the same principles, Raibert and his team built a 3D hopper that was able to run without being constrained on

the sagittal plane; [91, Chapter 3].

The success of these simple algorithms in the control of an apparently complex task such as running, led Raibert to build bipedal and quadrupedal extensions of his monopod and to apply the same basic ideas. In [92], [91, Chapter 4] and [88], Raibert extended the control algorithms developed for monopods to bipeds and quadrupeds. He investigated quadrupedal running gaits that use the legs in pairs: the trot (diagonal legs in pairs), the pace (lateral legs in pair) and the bound (front and rear pairs). In order to simplify the control problem, he proposed a *virtual leg* approach, according to which legs that operate in pairs can be substituted by an equivalent virtual leg. Raibert's approach separates the control problem into two parts. The first part is a high-level controller based on the three-part algorithm developed for the monopod, which produces the commands needed to control the body motions in achieving the desired behavior. The second part is a low-level controller that ensures the conditions for the virtual leg approach are met.

Motivated by Raibert's work, Buehler and his students developed dynamically stable running robots that employ low degree-of-freedom electrical actuation combined with a "minimalist" mechanical system; see [17] for an overview. Like Raibert, Buehler focused on dynamic mobility, but emphasized mostly energy efficiency and autonomy replacing the high-power pneumatic and hydraulic actuators in Raibert's robots with electrical motors. Monopod I consisted of a body connected to a compliant prismatic leg at the hip and it was able to run in the sagittal plane at a speed of 1.2 m/s with an average mechanical power of 125 W; [1]. The control algorithms for the pitch and forward speed were based on Raibert's decoupled controllers, while a "thrusting" control law based on the model of the transmission system was proposed to inject sufficient energy during the short stance phase; [44]. Energetic analysis of the experimental results showed that, at top speed, 40% of the energy goes to sweeping the leg forward. To reduce this energy, Monopod II was constructed; [44]. Monopod II inherited most of the features of Monopod I; however, compliance in series with the hip actuator was introduced, resulting in a sustained body-leg counter-oscillation, which dramatically decreased the total energy requirement: Monopod II was capable of achieving stable running at a speed of 1.25 m/s with total mechanical

power expenditure⁹ reduced to 70% of that required for Monopod I.

In the same vein, several other monopedal robots were built, including Ringrose’s self-stabilizing one-legged robot, [93], and Zeglin’s bow-leg hopper, [16]. For a comprehensive survey of monopedal robots and related control strategies, the reader is referred to [96].

2.4 On the Control of Hopping and Running

The complexity of the dynamics of one-legged hoppers precluded analytically tractable stability studies on realistic models of monopedal robots, and led to introducing various simplifications: point-mass body, massless leg, zero gravity in stance, to name a few. In one of the earliest analytical works, Koditschek and Buehler explain the robust behavior of Raibert’s vertical hopping controller by concentrating on the vertical oscillation of a simplified hopper; see [60]. This analysis is extended in [108] by considering the bifurcation diagram of the system’s return map. Forward dynamics is added to the vertical hopper in [72] with the purpose of investigating its effect on the vertical motion. The problem of controlling forward velocity alone is examined in [31] and [101], where no control input is available at the leg.

On the other hand, the combined difficulties of hybrid dynamics and underactuation inherent in dynamically stable legged systems stymied the direct application of nonlinear controller synthesis tools, such as those in [57], to induce provably stable motions to realistic models of running robots. Instead, many *empirical* control procedures have been employed over the past twenty years to control hopping and running robots or robot models; see [91], [2], [43], [32], [80], [56], [23], [3] for examples of one-legged robots.

In many cases, these control procedures are inspired by Raibert’s original three-part controller, [91]. In [2], the authors present a strategy, termed the controlled passive dynamic running (CPDR), for the control of a one-legged running robot featuring compliant elements in series with the hip and leg actuators. The proposed control law exploits the system’s passive dynamics, i.e. its unforced response, through imposing proper desired

⁹The total mechanical power expenditure is measured by the “specific resistance” introduced by Gabrieli and von Kármán in [38], and is defined as the ratio of the output power (mechanical or electrical) P over the product of the total weight of the vehicle mg with the maximum speed v_{\max} .

trajectories via inverse dynamics control on the actuated joints, while a modification of Raibert’s foot-placement controller is used for adapting the motion to varying forward velocity commands. This approach has been expanded and successfully implemented in experiments in [3]. A different class of controllers for monopedal running was introduced in [32]. These controllers apply impulsive (or, equivalently piecewise constant) feedback inputs at discrete time instants throughout a stride to stabilize unforced periodic solutions of a simplified model, and were found to perform well on an exact model of the hopper. The reliance of the control laws in [32] on a simplified model is removed in [56]. From a minimalist perspective, a realistic one-legged hopper is controlled using only a hip actuator in [23]. All the control laws mentioned so far incorporate sensory feedback to stabilize periodic running motions. However, as indicated in [80], stable running can be achieved using purely feed-forward periodic commands to the hip and leg motors.

A quite different paradigm for control law design combining *analytical tractability* with *realistic models* has been followed in [46], [110], and [24]; see also [109] for an integrative perspective. There, geometric nonlinear control methods have been developed that deal directly with the underactuation and hybrid dynamics present in legged robots, and induce provably asymptotically stable dynamic walking and running motions in bipedal robots. In particular, it has been shown that planar walking and running gaits can be “embedded” in the dynamics of a biped by defining a set of holonomic output functions with the control objective being to drive these outputs to zero; [46], [110]. In essence, this method asymptotically restricts the dynamics of the closed-loop hybrid model to a lower-dimensional attractive and invariant subset of the state space. The stable periodic solutions of the dynamics restricted on this subset, called the Hybrid Zero Dynamics (HZD), encode the desired task (walking or running).

The general idea of task encoding through the enforcement of a lower-dimensional target dynamics¹⁰, rather than through the prescription of a set of reference trajectories, has been employed in the control of dynamically dexterous machines, including juggling,

¹⁰Specifying the desired behavior of a plant through the definition of target dynamics is not a new concept in control theory; see for instance model reference adaptive controllers, [61], or model matching control designs, [28]. In the vast majority of these controllers, however, the target dynamics is usually a very simple system; in many cases a double integrator. In the work mentioned above, the target dynamics is a complex system—in legged locomotion, a hybrid dynamical system—that captures the task-level behavior.

brachiating and running robots, by Koditschek and his collaborators; [18], [86] and [94]. The same general idea, albeit in a fully actuated setting, has been employed in [10] and [9], where the method of controlled symmetries introduced in [107] together with a generalization of Routhian reduction for hybrid systems were combined to extend passive dynamic walking gaits, such as those obtained by McGeer’s passive walker [70], in three-dimensions.

Task encoding through imposing pre-specified target dynamics leaves one with the question of selecting a suitable candidate dynamical system for the targeted running behavior. On one hand, as was described in Section 2.2.2, a growing body of evidence in biomechanics indicates that diverse species, when they run, they tune their neural and musculoskeletal systems so that their COM bounces along as if it was following the dynamics of a SLIP; [11], [13], [33]. On the other hand, careful consideration of the SLIP gave insight into synthesizing empirical control laws capable of stabilizing running robots with one, two and four legs, as was demonstrated in [91]. In the light of this evidence, the SLIP is construed as a dynamic model of the observed running behavior, and thus can be used as the target dynamics for legged robots; see [33], and [49].

Up to this point, however, much of this research has been concentrated on the SLIP itself, and, as was indicated in [23], controllers specifically derived for the SLIP will have to be modified in order to be successful in inducing stable running in more complete models that include pitch dynamics or energy losses. Only preliminary results in this direction are available, including [95] and [94], in which controllers for running exploit results known for the SLIP. Furthermore, the majority of control laws suitable for one-legged robot models exhibiting pitch dynamics are derived based on the assumption that the torso COM *coincides* with the hip joint; for example, see [2], [32], [80], [56], [23], [3]. The purpose of this assumption, which is crucial for the success of the control laws, is that it results in trivial coupling between the torso and leg dynamics. To the best of the author’s knowledge, only [54] and [55] addressed the asymmetric case, but stability conclusions were drawn from numerical studies only.

These observations set the stage for this thesis. Chapters III and IV aim at establishing a more rigorous connection between the SLIP as a control target for running and more

complete plant models of legged robots, such as the ASLIP that includes nontrivial pitch dynamics. Then, in Chapters V and VI, the feedback ideas developed for the ASLIP are extended to derive control laws with provable stability properties that work harmoniously with the natural compliant dynamics of Thumper to induce elegant running motions on the robot.

CHAPTER III

Approximating Thumper: The Asymmetric Spring Loaded Inverted Pendulum

As was mentioned in the introduction, the first step toward the construction of controllers for running in Thumper is the introduction of an intermediate model, termed the *Asymmetric Spring Loaded Inverted Pendulum (ASLIP)*. This model is intended to bridge the gap between Thumper and point-mass hoppers that describe the center of mass dynamics of running, such as the Spring Loaded Inverted Pendulum (SLIP). Aiming to reflect a broader purpose, the ASLIP includes torso pitch dynamics nontrivially coupled to the leg motion, an issue not addressed in the widely studied SLIP or in its straightforward extensions, in which the torso COM coincides with the hip joint. Despite its importance, to the best of the author’s knowledge, no rigorous studies of the ASLIP exist in the relevant literature.

In this chapter, a mathematical model that governs the evolution of the hybrid dynamics of the ASLIP in running is developed. Section 3.1 provides the modeling hypotheses, based on which the equations of motion in the stance and flight phases will be derived. This is accomplished in Sections 3.2 and 3.3 through the use of the method of Lagrange. Transitions between phases are modeled in Sections 3.4 and 3.5, and the system is brought to the form of a system with “impulse” effects in Section 3.6. This form enables the use of results from the theory of systems with impulse effects—in particular, the hybrid zero dynamics method—to design controllers that induce provably exponentially stable periodic running motions in the ASLIP. This task is undertaken in Chapter IV.

3.1 Terminology, modeling hypotheses, and notation

A schematic for the Asymmetric Spring Loaded Inverted Pendulum (ASLIP) is presented in Fig. 3.1. During running, the ASLIP alternates between *stance* and *flight* phases. In the stance phase the leg-end is in contact with the ground, while in flight the ASLIP follows a ballistic trajectory under the influence of gravity. In what follows, the subscripts “f” and “s” denote “flight” and “stance,” respectively.

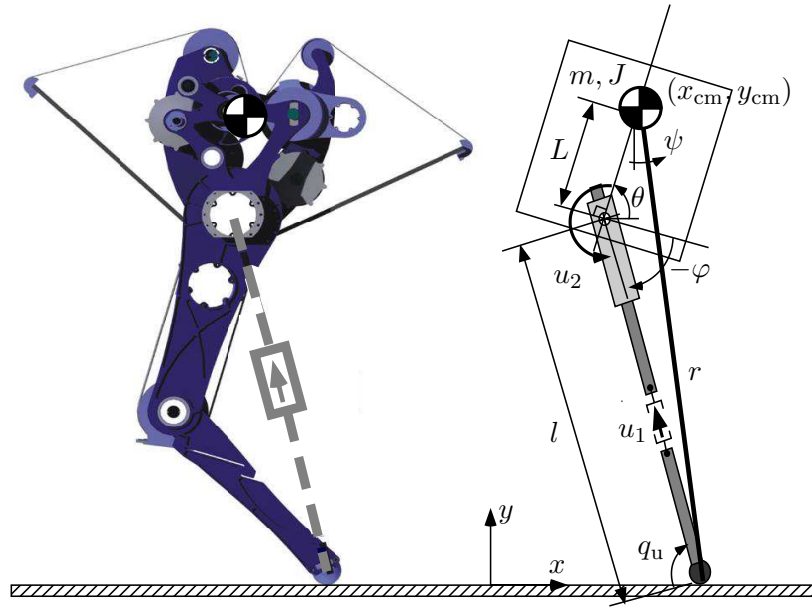


Figure 3.1: **Left:** The morphology of Thumper’s leg; see [52], [51] for design principles and hardware details. The knee has a revolute series compliant actuator. **Right:** The Asymmetric Spring Loaded Inverted Pendulum (ASLIP). The leg force u_1 will be modeled as a spring in parallel with a prismatic force source. The ASLIP is a more faithful representation of the robot on the left than a SLIP model.

As shown in Fig. 3.1, the ASLIP is composed by a torso and a single leg attached to the torso via a revolute joint, termed the *hip joint*. The hip joint does not coincide with the center of mass (COM) of the torso, which is modeled as a rigid body with mass m and moment of inertia J about the COM. The leg is composed by two links, the lower and the upper leg, which are connected via a prismatic joint, and are assumed to be massless. The contact of the leg with the ground, usually referred to as the *toe*, is modeled as an unactuated pin joint. The ASLIP is controlled by two inputs: a force u_1 acting along the leg, and a torque u_2 applied at the hip. In Section 4.6, the leg force u_1 will be modeled as a

spring in parallel with an ideal prismatic force source.

In the following list, the hypotheses underlying the derivation of the model of the ASLIP presented in this chapter are enumerated. The significance of these modeling hypotheses will become apparent in subsequent sections, where details on the model derivation are presented. Here, all hypotheses are collected for reference purposes.

Model Hypotheses: ASLIP

HMA1) The motion is planar, i.e., running is constrained in the sagittal plane;

HMA2) The torso is modeled as a rigid body with nonzero mass and distributed inertia.

The leg is assumed to be massless. The hip and knee joints are assumed to be ideal (frictionless) revolute and prismatic joints, respectively;

HMA3) The point of contact between the leg-end and the ground is unactuated; it is modeled as a frictionless pin joint; and

HMA4) The leg force u_1 will be modeled as a spring in parallel with an ideal prismatic force source.

Gait Hypotheses for Running: ASLIP

HGA1) Running is from left to right and takes place on a level surface;

HGA2) There are alternating phases of stance and flight separated by touchdown and liftoff events;

HGA3) During the single support phase the stance leg acts as an ideal pivot joint; in particular, throughout the stance phase it can be guaranteed that the vertical component of the ground reaction force is non-negative and that the ratio of the horizontal component over the vertical component does not exceed the coefficient of friction (the leg does not “pull” the ground and the toe does not slip);

HGA4) The COM of the robot travels a nonzero horizontal distance during the flight phase;

HGA5) The flight phase is terminated when the toe touches the ground. No impact occurs at this instant (the leg is assumed to be massless and there is a prismatic spring along its direction); and

HGA6) In the open-loop system, the stance phase is terminated when, in the absence of vertical ground reaction force component, the acceleration of the toe is positive, i.e., directed upwards. In the closed-loop system, switching from stance to flight is assumed to be control decision.

3.2 ASLIP Flight Dynamics

In accordance with hypotheses HMA1) and HMA2), the flight phase dynamics corresponds to a planar rigid body undergoing ballistic motion in a gravitational field. The configuration space Q_f of the flight phase is a simply-connected open subset of $\mathbb{R}^2 \times \mathbb{S}^1$ corresponding to physically reasonable configurations of the ASLIP, and it can be parameterized by the Cartesian coordinates x_{cm} and y_{cm} of the COM together with the pitch angle θ , i.e., $q_f := (x_{cm}, y_{cm}, \theta)' \in Q_f$; see Fig. 3.1.

The equations of motion of the ASLIP during the flight phase are obtained through the method of Lagrange; see [106, p. 255]. If $\mathcal{K}_f : TQ_f \rightarrow \mathbb{R}$ and $\mathcal{V}_f : Q_f \rightarrow \mathbb{R}$ denote the kinetic and potential energies of the ASLIP in flight, respectively, then the corresponding Lagrangian $\mathcal{L}_f : TQ_f \rightarrow \mathbb{R}$ is

$$\begin{aligned} \mathcal{L}_f(q_f, \dot{q}_f) &:= \mathcal{K}_f(q_f, \dot{q}_f) - \mathcal{V}_f(q_f) \\ &= \frac{1}{2}m(\dot{x}_{cm}^2 + \dot{y}_{cm}^2) + \frac{1}{2}J\dot{\theta}^2 - mgy_{cm}, \end{aligned} \tag{3.1}$$

where g is the gravitational acceleration. The flight dynamics of the ASLIP can then be described by the second-order system

$$D_f \ddot{q}_f + G_f = 0, \tag{3.2}$$

where $D_f = \text{diag}(m, m, J)$ and $G_f = (0, mg, 0)'$. The system (3.2) can easily be written in

state-space form as

$$\dot{x}_f := \frac{d}{dt} \begin{bmatrix} q_f \\ \dot{q}_f \end{bmatrix} = \begin{bmatrix} \dot{q}_f \\ -D_f^{-1}G_f \end{bmatrix} =: f_f(x_f), \quad (3.3)$$

evolving in $TQ_f := \{x_f = (q_f', \dot{q}_f')' \mid q_f \in Q_f, \dot{q}_f \in T_{q_f}Q_f \cong \mathbb{R}^3\}$.

As mentioned in Hypothesis HGA5), the flight phase terminates when the vertical distance of the toe from the ground becomes zero. To realize this condition, the flight state vector is augmented with $\alpha_f := (l^{\text{td}}, \varphi^{\text{td}})' \in \mathcal{A}_f$ an open subset of $\mathbb{R} \times \mathbb{S}^1$, where l^{td} and φ^{td} are the leg length and angle at touchdown, respectively, and $\dot{\alpha}_f = 0$. This means that, during flight, the leg is assumed to obtain the desired length and orientation instantaneously¹, without affecting the motion of the torso. The threshold function $H_{f \rightarrow s} : TQ_f \times \mathcal{A}_f \rightarrow \mathbb{R}$ given by

$$H_{f \rightarrow s}(x_f, \alpha_f) := y_{\text{cm}} - l^{\text{td}} \cos(\varphi^{\text{td}} + \theta) - L \sin \theta, \quad (3.4)$$

signifies the touchdown event at its zero crossing, and defines a smooth switching manifold $\mathcal{S}_{f \rightarrow s}$ in the augmented state space $\mathcal{X}_f := TQ_f \times \mathcal{A}_f$, given by

$$\mathcal{S}_{f \rightarrow s} := \{(x_f, \alpha_f) \in \mathcal{X}_f \mid H_{f \rightarrow s}(x_f, \alpha_f) = 0\}. \quad (3.5)$$

Note that in (3.4) and (3.5), the parameter α_f is an input available for discrete-time control, and will eventually be chosen according to an event-based feedback law.

3.3 ASLIP Stance Dynamics

During the stance phase the toe is in contact with the ground. By Hypothesis HMA3), the toe-ground interaction will be modeled as a frictionless pin joint; in particular the Cartesian velocity of the toe during the stance phase is assumed to be zero throughout stance. Attaching the frame of reference at the (motionless) toe, i.e., $(p_{\text{toe}}^h, p_{\text{toe}}^v) = (0, 0)$ results in

¹Instantaneous positioning of the leg during flight is only one possible foot placement strategy. Other possibilities include the case where appropriately selected functions govern the evolution of the leg variables (length and angle) in time. Such alternatives do not have any effect on the analysis of the following sections, because the motion of the leg does not affect the second-order dynamics of the body in the flight phase.

the (holonomic) constraint

$$\begin{bmatrix} p_{\text{toe}}^h \\ p_{\text{toe}}^v \end{bmatrix} = \begin{bmatrix} 0 \\ 0 \end{bmatrix} \Leftrightarrow \begin{bmatrix} x_{\text{cm}} \\ y_{\text{cm}} \end{bmatrix} = \begin{bmatrix} L \cos \theta - l \sin(\theta + \varphi) \\ L \sin \theta + l \cos(\theta + \varphi) \end{bmatrix}. \quad (3.6)$$

In view of this constraint, the configuration space Q_s of the stance phase can be parameterized by the joint coordinates: leg length l , leg angle with respect to the torso φ , and torso orientation θ , i.e. $q_s := (l, \varphi, \theta)' \in Q_s$; see Fig. 3.1. Hence, Q_s is a simply-connected open subset of $\mathbb{R} \times \mathbb{S}^2$ corresponding to physically reasonable configurations of the ASLIP.

Through the use of the method of Lagrange [106, p. 255], the equations of motion of the ASLIP during the stance phase can be computed by substituting the constraint equations to the unconstrained flight-phase Lagrangian (3.1). This procedure results in the second-order system

$$D_s(q_s)\ddot{q}_s + C_s(q_s, \dot{q}_s)\dot{q}_s + G_s(q_s) = B_s u, \quad (3.7)$$

where $u := (u_1, u_2)' \in \mathcal{U}$ an open subset of \mathbb{R}^2 , is the input vector during stance, and the matrices in (3.7) are given by

$$D_s(q_s) = \begin{bmatrix} m & 0 & mL \cos \varphi \\ 0 & ml^2 & ml(l - L \sin \varphi) \\ mL \cos \varphi & ml(l - L \sin \varphi) & J + mL^2 + ml(l - 2L \sin \varphi) \end{bmatrix}$$

$$C_s(q_s, \dot{q}_s)\dot{q}_s = \begin{bmatrix} mL \sin \varphi \dot{\theta}^2 - ml (\dot{\varphi} + \dot{\theta})^2 \\ mLl \cos \varphi \dot{\theta}^2 + 2ml \dot{l}(\dot{\varphi} + \dot{\theta}) \\ 2m(l - L \sin \varphi) \dot{l}(\dot{\varphi} + \dot{\theta}) - mLl \cos \varphi \dot{\varphi}(\dot{\varphi} + 2\dot{\theta}) \end{bmatrix}$$

$$G_s(q_s) = \begin{bmatrix} mg \cos(\varphi + \theta) \\ -mgl \sin(\varphi + \theta) \\ mgL \cos \theta - mgl \sin(\varphi + \theta) \end{bmatrix}, \quad B_s = \begin{bmatrix} 1 & 0 \\ 0 & 1 \\ 0 & 0 \end{bmatrix}.$$

The model (3.7) can be brought into standard state-space form by defining

$$\begin{aligned}\dot{x}_s &:= \frac{d}{dt} \begin{bmatrix} q_s \\ \dot{q}_s \end{bmatrix} = \begin{bmatrix} \dot{q}_s \\ D_s^{-1}(q_s)(-C_s(q_s, \dot{q}_s)\dot{q}_s - G_s(q_s) + B_s u) \end{bmatrix} \\ &=: f_s(x_s) + g_s(x_s)u,\end{aligned}\tag{3.8}$$

where $x_s \in TQ_s := \{(q'_s, \dot{q}'_s)' \mid q_s \in Q_s, \dot{q}_s \in T_{q_s}Q_s \cong \mathbb{R}^3\} =: \mathcal{X}_s$ is the state vector.

Remark 3.1. The resulting equations of motion (3.7) for the stance phase include only the gravitational potential energy. This is a consequence of the definition of the unconstrained Lagrangian (3.1), which does not include an elastic energy term. The leg spring will be introduced in Section 4.6 as part of the total leg force u_1 ; see (4.79) there. \triangleleft

Remark 3.2. The ground reaction forces $F_{\text{toe}} = (F_{\text{toe}}^T, F_{\text{toe}}^N)'$, where F_{toe}^T is the tangential and F_{toe}^N the normal component, respectively, can be computed provided that the input forces $u = (u_1, u_2)'$ are known through

$$\begin{bmatrix} F_{\text{toe}}^T \\ F_{\text{toe}}^N \end{bmatrix} = \begin{bmatrix} \sin(\varphi + \theta) & \frac{1}{l} \cos(\varphi + \theta) \\ -\cos(\varphi + \theta) & \frac{1}{l} \sin(\varphi + \theta) \end{bmatrix} \begin{bmatrix} u_1 \\ u_2 \end{bmatrix}.\tag{3.9}$$

For the stance model (3.7) to be physically meaningful, i.e., consistent with the hypotheses that were used to derive it—in particular, Hypothesis HGA3—it must be verified that

$$F_{\text{toe}}^N > 0\tag{3.10}$$

and

$$|F_{\text{toe}}^T| \leq \mu_s F_{\text{toe}}^N,\tag{3.11}$$

where μ_s is the coefficient of static friction. In words, (3.10) means that the toe is not “pulling” the ground, while (3.11) corresponds to the toe not slipping on the ground. \triangleleft

In agreement with Hypothesis HGA6), transition from stance into flight can be initiated by causing the acceleration of the stance leg end to be positive, i.e., directed upwards, when the ground force becomes zero. As explained in [26, Section 4], if torque discontinuities

are allowed²—as they are assumed to be in this model—when to transition into the flight phase becomes a control decision. Therefore, liftoff is assumed to occur at predetermined configurations in the stance state space that correspond to the distance between the leg end and the torso COM be equal to a constant r_0 , which will be fixed in the control system design; see Remark 4.6 in Section 4.3. Consequently, the threshold function $H_{s \rightarrow f} : TQ_s \rightarrow \mathbb{R}$ is defined by

$$H_{s \rightarrow f}(x_s) := r_0 - \sqrt{L^2 + l^2 - 2Ll \sin \varphi}, \quad (3.12)$$

and its zeroing defines the stance-to-flight switching surface

$$\mathcal{S}_{s \rightarrow f} := \{x_s \in \mathcal{X}_s \mid H_{s \rightarrow f}(x_s) = 0\}. \quad (3.13)$$

Remark 3.3. Equation (3.12) is physically meaningful since $L^2 + l^2 - 2Ll \sin \varphi \geq (L-l)^2 \geq 0$. Moreover, if $l \neq L$ so that $L^2 + l^2 - 2Ll \sin \varphi \neq 0$, and if r_0 is selected so that $\mathcal{S}_{s \rightarrow f}$ is nonempty, then $\mathcal{S}_{s \rightarrow f}$ is a five-dimensional C^1 embedded submanifold of TQ_s . This is a result of the regular value theorem, see Theorem (5.8) [15, p. 78], since $H_{s \rightarrow f}$ is C^1 and $\partial H_{s \rightarrow f} / \partial x_s \neq 0$ on $H_{s \rightarrow f}^{-1}(\{0\}) = \mathcal{S}_{s \rightarrow f}$. These conditions are easily met on a physical model; see for example Table 4.1. \triangleleft

Remark 3.4. It is apparent from (3.12) that the stance-to-flight switching surface $\mathcal{S}_{s \rightarrow f}$ depends *only* on the stance states, and not on the parameters α_f . This fact will be important for proving exponential stability by using the theorems developed in [83] for systems with impulse effects in the presence of parameters. \triangleleft

3.4 ASLIP Flight-to-stance Transition Map

The ASLIP flight-to-stance transition map $\Delta_{f \rightarrow s} : \mathcal{S}_{f \rightarrow s} \rightarrow TQ_s$ corresponds to the coordinate transformation taking the exit (final) conditions of the flight phase to the entry (initial) conditions of the ensuing stance phase. Since, according to Hypothesis HGA5), no impact occurs at the transition from flight to stance, the total energy is conserved and $\Delta_{f \rightarrow s}$ is a volume preserving mapping. Furthermore, it is independent of the parameters

²This is a modeling issue. In practice, the torque is continuous due to actuator dynamics. It is assumed here that the actuator time constant is small enough that it need not be modeled.

α_f , despite the fact that it is defined on the surface $\mathcal{S}_{f \rightarrow s}$, which, as can be seen from (3.5), depends on α_f . The map $\Delta_{f \rightarrow s}$ is given by

$$\Delta_{f \rightarrow s}(x_f) = \begin{bmatrix} \sqrt{(L \cos \theta - x_{cm})^2 + (L \sin \theta - y_{cm})^2} \\ \arctan\left(\frac{L \cos \theta - x_{cm}}{y_{cm} - L \sin \theta}\right) - \theta \\ \theta \\ \begin{bmatrix} j_{11}^{-1} & j_{12}^{-1} & j_{13}^{-1} \\ j_{21}^{-1} & j_{22}^{-1} & j_{23}^{-1} \\ j_{31}^{-1} & j_{32}^{-1} & j_{33}^{-1} \end{bmatrix} \begin{bmatrix} \dot{x}_{cm} \\ \dot{y}_{cm} \\ \dot{\theta} \end{bmatrix} \end{bmatrix} \quad (3.14)$$

where

$$\begin{aligned} j_{11}^{-1} &= \frac{x_{cm} - L \cos \theta}{A(x_{cm}, y_{cm}, \theta)}, & j_{12}^{-1} &= \frac{y_{cm} - L \sin \theta}{A(x_{cm}, y_{cm}, \theta)}, \\ j_{13}^{-1} &= \frac{L x_{cm} \sin \theta - L y_{cm} \cos \theta}{A(x_{cm}, y_{cm}, \theta)}, \\ j_{21}^{-1} &= \frac{L \sin \theta - y_{cm}}{A^2(x_{cm}, y_{cm}, \theta)}, & j_{22}^{-1} &= \frac{x_{cm} - L \cos \theta}{A^2(x_{cm}, y_{cm}, \theta)}, \\ j_{23}^{-1} &= \frac{x_{cm}(L \cos \theta - x_{cm}) + y_{cm}(L \sin \theta - y_{cm})}{A^2(x_{cm}, y_{cm}, \theta)}, \\ j_{31}^{-1} &= 0, & j_{32}^{-1} &= 0, & j_{33}^{-1} &= 1, \end{aligned}$$

with

$$A(x_{cm}, y_{cm}, \theta) = \sqrt{(L \cos \theta - x_{cm})^2 + (L \sin \theta - y_{cm})^2}.$$

3.5 ASLIP Stance-to-flight Transition Map

The ASLIP stance-to-flight transition map $\Delta_{s \rightarrow f} : \mathcal{S}_{s \rightarrow f} \rightarrow TQ_f$ corresponds to the coordinate transformation taking the exit (final) conditions of the stance phase to the entry (initial) conditions of the ensuing flight phase. In the absence of any (internal) impacts, the

total energy is conserved so that $\Delta_{s \rightarrow f}$ is a volume preserving map, and is given by

$$\Delta_{s \rightarrow f}(x_s) = \begin{bmatrix} L \cos \theta - l \sin(\varphi + \theta) \\ L \sin \theta + l \cos(\varphi + \theta) \\ \theta \\ \begin{bmatrix} j_{11} & j_{12} & j_{13} \\ j_{21} & j_{22} & j_{23} \\ j_{31} & j_{32} & j_{33} \end{bmatrix} \begin{bmatrix} \dot{l} \\ \dot{\varphi} \\ \dot{\theta} \end{bmatrix} \end{bmatrix}, \quad (3.15)$$

where

$$j_{11} = -\sin(\varphi + \theta), \quad j_{12} = -l \cos(\varphi + \theta),$$

$$j_{13} = -l \cos(\varphi + \theta) - L \sin \theta,$$

$$j_{21} = \cos(\varphi + \theta), \quad j_{22} = -l \sin(\varphi + \theta),$$

$$j_{23} = -l \sin(\varphi + \theta) + L \cos \theta, ,$$

$$j_{31} = 0, \quad j_{32} = 0, \quad j_{33} = 1.$$

3.6 ASLIP Hybrid Dynamics of Running

The open-loop hybrid model of the ASLIP can be written as

$$\Sigma_f : \begin{cases} \mathcal{X}_f = TQ_f \times \mathcal{A}_f \\ (\dot{x}'_f, \dot{\alpha}'_f)' = (f'_f(x_f), 0)' \\ \mathcal{S}_{f \rightarrow s} = \{(x_f, \alpha_f) \in \mathcal{X}_f \mid H_{f \rightarrow s}(x_f, \alpha_f) = 0\} \\ x_s^+ = \Delta_{f \rightarrow s}(x_f^-) \end{cases} \quad (3.16)$$

$$\Sigma_s : \begin{cases} \mathcal{X}_s = TQ_s \\ \dot{x}_s = f_s(x_s) + g_s(x_s)u \\ \mathcal{S}_{s \rightarrow f} = \{x_s \in \mathcal{X}_s \mid H_{s \rightarrow f}(x_s) = 0\} \\ x_f^+ = \Delta_{s \rightarrow f}(x_s^-), \end{cases}$$

where $x_i^- = \lim_{\tau \nearrow t} x_i(\tau)$ and $x_i^+ = \lim_{\tau \searrow t} x_i(\tau)$, $i \in \{f, s\}$, are the left and right limits of the stance and flight solutions. The structure of the system is depicted in Fig. 3.2.

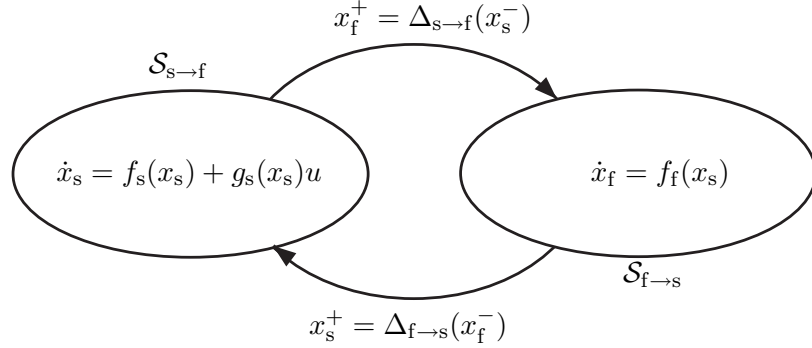


Figure 3.2: Representation of ASLIP's model in running as a hybrid system.

The subsystems Σ_f and Σ_s can be combined into a single system with “impulse” effects Σ^{ASLIP} describing the open-loop hybrid dynamics of the ASLIP; see [109, pp. 252-254], for a discussion of the related geometry. Let $\phi_f : [0, +\infty) \times TQ_f \rightarrow TQ_f$ denote the flow generated by the flight phase vector field f_f of (3.3). Note that the simplicity of f_f allows for explicit calculation of the flow ϕ_f . When the “augmented” flight flow (ϕ_f, α_f) intersects $\mathcal{S}_{f \rightarrow s}$, transition from flight to stance occurs. Define the time-to-touchdown function $T_f : \mathcal{X}_f \rightarrow \mathbb{R} \cup \{\infty\}$, as

$$T_f(x_{f,0}, \alpha_f) := \begin{cases} \inf \{t \in [0, +\infty) \mid (\phi_f(t, x_{f,0}), \alpha_f) \in \mathcal{S}_{f \rightarrow s}\}, \\ \text{if } \exists t \text{ such that } (\phi_f(t, x_{f,0}), \alpha_f) \in \mathcal{S}_{f \rightarrow s} \\ \infty, \text{ otherwise.} \end{cases} \quad (3.17)$$

The flow map³ $F_f : \mathcal{X}_f \rightarrow \mathcal{S}_{f \rightarrow s}$ for the (augmented) flight phase can then be given by the

³The definition of the flight flow map presupposes the existence of a time instant t such that $(\phi_f(t, x_{f,0}), \alpha_f) \in \mathcal{S}_{f \rightarrow s}$. The case where no such time instant exists does not correspond to periodic running motions.

rule $(x_{f,0}, \alpha_f) \mapsto (\phi_f(T_f(x_{f,0}, \alpha_f), x_{f,0}), \alpha_f) \in \mathcal{S}_{f \rightarrow s}$. Let $\Delta : \mathcal{S}_{s \rightarrow f} \times \mathcal{A}_f \rightarrow \mathcal{X}_s$ be the map

$$\Delta(x_s^-, \alpha_f) := \Delta_{f \rightarrow s} [F_f(\Delta_{s \rightarrow f}(x_s^-), \alpha_f)]. \quad (3.18)$$

The map Δ “compresses” the flight phase into an “event,” and can be thought of as a (generalized) “impact map” [26], or a “reset map” [10]. It should be emphasized here that the overall reset map Δ defined by (3.18) depends explicitly on the parameters α_f despite the fact that both transition maps $\Delta_{f \rightarrow s}$ and $\Delta_{s \rightarrow f}$ are independent of α_f ; this dependence arises from the flight flow map F_f defined above. In this setting, the hybrid dynamics of the ASLIP becomes

$$\Sigma^{\text{ASLIP}} : \begin{cases} \dot{x}_s = f_s(x_s) + g_s(x_s)u, & x_s^- \notin \mathcal{S}_{s \rightarrow f} \\ x_s^+ = \Delta(x_s^-, \alpha_f), & x_s^- \in \mathcal{S}_{s \rightarrow f}, \alpha_f \in \mathcal{A}_f. \end{cases} \quad (3.19)$$

The left and right limits x_s^- and x_s^+ correspond to the states “just prior to liftoff” and “just after touchdown,” respectively. Note also that in (3.19), *only* the argument $x_s^- \in \mathcal{S}_{s \rightarrow f}$ triggers liftoff; the surface $\mathcal{S}_{s \rightarrow f}$ does not depend on the parameters α_f , which affect the initial conditions of the continuous part of (3.19). The system Σ^{ASLIP} has the typical form of a system with impulse effects, i.e., it is defined on a single chart \mathcal{X}_s , where the states evolve, together with the map Δ , which reinitializes the differential equation at liftoff; see [113], [48] and [109] for general treatments of impulsive and hybrid dynamical systems.

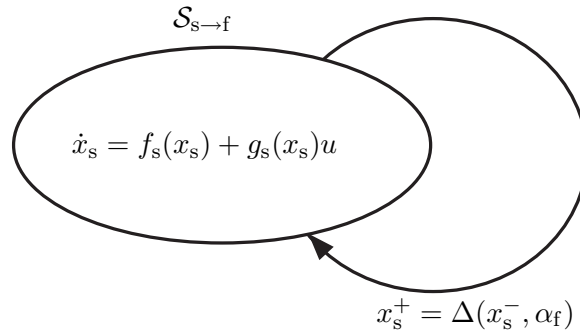


Figure 3.3: Representation of ASLIP’s model as a system with “impulse” effects.

CHAPTER IV

Controlling the ASLIP: SLIP-embedding and Rigid Target Model Controllers

This chapter is devoted to the development of control laws for running motions in the ASLIP, whose model was derived in Chapter III. A framework is proposed that combines established nonlinear controller synthesis tools, such as the Hybrid Zero Dynamics (HZD), with control laws obtained in the context of the SLIP to induce exponentially stable running motions on the ASLIP. A second aspect addressed in this chapter regards the performance benefits of designing the HZD to be a compliant system. These observations motivate the development of Thumper's *compliant hybrid zero dynamics* controllers, which will be detailed in Chapter VI.

The structure of this chapter is as follows. In Section 4.1, the general framework within which the controllers are developed is outlined. Following these general guidelines, two feedback controllers are proposed in Sections 4.3 and 4.4, and Section 4.5. In each case, feedback is used to create a lower-dimensional hybrid subsystem that determines the closed-loop behavior of the ASLIP. The first controller developed in Sections 4.3 and 4.4 creates a two-degree-of-freedom subsystem that is rendered *diffeomorphic* to an energy-stabilized variant of the standard SLIP, which is described in Section 4.2; this controller is referred to as the *SLIP-embedding controller*. Section 4.5 discusses the second controller, which creates a one degree-of-freedom *non-compliant* subsystem; this controller is referred to as the *rigid target model controller*. Finally, Section 4.6 highlights the fundamental differences in the two control designs, illustrating the benefits of designing the HZD so that it

accommodates compliance, such as in the SLIP embedding controller.

4.1 Overview of the Control Law

Generally speaking, the purpose of the feedback law is to coordinate the actuated degrees of freedom of the ASLIP so that a lower-dimensional hybrid subsystem “emerges” from the closed-loop ASLIP dynamics; this lower-dimensional dynamical subsystem serves as a target for the control of the ASLIP and governs its asymptotic behavior. This statement will be made mathematically precise in the following sections. In this section, only the general guidelines of the controller design are briefly described.

The feedback law exploits the hybrid nature of the system by introducing control action on two levels; see Fig. 4.1. On the first level, a continuous-time feedback law Γ_c is employed in the stance phase with the purpose of creating an invariant and attractive submanifold \mathcal{Z} embedded in the stance state space, on which the closed-loop dynamics have desired properties. On the second level, event-based updates of controller parameters are performed at transitions from stance to flight. Generally, the event-based parameter update law is organized in an inner/outer-loop architecture, with the inner-loop controller Γ_s intended to render the surface \mathcal{Z} invariant under the reset map. This condition is referred to as *hybrid invariance*, and it leads to the creation of a reduced-order hybrid subsystem called the *Hybrid Zero Dynamics* (HZD), which governs the stability properties of the full-order ASLIP; see [110] for details. In cases where the in-stride controller Γ_c achieves hybrid invariance, Γ_s is not needed and may be excluded from the controller design; Section 4.3 presents one such example. Finally, the outer-loop controller Γ_f completes the control design by ensuring that the resulting HZD is exponentially stable.

In Sections 4.3 and 4.4, and in Section 4.5 we particularize these ideas through explicit constructions of two sets of feedback laws Γ_c , Γ_s and Γ_f that achieve the control objectives. In Sections 4.3 and 4.4 the objective is to coordinate the actuated DOFs of the ASLIP so that the compliant SLIP emerges as the HZD; this controller is referred to as the *SLIP embedding controller*. In Section 4.5, the objective is to impose suitably parameterized virtual holo- nomic constraints on the ASLIP so that an one-DOF mechanical system arises as its HZD;

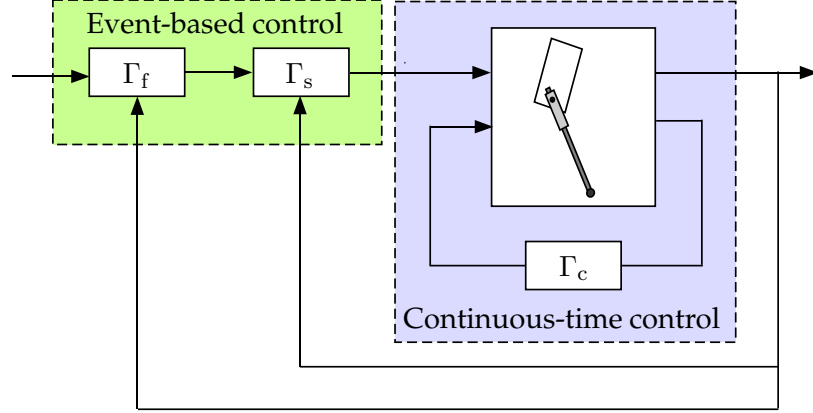


Figure 4.1: Feedback diagram presenting the basic structure of the ASLIP controllers.

because, in this case, the resulting HZD *cannot* be compliant, we refer to this controller as the *rigid target model controller*. Fundamental differences in the two control laws are highlighted in Section 4.6, illustrating the benefits of designing the HZD to accommodate compliance, such as in the SLIP embedding controller.

4.1.1 In-stride Continuous Control

To the continuous part of (3.19), associate the output

$$y = h(q_s, \alpha_s), \quad (4.1)$$

which depends on the configuration variables q_s , and on a set of parameters $\alpha_s \in \mathcal{A}_s$, which remain constant during the stance phase, i.e. $\dot{\alpha}_s = 0$. These parameters can be the coefficients of polynomials representing a set of virtual constraints as in the rigid target model controller, or the mechanical properties of a target model as in the SLIP embedding controller.

Given a set of values for the parameters α_s , differentiating (4.1) twice with respect to time results in

$$\frac{d^2 y}{dt^2} = L_{f_s}^2 h(q_s, \alpha_s) + L_{g_s} L_{f_s} h(q_s, \alpha_s) u, \quad (4.2)$$

where $L_{g_s} L_{f_s} h(q_s, \alpha_s)$ is the decoupling matrix. Under the condition that $L_{g_s} L_{f_s} h(q_s, \alpha_s)$ is

invertible,

$$u^*(x_s, \alpha_s) := - (L_{g_s} L_{f_s} h(q_s, \alpha_s))^{-1} L_{f_s}^2 h(x_s, \alpha_s) \quad (4.3)$$

is the unique control input that renders the surface

$$\mathcal{Z}_{\alpha_s} := \{x_s \in TQ_s \mid h(q_s, \alpha_s) = 0, L_{f_s} h(x_s, \alpha_s) = 0\} \quad (4.4)$$

invariant under the flow of the continuous part of the ASLIP dynamics (3.19), that is, for every $x \in \mathcal{Z}_{\alpha_s}$,

$$f^*(x, \alpha_s) = f_s(x) + g_s(x)u^*(x_s, \alpha_s) \in T_x \mathcal{Z}_{\alpha_s}. \quad (4.5)$$

Following standard terminology, the surface \mathcal{Z}_{α_s} is the stance phase zero dynamics manifold, and

$$\dot{z} = f^*|_{\mathcal{Z}_{\alpha_s}}(z, \alpha_s) \quad (4.6)$$

is the stance phase zero dynamics.

To establish *attractivity* of \mathcal{Z}_{α_s} , the input (4.3) is modified as

$$\begin{aligned} u &= \Gamma_c^\epsilon(x_s, \alpha_s) \\ &:= (L_{g_s} L_{f_s} h(q_s, \alpha_s))^{-1} [v^\epsilon(y, \dot{y}) - L_{f_s}^2 h(x_s, \alpha_s)], \end{aligned} \quad (4.7)$$

where

$$v^\epsilon(y, \dot{y}) := -\frac{1}{\epsilon^2} K_P^y y - \frac{1}{\epsilon} K_V^y \dot{y}, \quad (4.8)$$

and K_P^y and K_V^y are appropriately chosen gain matrices, and $\epsilon > 0$. Under the feedback law Γ_c^ϵ , the hybrid system (3.19) takes the form

$$\Sigma_{\text{cl}}^{\text{ASLIP}} : \begin{cases} \dot{x}_s = f_{s,\text{cl}}^\epsilon(x_s, \alpha_s), & x_s^- \in \mathcal{S}_{s \rightarrow f}, \alpha_s \in \mathcal{A}_s \\ x_s^+ = \Delta(x_s^-, \alpha_f), & x_s^- \in \mathcal{S}_{s \rightarrow f}, \alpha_f \in \mathcal{A}_f \end{cases}, \quad (4.9)$$

where the stance-to-flight switching surface has been defined in (3.13), and

$$f_{s,\text{cl}}^\epsilon(x_s, \alpha_s) := f_s(x_s) + g_s(x_s)\Gamma_c^\epsilon(x_s, \alpha_s). \quad (4.10)$$

4.1.2 Event-based Discrete Control

A key implication of the hybrid nature of (4.9) combined with the (trivial) dynamics $\dot{\alpha}_s = 0$ and $\dot{\alpha}_f = 0$ governing the parameters in (4.9), is the possibility of updating α_s and α_f in an event-based manner. More specifically, at each crossing of the surface $\mathcal{S}_{s \rightarrow f}$, α_s and α_f can be updated based on feedback of the liftoff state $x_s^- \in \mathcal{S}_{s \rightarrow f}$, i.e.,

$$\alpha_f = \Gamma_f(x_s^-), \quad (4.11)$$

$$\alpha_s^+ = \Gamma_s(x_s^-, \Gamma_f(x_s^-)), \quad (4.12)$$

with the purpose of the feedback laws Γ_s and Γ_f being to extend the notion of invariance in the hybrid setting, and to ensure stability of the resulting HZD. Loosely speaking, (4.11) introduces control authority over the initial conditions of the continuous part of (4.9). On the other hand, (4.12) allows for “real-time” motion planning in stance via updating α_s .

To ensure hybrid invariance, the inner-loop controller Γ_s is designed to provide updated values α_s^+ of the stance parameters so that the following conditions are satisfied, [83]:

- (i) the surface $\mathcal{S}_{s \rightarrow f} \cap \mathcal{Z}_{\alpha_s}$ is the same as $\mathcal{S}_{s \rightarrow f} \cap \mathcal{Z}_{\alpha_s^+}$; denote $\mathcal{S}_{s \rightarrow f} \cap \mathcal{Z}_{\alpha_s}$ by $\mathcal{S}_{s \rightarrow f} \cap \mathcal{Z}_\circ$,
- (ii) $\mathcal{S}_{s \rightarrow f} \cap \mathcal{Z}_\circ$ is invariant under the reset map Δ , i.e., $\Delta((\mathcal{S}_{s \rightarrow f} \cap \mathcal{Z}_\circ) \times \mathcal{A}_f) \subset \mathcal{Z}_{\alpha_s^+}$.

In words, (i) means that liftoff occurs where it would have occurred without updating α_s . Enforcing (i) and (ii) through the parameter update law Γ_s results in the creation of a well-defined lower-dimensional *hybrid* subsystem, the HZD, which has the form

$$\Sigma^{\text{HZD}} : \begin{cases} \begin{bmatrix} \dot{z} \\ \dot{\alpha}_s \end{bmatrix} = \begin{bmatrix} f^*|_{\mathcal{Z}_{\alpha_s}}(z, \alpha_s) \\ 0 \end{bmatrix}, & z^- \notin \mathcal{S}_{s \rightarrow f} \cap \mathcal{Z}_\circ \\ \begin{bmatrix} z^+ \\ \alpha_s^+ \end{bmatrix} = \begin{bmatrix} \Delta|_{\mathcal{S}_{s \rightarrow f} \cap \mathcal{Z}_\circ}(z^-, \alpha_f) \\ \Gamma_s|_{\mathcal{S}_{s \rightarrow f} \cap \mathcal{Z}_\circ}(z^-, \alpha_f) \end{bmatrix}, & z^- \in \mathcal{S}_{s \rightarrow f} \cap \mathcal{Z}_\circ \end{cases}, \quad (4.13)$$

A critical aspect of the resulting HZD is the dependence of the (extended) reset map on α_f , which can be selected according to the outer-loop feedback law Γ_f of Fig. 4.1, intended

to achieve exponential stability. It is mentioned here that one way of designing Γ_f is by using discrete LQR techniques. An alternative is to use a modification of Raibert’s forward speed controller. Both methods are explored in the following sections.

4.2 Target Model: The Energy-Stabilized SLIP

In this section, the target model for the SLIP embedding controller is introduced. The standard SLIP consists of a point mass attached to a massless prismatic spring, and it is passive and conservative¹, thus precluding the existence of exponentially stable periodic orbits; see [8], [42]. In this thesis, we consider a variant of the SLIP, where the leg force is allowed to be non-conservative. The purpose of this modification is to introduce control authority over the total energy, which is no more conserved as in the standard SLIP, thus leading to the existence of exponentially stable periodic orbits. This system, called the Energy-Stabilized SLIP (ES-SLIP), is presented in Fig. 4.2.

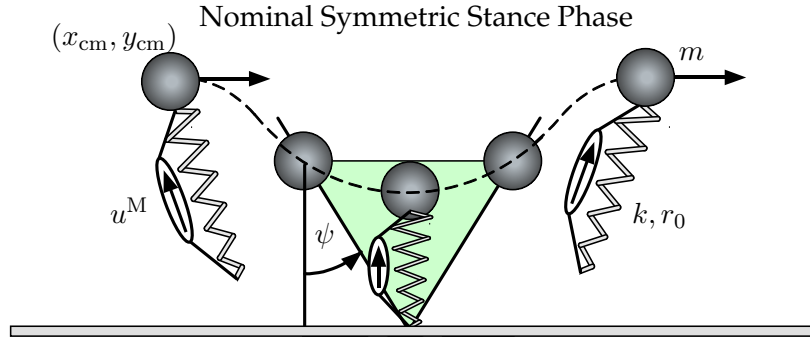


Figure 4.2: The Energy-Stabilized SLIP (ES-SLIP), with a prismatic actuator (force source) in parallel with the spring.

The derivation of the hybrid model for the ES-SLIP is similar to that of the ASLIP, thus the exposition in this section will be terse. Moreover, only the closed-loop hybrid dynamics of the ES-SLIP will be presented. In what follows, the superscript “M” denotes the ES-SLIP target model. The flight and stance configuration spaces Q_f^M and Q_s^M , respectively, will both be parameterized by the Cartesian coordinates of the COM $(x_{cm}, y_{cm}) \in Q_f^M = Q_s^M =: Q^M$ a simply-connected open subset of $\{(x_{cm}, y_{cm}) \in \mathbb{R}^2 \setminus \{(0, 0)\} \mid y_{cm} > 0\}$. Hence,

¹The SLIP has no actuator inputs and experiences no energy losses.

the system dynamics evolves in the state space

$$\mathcal{X}^M := TQ^M = \{x^M = \text{col}(q^M, \dot{q}^M) \mid q^M \in Q^M, \dot{q}^M \in \mathbb{R}^2\}.$$

In order to accommodate perturbations away from the nominal energy, the conservative force F_{el} developed by the springy leg of the standard SLIP is modified to include a nonconservative feedback component $u^M = \Gamma_c^M(x^M)$. The purpose of u^M is to stabilize the total energy of the system at a desired nominal level \bar{E} , and is achieved by

$$\Gamma_c^M(x^M) := -K_P^E \frac{x_{\text{cm}}\dot{x}_{\text{cm}} + y_{\text{cm}}\dot{y}_{\text{cm}}}{\sqrt{x_{\text{cm}}^2 + y_{\text{cm}}^2}} [E(x^M) - \bar{E}], \quad (4.14)$$

where $E(x^M)$ is the total energy, and K_P^E is a positive gain.

To regulate the forward speed, the following event-based control law is employed

$$\psi = \Gamma_f^M((x^M)^-) := \bar{\psi} + K_{\dot{x}}(\dot{x}_{\text{cm}}^- - \dot{\bar{x}}_{\text{cm}}); \quad (4.15)$$

$\bar{\psi}$ and $\dot{\bar{x}}_{\text{cm}}$ specify the nominal touchdown angle and forward speed, respectively, \dot{x}_{cm}^- is the actual forward speed just prior to liftoff, and $K_{\dot{x}}$ is a positive gain. It can be recognized that (4.15) corresponds to a variation of Raibert's speed controller; see [91, pp. 44–47].

Under the influence of the feedback laws (4.14) and (4.15), the closed-loop ES-SLIP hybrid dynamics can be obtained as

$$\Sigma_{\text{cl}}^M : \begin{cases} \dot{x}^M = f_{\text{s,cl}}^M(x^M), & (x^M)^- \notin \mathcal{S}_{\text{s} \rightarrow \text{f}}^M \\ (x^M)^+ = \Delta_{\text{cl}}^M((x^M)^-), & (x^M)^- \in \mathcal{S}_{\text{s} \rightarrow \text{f}}^M \end{cases}, \quad (4.16)$$

where $f_{\text{s,cl}}^M(x^M)$ is the closed-loop stance vector field, which is given below for future use,

$$f_{\text{s,cl}}^M(x^M) = \begin{bmatrix} \dot{x}_{\text{cm}} \\ \dot{y}_{\text{cm}} \\ \frac{1}{m} \frac{x_{\text{cm}}}{\sqrt{x_{\text{cm}}^2 + y_{\text{cm}}^2}} (F_{\text{el}} + \Gamma_c^M(x^M)) \\ \frac{1}{m} \frac{y_{\text{cm}}}{\sqrt{x_{\text{cm}}^2 + y_{\text{cm}}^2}} (F_{\text{el}} + \Gamma_c^M(x^M)) - g \end{bmatrix}; \quad (4.17)$$

F_{el} is the elastic force developed by the prismatic spring of the leg, which is assumed to be generated by a radial potential $\mathcal{V}_{\text{el}}^{\text{M}}(r(x_{\text{cm}}, y_{\text{cm}}))$ with $r(x_{\text{cm}}, y_{\text{cm}}) = \sqrt{x_{\text{cm}}^2 + y_{\text{cm}}^2}$ as

$$F_{\text{el}} = \frac{d\mathcal{V}_{\text{el}}^{\text{M}}(r)}{dr} \Big|_{r=\sqrt{x_{\text{cm}}^2 + y_{\text{cm}}^2}}. \quad (4.18)$$

Assuming, for definiteness, that the spring is linear gives

$$F_{\text{el}} = k \left(r_0 + \Delta r - \sqrt{x_{\text{cm}}^2 + y_{\text{cm}}^2} \right); \quad (4.19)$$

k is the spring constant, r_0 the nominal leg length (determining touchdown), and Δr a (constant) pretention; see Fig. 4.2.

In (4.16), the switching surface

$$\mathcal{S}_{\text{s} \rightarrow \text{f}}^{\text{M}} := \{x^{\text{M}} \in \mathcal{X}^{\text{M}} \mid H_{\text{s} \rightarrow \text{f}}^{\text{M}}(x^{\text{M}}) = 0\}, \quad (4.20)$$

where

$$H_{\text{s} \rightarrow \text{f}}^{\text{M}}(x^{\text{M}}) := r_0 - \sqrt{x_{\text{cm}}^2 + y_{\text{cm}}^2}, \quad (4.21)$$

is a three-dimensional C^1 embedded submanifold of \mathcal{X}^{M} , for reasons similar to those mentioned in Remark 3.3. Finally, the closed-loop reset map $\Delta_{\text{cl}}^{\text{M}} : \mathcal{S}_{\text{s} \rightarrow \text{f}}^{\text{M}} \rightarrow \mathcal{X}^{\text{M}}$ in (4.16) is defined by²

$$\Delta_{\text{cl}}^{\text{M}} := \Delta_{\text{f} \rightarrow \text{s}}^{\text{M}} \circ F_{\text{f}}^{\text{M}} \circ (\Delta_{\text{s} \rightarrow \text{f}}^{\text{M}} \times \Gamma_{\text{f}}^{\text{M}}), \quad (4.22)$$

where $\Delta_{\text{s} \rightarrow \text{f}}^{\text{M}} : \mathcal{S}_{\text{s} \rightarrow \text{f}}^{\text{M}} \rightarrow \mathcal{X}^{\text{M}}$ and $\Delta_{\text{f} \rightarrow \text{s}}^{\text{M}} : \mathcal{S}_{\text{f} \rightarrow \text{s}}^{\text{M}} \rightarrow \mathcal{X}^{\text{M}}$ are the ES-SLIP stance-to-flight and flight-to-stance transition maps, respectively. Due to the fact that both the flight and stance state spaces are parameterized by the same coordinates, the transition maps simply correspond to the identity map on \mathcal{X}^{M} , i.e. $\Delta_{\text{s} \rightarrow \text{f}}^{\text{M}} = \Delta_{\text{f} \rightarrow \text{s}}^{\text{M}} = \text{id}_{\mathcal{X}^{\text{M}}}$. In (4.22), $F_{\text{f}}^{\text{M}} : \mathcal{X}^{\text{M}} \times \mathcal{A}_{\text{f}}^{\text{M}} \rightarrow \mathcal{S}_{\text{s} \rightarrow \text{f}}^{\text{M}}$ is the ES-SLIP flight flow map, defined analogously with the ASLIP flight flow map; $\mathcal{A}_{\text{f}}^{\text{M}}$ is an open subset of \mathbb{S}^1 , containing physically reasonable values for the touchdown angle ψ .

²Notation: Let $f_1 : \mathcal{X} \rightarrow \mathcal{Y}_1$ and $f_2 : \mathcal{X} \rightarrow \mathcal{Y}_2$, and define $f_1 \times f_2 : \mathcal{X} \rightarrow \mathcal{Y}_1 \times \mathcal{Y}_2$ by $(f_1 \times f_2)(x) = (f_1(x), f_2(x))$, $x \in \mathcal{X}$.

Remark 4.1. To explain (4.20) and (4.21), the liftoff condition is assumed to occur when the leg length obtains a particular value, namely r_0 , as is the case for the conservative SLIP. \triangleleft

In order to study the stability properties of periodic orbits of Σ_{cl}^M , the method of Poincaré is used. The Poincaré section is selected to be the surface $\mathcal{S}_{s \rightarrow f}^M$ defined by (4.20). Let $\phi_{s,cl}^M : [0, +\infty) \times \mathcal{X}^M \rightarrow \mathcal{X}^M$ be the flow generated by $f_{s,cl}^M$, and define the time-to-liftoff function $T_s^M : \mathcal{X}^M \rightarrow \mathbb{R} \cup \{\infty\}$, in a similar fashion as (3.17), by

$$T_s^M(x_0^M) := \begin{cases} \inf \left\{ t \in [0, +\infty) \mid \phi_{s,cl}^M(t, x_0^M) \in \mathcal{S}_{s \rightarrow f}^M \right\}, \\ \text{if } \exists t \text{ such that } \phi_{s,cl}^M(t, x_0^M) \in \mathcal{S}_{s \rightarrow f}^M \\ \infty, \text{ otherwise.} \end{cases} \quad (4.23)$$

Then, the Poincaré map $\mathcal{P}^M : \mathcal{S}_{s \rightarrow f}^M \rightarrow \mathcal{S}_{s \rightarrow f}^M$ is defined by

$$\mathcal{P}^M := \phi_{s,cl}^M \circ [(T_s^M \circ \Delta_{cl}^M) \times \Delta_{cl}^M]. \quad (4.24)$$

Remark 4.2. Feedback control laws similar to (4.14) and (4.15) exist in the literature; the particular ones used here are for illustrative purposes only. It is emphasized that many other in-stride or event-based controllers could have been used to stabilize the SLIP. For instance, energy stabilization in nonconservative monopodal models has been demonstrated using linear (leg) and rotational (hip) actuation in [3] and [23], respectively. On the other hand, a large variety of event-based controllers exist for the SLIP, e.g., [8], [91], [100], [105], which are known to have very appealing properties. In the following section, we develop rigorously a controller for the ASLIP that affords the direct use of control laws available for the SLIP. \triangleleft

4.3 Main Result: The SLIP Embedding Controller

As was mentioned in Section 4.1, the control action takes place on two hierarchical levels. On the first level, continuous in-stride control is exerted during the stance phase to stabilize the torso at a desired posture, and to create an invariant manifold on which the ES-SLIP dynamics can be imposed. On the second level, an event-based SLIP controller

is used to stabilize a periodic orbit of the system. These results are summarized in the following theorem and corollary.

Theorem 4.3 (SLIP embedding controller). *Let $\hat{Q}_s := \{q_s \in Q_s \mid l \neq L \sin \varphi\}$. Then, for every $\epsilon > 0$, there exists a C^1 in-stride (continuous) control law $u = \Gamma_c^\epsilon(x_s)$, and a C^1 event-based (discrete) control law $\alpha_f = \Gamma_f(x_s^-)$ such that the following hold:*

A. In-stride Continuous Control

There exists a map $\Phi : T\hat{Q}_s \rightarrow \mathbb{R}^6$ that is a diffeomorphism onto its image, and such that, in coordinates $x = (\eta', z) := \Phi(x_s) \in \mathbb{R}^6$, the closed-loop model

$$f_{s,\text{cl}}^\epsilon(x_s) := f_s(x_s) + g_s(x_s)\Gamma_c^\epsilon(x_s) \quad (4.25)$$

satisfies:

A.1) the vector field

$$\tilde{f}_{s,\text{cl}}^\epsilon(x) := \left(\frac{\partial \Phi}{\partial x_s} f_{s,\text{cl}}^\epsilon(x_s) \right) \Big|_{x_s = \Phi^{-1}(x)} \quad (4.26)$$

has the form

$$\tilde{f}_{s,\text{cl}}^\epsilon(x) = \begin{bmatrix} \tilde{f}_{s,\text{cl},1:2}^\epsilon(\eta) \\ \tilde{f}_{s,\text{cl},3:6}^\epsilon(\eta, z) \end{bmatrix}; \quad (4.27)$$

A.2) the set $\mathcal{Z} := \{x \in \mathbb{R}^6 \mid \eta = 0\}$ is a smooth four-dimensional C^1 embedded submanifold of \mathbb{R}^6 that is invariant under the stance flow, i.e. $x \in \mathcal{Z}$ implies $\tilde{f}_{s,\text{cl}}^\epsilon(x) \in T_x \mathcal{Z}$, and the set $\mathcal{S}_{s \rightarrow f} \cap \mathcal{Z}$, where $\mathcal{S}_{s \rightarrow f}$ is given by (3.13), is a co-dimension one C^1 submanifold of \mathcal{Z} ;

A.3) the transverse dynamics $\tilde{f}_{s,\text{cl},1:2}^\epsilon(\eta)$ takes the form

$$\tilde{f}_{s,\text{cl},1:2}^\epsilon(\eta) = A(\epsilon) \eta, \quad (4.28)$$

and it exponentially contracts as $\epsilon \rightarrow 0$, i.e. $\lim_{\epsilon \searrow 0} e^{A(\epsilon)} = 0$;

A.4) the restriction dynamics

$$\tilde{f}_{s,\text{cl}}^\epsilon(x)|_{\mathcal{Z}} = \tilde{f}_{s,\text{cl},3:6}^\epsilon(0, z) \quad (4.29)$$

is diffeomorphic to the ES-SLIP stance phase closed-loop dynamics $f_{s,\text{cl}}^M$ given by (4.17).

B. Event-based Discrete Control

The closed-loop reset map $\Delta_{\text{cl}} : \mathcal{S}_{\text{s} \rightarrow \text{f}} \rightarrow T\hat{Q}_{\text{s}}$ defined by

$$\Delta_{\text{cl}} = \Delta_{\text{f} \rightarrow \text{s}} \circ F_{\text{f}} \circ (\Delta_{\text{s} \rightarrow \text{f}} \times \Gamma_{\text{f}}), \quad (4.30)$$

where the maps $\Delta_{\text{f} \rightarrow \text{s}}$, $\Delta_{\text{s} \rightarrow \text{f}}$ and F_{f} have been defined in Sections 3.4, 3.5 and 3.6, satisfies

B.1) $\Delta_{\text{cl}}(\mathcal{S}_{\text{s} \rightarrow \text{f}} \cap \mathcal{Z}) \subset \mathcal{Z}$, i.e. $\mathcal{S}_{\text{s} \rightarrow \text{f}} \cap \mathcal{Z}$ is hybrid invariant;

B.2) the restricted reset map $\Delta_{\text{cl}}|_{\mathcal{Z}}$ is diffeomorphic to the ES-SLIP closed-loop reset map $\Delta_{\text{cl}}^{\text{M}}$ defined by (4.22).

For $\epsilon > 0$ a given constant, the closed-loop hybrid dynamics of the ASLIP under the continuous and event-based feedback control laws of Theorem 4.3 takes the form

$$\Sigma_{\text{cl}}^{\text{ASLIP}} : \begin{cases} \dot{x} = \tilde{f}_{\text{s,cl}}^{\epsilon}(x), & x^- \notin \mathcal{S}_{\text{s} \rightarrow \text{f}} \\ x^+ = \tilde{\Delta}_{\text{cl}}(x^-), & x^- \in \mathcal{S}_{\text{s} \rightarrow \text{f}} \end{cases}, \quad (4.31)$$

where $\mathcal{S}_{\text{s} \rightarrow \text{f}}$ was defined in (3.13), and $\tilde{\Delta}_{\text{cl}} := \Phi \circ \Delta_{\text{cl}} \circ \Phi^{-1}$ is the representation of the closed-loop reset map in the x -coordinates. The stability properties of $\Sigma_{\text{cl}}^{\text{ASLIP}}$ will be studied via the corresponding Poincaré return map $\mathcal{P}^{\epsilon} : \mathcal{S}_{\text{s} \rightarrow \text{f}} \rightarrow \mathcal{S}_{\text{s} \rightarrow \text{f}}$, which is defined analogously to \mathcal{P}^{M} of Section 4.2; see (4.24). As is described in detail in [82], the structure imposed on the ASLIP by the feedback laws of Theorem 4.3 results in the map $\mathcal{P}^{\epsilon}|_{\mathcal{Z}} : \mathcal{S}_{\text{s} \rightarrow \text{f}} \cap \mathcal{Z} \rightarrow \mathcal{S}_{\text{s} \rightarrow \text{f}} \cap \mathcal{Z}$ being independent of ϵ and $\mathcal{P}^{\epsilon}|_{\mathcal{Z}} \cong \mathcal{P}^{\text{M}}$, i.e. the restricted Poincaré map is well defined and is diffeomorphic to the ES-SLIP Poincaré map. The following corollary is an immediate consequence of Theorem 4.3 in view of the results in [82].

Corollary 4.4 (Exponential Stability of $\Sigma_{\text{cl}}^{\text{ASLIP}}$). *Let $(x^{\text{M}})^*$ be a fixed point of \mathcal{P}^{M} and x^* a fixed point of \mathcal{P}^{ϵ} . There exist $\bar{\epsilon} > 0$ such that, for all $\epsilon \in (0, \bar{\epsilon})$, x^* is exponentially stable, if, and only if, $(x^{\text{M}})^*$ is exponentially stable.*

Before continuing with the proof of Theorem 4.3, which will be given in Section 4.4, a few remarks are in order.

Remark 4.5. The conditions $l \neq L$ of Remark 3.3 and $l \neq L \sin \varphi$ of Theorem 4.3 are both satisfied whenever $l > L$, which is the case of most upright runners. \triangleleft

Remark 4.6. Intuitively, the definition of $\mathcal{S}_{s \rightarrow f}$ as in Theorem 4.3, that is, by (3.13), means that liftoff occurs when the distance between the foot and the COM becomes equal to the nominal length of the ES-SLIP leg, r_0 ; see also Remark 4.1. \triangleleft

Remark 4.7. To help develop some intuition on Theorem 4.3, it is noted that the two-dimensional state vector η corresponds to the output dynamics; in particular, it corresponds to the pitch error dynamics. The four-dimensional state vector z is suitable for describing the associated zero dynamics. The theorem provides conditions under which, for sufficiently fast exponentially contracting pitch error dynamics, an exponentially stable periodic orbit of the *restriction dynamics* is also an exponentially stable orbit of the ASLIP. Furthermore, the restriction dynamics, which corresponds to the translational dynamics of the COM of the ASLIP, is rendered diffeomorphic to the ES-SLIP dynamics. Intuitively, the feedback laws of Theorem 4.3 “coordinate” the actuated degrees of freedom of the ASLIP so that a lower-dimensional subsystem, more specifically the ES-SLIP, “emerges” from the closed-loop dynamics, and it governs the behavior —i.e. the existence and stability properties of periodic orbits of interest— of the full-order ASLIP. \triangleleft

Remark 4.8. The importance of Corollary 4.4 is that, for given controllers that create an exponentially stable periodic orbit of the ES-SLIP, the feedback laws $u = \Gamma_c^\epsilon(x_s)$ and $\alpha_f = \Gamma_f(x_s^-)$ of Theorem 4.3 render this orbit exponentially stable in the ASLIP. \triangleleft

4.4 Proof of the SLIP Embedding Theorem

In this section, Theorem 4.3 is proved through a sequence of lemmas. The procedure is constructive, and results in a control law satisfying the requirements of Theorem 4.3. Figure 4.3 summarizes the continuous-time control action during the ASLIP stance phase, whose objective is to render the translational dynamics of the ASLIP COM diffeomorphic to the ES-SLIP dynamics.

4.4.1 In-stride Continuous Control

The purpose of the in-stride control action during the stance phase is twofold. First, it ensures that the torso remains at a desired (constant and upright) pitch angle, and second,

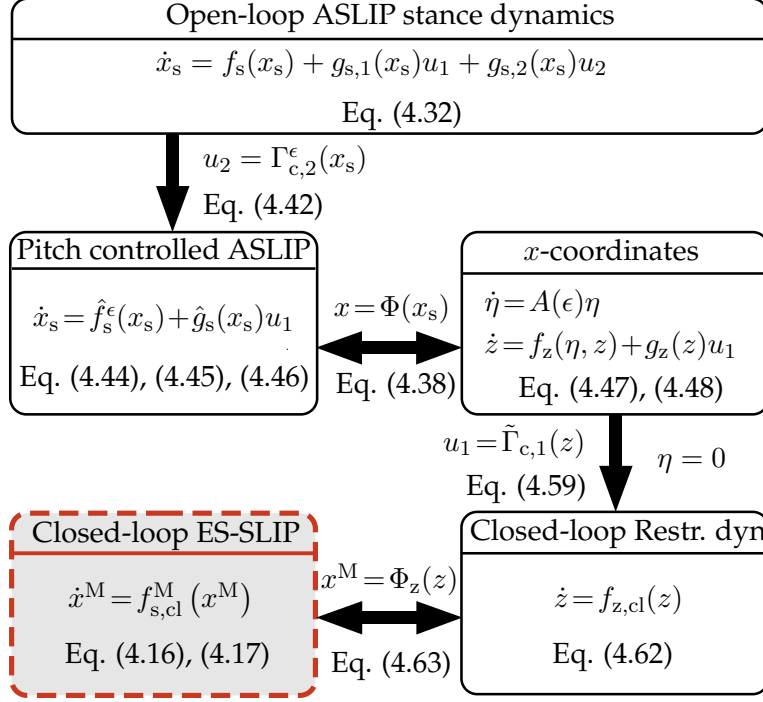


Figure 4.3: A diagram summarizing the control procedure through which the ASLIP restriction dynamics is rendered diffeomorphic to the ES-SLIP closed-loop dynamics. Vertical arrows correspond to control actions; horizontal arrows relate diffeomorphic dynamics. The dashed box includes the ES-SLIP closed-loop target dynamics. Equation numbers refer to the text.

it renders the translational stance dynamics of the ASLIP diffeomorphic to the ES-SLIP closed-loop stance dynamics. In view of the underactuated nature of the stance phase, the two control objectives will be achieved in different time scales. Since the requirement for the torso being upright throughout the motion is more stringent, high-gain control will be imposed on the pitch rotational motion. Hence, the system will be decomposed into fast and slow dynamics governing the rotational and the translational dynamics of the torso, respectively.

The continuous part of Σ^{ASLIP} in (3.19), can be written as

$$\dot{x}_s = f_s(x_s) + g_{s,1}(x_s)u_1 + g_{s,2}(x_s)u_2. \quad (4.32)$$

Define the output $h : \hat{Q}_s \rightarrow \mathbb{R}$ by

$$y := h(q_s) := \theta - \bar{\theta}, \quad (4.33)$$

where $\bar{\theta}$ is a desired pitch angle, taken to be a constant³. The output defined by (4.33) results in the second-order input-output dynamics

$$\frac{d^2y}{dt^2} = [L_{f_s}^2 h(x_s) + L_{g_{s,1}} L_{f_s} h(q_s) u_1] + L_{g_{s,2}} L_{f_s} h(q_s) u_2, \quad (4.34)$$

where

$$\begin{aligned} L_{f_s}^2 h(x_s) &= 0, \\ L_{g_{s,1}} L_{f_s} h(q_s) &= \frac{-L \cos \varphi}{J}, \quad L_{g_{s,2}} L_{f_s} h(q_s) = \frac{L \sin \varphi - l}{Jl}. \end{aligned} \quad (4.35)$$

Equation (4.34) shows that two inputs are available for zeroing the (single) output (4.33). In what follows, the hip torque u_2 is solely devoted to pitch control, while the leg input u_1 is reserved for controlling the zero dynamics.

Lemma 4.9 (Stance Phase Zero Dynamics). *Under the output function h defined by (4.33), and for $q_s \in \hat{Q}_s := \{q_s \in Q_s \mid l \neq L \sin \varphi\}$,*

1) *the set $\mathcal{Z} := \{x_s \in T\hat{Q}_s \mid h(x_s) = 0, L_{f_s} h(x_s) = 0\}$ is a smooth four-dimensional embedded submanifold of $T\hat{Q}_s$;*

2) *the feedback control law*

$$u_2^* = -\frac{L_{g_{s,1}} L_{f_s} h(q_s)}{L_{g_{s,2}} L_{f_s} h(q_s)} u_1 \quad (4.36)$$

renders \mathcal{Z} invariant under the stance dynamics; that is, for $x_s \in \mathcal{Z}$, $u_1 \in \mathbb{R}$,

$$f_s(x_s) + g_{s,1}(x_s) u_1 + g_{s,2}(x_s) u_2^* \in T_{x_s} \mathcal{Z};$$

3) *there exist smooth functions $\gamma_1(x_s)$ and $\gamma_2(x_s)$ so that the map $\Phi : T\hat{Q}_s \rightarrow \mathbb{R}^6$,*

$$\Phi(x_s) =: (\eta_1, \eta_2, z_1, z_2, z_3, z_4)' =: x, \quad (4.37)$$

where

$$\eta_1 := h(q_s), \quad \eta_2 := L_{f_s} h(x_s), \quad (4.38)$$

³It can rigorously be shown using arguments from model matching, e.g. [28], that $\bar{\theta}$ being constant is a *necessary* condition for the existence of an embedding control law for realistic hopping motions. Due to limited space, the proof of this statement will not be presented here.

$$(z_1, z_2)' := (l, \varphi)', \quad (z_3, z_4)' := (\gamma_1(x_s), \gamma_2(x_s))', \quad (4.39)$$

is a valid coordinate transformation, i.e. Φ is a diffeomorphism onto its image, and

$$L_{g_{s,2}}\gamma_1(x_s) = 0, \quad L_{g_{s,2}}\gamma_2(x_s) = 0;$$

4) the set $\mathcal{S}_{s \rightarrow f} \cap \mathcal{Z}$ with $\mathcal{S}_{s \rightarrow f}$ defined by (3.13) is a co-dimension one C^1 -submanifold of \mathcal{Z} .

Proof. Parts 1) and 2) of Lemma 4.9 follow from general results in [57, pp. 169-170]. For part 3), consider the distribution $G := \text{span}\{g_{s,2}\}$, which has constant dimension $d = 1$ on $T\hat{Q}_s$. Since G is one dimensional, it is involutive, and thus, by the Frobenius theorem (Theorem 1.4.1, [57, p. 23]), integrable. As a result there exist $n - d = 6 - 1 = 5$ real-valued functions defined on $T\hat{Q}_s$ such that the annihilator of G is $G^\perp = \text{span}\{dl, d\varphi, d\theta, d\gamma_1, d\gamma_2\}$. A straightforward application of the constructive proof of the sufficiency part of Frobenius theorem [57, pp. 24-28] results in

$$\gamma_1(x_s) = \dot{l} + (L \cos \varphi)\dot{\theta}, \quad (4.40)$$

$$\gamma_2(x_s) = \dot{\varphi} + \left[-1 + \frac{L \sin \varphi}{l} + \frac{J}{ml(L \sin \varphi - l)} \right] \dot{\theta}. \quad (4.41)$$

It is straightforward to check that Φ is a diffeomorphism onto its image in \mathbb{R}^6 . Finally, for part 4), note that, in x -coordinates, $\tilde{H}_{s \rightarrow f}(x) := (H_{s \rightarrow f} \circ \Phi^{-1})(x) = r_0 - \sqrt{L^2 + z_1^2 - 2Lz_1 \sin z_2}$, i.e. $\tilde{H}_{s \rightarrow f}$ is a function of z only. In particular, it does not depend on θ and $\dot{\theta}$. The result now follows from the regular value theorem (Theorem (5.8) [15, p. 78]), in view of Remark 3.3 and of the fact that $\text{rank}\{(h, L_f h, H_{s \rightarrow f})'\} = 2 + \text{rank}\{H_{s \rightarrow f}\} = 3$. \square

It should be noted that, contrary to the HZD designed in [110] and [26], the zero dynamics manifold \mathcal{Z} is a four-dimensional embedded submanifold of the six-dimensional stance state space $T\hat{Q}_s$. This significantly complicates stability analysis of the resulting HZD, which no longer is a one-DOF system as in [110] and [26]. However, the presence of u_1 in the zero dynamics allows for further control action. A feedback law can be devised for u_1 so that the zero dynamics associated with the output (4.33) matches exactly the differential equations of the ES-SLIP stance phase dynamics. To do this, let $\epsilon > 0$ and define

the feedback

$$\begin{aligned} u_2 &= \Gamma_{c,2}^\epsilon(x_s) \\ &:= \frac{1}{L_{g_{s,2}}L_{f_s}h(q_s)} \left[v^\epsilon(\theta, \dot{\theta}) - L_{g_{s,1}}L_{f_s}h(q_s)u_1 \right], \end{aligned} \quad (4.42)$$

where

$$v^\epsilon(\theta, \dot{\theta}) := -\frac{1}{\epsilon^2}K_P^\theta(\theta - \bar{\theta}) - \frac{1}{\epsilon}K_V^\theta\dot{\theta}, \quad (4.43)$$

and K_P^θ, K_V^θ are positive constants. Under this feedback law, the model (4.32) becomes

$$\dot{x}_s = \hat{f}_s^\epsilon(x_s) + \hat{g}_s(x_s)u_1, \quad (4.44)$$

where

$$\hat{f}_s^\epsilon(x_s) := f_s(x_s) + \left[\frac{1}{L_{g_{s,2}}L_{f_s}h(q_s)} v^\epsilon(\theta, \dot{\theta}) \right] g_{s,2}(x_s), \quad (4.45)$$

$$\hat{g}_s(x_s) := g_{s,1}(x_s) - \frac{L_{g_{s,1}}L_{f_s}h(q_s)}{L_{g_{s,2}}L_{f_s}h(q_s)} g_{s,2}(x_s). \quad (4.46)$$

Under the coordinates of Lemma 4.9, (4.44) has the form

$$\dot{\eta} = A(\epsilon)\eta, \quad (4.47)$$

$$\dot{z} = f_z(\eta, z) + g_z(z)u_1, \quad (4.48)$$

where

$$A(\epsilon) = \begin{bmatrix} 0 & 1 \\ -K_P^\theta/\epsilon^2 & -K_V^\theta/\epsilon \end{bmatrix}. \quad (4.49)$$

With the additional change of coordinates $\eta = \Pi(\epsilon)\tilde{\eta}$, defined by $\eta_1 = \epsilon\tilde{\eta}_1$ and $\eta_2 = \tilde{\eta}_2$, the model (4.47)-(4.48) takes the form

$$\epsilon\dot{\tilde{\eta}} = \tilde{A}\tilde{\eta}, \quad (4.50)$$

$$\dot{z} = f_z(\Pi(\epsilon)\tilde{\eta}, z) + g_z(z)u_1, \quad (4.51)$$

and

$$\frac{1}{\epsilon}\tilde{A} = \Pi^{-1}(\epsilon)A(\epsilon)\Pi(\epsilon) \Rightarrow \tilde{A} = \begin{bmatrix} 0 & 1 \\ -K_P^\theta & -K_V^\theta \end{bmatrix}. \quad (4.52)$$

Since the gains $\{K_p^\theta, K_V^\theta\}$ in (4.52) are strictly positive, the matrix \tilde{A} is Hurwitz and $e^{\frac{1}{\epsilon}\tilde{A}}$ converges to zero exponentially fast as $\epsilon \rightarrow 0$. Hence, $\lim_{\epsilon \searrow 0} e^{A(\epsilon)} = 0$. This verifies condition A.3) of Theorem 4.3. Moreover, setting $\epsilon = 0$, (4.50) reduces to the algebraic equation $\tilde{A}\tilde{\eta} = 0$, which has the origin as its unique solution. Hence, (4.50)-(4.51) is in standard singular perturbation form, see [58, p. 424], and the corresponding reduced model is obtained by substituting $\epsilon = 0$ and $\tilde{\eta} = 0$ in the slow part of the dynamics (4.51), i.e.

$$\dot{z} = f_z(0, z) + g_z(z)u_1, \quad (4.53)$$

where direct calculation leads to

$$f_z(z) = \begin{bmatrix} z_3 \\ z_4 \\ z_1 z_4^2 - g \cos(\bar{\theta} + z_2) \\ \frac{-2z_3 z_4 + g \sin(\bar{\theta} + z_2)}{z_1} \end{bmatrix}, \quad (4.54)$$

$$g_z(z) = \begin{bmatrix} 0 \\ 0 \\ 1/m \\ \frac{L \cos z_2}{m z_1 (L \cos z_2 - z_1)} \end{bmatrix}. \quad (4.55)$$

The following lemma completes the continuous stance controller design by providing a procedure for constructing u_1 .

Lemma 4.10 (Restriction dynamics). *If $\bar{\theta}$ is the desired pitch angle in (4.33), define*

$$r(z) := \sqrt{L^2 + z_1^2 - 2Lz_1 \sin z_2}, \quad (4.56)$$

$$\dot{r}(z) := \frac{z_1 - L \sin z_2}{r(z)} z_3 - \frac{L z_1 \cos z_2}{r(z)} z_4, \quad (4.57)$$

$$y_z(z) := z_1 \cos(z_2 + \bar{\theta}) + L \sin \bar{\theta}. \quad (4.58)$$

Then, if \bar{E} is the desired energy level, the feedback law

$$u_1 = \tilde{\Gamma}_{c,1}(z) := \frac{z_1 - L \sin z_2}{r(z)} F_{\text{ES-SLIP}}(z), \quad (4.59)$$

with

$$F_{\text{ES-SLIP}}(z) := k[r_0 + \Delta r - r(z)] - K_P^E \dot{r}(z)[E(z) - \bar{E}], \quad (4.60)$$

$$E(z) := \frac{1}{2}m(z_3^2 + z_1^2 z_4^2) + mgy_z(z) + \frac{1}{2}k[r_0 + \Delta r - r(z)]^2, \quad (4.61)$$

and $K_P^E > 0$, renders the restriction dynamics (4.53) diffeomorphic to the ES-SLIP closed-loop dynamics $f_{s,\text{cl}}^M(x^M)$ defined by (4.17).

Proof. Substitution of (4.59) into (4.53) gives

$$\dot{z} = f_z(z) + g_z(z)\tilde{\Gamma}_{c,1}(z) =: f_{z,\text{cl}}(z). \quad (4.62)$$

Define the map $\Phi_z : \mathcal{Z} \rightarrow \mathbb{R}^4$ by

$$\Phi_z(z) := \begin{bmatrix} -z_1 \sin(z_2 + \bar{\theta}) + L \cos \bar{\theta} \\ z_1 \cos(z_2 + \bar{\theta}) + L \sin \bar{\theta} \\ -z_3 \sin(z_2 + \bar{\theta}) - z_1 z_4 \cos(z_2 + \bar{\theta}) \\ z_3 \cos(z_2 + \bar{\theta}) - z_1 z_4 \sin(z_2 + \bar{\theta}) \end{bmatrix}. \quad (4.63)$$

It is straightforward to check that Φ_z is a diffeomorphism onto its image, thus it describes a valid coordinate transformation on \mathcal{Z} . Observe that $\Phi_z(z) = x^M$. The result

$$\left(\frac{\partial \Phi_z}{\partial z} f_{z,\text{cl}}(z) \right) \Big|_{z=\Phi_z^{-1}(x^M)} = f_{s,\text{cl}}^M(x^M) \quad (4.64)$$

is obtained after straightforward algebraic manipulations. \square

Remark 4.11. Careful inspection of (4.59) reveals that under the proposed feedback law the total ASLIP leg force, u_1 , becomes equal to the projection of the ES-SLIP force, $F_{\text{ES-SLIP}}$, along the direction of the actual (ASLIP) leg; see Fig. 4.4. Indeed, in the coordinates x

defined by (4.37) and (4.39), the control law (4.59) takes the form

$$u_1 = \frac{l - L \sin \varphi}{r} F_{\text{ES-SLIP}} \Leftrightarrow u_1 = (\cos \chi) F_{\text{ES-SLIP}}, \quad (4.65)$$

where the angle χ is shown in Fig. 4.4. As will be explained in Section 4.6.4, this property can be used to provide a qualitative explanation of the superiority of the SLIP-embedding controller against controllers that create non-compliant HZD. \triangleleft

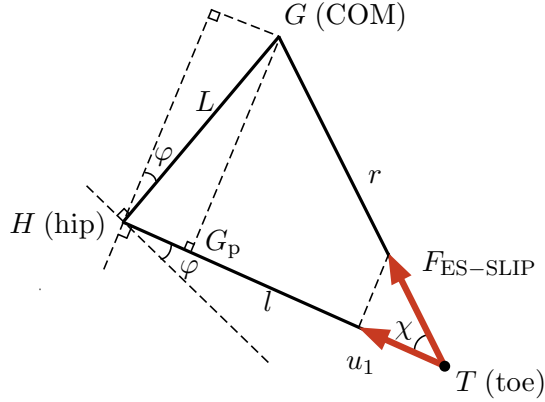


Figure 4.4: The controller (4.59) makes the actual total leg force u_1 equal to the projection of the virtual leg force $F_{\text{ES-SLIP}}$ along the direction of the ASLIP (actual) leg.

Remark 4.12. Combining (4.42)-(4.59), a feedback controller of the form $u = \Gamma_c^\epsilon(x_s, \alpha_s)$ is obtained. The vector $\alpha_s := (\bar{\theta}, k, r_0, \Delta r)'$ corresponds to parameters introduced by the control law, and includes the mechanical properties of the target model. The nominal values of these parameters will be selected via an optimization procedure, which will be presented in Section 4.6. As was mentioned in Section 4.1, α_s can be updated in an event-based manner through the inner-loop feedback law Γ_s of Fig. 4.1 to achieve hybrid invariance. However, Lemma 4.13 below shows that this is not necessary for the SLIP embedding controller, and thus α_s need not be updated. This is the reason why α_s did not explicitly appear as one of the arguments of the continuous-time controller Γ_c^ϵ . \triangleleft

4.4.2 Event-Based Discrete Control

The purpose of the stride-to-stride controller is twofold. First, it ensures that the manifold $\mathcal{S}_{s \rightarrow f} \cap \mathcal{Z}$ is invariant under the reset map Δ_{cl} . Second, it arranges the configuration

of the ASLIP at liftoff so that the restriction of the ASLIP reset map on $\mathcal{S}_{s \rightarrow f} \cap \mathcal{Z}$ is equal to the SLIP closed-loop reset map. Both requirements can be satisfied through the outer-loop event-based controller Γ_f of Fig. 4.1, whose design is the subject of the following lemma.

Lemma 4.13 (Event-based controller). *Let \dot{x}_{cm} and $\bar{\psi}$ be the forward running speed at liftoff and the touchdown angle, respectively, corresponding to a (desired) fixed point of the ES-SLIP. Define*

$$\psi(x_s^-) := \bar{\psi} + K_{\dot{x}} [\dot{x}_{\text{cm}}^-(x_s^-) - \dot{x}_{\text{cm}}], \quad (4.66)$$

where \dot{x}_{cm}^- is the forward running speed of the ASLIP prior to liftoff. Then, the controller $\alpha_f = \Gamma_f(x_s^-) := (l^{\text{td}}(x_s^-), \varphi^{\text{td}}(x_s^-))'$,

$$l^{\text{td}}(x_s^-) = \sqrt{L^2 + r_0^2 + 2Lr_0 \sin(\psi(x_s^-) - \bar{\theta})}, \quad (4.67)$$

$$\varphi^{\text{td}}(x_s^-) = \arcsin \left[\frac{(l^{\text{td}}(x_s^-))^2 + L^2 - r_0^2}{2Ll^{\text{td}}(x_s^-)} \right], \quad (4.68)$$

where $\bar{\theta}$ is the desired pitch angle in (4.33), achieves B.1) and B.2) of Theorem 4.3.

Proof. Suppose $x_s^- \in \mathcal{S}_{s \rightarrow f} \cap \mathcal{Z}$. To show B.1), notice that this implies $\dot{\theta}^- = 0$ and $\theta^- = \bar{\theta}$ just prior to liftoff. Since during the flight phase $\ddot{\theta} = 0$, i.e. $\theta(t) \equiv \bar{\theta}$, at touchdown we have $\dot{\theta}^+ = 0$ and $\theta^+ = \bar{\theta}$, which means that $x_s^+ \in \mathcal{Z}$. This establishes hybrid invariance, i.e. $\Delta_{\text{cl}}(\mathcal{S}_{s \rightarrow f} \cap \mathcal{Z}) \subset \mathcal{Z}$. To show B.2), observe that, in coordinates (4.63), the surface $\mathcal{S}_{s \rightarrow f} \cap \mathcal{Z}$ with $\mathcal{S}_{s \rightarrow f}$ defined by (3.13), is equal to $\mathcal{S}_{s \rightarrow f}^{\text{M}}$, given by (4.20), i.e. the domains of definition of the maps $\Delta_{\text{cl}}|_{\mathcal{Z}}$ and $\Delta_{\text{cl}}^{\text{M}}$ are equal. The rest of the proof is a consequence of the fact that the flight flow of the ES-SLIP is the same as the translational part of the flight flow of the ASLIP. Equations (4.66)-(4.68) ensure that, not only the flight flows are identical, but also the corresponding closed-loop reset maps $\Delta_{\text{cl}}|_{\mathcal{Z}}$ and $\Delta_{\text{cl}}^{\text{M}}$, are diffeomorphic. \square

Remark 4.14. The proof of Lemma 4.13 depends only upon the restriction of the functions l^{td} and φ^{td} on $\mathcal{S}_{s \rightarrow f} \cap \mathcal{Z}$. Hence, l^{td} and φ^{td} can be replaced with any smooth functions whose restrictions on $\mathcal{S}_{s \rightarrow f} \cap \mathcal{Z}$ are equal to (4.67) and (4.68), respectively. This property will be brought into use in Section 4.6.1 to modify (4.67) and (4.68) in order to enlarge the basin of attraction of the nominal orbit; see (4.75) and (4.76) there. \triangleleft

4.4.3 Proof of Theorem 4.3

The proof of Theorem 4.3 is an immediate consequence of Lemmas 4.9, 4.10 and 4.13.

4.5 One DOF Hybrid Zero Dynamics: The Rigid Target Model

This section describes the second of the controllers presented in this paper. The design procedure provides the feedback laws Γ_c , Γ_s and Γ_f , whose function was described in Section 4.1. This controller, whose stability proof follows from previous results in [26] and [83], is included here because its comparison with the SLIP embedding controller will reveal some beneficial aspects of designing the HZD to accommodate compliance. Thus, the presentation will be terse leaving the details of the design for Appendix A; the interested reader is referred to supplemental material in [45] for further implementation details and in [83] for the general framework. It is important to emphasize that this controller is fundamentally different from the SLIP embedding controller of Sections 4.3 and 4.4 in that it results in a one-DOF HZD, a fact that greatly simplifies stability analysis, but leaves no room for compliance. Hence, we refer to this controller as the *rigid target model controller*.

4.5.1 In-stride Continuous Control

During the stance phase, the ASLIP exhibits one degree of underactuation. The two inputs $u = (u_1, u_2)'$ will be used to asymptotically impose two virtual holonomic constraints on two of the models' three DOF, which are chosen to be the leg length and the pitch angle, i.e. $q_a := (l, \theta)'$. Other choices are possible; however, this particular one allows for the direct comparison with the SLIP embedding controller of Sections 4.3 and 4.4. Here, the virtual constraints are chosen to be polynomials parameterized by the monotonic quantity $q_u = \pi/2 - \varphi - \theta$, representing the angle of the leg with respect to the ground, as shown in Fig. 3.1. The virtual constraints are imposed through zeroing the output

$$y = h(q_s, \alpha_s) = q_a - h_d(q_u, \alpha_s), \quad (4.69)$$

where h_d are the polynomial functions of q_u describing the desired evolution of q_{av} and α_s includes the corresponding polynomial coefficients; see Appendix A.

Following the procedure that was outlined in Section 4.1.1, the continuous feedback controller Γ_c is designed to render the surface

$$\mathcal{Z}_{\alpha_s} := \{x_s \in TQ_s \mid h(q_s, \alpha_s) = 0, L_f h(x_s, \alpha_s) = 0\} \quad (4.70)$$

invariant under the flow of the continuous part of the ASLIP dynamics and attractive. It is emphasized here that *two* virtual constraints are imposed by zeroing (4.69), thus resulting in a *one-DOF* HZD evolving on a two-dimensional surface \mathcal{Z}_{α_s} .

4.5.2 Event-Based Discrete Control

The development of the event-based control law closely follows the structure outlined in Section 4.1. In this case, to achieve hybrid invariance, it is necessary to include the inner-loop controller Γ_s of Fig. 4.1 in the feedback design. Details on how to construct Γ_s can be found in Appendix A.

The outer-loop control law Γ_f updates $\alpha_f = (l^{\text{td}}, \varphi^{\text{td}})'$ in order to exponentially stabilize the HZD. In the rigid target model controller, we do not explore the possibility of updating the leg length l^{td} at touchdown; l^{td} is assumed to be always equal to its nominal value l_0 . This leaves the touchdown angle φ^{td} as the only parameter available for control. The Poincaré map \mathcal{P} associated with the hybrid system under the feedback laws Γ_c and Γ_s gives rise to the discrete-time control system,

$$x_s^- [k + 1] = \mathcal{P} \left(x_s^- [k], \varphi^{\text{td}} [k] \right), \quad (4.71)$$

defined on the surface

$$\mathcal{S}'_{s \rightarrow f} := \left\{ x_s \in \mathcal{X}_s \mid l - l_0 = 0, i > 0 \right\}. \quad (4.72)$$

where $x_s^- (k)$ is the state just prior to the k -th liftoff. Linearizing (4.71) about a fixed point \bar{x}_s^- and $\bar{\varphi}^{\text{td}}$ corresponding to the nominal values of the state just prior liftoff and the touch-

down angle, respectively, results in a discrete-time linear-time-invariant control system

$$\delta x_s^- [k + 1] = \left(\frac{\partial \mathcal{P}}{\partial x_s^-} \right) \Big|_{(x_s^- = \bar{x}_s^-, \varphi^{\text{td}} = \bar{\varphi}^{\text{td}}} \delta x_s^- [k] + \left(\frac{\partial \mathcal{P}}{\partial \varphi^{\text{td}}} \right) \Big|_{(x_s^- = \bar{x}_s^-, \varphi^{\text{td}} = \bar{\varphi}^{\text{td}}} \delta \varphi^{\text{td}} [k], \quad (4.73)$$

where $\delta x_s^- = x_s^- - \bar{x}_s^-$ and $\delta \varphi^{\text{td}} = \varphi^{\text{td}} - \bar{\varphi}^{\text{td}}$. Implementing a discrete LQR controller using the linearization (4.73) gives

$$\varphi^{\text{td}} [k] = \Gamma_f (x_s^- [k]) := \bar{\varphi}^{\text{td}} + K (x_s^- [k] - \bar{x}_s^-). \quad (4.74)$$

The feedback controller (4.74) guarantees that the eigenvalues of the linearization of (4.71) are all within the unit circle, and completes the control design. Note that instead of the full model Poincaré map (4.71), the one-dimensional Poincaré map associated with the HZD could have been used, affording a reduced-order stability test; see [110], [26], [83].

4.6 Controller Evaluation via Simulation

This section presents simulation results that compare the performance of the SLIP embedding controller presented in Sections 4.3 and 4.4, with that of the rigid target model controller of Section 4.5. Both the steady-state and the transient behavior of the controllers are discussed.

4.6.1 Implementation Issues and Nominal Orbit Design

The mechanical properties of the ASLIP used in the simulations of this section roughly correspond to Thumper, and are presented in Table 4.1 (see also Fig. 3.1).

Table 4.1: ASLIP Mechanical Parameters

Parameter	Value	Units
Torso Mass (m)	27	kg
Torso Inertia (J)	1	kg m ²
Hip-to-COM spacing (L)	0.25	m
Nominal Leg Length (l_0)	0.9	m
Uncompressed Spring Length (l_{nat})	0.91	m
ASLIP Spring Constant (k_A)	7578	N/m

In implementing the SLIP embedding controller, simulation shows that, while the event-based controller developed in Lemma 4.13 of Section 4.4.2 achieves exponential stability of the ASLIP, letting the pitch angle in (4.67)-(4.68) off the zero dynamics be equal to its actual value, instead of its nominal value $\bar{\theta}$, enlarges the domain of attraction of the controller, i.e.

$$l^{\text{td}}(x_f, x_s^-) = \sqrt{L^2 + r_0^2 + 2Lr_0 \sin(\psi(x_s^-) - \theta)}, \quad (4.75)$$

$$\varphi^{\text{td}}(x_f, x_s^-) = \arcsin \left[\frac{(l^{\text{td}}(x_f, x_s^-))^2 + L^2 - r_0^2}{2Ll^{\text{td}}(x_f, x_s^-)} \right], \quad (4.76)$$

whose restrictions on $\mathcal{S}_{s \rightarrow f} \cap \mathcal{Z}$ are equal to (4.67) and (4.68), respectively. By Remark 4.14, the stability conclusion of Theorem 4.3 remains valid. This modification is similar to what was done in [26], and it will be included in the simulations of the SLIP embedding controller without further comment.

To implement the rigid target model controller, a sixth order polynomial was used for the desired leg length, and a constant polynomial for the desired pitch angle; refer to Appendix A for details. Generally, the rigid target model controller allows for the desired pitch angle θ being any suitably parameterized function of the unactuated variable q_u , thus allowing for nontrivial motions of the torso. However, this is not possible in the SLIP embedding controller, due to the fact that constant pitch angle throughout the nominal (steady-state) motion is a necessary condition for its implementation.

Both controllers introduce a set of parameters α_s , whose values along the nominal orbit can be selected using the optimization technique developed in [110]. Consider the hybrid dynamics of the ASLIP in closed-loop with the feedback controllers developed in Sections 4.3, and 4.4, and in Section 4.5 with cost function

$$\hat{J}(\alpha_s) = \frac{1}{T_s} \int_0^{T_s} u_2^2(t) dt + \max_{t \in [0, T_s]} \left\{ [u_1(t) - k_A (l_{\text{nat}} - l(t))]^2 \right\}, \quad (4.77)$$

where T_s is the duration of the stance phase, k_A is the stiffness of the ASLIP leg, and l_{nat} its natural length; see Table 4.1. Append to (4.77) the constraint

$$x_s^- - \mathcal{P}(x_s^-, \alpha_s, \alpha_f) = 0, \quad (4.78)$$

so that the nominal orbit is periodic. One can also include constraints that correspond to requirements such as the desired nominal forward speed, or the normal ground force component be non-negative etc. Then, the problem of finding the nominal values of the coefficients α_s and α_f reduces to a constrained minimization problem, which can be (numerically) solved using MATLAB's `fmincon`. It worth mentioning here, that the specific choice of performance index (4.77) reflects our desire to find a nominal orbit for the ASLIP, on which the amount of work produced by the hip actuator and the peak force developed by the leg actuator given by

$$u_1^a = u_1 - k_A(l_{\text{nat}} - l), \quad (4.79)$$

are minimized.

4.6.2 Steady-State Behavior

In order to compare the behavior of the two controllers under perturbations, it would be ideal to have identical nominal orbits. Despite the fact that relatively low degree polynomials have been used in the rigid target model controller, an almost exact match in the resulting nominal orbits was obtained, as Fig. 4.5 presents. Figure 4.5 also shows that both controllers take advantage of the leg spring on the nominal (steady-state) motion, since the leg actuator force u_1^a is below 6 N while the total leg forces are on the order of 900 N in both cases.

4.6.3 Transient Behavior and Performance Evaluation

The gains used in the SLIP embedding controller are

$$K_P^\theta = 300, K_V^\theta = 2\sqrt{K_P^\theta}, \epsilon = 1.2, K_P^E = 2, \text{ and } K_{\dot{x}} = 0.2,$$

while the gains for the rigid target model controller are

$$K_P^y = \text{diag}\{100, 100\}, K_V^y = 2\sqrt{K_P^y}, \epsilon = 1, \text{ and}$$

$$K = (0.1839, 0.4555, -0.0048, 0.0887, 0.1902).$$

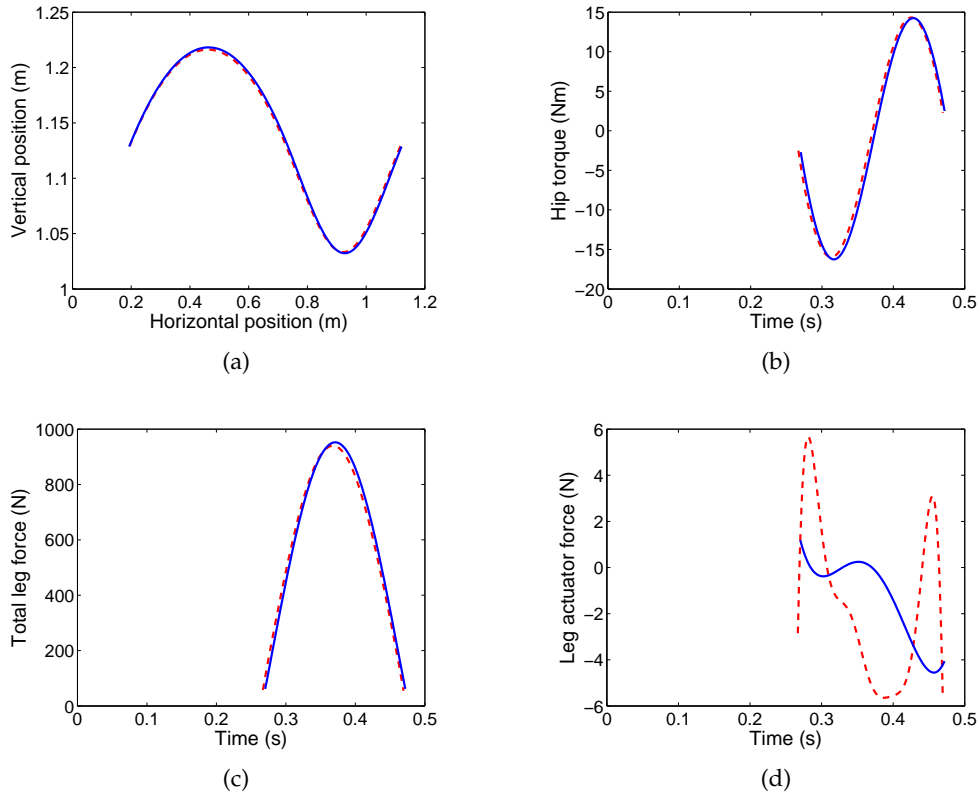


Figure 4.5: Nominal orbits in physical space (a), and corresponding hip torques (b), total leg forces (c), and leg actuator forces (d) computed by (4.79), for the rigid target model controller (dashed lines) and the SLIP embedding controller (solid lines).

Note that K has been selected using MATLAB's `d1qr` on the linear time invariant discrete system (4.73) evolving on the Poincaré section (4.72).

Using these data, both controllers have been simulated in MATLAB. It was observed that the rigid target model controller tends to violate the unilateral constraint between the ground and the toe by developing control forces which “pull” against the ground (i.e. the normal force becomes negative). To enlarge the domain of attraction, it was necessary to include saturation on the control forces so that the ground constraints are respected; details on the saturation procedure [45]. The SLIP embedding controller did not violate these constraints, except at very large perturbations.

Figure 4.6 presents pitch angle and forward velocity as the ASLIP recovers from a perturbation $\delta\theta = -6$ deg using both controllers. The perturbation occurs at the liftoff of the second stride. Notice that in both cases, the response of the pitch angle is similar; however,

larger excursions from the nominal forward speed are observed in the rigid target model controller.

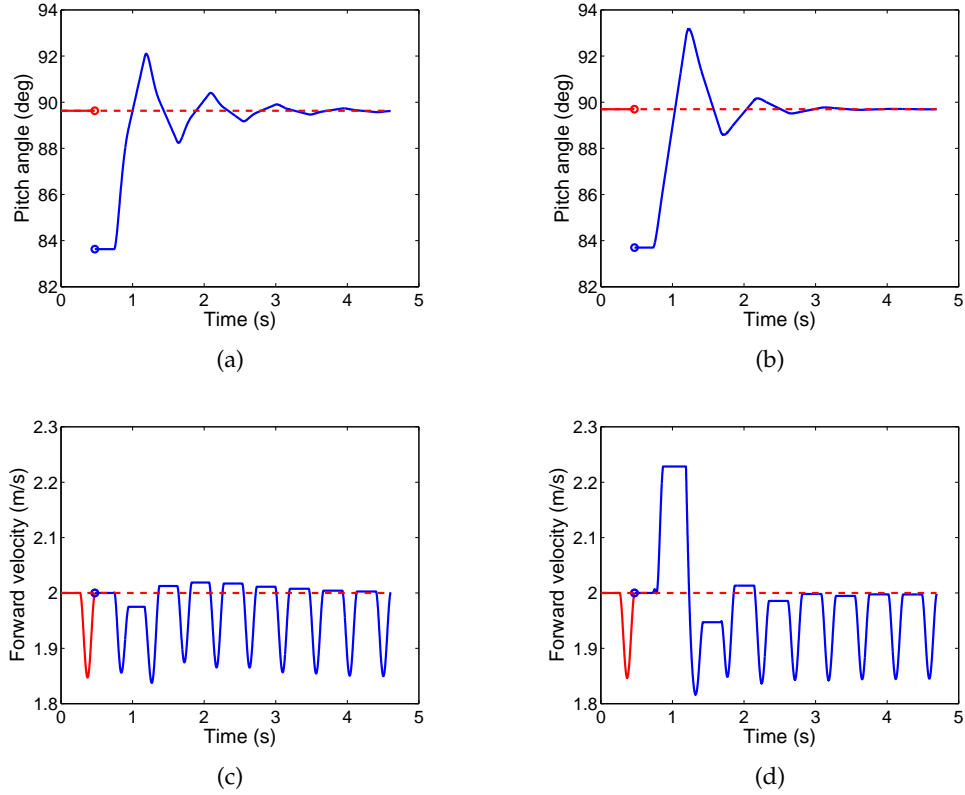


Figure 4.6: Ten strides showing convergence from $\delta\theta = -6$ deg, for the the SLIP embedding controller (a), (c), and the rigid target model controller (b),(d). Dashed lines show desired values; the circles correspond to the instant when the perturbation occurs (liftoff of the second stride).

Figure 4.7 presents the total leg forces and the leg actuator forces corresponding to Fig. 4.6. It is seen that, in the SLIP embedding controller, the profile of the leg actuator forces u_1^a computed by (4.79) remains close to that of a spring force, even during transients. On the contrary, in the rigid target model controller, the profile of the total leg force u_1 significantly differs from that of the spring force, resulting in large actuator forces u_1^a . This means that the rigid target model controller in closed loop with the ASLIP effectively “cancels” the compliance of the leg in the open-loop ASLIP. It is emphasized that, on the nominal orbit, both controllers exploit the leg spring equally well, since as shown in Fig. 4.5, the leg actuator force never exceeds 6 N, while the total forces are on the order of 900 N.

These features have significant implications for the domain of attraction of the two con-

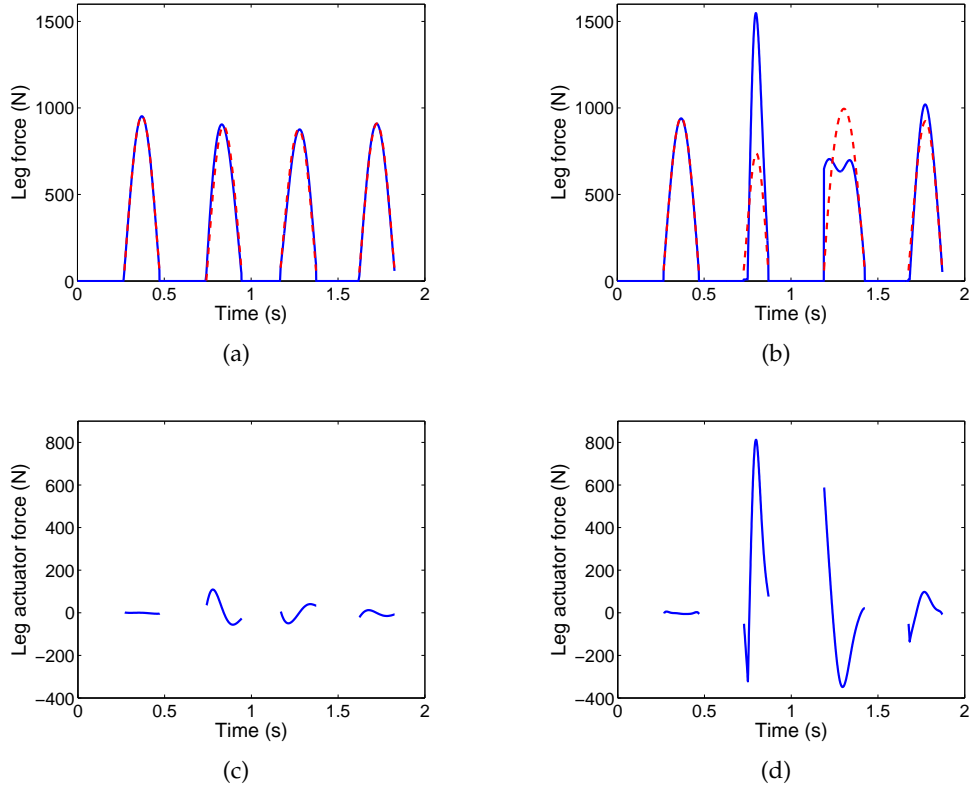


Figure 4.7: Leg forces for the SLIP embedding controller (left), and the rigid target model controller (right), and for the first four steps of Fig. 4.6. Upper plots show total leg forces; bottom plots show leg actuator forces computed by (4.79). The dashed lines in the upper plots show spring forces.

trollers. This is demonstrated in Table 4.2, which presents the number of strides until convergence within 5% of the steady-state value (strides), the peak actuator forces $(u_1^a, u_2)^{\max}$ in N, and the total work $(W_1, W_2)^{\text{total}}$ in J, required to reject perturbations $\delta\theta$ in the pitch angle and $\delta\dot{x}_{\text{cm}}$ in the forward velocity using the SLIP embedding controller (SLIP) and the Rigid Target Model controller (RTM). The perturbations reported in Table 4.2 correspond to the maximum values that can be rejected with the RTM controller, while the leg actuator force satisfies $u_1^a \leq 500$ N (almost double the weight of the robot). As is shown in Table 4.2, significantly lower peak leg actuator forces and total work are required from the SLIP embedding controller. As a result, larger perturbations than those in Table 4.2 can be rejected by the SLIP embedding controller respecting the constraint $u_1^a \leq 500$ N. This is due to the fact that the SLIP embedding controller acts in concert with the spring. These results demonstrate the significance of designing the HZD of running to respect the compliance

available in the open-loop system. Otherwise, the beneficial effects of the actual leg spring may be canceled by the control inputs during transients.

Table 4.2: Control Effort: SLIP Embedding and RTM Controllers

Perturbation	Control	Stride	$(u_1^a, u_2)^{\max}$	$(W_1, W_2)^{\text{total}}$
$\delta\theta = +4\text{deg}$	SLIP	4	(54, 28)	(24, 18)
	RTM	6	(442, 15)	(71, 24)
$\delta\theta = -3\text{deg}$	SLIP	4	(50, 26)	(16, 19)
	RTM	4	(382, 21)	(55, 19)
$\delta\dot{x}_{\text{cm}} = +0.9\frac{\text{m}}{\text{s}}$	SLIP	6	(418, 64)	(110, 40)
	RTM	12	(448, 37)	(242, 76)
$\delta\dot{x}_{\text{cm}} = -1.4\frac{\text{m}}{\text{s}}$	SLIP	Such a large perturbation could not be rejected without input saturation.		
	RTM	15	(486, 15)	(236, 47)

4.6.4 Qualitative Discussion

The significantly lower leg actuator forces reported for the SLIP-embedding controller in Table 4.2 are due to the fact that, in this case, the control input acts in concert with the spring. To be precise, as was mentioned in Remark 4.11, the intuitive meaning of the feedback law given by (4.59) is that the ASLIP (actual) leg force, u_1 , is rendered equal to the projection of the SLIP (virtual) leg force, $F_{\text{ES-SLIP}}$, along the direction of the actual leg. In view of (4.79), to achieve this prescription the leg actuator u_1^a is only required to “shape” the actual spring force $k_A(l_{\text{nat}} - l)$, so that the required central spring force, $F_{\text{ES-SLIP}}$, along the virtual (SLIP) leg direction is developed. As can be seen in Fig. 3.1, for physically reasonable torso pitch angles, the angle between the actual leg and the virtual leg direction is small. Consequently, small actuator effort suffices to “shape” the spring force of the actual leg to achieve this projection.

Concerning the lower power required by the SLIP-embedding controller, this is attributed to the fact that much of the work done on the leg is provided by the spring. Hence, in decelerating the COM during the compression part of the stance phase, only a small amount of energy is dissipated in the leg actuator. Finally, another particularly

important advantage of the SLIP-embedding controller is that, under reasonable conditions, it does not violate the ground contact constraints. In contrast, the rigid target model controller frequently commands leg forces that violate the unilateral constraints characterizing the toe/ground interaction. For instance, this occurs when the current leg length exceeds the commanded value. On such occasions, the controller attempts to shorten the leg by “pulling” the ground, often resulting in forces that violate the unilateral ground constraint.

These results demonstrate the significance of designing the HZD of running to respect the compliance available in the open-loop system. Otherwise, the beneficial effects of the actual leg spring may be canceled by the control inputs during transients. These ideas will be exploited in Chapter VI, where a feedback control law that induces stable running motions on Thumper is designed.

CHAPTER V

The Monopedal Robot Thumper

In this section, the mathematical equations governing the behavior of Thumper in running are derived. As was mentioned in the introduction, Thumper can be thought of as a rigid open kinematic chain composed of three links, which is driven by a compliant transmission system. To derive the equations of motion of Thumper, the transmission dynamics will be *included* as part of the model. This is necessary because of the way the compliance enters the system. In particular, the spring is part of the transmission system and it does not act directly on any of the physical joints of the linkage representing the robot. This is one of the main differences with the ASLIP model of Chapter III, where the spring was directly associated with the prismatic leg joint and the control inputs were assumed to act on the leg angle and leg length joints without dynamics involved.

The structure of this chapter is as follows. Section 5.1 clarifies the notation used in subsequent sections and contains the modeling hypotheses used to derive a mathematical model for Thumper's dynamics in running. Section 5.2 contains a model of the transmission along with some design details that are important for understanding its role as part of the system. Finally, in Section 5.3, a mathematical model of Thumper in running is derived, including the flight and stance dynamics, and the corresponding flight-to-stance and stance-to-flight transition maps.

5.1 Terminology, modeling hypotheses, and notation

Similarly to the ASLIP, during running, Thumper alternates between *stance* and *flight* phases. In the stance phase, which sometimes is called the (single) support phase, the leg-end, referred to as the *toe*, is in contact with the ground, while in flight the robot follows a ballistic trajectory under the influence of gravity. Thumper is composed of a torso and a single leg attached to the torso via a revolute joint, which is termed the *hip* joint. The leg is composed by two links, called the *thigh* and the *shin*, which are connected with another revolute joint, called the *knee*. The torso, thigh and shin form a rigid open kinematic chain, which is driven by two actuators—the *leg angle* and the *leg shape* actuators—via a compliant transmission system contained inside the torso. The transmission delivers actuator torques to the thigh and shin through a system of differentials implemented by cable-driven pulleys in such a way that the compliance acts in the direction of the line connecting the toe with the hip joint.

In the following list, the hypotheses used to derive the mathematical model of Thumper in running are enumerated. The significance of each of these modeling hypotheses will become apparent in subsequent sections, where details on the model derivation are presented. Here, all the hypotheses are collected for reference purposes.

Model Hypotheses: Thumper

HMT1) The motion is planar, i.e., running is constrained in the sagittal plane;

HMT2) The torso, thigh and shin are modeled as rigid bodies with nonzero mass and distributed inertia. The hip and knee joints are assumed to be ideal (frictionless) revolute joints;

HMT3) The point of contact between the leg-end and the ground is unactuated and it is modeled as a frictionless pin joint;

HMT4) The pulleys of the differentials in the transmission are modeled as cylindrical rigid bodies with distributed inertia about their COM. Their mass is included in the torso total mass. The cables connecting the pulleys are assumed to be massless;

HMT5) The spring is assumed to be linear and unilateral; it can be deformed in one direction only. The deformation of the spring in flight is assumed to be negligible; and

HMT6) The transmission system contributes to the gravitational potential energy of the mechanism only through increasing the torso mass.

Gait Hypotheses for Running: Thumper

The following properties consistent with the notion of monopedal running will be satisfied by the robot's motion as a result of the control action:

HGT1) Running is from left to right and takes place on a level surface;

HGT2) There are alternating phases of stance and flight separated by touchdown and liftoff events;

HGT3) During the single support phase the stance leg acts as an ideal pivot joint; in particular, throughout the stance phase it can be guaranteed that the vertical component of the ground reaction force is non-negative and that the ratio of the horizontal component over the vertical component does not exceed the coefficient of friction (the leg does not "pull" the ground and the toe does not slip);

HGT4) The COM of the robot travels a nonzero horizontal distance during the flight phase;

HGT5) The flight phase is terminated when the toe touches the ground. At this point an impact occurs;

HGT6) The stance phase is terminated when the vertical component of the ground reaction force becomes zero. At this point, the spring reaches its natural length and an (internal) impact occurs between the pulley attached to the spring in the transmission system and a mechanical (hard) stop, not allowing the spring to extend.

Rigid Impact Model Hypothesis: Thumper

By Hypotheses HGT5) and HGT6), impacts occur during the motion of the robot on two occasions. First, at touchdown, when the toe collides with the ground signifying the end

of the flight phase. Second, at liftoff, when a mechanical stop in the transmission system is hit by one of the pulleys associated with the spring, not allowing the spring to extend. This is a result of the specific design of the transmission system, which introduces a unilateral spring action as was mentioned in hypothesis HMT5). The impacts are modeled as contacts between two rigid bodies according to the model in [50]. In particular, the following hypotheses are used to model impacts:

HIT1) Impacts are instantaneous;

HIT2) The impact associated with the collision of the toe with the ground results in no rebound and no slipping; the internal impact associated with hitting the mechanical stop results in no rebound of the colliding pulley;

HIT3) The externally applied forces during an impact can be represented by impulses;

HIT4) The actuators do not generate impulses; hence, they can be ignored during impact; and

HIT5) The impulsive forces may result in instantaneous change in the robot's velocities, but there is no instantaneous change in configuration.

Finally, before continuing with the derivation of the model of Thumper in running, a few remarks on notation are in order. As in the ASLIP, the subscripts “f” and “s” will be used to denote the “flight” and “stance” phases, respectively. Moreover, the subscript “e” will be used to denote quantities associated with the “extended,” i.e., unconstrained, dynamics of Thumper. The symbol “ q ” will be used to denote *both* a point in the configuration manifold Q and its coordinate representation with respect to a coordinate chart of Q . Similarly, “ \dot{q} ” will be used to denote *both* a tangent vector, i.e., an element of the vector space T_qQ , and its coordinate representation, i.e., a column array in \mathbb{R}^n . In general, there will be no distinction between a map relating two manifolds and its coordinate representation. On some occasions, a distinction is made between maps between tangent spaces and their corresponding representations. For instance, let $\Upsilon : Q_1 \rightarrow Q_2$ be a smooth map between two manifolds Q_1 and Q_2 . The differential of Υ will be denoted by $(D\Upsilon)_q : T_qQ_1 \rightarrow T_{\Upsilon(q)}Q_2$, $q \in Q_1$, while its coordinate representation is denoted by the Jacobian matrix $J(q)$.

In general, a point on the robot will be denoted by its Cartesian coordinates $p = (p^h; p^v)$ with respect to the inertia frame. An exception to this general rule corresponds to the Cartesian coordinates of the COM, which will be denoted as (x_{cm}, y_{cm}) . The purpose of this exemption is to emphasize the use of the Cartesian coordinates of the COM (x_{cm}, y_{cm}) as part of the configuration variables during the flight phase. Note that augmenting the stance configuration variables with the Cartesian coordinates of the COM is a common, but not unique, choice of generalized coordinates for the flight phase.

5.2 Transmission Dynamics

The novel aspects of Thumper, and there are many, appear in the transmission or powertrain; see [52], [53] and [51]. First of all, all of the actuators (two DC-brushless motors) are located in the torso¹, so that the legs are as light as possible. Secondly, the actuated degrees of freedom of each leg do not correspond to the knee and hip angles –the hip angle being the relative angle between the torso and the thigh. Instead, a collection of differentials is used to connect the two motors to the hip and knee joints in such a way that one motor actuates the angle of the *virtual leg* consisting on the line connecting the hip to the toe, and the second motor is connected *in series with a spring* to control the *length* or *shape* of the virtual leg; see Fig. 5.1.

Roughly speaking, the rationale for this design is that, despite the presence of a revolute knee joint, Thumper’s leg resembles kinematically the prismatic leg of a Spring Loaded Inverted Pendulum (SLIP). In fact, the powertrain ensures that compliance is present along the virtual leg direction shown in Fig. 5.1(a), in much the same way as the prismatic spring acts in the SLIP. The transmission system introduces dynamic effects not present in other robot designs, and it needs to be included in the model of the system. The purpose of this section is to provide the essential features characterizing the behavior of the transmission system leaving the corresponding details for Appendix B.

As was mentioned above, there are two actuators, namely, the leg-angle and the leg-shape actuators, providing torque inputs u_{LA} and u_{LS} , respectively; see Fig. 5.1(b). The

¹This is different from RABBIT and most other robots, in which the knee actuators are mounted on the thigh; see for instance [24].

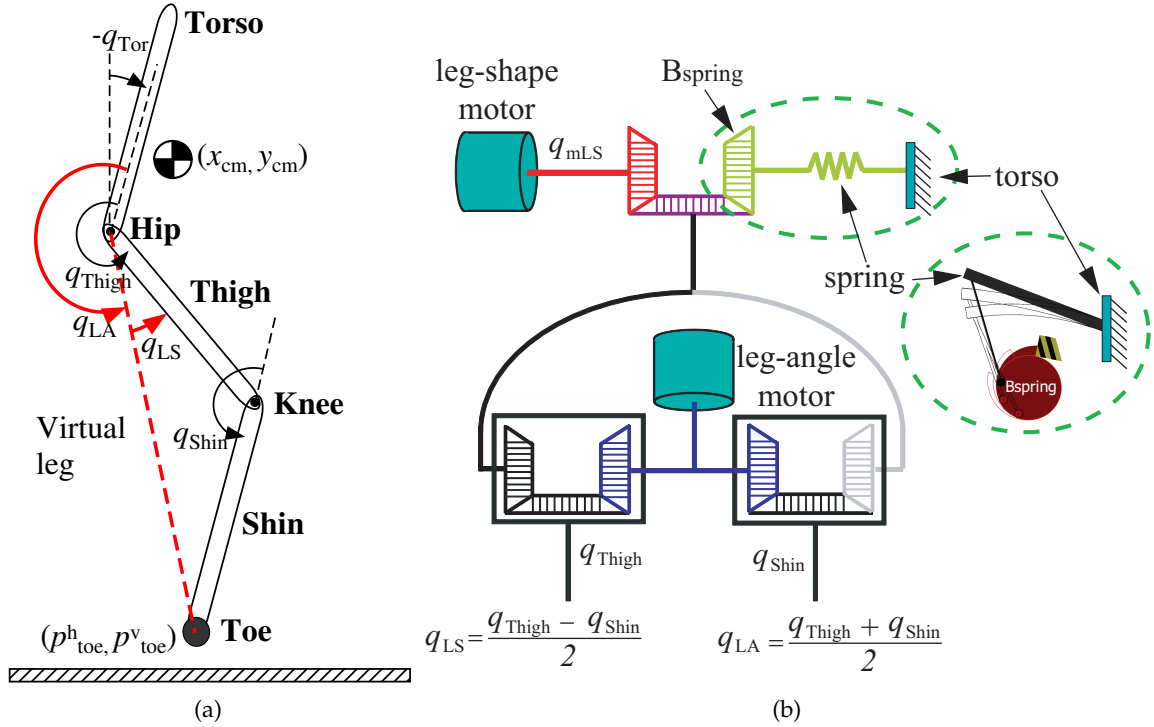


Figure 5.1: **Left:** Basic robot configuration. The dashed line connecting the toe with the hip corresponds to the “leg direction;” its length l and angle q_{LA} are the virtual “leg length” and “leg angle,” respectively. The leg length l is uniquely determined by the “leg shape” angle, q_{LS} . **Right:** Thumper’s powertrain system (courtesy of Hae-Won Park). The motors and spring are connected to the hip and knee joints via three differentials connected so that the actuated variables are the leg and leg-shape angles, q_{LA} and q_{LS} , respectively; see Fig. 5.1(a). The spring is *in series* with the leg-shape motor: one end is connected to the torso and the other to the B_{spring} pulley via a cable, which makes the spring *unilateral*. When the spring reaches its rest position, the B_{spring} pulley hits a hard stop, as shown in the detail. When this happens, the leg-shape motor is, for all intents and purposes, rigidly connected to leg shape through a gear ratio. Design details of the transmission can be found in [51].

transmission consists of three cable-driven differentials, whose placement is according to the conceptual diagram shown in Fig. 5.1(b); a more detailed figure, Fig. B.1, is given in Appendix B. The kinematics of the transmission involves eighteen variables corresponding to the angular positions of the pulleys, among which there exist fifteen constraints imposed by their interconnections. To improve readability, these constraints are provided in Appendix B. Here, only their implications for the kinematics and dynamics of the robot are discussed.

First, special attention is given to two of the constraints imposed by the transmission,

namely, those constraints that relate the “internal” variables of the transmission with the external linkage kinematics. Let q_{Thigh} and q_{Shin} be the angles of the thigh and the shin relative to the torso², respectively, see Fig. 5.1(a). Then, the placement of the differentials in the transmission and the geometry of the associated pulleys ensure that the leg angle q_{LA} and the leg shape q_{LS} are constrained according to

$$q_{\text{LA}} = \frac{q_{\text{Thigh}} + q_{\text{Shin}}}{2} \quad (5.1)$$

$$q_{\text{LS}} = \frac{q_{\text{Thigh}} - q_{\text{Shin}}}{2} \quad (5.2)$$

Notice that the angles q_{LA} and q_{LS} given by (5.1) and (5.2), respectively, uniquely determine the orientation with respect to the torso of the line segment connecting the hip and the toe, and its length through the relation

$$l = 2d \cos(q_{\text{LS}}), \quad (5.3)$$

respectively. In (5.3), d refers to the length of the thigh and shin; see Fig. 5.1(a). Consequently, from a kinematics perspective, the transmission system can be viewed as a system with leg length and leg angle as inputs, and thigh angle and shin angle as outputs. In other words, given some desired values of q_{LA} and l (or, equivalently q_{LS}), the transmission guarantees mechanically that the hip and knee joints are placed appropriately so that these desired values are achieved. Intuitively, (5.1), (5.2) and the constraints listed in Appendix B ensure that the toe is *mechanically* constrained to move along the virtual leg length line shown in Fig. 5.1(a).

The second point that will be addressed in this section, and is related to the constraints imposed by the differentials and their interconnections, regards the degrees of freedom of the transmission system. Since the transmission involves eighteen variables and fifteen constraints among them —see Appendix B— there will be three independent variables, which completely determine the configuration of all the pulleys in the transmission. In

²By design, these are the angles of the “C” pulleys of the thigh and shin differentials $\theta_{C_{\text{Thigh}}}$ and $\theta_{C_{\text{Shin}}}$, respectively; see Table B.1 and Fig. B.1 in Appendix B.

what follows, the triplet $(q_{LA}, q_{LS}, q_{mLS})$ — q_{LA}, q_{LS} have been described above and q_{mLS} is the position of the motorshaft of the leg-shape motor; see Fig. 5.1— is selected as the set of configuration variables for the transmission system. It should be emphasized here that, since only two actuator torques u_{LA} and u_{LS} act as inputs, the transmission is an underactuated system with one degree of underactuation.

The source of underactuation of the transmission is the existence of the spring depicted in Fig. 5.1(b). If $\theta_{B_{\text{Spring}}}$ denotes the deformation of the spring, then

$$\theta_{B_{\text{Spring}}} = \mu_1 q_{LS} - \mu_2 q_{mLS}, \quad (5.4)$$

where $\mu_1 = 5.196$ and $\mu_2 = 0.1646$ are constants whose values depend on the geometric characteristics of the pulleys. Equation (5.4) is quite revealing for the role of the spring. It shows that compliance acts between the leg shape angle, q_{LS} , and the motorshaft angular position, q_{mLS} , in roughly the same way as in the case of a motor connected in series with a spring moving a load. In fact, this would have been exactly the case if $\mu_1 = \mu_2 = 1$. Note also that the spring does not affect the relation between the leg angle q_{LA} and the corresponding motorshaft position q_{mLA} ; thus, the torque u_{LA} is rigidly transmitted to the linkage. Only the torque u_{LS} developed at the leg shape motor is transmitted to the linkage through the compliant element.

Remark 5.1. Equation (5.4) highlights that holding the motorshaft at a constant angle q_{mLS} , and given the one-to-one relation between the virtual leg length l and q_{LS} imposed by (5.3), equation (5.4) shows that the spring action is “visible” only when l changes, in much the same way the prismatic spring acts in the SLIP. Indeed, as the knee flexes during the compression part of the stance phase, holding the leg-shape motorshaft at a constant position ensures that elastic energy is stored in the spring; this energy can be returned in the system during the decompression part of the stance phase. This fact will be used in Section 6.2 to design a controller for Thumper that takes advantage of the spring. \triangleleft

The third novelty in Thumper’s powertrain is that the spring in series with the leg-shape motor is *unilateral* in the sense that it compresses, but does not extend beyond its nominal rest length; instead, once the spring reaches its rest length, the position of the leg-

shape motor and the shape of the virtual leg are rigidly connected, i.e., directly, through a gear ratio, and no longer through a compliant element; see Fig. 5.1(b) for how this is achieved. This is a big advantage in initiating take-off in running since when the leg is lifted from the ground its motion does not have to “fight” a spring that is trying to extend due to the non-zero mass of the shin. Roughly speaking, the spring is present when it is useful for shock attenuation and energy storage, and absent when it would be a hinderance for lifting the leg from the ground.

It is apparent from the above discussion that the presence of the spring and the inertias of the rotating pulleys inside the transmission system introduce dynamic effects that need to be included in a full model of the robot in order to accurately describe its dynamics. This can be done easily by computing the kinetic and potential energies of the transmission, which can then be added (in a scalar fashion) to the kinetic and potential energies of the linkage. Let Q^{tr} be the configuration space of the transmission system, considered to be a simply-connected open subset of \mathbb{S}^3 parameterized by the coordinates³ $q^{\text{tr}} = (q_{LA}; q_{LS}; q_{mLS})$. The kinetic energy $\mathcal{K}^{\text{tr}} : TQ^{\text{tr}} \rightarrow \mathbb{R}$ of the transmission can be computed based on Hypothesis HMT4) and its expression in coordinates is given in Appendix B. Consistent with Hypothesis HMT6), the potential energy $\mathcal{V}^{\text{tr}} : Q^{\text{tr}} \rightarrow \mathbb{R}$ associated with the transmission system corresponds only to the elastic energy of the spring, and in the given coordinates it is obtained by

$$\mathcal{V}^{\text{tr}}(q_{\text{tr}}) = \frac{1}{2}k\theta_{\text{BSpring}}^2 = \frac{1}{2}k_{\text{T}}(\mu_1q_{LS} - \mu_2q_{mLS})^2, \quad (5.5)$$

where k_{T} is the stiffness of the spring. Given the kinetic and potential energies, a model of the dynamics in the transmission can be found using the Lagrangian framework. Such a model for the transmission alone will not be presented here. Instead, the kinetic and potential energies, given by (B.3) of Appendix B and (5.5) above, respectively, will be used in the following section to include the transmission dynamics in the model of Thumper, which will be used for control.

³Notation: semicolons are used to form columns vectors in line, for instance $(q_s; x_{\text{cm}}; y_{\text{cm}})$ will be used instead of $(q'_s, x_{\text{cm}}, y_{\text{cm}})'$

5.3 Dynamics of Thumper in Running

The mathematical model of the dynamics of Thumper in running will be derived in this section according to the hypotheses enumerated in Section 5.1. Figure 5.2 shows a schematic of three links representing Thumper’s torso, thigh, and shin. The figure includes the generalized coordinates describing the configuration of the mechanism and also the mechanical properties of the links.

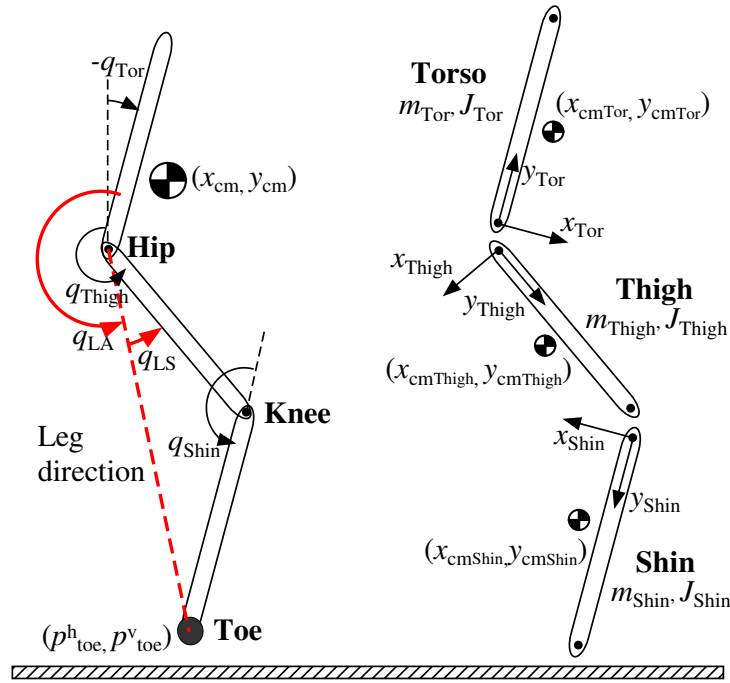


Figure 5.2: A schematic of Thumper used to model running. The transmission system is not shown. Left: “Official” generalized coordinates (q_{LA} ; q_{LS} ; q_{Tor} ; x_{cm} ; y_{cm}) describing linkage configuration, and other important quantities. Right: Mechanical properties of Thumper. The COM of each link is placed outside from the corresponding link to emphasize asymmetry. The moment of inertia of each link is with respect to its COM.

As was mentioned in Section 5.2, the model will include the transmission dynamics, because its role in determining the dynamics of the robot is important. This is one of the main differences with the ASLIP model of Chapter III, where actuation was assumed to be directly available at the leg-angle and leg-length joints without any dynamics involved. Other differences with the model of the ASLIP dynamics include the fact that, as noted in Hypothesis HMT2), Thumper’s model incorporates leg mass and inertia, while

the ASLIP's leg was assumed to be massless. These differences between Thumper and the ASLIP will have significant implications to control design as will be shown in Chapter VI.

5.3.1 Thumper's Unconstrained Dynamics

The configuration space Q_e of the unconstrained dynamics of Thumper is a simply-connected open subset of $\mathbb{S}^4 \times \mathbb{R}^2$ corresponding to physically reasonable configurations of the robot when no constraints act on it, i.e., when the robot does not touch the ground and the spring in the transmission system is allowed to act in both directions, extension and compression. As suggested by Fig. 5.2, a set of coordinates suitable for parameterizing the configuration of the robot's linkage composed by the torso, thigh and shin, is $(q_{LA}; q_{LS}; q_{Tor}; x_{cm}; y_{cm})$. On the other hand, based on the discussion of Section 5.2, the triplet $(q_{LA}; q_{LS}; q_{mLS})$ completely describes the configuration of the transmission system. As a result, the configuration space Q_e of the unconstrained dynamics of Thumper can be parameterized by $q_e := (q_{LA}; q_{LS}; q_{mLS}; q_{Tor}; x_{cm}; y_{cm}) \in Q_e$, describing both the dynamics of the linkage and the transmission system.

The corresponding equations of motion will be obtained using the method of Lagrange. The total kinetic energy $\mathcal{K}_e : TQ_e \rightarrow \mathbb{R}$ of the mechanism can be computed by adding the corresponding kinetic energies \mathcal{K}^{tr} and $\mathcal{K}_e^{\text{link}}$ of the transmission system and the linkage composed by the the torso, thigh and shin, respectively, i.e.,

$$\mathcal{K}_e(q_e, \dot{q}_e) = \mathcal{K}^{tr}(q_e, \dot{q}_e) + \mathcal{K}_e^{\text{link}}(q_e, \dot{q}_e), \quad (5.6)$$

where $\mathcal{K}^{tr}(q_e, \dot{q}_e)$ is given by (B.3) of Appendix B and

$$\begin{aligned} \mathcal{K}_e^{\text{link}}(q_e, \dot{q}_e) &= \frac{1}{2}m_{\text{Tor}}(\dot{x}_{\text{cmTor}}^2 + \dot{y}_{\text{cmTor}}^2) + \frac{1}{2}J_{\text{Tor}}\dot{q}_{\text{Tor}}^2 \\ &+ \frac{1}{2}m_{\text{Thigh}}(\dot{x}_{\text{cmThigh}}^2 + \dot{y}_{\text{cmThigh}}^2) + \frac{1}{2}J_{\text{Thigh}}\dot{q}_{\text{Thigh}}^2 \\ &+ \frac{1}{2}m_{\text{Shin}}(\dot{x}_{\text{cmShin}}^2 + \dot{y}_{\text{cmShin}}^2) + \frac{1}{2}J_{\text{Shin}}\dot{q}_{\text{Shin}}^2. \end{aligned} \quad (5.7)$$

In (5.7), $(\dot{x}_{\text{cm}_i}, \dot{y}_{\text{cm}_i})$, $i \in \{\text{Tor}, \text{Thigh}, \text{Shin}\}$ correspond to the Cartesian velocities of the COM of the torso, thigh, and shin, respectively, and \dot{q}_{Tor} , \dot{q}_{Thigh} , and \dot{q}_{Shin} are the rates of

the absolute angles of the torso, thigh, and shin, respectively, relative to the vertical; see Fig. 5.2. In terms of the generalized coordinates q_e and the corresponding velocities \dot{q}_e , the total kinetic energy \mathcal{K}_e can be written in the quadratic form

$$\mathcal{K}_e(q_e, \dot{q}_e) = \frac{1}{2} \dot{q}_e' D_e(q_s) \dot{q}_e, \quad (5.8)$$

where

$$D_e(q_s) = \begin{bmatrix} A(q_s) & 0_{4 \times 2} \\ 0_{2 \times 4} & mI_{2 \times 2} \end{bmatrix} \quad (5.9)$$

is the unconstrained inertia matrix. In (5.9), $m := m_{\text{Tor}} + m_{\text{Thigh}} + m_{\text{Shin}}$ is the total mass of the robot, and $A \in \mathbb{R}^{4 \times 4}$ is a matrix that depends only on the angular coordinates $q_s := (q_{\text{LA}}; q_{\text{LS}}; q_{\text{mLS}}; q_{\text{Tor}})$, i.e., it is independent of the Cartesian coordinates $(x_{\text{cm}}, y_{\text{cm}})$ of the robot's COM. The block diagonal structure of the inertia matrix D_e reflects the fact that the total kinetic energy is invariant under translations of the body, and it will be put to use in Sections 5.3.4 and 5.3.5 below, where the flight-to-stance and stance-to-flight transition maps representing the impacts that occur at touchdown and liftoff are derived.

Similarly, the total potential energy $\mathcal{V}_e : Q_e \rightarrow \mathbb{R}$ of the mechanism is computed by adding the corresponding potential energies $\mathcal{V}_e^{\text{tr}}$ and $\mathcal{V}_e^{\text{link}}$ of the transmission and the linkage, respectively, that is,

$$\mathcal{V}_e(q_e) = \mathcal{V}_e^{\text{tr}}(q_e) + \mathcal{V}_e^{\text{link}}(q_e), \quad (5.10)$$

where $\mathcal{V}_e^{\text{tr}}$ is given by (5.5) and

$$\mathcal{V}_e^{\text{link}}(q_e) = mgy_{\text{cm}}. \quad (5.11)$$

Notice that, by Hypothesis HMT6), the transmission system contributes to the potential energy of the system only via its elastic energy.

The (unconstrained) Lagrangian $\mathcal{L}_e : TQ_e \rightarrow \mathbb{R}$ can then be defined as usual by

$$\mathcal{L}_e := \mathcal{K}_e - \mathcal{V}_e, \quad (5.12)$$

and the model of the unconstrained robot dynamics can be determined through Lagrange's

equations

$$\frac{d}{dt} \frac{\partial \mathcal{L}_e}{\partial \dot{q}_e} - \frac{\partial \mathcal{L}_e}{\partial q_e} = \Gamma_e, \quad (5.13)$$

where Γ_e is a column array containing the components of the generalized forces⁴ acting on the robot. Using the principle of virtual work, Γ_e is found to be

$$\Gamma_e = B_e u, \quad (5.14)$$

where $u = (u_{LA}; u_{LS}) \in \mathcal{U} \subset \mathbb{R}^2$ contains the actuator torques applied at the robot, and B_e is the corresponding actuation distribution matrix, which, in this particular case, is independent of q_e .

Applying Lagrange's equations (5.13) with the kinetic and potential energies defined by (5.6) and (5.10), respectively, results in the second-order model

$$D_e(q_e)\ddot{q}_e + C_e(q_e, \dot{q}_e)\dot{q}_e + G_e(q_e) = B_e u \quad (5.15)$$

describing the unconstrained dynamics of Thumper. In (5.15), D_e is the mass matrix given by (5.9), C_e contains Coriolis and centrifugal terms, and G_e is the vector of the configuration dependent forces, gravitational and elastic.

5.3.2 Thumper Flight Dynamics

In the flight phase, the robot follows a ballistic motion under the influence of gravity, and hence its dynamics could accurately be represented by the second-order model (5.15). However, based on the fact that the stiffness and damping associated with the spring in the transmission system are large compared to the relatively small mass and inertia of the leg (thigh and shin), it will be assumed that the spring deformation can be neglected

⁴To be precise, a generalized force F should be viewed as a map $F : I \times TQ \rightarrow T^*Q$, $I \subset [0, +\infty)$, that depends (at least) continuously on time $t \in I$, for which $F(t, \dot{q}) \in T_q^*Q$, for each $(t, \dot{q}) \in I \times T_qQ$, $q \in Q$; see [19, p. 189] or [14, pp. 128-130]. Note that if $\gamma : I \rightarrow Q$ is a smooth curve on Q , the force along γ is a *covector* field $\alpha : I \rightarrow TQ^*$ with $\alpha(t) := F(t, \gamma'(t))$. This level of abstractness in defining the notion of a generalized force will not be necessary for developing the models, and hence, by (the usual) abuse of notation, the generalized force is viewed as a column vector.

during the flight phase⁵. This assumption was summarized in Hypothesis HMT5), and it results in a relation constraining the motor position q_{mLS} and the leg shape q_{LS} , obtained by setting $\theta_{\text{Bspring}} = 0$ in (5.4), i.e.

$$q_{\text{mLS}} = \mu q_{\text{LS}}, \quad (5.16)$$

where $\mu = \frac{\mu_1}{\mu_2} = 31.57$ is a constant that depends on the geometry of the pulleys in the transmission system. Equation (5.16) results in the constraint

$$c_f(q_e) = 0, \quad (5.17)$$

where $c_f : Q_e \rightarrow \mathbb{R}$ is a smooth real-valued linear map represented in coordinates by

$$c_f(q_e) := \begin{bmatrix} 0 & -\mu & 1 & 0 & 0 & 0 \end{bmatrix} q_e.$$

Equation (5.17) is an example of a *holonomic* constraint imposed on the configuration space Q_e ; see [85, pp. 265-276] for a detailed treatment of such constraints. This constraint reduces the number of degrees of freedom of the unconstrained model by one. To be precise, (5.17) restricts the motion of the system to a smooth five-dimensional submanifold $Q_f := \{q_e \in Q_e \mid c_f(q_e) = 0\}$ embedded⁶ in the (unconstrained) configuration space Q_e . Note that by differentiating (5.17) with respect to time, the following relation is imposed upon the velocities $\dot{q}_e \in T_{q_e} Q_e$ of the unconstrained system

$$\begin{bmatrix} 0 & -\mu & 1 & 0 & 0 & 0 \end{bmatrix} \dot{q}_e = 0 \Rightarrow E_f \dot{q}_e = 0. \quad (5.18)$$

Geometrically, (5.18) means that the allowable velocities of the system under the (holonomic) constraint (5.17) must be orthogonal to the row matrix E_f . In other words, E_f represents the direction in Q_e along which the system *cannot* move.

To derive the equations of motion for the flight phase, the constraint (5.17) will be

⁵The situation is similar to that of an actuator connected in series with a spring/damper system that pushes a small mass. When the spring stiffness and damping constant are large enough, the spring/damper system can be approximated with a rigid link (for reasonably small accelerations). Remember that the spring in the transmission acts only in the direction of the leg shape, that is, in the direction of the virtual leg length.

⁶This is a consequence of the regular value theorem, see Theorem (5.8), [15, p. 78], in view of the smoothness of the map c_f and the fact that $\partial c_f / \partial x_f \neq 0$ on $c_f^{-1}(\{0\})$.

“eliminated” by representing the dynamics with respect to a set of coordinates parameterizing Q_f . In essence, these new coordinates parameterize the “allowable” motions of the system, and are not subjected to any further constraints. As a result, the generalized coordinates of the flight phase can be selected to be $q_f := (q_{LA}; q_{LS}; q_{Tor}; x_{cm}; y_{cm})$. Then,

$$q_e = \Upsilon_f(q_f), \quad (5.19)$$

where $\Upsilon_f : Q_f \rightarrow Q_e$ is a smooth linear map, which, in coordinates, can be represented by the matrix $Y_f \in \mathbb{R}^{6 \times 5}$,

$$Y_f := \begin{bmatrix} I_{2 \times 2} & 0_{2 \times 3} \\ [0 \ \mu] & 0_{1 \times 3} \\ 0_{3 \times 2} & I_{3 \times 3} \end{bmatrix}. \quad (5.20)$$

Note that, for future use, the flight coordinates q_f can be recovered from the extended model coordinates q_e through the map $\Pi_f : Q_e \rightarrow Q_f$,

$$q_f = \Pi_f(q_e), \quad (5.21)$$

which, in coordinates, is given by the matrix $P_f \in \mathbb{R}^{5 \times 6}$ as

$$P_f := \begin{bmatrix} I_{2 \times 2} & 0_{2 \times 1} & 0_{2 \times 3} \\ 0_{3 \times 2} & 0_{3 \times 1} & I_{3 \times 3} \end{bmatrix}, \quad (5.22)$$

and $\Pi_f \circ \Upsilon_f = \text{id}_{Q_f}$ as suggested by the commutative diagram of Fig. 5.3.

Let $(\mathbf{D}\Upsilon_f)_{q_f} : T_{q_f}Q_f \rightarrow T_{\Upsilon_f(q_f)}Q_e$ denote the differential at a point $q_f \in Q_f$ of the map Υ_f defined by (5.19). Then,

$$\dot{q}_e = (\mathbf{D}\Upsilon_f)_{q_f}(\dot{q}_f), \quad (5.23)$$

where $\dot{q}_f \in T_{q_f}Q_f$ and $\dot{q}_e \in T_{\Upsilon_f(q_f)}Q_e$ are the flight and unconstrained velocity (i.e., tangent) vectors, respectively. The map $(\mathbf{D}\Upsilon_f)_{q_f}$ can be represented in coordinates by the Jacobian matrix $J_f \in \mathbb{R}^{6 \times 5}$, which, in view of (5.20), is simply $J_f = Y_f$, i.e., it is independent of the point $q_f \in Q_f$, resulting in the following relation between the components of the uncon-

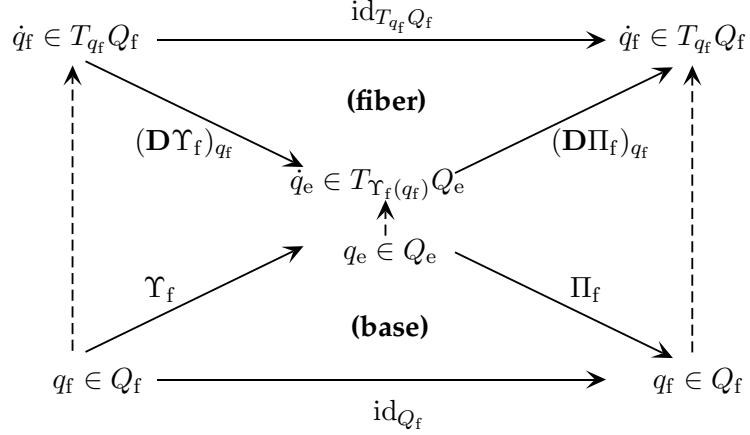


Figure 5.3: A commutative diagram showing mappings between the flight and unconstrained state spaces, TQ_f and TQ_e , respectively.

strained and flight velocities

$$\dot{q}_e = J_f \dot{q}_f. \quad (5.24)$$

In a similar fashion, the differential $D\Pi_f : T_{q_e} Q_e \rightarrow T_{\Pi_f(q_e)} Q_f$ of the map Π_f at a point $q_e \in Q_e$,

$$\dot{q}_f = (D\Pi_f)_{q_e}(\dot{q}_e), \quad (5.25)$$

can be defined in coordinates by the matrix P_f given by (5.22). Note that $(D\Pi_f)_{\Upsilon(q_f)} \circ (D\Upsilon_f)_{q_f} = \text{id}_{T_{q_f} Q_f}$, which, in coordinates, corresponds to $P_f Q_f = I$, $I \in \mathbb{R}^{5 \times 5}$ is the identity matrix.

Remark 5.2. To avoid confusion between the (different) meanings of (5.23) and (5.24), it is clarified that, for reasons of notational convenience, the same symbol \dot{q} is used to denote *both* a tangent vector $\dot{q} \in T_q Q$, and its coordinate representation $[\dot{q}]_{(U, \phi)} \in \mathbb{R}^n$ with respect to a given chart (U, ϕ) of Q . This is standard practice in the control and classical mechanics literature. \triangleleft

Due to the fact that the constraint (5.17) is holonomic, substitution of the constraint equations in the unconstrained Lagrangian \mathcal{L}_e defined by (5.12) is permitted, and will result in the correct equations of motion⁷. Substituting (5.24) in the kinetic energy of the

⁷This *not* true when the constraint is nonholonomic; see [85, p. 274]. In general, for nonholonomic constraints, substitution of the constraint equations to the unconstrained Lagrangian will result in wrong equations of motion.

unconstrained model (5.8), the kinetic energy $\mathcal{K}_f : TQ_f \rightarrow \mathbb{R}$ in the flight phase is found

$$\mathcal{K}_f(q_f, \dot{q}_f) = \frac{1}{2} \dot{q}_f' D_f(q_s) \dot{q}_f, \quad (5.26)$$

with

$$D_f(q_s) = J_f' D_e(q_s) J_f, \quad (5.27)$$

where D_e has been defined in (5.9). Moreover, the total potential energy $\mathcal{V}_f : Q_f \rightarrow \mathbb{R}$ of the mechanism in the flight phase corresponds to the gravitational potential energy of the rigid linkage composed by the torso, thigh and shin. In particular, since, by Hypothesis HMT5), the spring deformation is assumed to be zero in flight, the elastic energy of the spring does not contribute to the total potential energy. Hence,

$$\mathcal{V}_f(q_f) = mgy_{\text{cm}}. \quad (5.28)$$

The Lagrangian $\mathcal{L}_f : TQ_f \rightarrow \mathbb{R}$ can then be defined by $\mathcal{L}_f := \mathcal{K}_f - \mathcal{V}_f$, with the kinetic and potential energies computed by (5.26) and (5.28), respectively⁸, and the model of the robot dynamics in flight can be determined through Lagrange's equations

$$\frac{d}{dt} \frac{\partial \mathcal{L}_f}{\partial \dot{q}_f} - \frac{\partial \mathcal{L}_f}{\partial q_f} = \Gamma_f, \quad (5.29)$$

where Γ_f is an column array containing the components of the generalized forces applied to the robot. By the principle of virtual work, Γ_f is found to be

$$\Gamma_f = B_f u, \quad (5.30)$$

where $u = (u_{LA}; u_{LS}) \in \mathcal{U} \subset \mathbb{R}^2$ contains the actuator torques applied at the robot, and B_f is the corresponding actuation distribution matrix. Applying Lagrange's equations (5.29)

⁸Note that, in view of the substitutions for computing the constrained kinetic and potential energy in (5.26) and (5.28), respectively, $\mathcal{L}_f(q_f, \dot{q}_f) := \mathcal{L}_e(\Upsilon_f(q_f), (\mathbf{D}\Upsilon_f)_{q_f}(\dot{q}_f))$, where \mathcal{L}_e is the unconstrained Lagrangian.

results in the second-order model

$$D_f(q_f)\ddot{q}_f + C_f(q_f, \dot{q}_f)\dot{q}_f + G_f(q_f) = B_f u, \quad (5.31)$$

describing the dynamics of Thumper in flight. The various matrices participating in (5.31) have the meaning described in (5.15). Equation (5.31) illustrates the degree of underactuation of the system in the flight phase. Indeed, during flight the system has five degrees of freedom and only two actuator inputs. As expected, this limited control authority is one of the sources of complexity in the process of designing controllers capable of inducing stable running in Thumper.

Finally, introducing the state vector $x_f := (q_f; \dot{q}_f) \in TQ_f$, the model (5.31) can be brought into standard state-space form by defining

$$\begin{aligned} \dot{x}_f &:= \frac{d}{dt} \begin{bmatrix} q_f \\ \dot{q}_f \end{bmatrix} = \begin{bmatrix} \dot{q}_f \\ D_f^{-1}(q_f)(-C_f(q_f, \dot{q}_f)\dot{q}_f - G_f(q_f) + B_f u) \end{bmatrix} \\ &=: f_f(x_f) + g_f(x_f)u, \end{aligned} \quad (5.32)$$

where $x_f \in TQ_f := \{(q_f; \dot{q}_f) \mid q_f \in Q_f, \dot{q}_f \in T_{q_f}Q_f \cong \mathbb{R}^5\} =: \mathcal{X}_f$ is the state vector.

according to Hypothesis HGT5), the flight phase is terminated when the vertical distance of the toe from the ground becomes zero. The threshold function $H_{f \rightarrow s} : \mathcal{X}_f \rightarrow \mathbb{R}$ given by $H_{f \rightarrow s}(x_f) := p_{\text{toe}}^v$, with p_{toe}^v denoting the vertical distance between the toe and the ground, see Fig. 5.2, signifies the touchdown event at its zero crossing, and defines a smooth switching manifold $\mathcal{S}_{f \rightarrow s}$ in the flight state space \mathcal{X}_f , given by

$$\mathcal{S}_{f \rightarrow s} := \{x_f \in \mathcal{X}_f \mid H_{f \rightarrow s}(x_f) = 0\}. \quad (5.33)$$

Mathematically, transition from flight to stance occurs when the solution of (5.32) pierces the flight-to-stance switching surface $\mathcal{S}_{f \rightarrow s}$.

5.3.3 Thumper Stance Dynamics

In the unconstrained model of Thumper, the Cartesian position $(p_{\text{toe}}^h, p_{\text{toe}}^v)$ of the toe can be expressed in terms of the Cartesian position $(x_{\text{cm}}, y_{\text{cm}})$ of the center of mass and the robot's angular coordinates $q_s := (q_{\text{LA}}; q_{\text{LS}}; q_{\text{mLS}}; q_{\text{Tor}})$ as

$$\begin{bmatrix} p_{\text{toe}}^h \\ p_{\text{toe}}^v \end{bmatrix} = \begin{bmatrix} x_{\text{cm}} \\ y_{\text{cm}} \end{bmatrix} - \Upsilon_{\text{toe}}(q_s), \quad (5.34)$$

where Υ_{toe} is a smooth function of q_s that depends on the robot's geometric parameters, namely, the length, mass, and position of center of mass of each link.

During the stance phase, the toe is in contact with the ground. By Hypothesis HMT3), the toe-ground interaction will be modeled as a frictionless pin-joint rigidly attached to the ground; in particular, the Cartesian velocity of the toe is assumed to be zero throughout the stance phase. Attaching the frame of reference at the (motionless) toe, i.e. $(p_{\text{toe}}^h, y_{\text{toe}}^v) = (0, 0)$, and using (5.34), results in the constraint

$$c_s(q_e) = 0, \quad (5.35)$$

where the map $c_s : Q_e \rightarrow \mathbb{R}^2$ is defined in coordinates by

$$c_s(q_e) := \begin{bmatrix} x_{\text{cm}} \\ y_{\text{cm}} \end{bmatrix} - \Upsilon_s(q_s), \quad (5.36)$$

and it is smooth, a property inherited by the smoothness of Υ_{toe} . The rank⁹ of c_s is equal to two everywhere in Q_e , reflecting the independence of the constraints defined by (5.35).

Equation (5.35) restricts the motion of the system on a smooth four-dimensional sub-manifold

$$Q_s := \{q_e \in Q_e \mid c_s(q_e) = 0\} \quad (5.37)$$

embedded in the (unconstrained) configuration space Q_e , and, similarly to the constraint

⁹Let $c : \mathcal{U} \rightarrow \mathbb{R}^m$ be a C^1 -mapping of an open set $\mathcal{U} \subset \mathbb{R}^n$. Then, the rank of c at a point $q \in \mathcal{U}$ is simply the rank of the Jacobian $\frac{\partial c}{\partial q}(q)$ of c at q ; see [15, p. 46].

(5.17) imposed in the flight phase, it belongs to the family of holonomic constraints. Intuitively, the space Q_s contains all the configurations in Q_e that are compatible with (5.35). Therefore, as was done in deriving the flight dynamics, the constraint can be “eliminated” by choosing to represent the system’s dynamics with respect to a set of coordinates on Q_s , essentially parameterizing the “allowable” motions of the system. These new coordinates subject to no further constraints.

In what follows, the generalized coordinates for the stance phase are selected to be $q_s := (q_{LA}; q_{LS}; q_{mLS}; q_{Tor})$ so that

$$q_e = \Upsilon_s(q_s), \quad (5.38)$$

where $\Upsilon_s : Q_s \rightarrow Q_e$ is a (smooth) map whose representation in coordinates is given by

$$\Upsilon_s(q_s) := \begin{bmatrix} q_s \\ \Upsilon_{toe}(q_s) \end{bmatrix}. \quad (5.39)$$

For future use, it is mentioned here that the stance coordinates q_s can be recovered from the extended model coordinates q_e through the map $\Pi_s : Q_e \rightarrow Q_s$,

$$q_s = \Pi_s(q_e), \quad (5.40)$$

which, in coordinates, is given by the matrix $P_s \in \mathbb{R}^{5 \times 6}$ as

$$P_s := \begin{bmatrix} I_{4 \times 4} & 0_{4 \times 2} \end{bmatrix}, \quad (5.41)$$

and $\Pi_s \circ \Upsilon_s = \text{id}_{Q_s}$ as suggested by the commutative diagram of Fig. 5.4.

Let $(\mathbf{D}\Upsilon_s)_{q_s} : T_{q_s}Q_s \rightarrow T_{\Upsilon_s(q_s)}Q_e$ denote the differential at the point $q_s \in Q_s$ of the map Υ_s defined by (5.38). Then the unconstrained and the stance velocity vectors, \dot{q}_e , \dot{q}_s , respectively, are related via

$$\dot{q}_e = (\mathbf{D}\Upsilon_s)_{q_s}(\dot{q}_s). \quad (5.42)$$

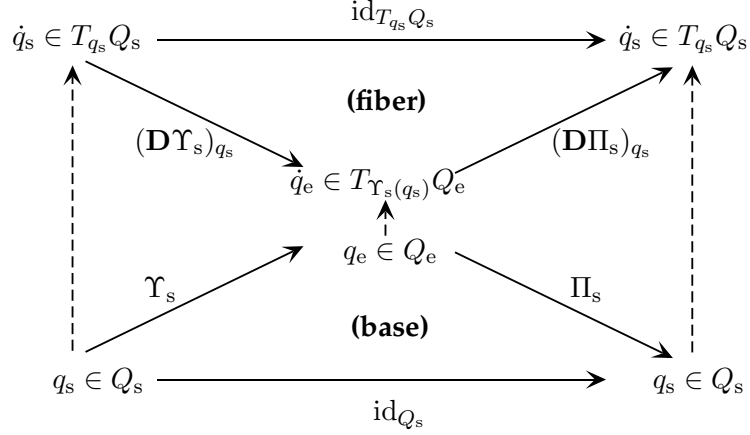


Figure 5.4: A commutative diagram showing mappings between the stance and unconstrained model state spaces, TQ_s and TQ_e , respectively.

The map $(D\Upsilon_s)_{q_s}$ can be represented in coordinates by the Jacobian matrix $J_s(q_s) \in \mathbb{R}^{6 \times 4}$

$$J_s(q_s) := \begin{bmatrix} I_{4 \times 4} \\ \frac{\partial \Upsilon_{\text{toe}}}{\partial q_s}(q_s) \end{bmatrix}, \quad (5.43)$$

resulting in the following relation between the coordinate arrays of the tangent vectors \dot{q}_s and \dot{q}_e ,

$$\dot{q}_e = J_s(q_s)\dot{q}_s. \quad (5.44)$$

In a similar fashion, the differential $D\Pi_s : T_{q_e} Q_e \rightarrow T_{\Pi_s(q_e)} Q_s$, at a point $q_e \in Q_e$ of the map Π_s is defined, so that

$$\dot{q}_s = (D\Pi_s)_{q_e}(\dot{q}_e), \quad (5.45)$$

and it can be represented by the matrix $P_s \in \mathbb{R}^{4 \times 6}$, defined by (5.41). Note that $(D\Pi_s)_{\Upsilon(q_s)} \circ (D\Upsilon_s)_{q_s} = \text{id}_{T_{q_s} Q_s}$, which, in coordinates, corresponds to the matrix product $P_s J_s = I$; $I \in \mathbb{R}^{4 \times 4}$ is the identity matrix. As a reminder, note that, according to Remark 5.2, the same symbol q is used to denote both a point on a manifold and its coordinate representation. The same holds for tangent vectors and their coordinate representations, which are both denoted by \dot{q} . Then, (5.42) refers to relating tangent vectors, while (5.44) refers to relating their coordinate representations.

Substituting (5.44) in the coordinate representation of the kinetic energy of the uncon-

strained model (5.8), the stance phase kinetic energy $\mathcal{K}_s : TQ_s \rightarrow \mathbb{R}$ can be computed by

$$\mathcal{K}_s(q_s, \dot{q}_s) = \frac{1}{2} \dot{q}_s' D_s(q_s) \dot{q}_s, \quad (5.46)$$

where

$$D_s(q_s) = J_s'(q_s) D_e(q_s) J_s(q_s) = A(q_s) + m \left(\frac{\partial \Upsilon_{\text{toe}}}{\partial q_s}(q_s) \right)' \left(\frac{\partial \Upsilon_{\text{toe}}}{\partial q_s}(q_s) \right), \quad (5.47)$$

in view of (5.9) for substituting D_e . On the other hand, the potential energy $\mathcal{V}_s : Q_s \rightarrow \mathbb{R}$ during the stance phase can be computed in coordinates as in the case of the unconstrained system (5.10), i.e.

$$\mathcal{V}_s(q_s) = mgy_{\text{cm}}(q_s) + \frac{1}{2} k_T (\theta_{\text{Bspring}}(q_s))^2, \quad (5.48)$$

where k_T is the stiffness of the spring and θ_{Bspring} its deformation computed by (5.4) as a function of the stance configuration variables.

Define the (constrained) Lagrangian $\mathcal{L}_s : TQ_s \rightarrow \mathbb{R}$ in the usual way by $\mathcal{L}_s := \mathcal{K}_s - \mathcal{V}_s$, with the kinetic and potential energy computed by (5.46) and (5.48), respectively. Then, the model of Thumper in the stance phase can be determined through Lagrange's equations

$$\frac{d}{dt} \frac{\partial \mathcal{L}_s}{\partial \dot{q}_s} - \frac{\partial \mathcal{L}_s}{\partial q_s} = \Gamma_s, \quad (5.49)$$

where Γ_s is a column array containing the components of the generalized forces applied at the robot. By the principle of virtual work, Γ_s is given by

$$\Gamma_s = B_s u. \quad (5.50)$$

As before, $u = (u_{\text{LA}}; u_{\text{LS}}) \in \mathcal{U} \subset \mathbb{R}^2$ is the vector of the actuator inputs and B_s is the corresponding actuation distribution matrix. Applying Lagrange's equations (5.49) results in the second-order model

$$D_s(q_s) \ddot{q}_s + C_s(q_s, \dot{q}_s) \dot{q}_s + G_s(q_s) = B_s u, \quad (5.51)$$

describing the dynamics of Thumper in stance. The various matrices participating in (5.51) have the usual interpretations as in (5.15).

By Hypothesis HMT3), one of the key assumptions in deriving (5.51) is that the toe-ground interaction can be captured by a frictionless unactuated revolute joint. This approximation, however, would require the development of bilateral constraint forces that can keep the toe in contact with the ground throughout the stance phase. In reality, this cannot happen for two reasons. First, the associated friction cone limitations restrict the magnitude of the developed ground reaction forces. Second, the toe can only push against the ground, it cannot pull the ground (unilateral vertical component of the ground reaction force). As a result, the validity of the model (5.51) must be checked by computing the associated constraint forces, that is, the forces required to ensure that the system remains on the constraint surface Q_s defined by the constraint (5.35). This computation can be done by incorporating the constraint forces in the unconstrained dynamics using Lagrange multipliers, and is detailed below.

As was mentioned in the derivation of the constraint (5.35), the Cartesian velocity of the toe is assumed to be zero throughout the stance phase, i.e., $\dot{p}_{\text{toe}}^h = \dot{p}_{\text{toe}}^v = 0$. By differentiating (5.35) with respect to time, this assumption results in the following relation imposed upon the velocities $\dot{q}_e \in T_{q_e}Q_e$ of the unconstrained system

$$\begin{bmatrix} -\frac{\partial \Upsilon_{\text{toe}}}{\partial q_s}(q_s) & I_{2 \times 2} \end{bmatrix} \begin{bmatrix} \dot{q}_s \\ \dot{x}_{\text{cm}} \\ \dot{y}_{\text{cm}} \end{bmatrix} = 0 \Leftrightarrow E_s(q_s)\dot{q}_e = 0, \quad (5.52)$$

where $E_s \in \mathbb{R}^{2 \times 6}$. Geometrically, (5.52) means that the allowable velocities of the system under the (holonomic) constraint (5.35) must be orthogonal to the rows of the matrix E_s . In other words, the rows of E_s represent the directions in Q_e along which the system *cannot* move. Notice that, by (5.52), $\dot{q}_e \in \mathcal{N}(E_s)$, the nullspace of E_s . Hence, the unconstrained velocity \dot{q}_e can be written as a linear combination of any set of basis vectors of $\mathcal{N}(E_s)$, whose coefficients correspond to the components of the independent velocity. Selecting the columns of the matrix J_s defined in (5.43) as the basis of $\mathcal{N}(E_s)$ results in \dot{q}_s being the

independent velocities, consistent to the coordinates selected to parameterize Q_s .

Let F_{ext} denote the *constraint forces*¹⁰ associated with the constraint (5.52). In words, these are the forces that are generated during stance to ensure that the system does not move in the directions given by the rows of E_s . Therefore, the constraint forces can be viewed as acting along the directions of the rows of E_s with magnitude chosen so that the system remains on the constraint hypersurface Q_s . As a result, these forces can be written as linear combinations of the rows of E_s —equivalently, of the columns of E'_s —i.e.,

$$F_{\text{ext}} = E'_s(q_s)F_{\text{toe}}, \quad (5.53)$$

where $F_{\text{toe}} = (F_{\text{toe}}^T; F_{\text{toe}}^N)$ includes the relative magnitudes of the constraint forces, and corresponds to the ground reaction forces applied at the toe. Note that the constraint forces, so defined, do no work on the system since

$$\begin{aligned} F'_{\text{ext}}\dot{q}_e &= F'_{\text{toe}}E_s(q_s)J_s(q_s)\dot{q}_s \\ &= F'_{\text{toe}} \begin{bmatrix} -\frac{\partial \Upsilon_{\text{toe}}}{\partial q_s}(q_s) & I_{2 \times 2} \end{bmatrix} \begin{bmatrix} I_{4 \times 4} \\ \frac{\partial \Upsilon_{\text{toe}}}{\partial q_s}(q_s) \end{bmatrix} \dot{q}_s \\ &= 0 \end{aligned}$$

Therefore, using the Lagrange-d'Alembert principle, the constraint forces can be incor-

¹⁰In precise terms, and for constraints linear in the velocities such as (5.52), the *constraint force* is formally defined as a force taking values in the annihilator of the distribution

$$\mathcal{D}_q := \{\dot{q} \in T_q Q \mid E(q)\dot{q} = 0\};$$

see [14, p. 212] and [19, p. 204]. This distribution is the subspace of the tangent space $T_q Q$ of Q at q consisting of the vectors \dot{q} satisfying the constraints. To understand the physical motivation for this definition note that a (time-independent) generalized force F should be viewed as a map $F : TQ \rightarrow T^*Q$, for which $F_q(\dot{q}) \in T^*_q Q$, for each $\dot{q} \in T_q Q$, $q \in Q$. On the other hand, in the Lagrangian setting, if $\gamma : I \subset \mathbb{R} \rightarrow Q$ is a smooth curve on Q , the work W done by F along γ is

$$W(F, \gamma) = \int_I \langle F_{\gamma(t)}(\gamma'(t)); \gamma'(t) \rangle dt,$$

where $\langle \cdot; \cdot \rangle$ is the natural pairing between vectors and covectors. With these in mind, the physical motivation for the definition of the constraint forces becomes apparent: constraint forces do no work along curves that satisfy the constraint, so that the Lagrange-d'Alembert principle is satisfied. Indeed, if the path γ is such that $\gamma'(t) \in \mathcal{D}_{\gamma(t)}$, for all $t \in I$, then the corresponding constraint force $F_{\gamma(t)}(\gamma'(t)) \in \text{ann}(\mathcal{D}_{\gamma(t)})$, the annihilator of $\mathcal{D}_{\gamma(t)}$, so that the work $W(F, \gamma) = 0$.

porated in the dynamics, which now takes the form

$$\frac{d}{dt} \frac{\partial \mathcal{L}_e}{\partial \dot{q}_e} - \frac{\partial \mathcal{L}_e}{\partial q_e} = \Gamma_e + F_{\text{ext}}, \quad (5.54)$$

resulting in the following system of second-order differential equations describing the constrained dynamics

$$D_e(q_e)\ddot{q}_e + C_e(q_e, \dot{q}_e)\dot{q}_e + G_e(q_e) = B_e u + E'_s(q_s)F_{\text{toe}}. \quad (5.55)$$

Given (5.52) and (5.55), the ground reaction force F_{toe} can be computed as follows. Differentiating (5.52) with respect to time yields

$$E_s(q_s)\ddot{q}_e + \dot{E}_s(q_s)\dot{q}_e = 0 \quad (5.56)$$

and, solving for \ddot{q}_e from (5.55) and substituting to (5.56) results in the following expression for F_{toe} ,

$$F_{\text{toe}} = (E_s(q_s)D_e(q_s)E'_s(q_s))^{-1} \left(E_s(q_s)D_e^{-1}(q_s) (-C_e(q_e, \dot{q}_e)\dot{q}_e - G_e(q_e) + B_e u) + \dot{E}_s(q_s)\dot{q}_s \right), \quad (5.57)$$

where the invertibility of the configuration-dependent matrix $E_s D_e E'_s$ is a consequence of the independence of the constraints. Using (5.57), the constraint forces F_{toe} can be computed based on knowledge of the input u , the current state $(q_s; \dot{q}_s)$, and equations (5.38) and (5.42).

Therefore, for the stance model (5.51) to be valid, i.e., consistent with the hypotheses that were used to derive it—in particular, with Hypothesis HGT3—it must be verified that

$$F_{\text{toe}}^N > 0 \quad (5.58)$$

and

$$|F_{\text{toe}}^T| \leq \mu_s F_{\text{toe}}^N, \quad (5.59)$$

where μ_s is the assumed coefficient of static friction. In words, (5.58) means that toe is never pulling the ground, while (5.59) corresponds to no sliding occurring at the toe-ground contact.

Finally, introducing the state vector $x_s := (q_s; \dot{q}_s) \in TQ_s$, the model (5.51) can be brought into standard state-space form as

$$\begin{aligned} \dot{x}_s &:= \frac{d}{dt} \begin{bmatrix} q_s \\ \dot{q}_s \end{bmatrix} = \begin{bmatrix} \dot{q}_s \\ D_s^{-1}(q_s)(-C_s(q_s, \dot{q}_s)\dot{q}_s - G_s(q_s) + B_s u) \end{bmatrix} \\ &=: f_s(x_s) + g_s(x_s)u, \end{aligned} \quad (5.60)$$

where $x_s \in TQ_s := \{(q_s; \dot{q}_s) \mid q_s \in Q_s, \dot{q}_s \in T_{q_s}Q_s \cong \mathbb{R}^4\}$ is the state vector.

The stance phase is terminated when the vertical component F_{toe}^N of the ground reaction force becomes zero. Then, the threshold function $H_{s \rightarrow f} : TQ_s \times \mathcal{U} \rightarrow \mathbb{R}$ given by $H_{s \rightarrow f}(x_s, u) := F_{\text{toe}}^N$, signifies the liftoff event at its zero crossing, and defines a smooth switching manifold $\mathcal{S}_{s \rightarrow f}$ in the product space¹¹, $TQ_s \times \mathcal{U}$ given by

$$\mathcal{S}_{s \rightarrow f} := \{(x_s, u) \in TQ_s \times \mathcal{U} \mid H_{s \rightarrow f}(x_s, u) = 0\}. \quad (5.61)$$

Mathematically, transition from flight to stance occurs when the solution of (5.60) pierces $\mathcal{S}_{s \rightarrow f}$.

Remark 5.3. It should be mentioned here that, when the stance feedback controller $\Gamma_s^c : TQ_s \rightarrow \mathcal{U}$, $u = \Gamma_s^c(x_s)$ is introduced, transition from stance to flight is a control decision; see Remark 6.5 and (6.32) in Chapter VI for details. \triangleleft

5.3.4 Thumper Flight-to-Stance Transition Model

The purpose of this section is to provide a model that describes the behavior of the robot in transition from the flight to the stance phase. Mathematically, the flight-to-stance

¹¹Since by (5.57) the value of F_{toe}^N depends on the input $u \in \mathcal{U}$, the stance-to-flight threshold function $H_{s \rightarrow f}$ is a real-valued function defined on the fiber bundle $(\pi, B, TQ_s, \mathcal{U})$, where $\pi : B \rightarrow TQ_s$ is a surjective submersion and, for each $x_s \in TQ_s$, the fibers $\pi^{-1}(x_s)$ are (locally) diffeomorphic to $\{x_s\} \times \mathcal{U}$. Due to the fact that the input space $\mathcal{U} = \mathbb{R}^2$ is independent of the state, the fiber bundle $(\pi, B, TQ_s, \mathcal{U})$ is a trivial bundle, hence, it (globally) possesses the product structure $TQ_s \times \mathcal{U}$, i.e., $B = TQ_s \times \mathcal{U}$.

transition can be modeled as a discrete map $\Delta_{f \rightarrow s} : \mathcal{S}_{f \rightarrow s} \rightarrow \mathcal{X}_s$ taking the (final) states $x_f^- \in \mathcal{S}_{f \rightarrow s} \subset \mathcal{X}_f$ of the flight phase to the (initial) states $x_s^+ \in \mathcal{X}_s$ of the stance phase. This is similar to what was done in the ASLIP, where, though, the flight-to-stance transition map was merely a coordinate transformation, reflecting the fact that no energy was lost at impact due to the leg being massless and the spring acting in the leg direction.

Instead, in Thumper, the flight-to-stance transition map $\Delta_{f \rightarrow s}$ should capture the physics of the impact and, in particular, it should include the effects of the compliance in the transmission system. Indeed, as was mentioned in the introduction, one of the beneficial aspects of physical series compliance is the effect of isolating the impulsive forces developed during impact from the motorshaft. Hence, it is imperative that the impact model *includes* the spring of the transmission system, which was, however, *excluded* from the flight dynamics model derived in Section 5.3.2. As a result, to develop the impact model, the unconstrained model of the robot developed in Section 5.3.1 will be used in a way that is detailed below.

Let $x_f^- = (q_f^-; \dot{q}_f^-) \in \mathcal{S}_{f \rightarrow s}$ be the final state of the flight phase. The flight-to-stance transition map $\Delta_{f \rightarrow s} : \mathcal{S}_{f \rightarrow s} \rightarrow \mathcal{X}_s$,

$$x_s^+ = \Delta_{f \rightarrow s}(x_f^-), \quad (5.62)$$

where $x_s^+ \in \mathcal{X}_s$ is the initial state in the stance phase, will be derived by constructing the corresponding base and fiber components $\Delta_{f \rightarrow s}^q : Q_f \rightarrow Q_s$ and $(\Delta_{f \rightarrow s}^{\dot{q}})_{q_f} : T_{q_f} Q_f \rightarrow T_{\Delta_{f \rightarrow s}^q(q_f)} Q_s$, respectively, i.e.,

$$\Delta_{f \rightarrow s}(x_f^-) := \begin{bmatrix} \Delta_{f \rightarrow s}^q(q_f^-) \\ (\Delta_{f \rightarrow s}^{\dot{q}})_{q_f^-}(\dot{q}_f^-) \end{bmatrix}, \quad (5.63)$$

so that the diagram in Fig. 5.5 commutes.

First, the initial configuration $q_s^+ \in Q_s$ of the upcoming stance phase is computed, given the final configuration $q_f^- \in Q_f$ of the previous flight phase. By (5.19), $q_e^- = \Upsilon_f(q_f^-)$. Since, by Hypothesis HIT5), the configuration is assumed to be invariant under impact, we have that $q_e^+ = q_e^-$; in the notation of Fig. 5.5, this corresponds to the action of the identity

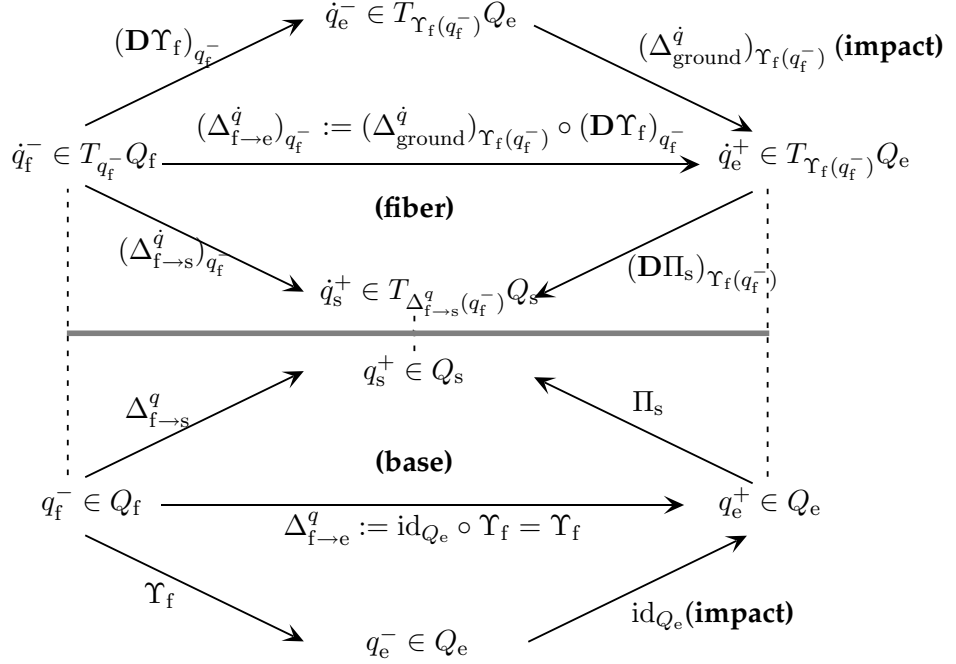


Figure 5.5: A commutative diagram showing the construction of the flight-to-stance transition map $\Delta_{f \to s}$. The coordinate representations of the various maps appearing in this figure are provided in the text. The bottom part corresponds to the construction of the base component $\Delta_{f \to s}^q$ and the upper part to the construction of the fiber component $\Delta_{f \to s}^{\dot{q}}$, which is *not* the differential of $\Delta_{f \to s}^q$ as in the ASLIP. Note that the “lift” to TQ_e is necessary for including the effects of compliance in the impact model.

map id_{Q_e} on Q_e . Then, the initial configuration q_s^+ is computed via (5.40) as $q_s^+ = \Pi_s(q_e^+)$.

Thus, the map $\Delta_{f \to s}^q$ can be defined by the composition,

$$\Delta_{f \to s}^q := \Pi_s \circ \text{id}_{Q_e} \circ \Upsilon_f = \Pi_s \circ \Upsilon_f, \quad (5.64)$$

as suggested by the bottom part of Fig. 5.5. Finally, using the coordinate representation Y_f and P_s of the maps Υ_f and Π_s , defined by (5.20) and (5.41), respectively, the map $\Delta_{f \to s}^q$ can be represented in coordinates by the matrix

$$P_s Y_f = \begin{bmatrix} 1 & 0 & 0 & 0 & 0 \\ 0 & 1 & 0 & 0 & 0 \\ 0 & \mu & 0 & 0 & 0 \\ 0 & 0 & 1 & 0 & 0 \end{bmatrix}. \quad (5.65)$$

The next step is to derive the map $(\Delta_{f \rightarrow s}^{\dot{q}})_{q_f^-} : T_{q_f^-} Q_f \rightarrow T_{\Delta_{f \rightarrow s}^q(q_f^-)} Q_s$, which, given the final configuration $q_f^- \in Q_f$ of the flight phase, takes its final velocities $\dot{q}_f^- \in T_{q_f^-} Q_f$ into the initial velocities $\dot{q}_s^+ \in T_{q_s^+} Q_s$ of the stance phase. By (5.23), $\dot{q}_e^- = (\mathbf{D}\Upsilon_f)_{q_f^-}(\dot{q}_f^-)$. If $(\Delta_{\text{ground}}^{\dot{q}})_{q_e} : T_{q_e} Q_e \rightarrow T_{q_e} Q_e$ denotes the impact map taking pre-impact to post-impact velocities, then $\dot{q}_e^+ = (\Delta_{\text{ground}}^{\dot{q}})_{q_e^+}(\dot{q}_e^-)$ is the post-impact unconstrained velocity vector. From \dot{q}_e^+ the required stance phase initial velocities can be computed by (5.45), i.e., $\dot{q}_s^+ = (\mathbf{D}\Pi_s)_{q_e^+}(\dot{q}_e^+)$, so that, consistent with the upper part of Fig. 5.5, the desired map $(\Delta_{f \rightarrow s}^{\dot{q}})_{q_f^-} : T_{q_f^-} Q_f \rightarrow T_{\Delta_{f \rightarrow s}^q(q_f^-)} Q_s$ can be defined by the composition

$$(\Delta_{f \rightarrow s}^{\dot{q}})_{q_f^-} := (\mathbf{D}\Pi_s)_{\Upsilon_f(q_f^-)} \circ (\Delta_{\text{ground}}^{\dot{q}})_{\Upsilon_f(q_f^-)} \circ (\mathbf{D}\Upsilon_f)_{q_f^-}. \quad (5.66)$$

Since the coordinate representations of the maps $(\mathbf{D}\Upsilon_f)_{q_f}$ and $(\mathbf{D}\Pi_s)_{q_e}$ are given by the matrices Y_f and P_s specified by (5.20) and (5.41), respectively, the focus will be on obtaining the map $(\Delta_{\text{ground}}^{\dot{q}})_{q_e}$ in coordinates.

In what follows, and according to what mentioned in Remark 5.2, let q_e^+ and \dot{q}_e^+ denote the *coordinates* of the post-impact configuration and velocity vector of the unconstrained model, respectively. As was indicated by Hypothesis HIT2), after impact the toe does not slip or rebound, i.e., the velocity of the toe after impact is assumed to be zero. Consistent with the development in Section 5.3.3 for deriving the stance dynamics, this condition can be described by the holonomic constraint

$$E_s(q_{e,1:4}^-) \dot{q}_{e,1:4}^+ = 0, \quad (5.67)$$

which corresponds to (5.52) *evaluated* at the post-impact instant, where the stance kinematics is in effect. In (5.67) and according to hypothesis HIT5), the invariance of configuration under the impact, i.e., $q_{e,1:4}^+ = q_{e,1:4}^-$ was used.

Let δF_{ext} be the vector of the constraint forces developed at impact to ensure that the toe neither slips not rebounds. From Hypothesis HIT3), these forces are impulsive, hence the notation δF_{ext} . In accordance to (5.53) for computing the stance phase constraint forces,

δF_{ext} can be written as

$$\delta F_{\text{ext}} = E'_s(q_{e,1:4})\delta F_{\text{toe}}, \quad (5.68)$$

and, similarly to what was done in Section 5.3.3, it can be incorporated to the dynamics, which takes the form

$$D_e(q_e)\ddot{q}_e + C_e(q_e, \dot{q}_e)\dot{q}_e + G_e(q_e) = B_e u + \delta F_{\text{ext}}. \quad (5.69)$$

Under Hypotheses HIT1)-HIT5), (5.69) can be “integrated” over the “duration” of the impact to obtain

$$D_e(q_{e,1:4}^+)\dot{q}_e^+ - D_e(q_{e,1:4}^-)\dot{q}_e^- = F_{\text{ext}}^\uparrow, \quad (5.70)$$

where $F_{\text{ext}}^\uparrow := \int_{t^-}^{t^+} \delta F_{\text{ext}}(\tau) d\tau$ is the result of integrating the impulsive constraint forces over the impact duration. Notice that the notation “ F_{ext}^\uparrow ” was used to distinguish external forces during impact from the external forces “ F_{ext} ” during the stance phase in (5.54). Due to the invariance of configuration at impact and using (5.68), we have

$$\begin{aligned} F_{\text{ext}}^\uparrow &= \int_{t^-}^{t^+} \delta F_{\text{ext}}(\tau) d\tau \\ &= \int_{t^-}^{t^+} E'_s(q_{e,1:4}(\tau)) \delta F_{\text{toe}}(\tau) d\tau \\ &= E'_s(q_{e,1:4}^-) \int_{t^-}^{t^+} \delta F_{\text{toe}}(\tau) d\tau \\ &= E'_s(q_{e,1:4}^-) F_{\text{toe}}^\uparrow, \end{aligned}$$

where $F_{\text{toe}}^\uparrow := \int_{t^-}^{t^+} \delta F_{\text{toe}}(\tau) d\tau$ is the result of integrating the impulsive ground reaction forces over the impact duration. Again, the notation “ F_{toe}^\uparrow ” was used to distinguish the ground reaction forces developed at impact from the ground reaction forces “ F_{toe} ” during the stance phase in (5.55). Then, substitution to (5.70) gives

$$D_e(q_{e,1:4}^+)\dot{q}_e^+ - D_e(q_{e,1:4}^-)\dot{q}_e^- = E'_s(q_{e,1:4}^-)F_{\text{toe}}^\uparrow,$$

which, combined with (5.67), results in

$$\begin{bmatrix} D_e(q_{e,1:4}^-) & -E_s'(q_{e,1:4}^-) \\ E_s(q_{e,1:4}^-) & 0_{2 \times 2} \end{bmatrix} \begin{bmatrix} \dot{q}_e^+ \\ F_{\text{toe}}^\uparrow \end{bmatrix} = \begin{bmatrix} D_e(q_{e,1:4}^-) \dot{q}_e^- \\ 0_{2 \times 1} \end{bmatrix}. \quad (5.71)$$

Equation (5.71) represents an algebraic system of eight equations with eight unknowns, namely the six entries of the array \dot{q}_e^+ and the two components—tangential and normal, $(F_{\text{toe}}^\uparrow)^T$ and $(F_{\text{toe}}^\uparrow)^N$, respectively—of the ground reaction force F_{toe}^\uparrow . Equivalently, using the block-diagonal structure of D_e presented in (5.9) and the definition of E_s by (5.52), the system (5.71) can be expanded as

$$\begin{bmatrix} A(q_{e,1:4}^-) & 0_{4 \times 2} & \left(\frac{\partial \Upsilon_{\text{toe}}}{\partial q_s}(q_{e,1:4}^-) \right)' \\ 0_{2 \times 4} & mI_{2 \times 2} & -I_{2 \times 2} \\ -\frac{\partial \Upsilon_{\text{toe}}}{\partial q_s}(q_{e,1:4}^-) & I_{2 \times 2} & 0_{2 \times 2} \end{bmatrix} \begin{bmatrix} \dot{q}_{e,1:4}^+ \\ \begin{bmatrix} \dot{x}_{\text{cm}}^+ \\ \dot{y}_{\text{cm}}^+ \end{bmatrix} \\ F_{\text{toe}}^\uparrow \end{bmatrix} = \begin{bmatrix} A(q_{e,1:4}^-) \dot{q}_{e,1:4}^- \\ m \begin{bmatrix} \dot{x}_{\text{cm}}^- \\ \dot{y}_{\text{cm}}^- \end{bmatrix} \\ 0_{2 \times 1} \end{bmatrix}. \quad (5.72)$$

Remark 5.4. The notation “ $\frac{\partial \Upsilon_{\text{toe}}}{\partial q_s}(q_{e,1:4}^-)$ ” is to be understood as “ $\frac{\partial \Upsilon_{\text{toe}}}{\partial q_s}$ evaluated at a point $q_s \in Q_s$ with coordinates equal to $q_{e,1:4}^-$.” This is because, in coordinates $q_s^+ = q_{e,1:4}^+ = q_{e,1:4}^-$, although, as points, q_s^+ and q_e^+ belong to different manifolds. \triangleleft

Using the last two lines of the matrix equation (5.72), the vector F_{toe}^\uparrow can be found as

$$F_{\text{toe}}^\uparrow = m \left(\frac{\partial \Upsilon_{\text{toe}}}{\partial q_s}(q_{e,1:4}^-) \dot{q}_{e,1:4}^+ - \begin{bmatrix} \dot{x}_{\text{cm}}^- \\ \dot{y}_{\text{cm}}^- \end{bmatrix} \right). \quad (5.73)$$

Substituting this into the first and second lines of (5.72) and rearranging yields

$$\begin{aligned} \dot{q}_{e,1:4}^+ &= \left[A(q_{e,1:4}^-) + m \left(\frac{\partial \Upsilon_{\text{toe}}}{\partial q_s}(q_{e,1:4}^-) \right)' \left(\frac{\partial \Upsilon_{\text{toe}}}{\partial q_s}(q_{e,1:4}^-) \right) \right]^{-1} \\ &\quad \left[A(q_{e,1:4}^-) \mid m \left(\frac{\partial \Upsilon_{\text{toe}}}{\partial q_s}(q_{e,1:4}^-) \right)' \right] \dot{q}_{e,1:4}^-, \end{aligned} \quad (5.74)$$

and

$$\begin{bmatrix} \dot{x}_{\text{cm}}^+ \\ \dot{y}_{\text{cm}}^+ \end{bmatrix} = \frac{\partial \Upsilon_{\text{toe}}}{\partial q_s}(q_{e,1:4}^-) \dot{q}_{e,1:4}^+, \quad (5.75)$$

as was expected from the stance phase geometry, which is in effect at the post-impact instant. In (5.73), (5.74) and (5.75), the dependence on $q_{e,1:4}^-$ is to be understood in the meaning explained in Rem. 5.4. Notice that the matrix inverted in (5.74) corresponds to the inertia matrix D_s of the stance phase as suggested by (5.47), whose inverse always exists. This is a consequence of the independence of the constraints. Equation (5.74) indicates that the robot's velocity vector after impact $\dot{q}_{e,1:4}^+$ is a linear expression of the unconstrained velocity vector \dot{q}_e^- before impact.

From (5.74) and (5.75), the coordinate representation $J_{\text{ground}}(q_e) \in \mathbb{R}^{6 \times 6}$ of the map $(\Delta_{\text{ground}}^{\dot{q}})_{q_e}$ used in (5.66) can be written as follows

$$J_{\text{ground}}(q_e^-) = \begin{bmatrix} M(q_e^-) & 0_{4 \times 2} \\ \frac{\partial \Upsilon_{\text{toe}}}{\partial q_s}(q_e^-) M(q_e^-) & 0_{2 \times 2} \end{bmatrix}, \quad (5.76)$$

where

$$M(q_e^-) = \begin{bmatrix} A(q_{e,1:4}^-) + m \left(\frac{\partial \Upsilon_{\text{toe}}}{\partial q_s}(q_{e,1:4}^-) \right)' \left(\frac{\partial \Upsilon_{\text{toe}}}{\partial q_s}(q_{e,1:4}^-) \right) \\ \left[A(q_{e,1:4}^-) \mid m \left(\frac{\partial \Upsilon_{\text{toe}}}{\partial q_s}(q_{e,1:4}^-) \right)' \right] \end{bmatrix}^{-1}$$

Given (5.76), the fiber component $(\Delta_{f \rightarrow s}^{\dot{q}})_{q_f}$ of the flight-to-stance transition map $\Delta_{f \rightarrow s}$ can be computed with respect to the chosen coordinates for Q_f and Q_s using the corresponding representations of the maps participating in (5.66). Putting all the ingredients together, namely, the coordinate representations of the maps (5.64) and (5.66) determined in this section, the flight-to-stance transition map $\Delta_{f \rightarrow s}$ can be specified in a form useful for computations.

Remark 5.5. It is important to note that the validity of the impact model must be checked at each impact. More specifically, each time (5.62) is evaluated, the corresponding ground reaction forces F_{toe}^\uparrow must be computed using (5.73). For the impact model to be valid, it must be verified that $(F_{\text{toe}}^\uparrow)^N > 0$ and $|(F_{\text{toe}}^\uparrow)^T| \leq \mu_s (F_{\text{toe}}^\uparrow)^N$, where μ_s is the assumed

coefficient of static friction. Intuitively, it must be verified that the robot does not slide or “pull” the ground at impact, as was the case for the validity of the stance model. \triangleleft

5.3.5 Thumper Stance-to-Flight Transition Model

Consistent with Hypothesis HGT6), transition from stance to flight is assumed to occur when the vertical component of the ground reaction force becomes zero; this event signifies the end of stance and is mathematically captured by the definition of the stance-to-flight switching surface $\mathcal{S}_{s \rightarrow f}$ according to (5.61).

Ideally, to take full advantage of the spring, it is desirable that by the time the stance-to-flight transition occurs, the spring has returned the energy stored in it throughout the stance phase by the compression of the leg. Therefore, it will be assumed that at liftoff—more precisely, *just after*¹² the vertical component of the ground reaction force becomes zero—the spring reaches its natural length, that is, $\theta_{\text{Bspring}} = 0$. When this condition is satisfied, an “internal” impact occurs due to the fact that the pulley “Bspring” of the spring differential, see Fig. 5.1, hits a mechanical (hard) stop, not allowing the spring to enter its extension phase: the spring is one directional, it can only compress as the virtual leg compresses; see Hypothesis HMT5). The stance-to-flight transition model should capture the impact occurring at the end of the stance phase to compute the initial conditions of the upcoming flight phase. The impact model is derived similarly to the ground impact described in Section 5.3.4, hence the exposition in this section will be terse.

Let $x_s^- = (q_s^-; \dot{q}_s^-) \in \mathcal{S}_{s \rightarrow f}$ be the final state of the stance phase. As in Section 5.3.4, the goal is to find a map $\Delta_{s \rightarrow f} : \mathcal{S}_{s \rightarrow f} \rightarrow \mathcal{X}_f$,

$$x_f^+ = \Delta_{s \rightarrow f}(x_s^-), \quad (5.77)$$

where $x_f^+ \in \mathcal{X}_f$ is the initial state in the flight phase. This map will be derived by constructing the corresponding base and fiber components $\Delta_{s \rightarrow f}^q : Q_s \rightarrow Q_f$ and $(\Delta_{s \rightarrow f}^{\dot{q}})_{q_s} : T_{q_s} Q_s \rightarrow$

¹²Note that the one could define the stance-to-flight threshold function by $H_{s \rightarrow f}(x_s) = \theta_{\text{Bspring}}$, so that the event triggering transition to flight is the spring obtaining its natural length. Although such definition would result in different nominal orbits than the ones studied here, it is an equally valid choice for a threshold function. However, what is assumed here by defining $\mathcal{S}_{s \rightarrow f}$ by (5.61) is that *first* the vertical component of the ground reaction force becomes zero and *then* the spring reaches its natural length. Nominal orbits consistent with this assumption will be the result of controller action.

$T_{\Delta_{s \rightarrow f}^q(q_s)}Q_f$, respectively, i.e.,

$$\Delta_{s \rightarrow f}(x_s^-) := \begin{bmatrix} \Delta_{s \rightarrow f}^q(q_s^-) \\ (\Delta_{s \rightarrow f}^{\dot{q}})_{q_s^-}(\dot{q}_s^-) \end{bmatrix}, \quad (5.78)$$

so that the diagram in Fig. 5.6 commutes.

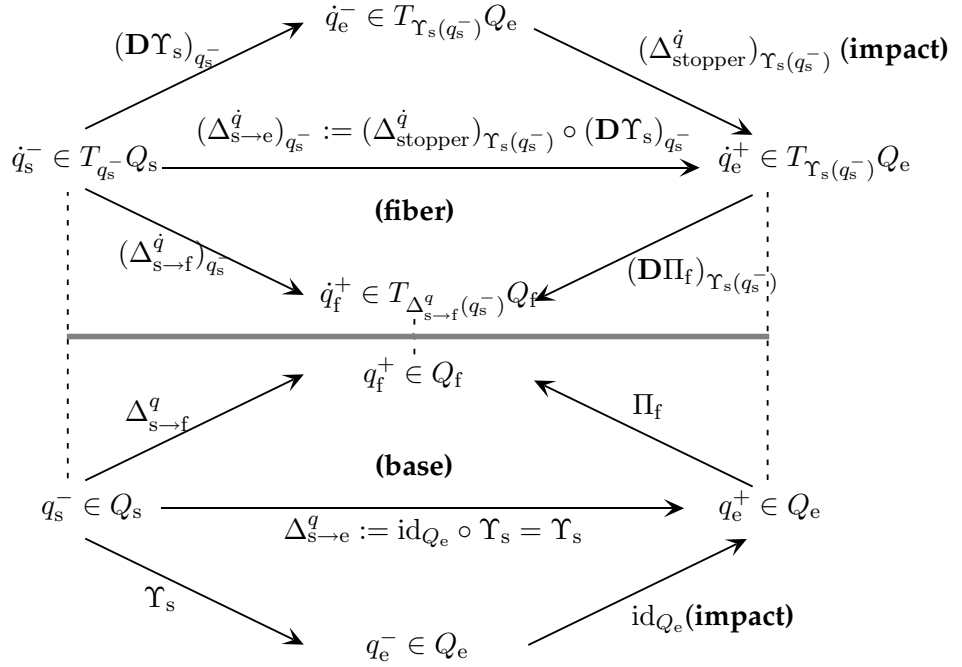


Figure 5.6: A commutative diagram showing the construction of the stance-to-flight transition map $\Delta_{s \rightarrow f}$. The bottom part corresponds to the base component $\Delta_{s \rightarrow f}^q$ and the upper part to the fiber component $\Delta_{s \rightarrow f}^{\dot{q}}$. The coordinate representations of the various maps appearing in this figure are provided in the text. Notice that the fiber component $\Delta_{s \rightarrow f}^{\dot{q}}$ of $\Delta_{s \rightarrow f}$ is not the differential of its base component $\Delta_{s \rightarrow f}^q$ as was in the ASLIP.

First, to derive the base component $\Delta_{f \rightarrow s}^q$, note that by (5.38), $q_e^- = \Upsilon_s(q_s^-)$ and since, by Hypothesis HIT5), the configuration is assumed to be invariant under impact, we have that $q_e^+ = q_e^-$. Hence, the initial configuration q_f^+ is computed via (5.21) as $q_f^+ = \Pi_f(q_e^+)$ resulting in the following expression defining the map $\Delta_{f \rightarrow s}^q$,

$$\Delta_{s \rightarrow f}^q := \Pi_f \circ \text{id}_{Q_e} \circ \Upsilon_s = \Pi_f \circ \Upsilon_s, \quad (5.79)$$

as suggested by the bottom part of Fig. 5.6. More explicitly, using the coordinate represen-

tation of the map Υ_s defined by (5.39), and of the map Π_f defined by the matrix P_f given by (5.22), the map $\Delta_{s \rightarrow f}^q$ can be represented in coordinates by

$$\Delta_{s \rightarrow f}^q(q_s^-) = P_f \begin{bmatrix} q_s^- \\ \Upsilon_{\text{toe}}(q_s^-) \end{bmatrix}.$$

This completes the construction of $\Delta_{f \rightarrow s}^q$, which is now known in a coordinate form suitable for computations.

Next, given the final configuration of the stance phase $q_s^- \in Q_s$, the map $(\Delta_{s \rightarrow f}^{\dot{q}})_{q_s^-} : T_{q_s^-} Q_s \rightarrow T_{\Delta_{s \rightarrow f}^q(q_s^-)} Q_f$ taking the final velocities \dot{q}_s^- of the stance phase into the initial velocities \dot{q}_f^+ of the upcoming flight phase is derived. By (5.42), $\dot{q}_e^- = (\mathbf{D}\Upsilon_s)_{q_s^-}(\dot{q}_s^-)$, and if $(\Delta_{\text{stopper}}^{\dot{q}})_{q_e} : T_{q_e} Q_e \rightarrow T_{q_e} Q_e$ denotes the impact map taking pre-impact to post-impact unconstrained velocities, then $\dot{q}_e^+ = (\Delta_{\text{stopper}}^{\dot{q}})_{q_e^+}(\dot{q}_e^-)$. Thus, the required flight phase initial velocities can be computed by (5.25), i.e., $\dot{q}_f^+ = (\mathbf{D}\Pi_f)_{q_e^+}(\dot{q}_e^+)$, so that, consistent with the upper part of Fig. 5.6, the fiber component $(\Delta_{s \rightarrow f}^{\dot{q}})_{q_s}$ can be defined by the composition

$$(\Delta_{s \rightarrow f}^{\dot{q}})_{q_s^-} := (\mathbf{D}\Pi_f)_{\Upsilon_s(q_s^-)} \circ (\Delta_{\text{stopper}}^{\dot{q}})_{\Upsilon_s(q_s^-)} \circ (\mathbf{D}\Upsilon_s)_{q_s^-}. \quad (5.80)$$

Since the coordinate representations of the maps $(\mathbf{D}\Upsilon_s)_{q_s}$ and $(\mathbf{D}\Pi_f)_{q_e}$ are given by the matrices J_s and P_f specified by (5.43) and (5.22), respectively, the coordinate representation of the map $(\Delta_{\text{stopper}}^{\dot{q}})_{q_e^-}$ is the only missing ingredient for computing $(\Delta_{s \rightarrow f}^{\dot{q}})_{q_s^-}$ in coordinate form. Computing the map $(\Delta_{\text{stopper}}^{\dot{q}})_{q_e^-}$ with respect to the selected coordinates for Q_e is the focus of what follows.

According to what was mentioned in Remark 5.2, q_e^+ and \dot{q}_e^+ denote the *coordinates* of the post-impact configuration point and velocity vector of the unconstrained system, respectively. As was indicated by Hypothesis HIT2), after the impact of the pulley with the mechanical stop, the pulley does not rebound, i.e., the rate of the spring deformation after impact is assumed to be zero. Consistent to the development in Section 5.3.2 for deriving the flight dynamics, this condition can be described by the holonomic constraint

$$E_f \dot{q}_e^+ = 0, \quad (5.81)$$

which corresponds to (5.18) *evaluated* at the post-impact instant. Note that E_f does not depend on the configuration variables.

The impulsive forces developed at impact to ensure that the constraint (5.81) is satisfied can be included in the dynamics of the unconstrained system, which is then “integrated” over the infinitesimally small duration of the impact according to Hypotheses HIT1-HIT5), precisely as was done in Section 5.3.4 for deriving the flight-to-stance model. If $F_{\text{stopper}}^\uparrow$ denotes the reaction force from the stopper at impact, the procedure of Section 5.3.4 results in

$$D_e(q_{e,1:4}^+) \dot{q}_e^+ - D_e(q_{e,1:4}^-) \dot{q}_e^- = E_f' F_{\text{stopper}}^\uparrow, \quad (5.82)$$

which, combined with (5.81), gives the following system of equations

$$\begin{bmatrix} D_e(q_{e,1:4}^-) & -E_f' \\ E_f & 0 \end{bmatrix} \begin{bmatrix} \dot{q}_e^+ \\ F_{\text{stopper}}^\uparrow \end{bmatrix} = \begin{bmatrix} D_e(q_{e,1:4}^-) \dot{q}_e^- \\ 0 \end{bmatrix}. \quad (5.83)$$

Equation (5.83) represents an algebraic system of seven equations with seven unknowns, namely the six entries of the vector \dot{q}_e^+ and the constraint force $F_{\text{stopper}}^\uparrow$. Using the block-diagonal structure of D_e presented in (5.9) and the definition of E_f by (5.18), the system (5.83) can be expanded as

$$\begin{bmatrix} A(q_{e,1:4}^-) & 0_{4 \times 2} & -E_{f,1:4}' \\ 0_{2 \times 4} & mI_{2 \times 2} & 0_{2 \times 1} \\ E_{f,1:4} & 0_{2 \times 1} & 0 \end{bmatrix} \begin{bmatrix} \dot{q}_{e,1:4}^+ \\ \begin{bmatrix} \dot{x}_{\text{cm}}^+ \\ \dot{y}_{\text{cm}}^+ \end{bmatrix} \\ F_{\text{stopper}}^\uparrow \end{bmatrix} = \begin{bmatrix} A(q_{e,1:4}^-) \dot{q}_{e,1:4}^- \\ m \begin{bmatrix} \dot{x}_{\text{cm}}^- \\ \dot{y}_{\text{cm}}^- \end{bmatrix} \\ 0_{2 \times 1} \end{bmatrix}. \quad (5.84)$$

The solution of (5.84) is found to be

$$\begin{aligned} \dot{q}_{e,1:4}^+ &= N_1(q_{e,1:4}^-) \dot{q}_{e,1:4}^-, \\ \begin{bmatrix} \dot{x}_{\text{cm}}^+ \\ \dot{y}_{\text{cm}}^+ \end{bmatrix} &= \begin{bmatrix} \dot{x}_{\text{cm}}^- \\ \dot{y}_{\text{cm}}^- \end{bmatrix}, \end{aligned} \quad (5.85)$$

and

$$F_{\text{stopper}}^{\uparrow} = N_2(q_{e,1:4}^-) \dot{q}_{e,1:4}^- \quad (5.86)$$

where

$$\begin{aligned} N_1(q_{e,1:4}^-) &:= \left(I_{4 \times 4} - \frac{1}{\nu} A^{-1}(q_{e,1:4}^-) E'_{f,1:4} E_{f,1:4} \right) \left[A^{-1}(q_{e,1:4}^-) A(q_{e,1:4}^-) \right], \\ N_2(q_{e,1:4}^-) &:= -\frac{1}{\nu} E_{f,1:4} \left[A^{-1}(q_{e,1:4}^-) A(q_{e,1:4}^-) \right], \end{aligned}$$

and $\nu = E_{f,1:4} A^{-1}(q_{e,1:4}^-) E'_{f,1:4}$ is a 1×1 nonzero matrix. From (5.85), the coordinate representation $J_{\text{stopper}}(q_e) \in \mathbb{R}^{6 \times 6}$ of the fiber component $(\Delta_{\text{stopper}}^{\dot{q}})_{q_e}$ of the impact map is found to be

$$J_{\text{stopper}}(q_e^-) = \begin{bmatrix} N_1(q_{e,1:4}^-) & 0_{4 \times 2} \\ 0_{2 \times 4} & I_{2 \times 2} \end{bmatrix}. \quad (5.87)$$

It is interesting to note that, as indicated by (5.87), the impact model results in no discontinuity of the cartesian velocities of the robot's COM.

Given (5.87), the fiber component $(\Delta_{s \rightarrow f}^{\dot{q}})_{q_s}$ of the stance-to-flight transition map $\Delta_{s \rightarrow f}$ can be computed with respect to the chosen coordinates for Q_s and Q_f through the corresponding representations of the maps participating in (5.80). Putting all the ingredients together, namely, the coordinate representations of the maps (5.79) and (5.80) determined in this section, the flight-to-stance transition map $\Delta_{f \rightarrow s}$ can be specified in a form useful for computations.

Remark 5.6. The validity of the (internal) impact model, thus of the transition map, must be checked at each impact. More specifically, each time (5.77) is evaluated, the corresponding reaction forces $F_{\text{stopper}}^{\uparrow}$ must be computed using (5.86). For the impact model to be valid, it must be verified that $F_{\text{stopper}}^{\uparrow} > 0$. Furthermore, the use of the unconstrained model of Thumper to model the impact implies that the leg-end is not constrained to be in contact with the ground just after impact. In particular, the impact may result in a toe velocity with negative vertical component, a situation that corresponds to toe-scuffing and is not acceptable. Hence, it must be checked that, immediately after impact, $(\dot{p}_{\text{toe}}^v)^+ > 0$. \triangleleft

5.3.6 Thumper Hybrid Dynamics of Running

Similarly to the ASLIP, see Section 3.6, the overall hybrid dynamics of Thumper in running can be represented as a hybrid nonlinear system comprising two state manifolds (charts), where the stance and flight continuous dynamics evolve, and discrete transitions between them, as is shown in Fig. 5.7, i.e.,

$$\Sigma_f : \begin{cases} \mathcal{X}_f = TQ_f \\ \dot{x}_f = f_f(x_f) + g_f(x_f)u \\ \mathcal{S}_{f \rightarrow s} = \{x_f \in \mathcal{X}_f \mid H_{f \rightarrow s}(x_f) = 0\} \\ x_s^+ = \Delta_{f \rightarrow s}(x_f^-) \end{cases} \quad (5.88)$$

$$\Sigma_s : \begin{cases} \mathcal{X}_s = TQ_s \times \mathcal{U} \\ \dot{x}_s = f_s(x_s) + g_s(x_s)u \\ \mathcal{S}_{s \rightarrow f} = \{(x_s, u) \in \mathcal{X}_s \mid H_{s \rightarrow f}(x_s, u) = 0\} \\ x_f^+ = \Delta_{s \rightarrow f}(x_s^-), \end{cases}$$

where $x_i^- = \lim_{\tau \nearrow t} x_i(\tau)$ and $x_i^+ = \lim_{\tau \searrow t} x_i(\tau)$, $i \in \{f, s\}$, are the left and right limits of the stance and flight solutions. All the components participating in the definition of stance Σ_s and flight Σ_f components of the hybrid system have been defined in the previous sections.

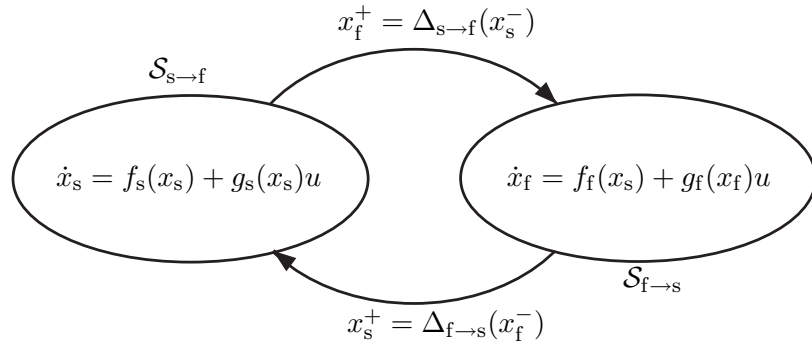


Figure 5.7: Representation of Thumper's model in running as a hybrid system.

Remark 5.7. Note that for a solution of the hybrid system (5.88) to correspond to running,

Hypothesis HGT4) requires that during flight $\dot{x}_{\text{cm}} > 0$. This requirement could have been built into the definition of the flight state manifold, which could have been defined by

$$\mathcal{X}_f := \{x_f := (q_f; \dot{q}_f) \mid q_f \in Q_f, \dot{q}_f \in T_{q_f} Q_f \simeq \mathbb{R}^6, \dot{x}_{\text{cm}} > 0\}.$$

Instead, we will seek for solutions of (5.88) respecting $\dot{x}_{\text{cm}} > 0$ during flight. ◁

CHAPTER VI

Controlling Thumper: A Compliant Hybrid Zero Dynamics Controller

In this chapter, a controller for inducing stable running motions on Thumper is presented. The framework, within which the control law is developed, is similar to that of the ASLIP. However, as was described in detail in Chapter V, the morphology of Thumper deviates significantly from that of the ASLIP in at least three ways. First, the spring in Thumper is connected in series with the actuator; not in parallel as was the case in the ASLIP. Hence, Thumper has two degrees of underactuation in the stance phase. Second, the mass of Thumper's leg is significant and it cannot be neglected as was done in the ASLIP. As a result, the torso is affected by the leg's motion during the flight phase through the conservation of angular momentum. Third, Thumper's transmission system introduces nontrivial dynamics in delivering the actuator inputs to the robot structure. Consequently, a different coordination strategy is required to realize running in Thumper. The control laws proposed for the ASLIP should be modified to accommodate these morphological discrepancies. Nevertheless, consistent to the SLIP embedding controller of Chapter IV, the proposed control laws must guarantee that the compliance present in the open-loop dynamics of Thumper dominates the behavior of the closed-loop system. In other words, the feedback action should *preserve* the compliant nature of the system. This specification will be met by ensuring that the virtual holonomic constraints imposed by the control action result in *compliant hybrid zero dynamics* governing the closed-loop behavior of Thumper, as was the case with the SLIP embedding controller for the ASLIP.

The structure of this chapter is as follows. In Section 6.1, the general framework within which the Thumper’s controller is developed is outlined. In Section 6.2 the control objectives are translated into virtual holonomic constraints, which are imposed on the robot’s dynamics by following the procedure of Section 6.3. Sections 6.4 and 6.5 provides the general strategy and implementation details of the event-based control action that updates the parameters introduced by the virtual holonomic constraints to achieve invariance in a hybrid setting and stability. Finally, Sections 6.6 and 6.7 present simulation results of the proposed control law.

6.1 Overview of the Control Method

This section outlines the general framework for the design of a controller for Thumper. In accordance to Raibert’s observations for monopedal running, a running gait in Thumper can be divided into three control objectives, namely, regulate torso angle, hopping height, and forward velocity.

The control objectives can be encoded in a set of suitably designed constraints that are imposed on the robot dynamics during the stance and flight phases through its actuators. These constraints are parameterized with respect to monotonic quantities that are functions of the state –not time– and can be interpreted as (*virtual*) *holonomic constraints*, which restrict Thumper’s dynamics on lower-dimensional surfaces embedded in the stance and flight state spaces, respectively. Loosely speaking, this *reduction-by-feedback*¹ procedure effectively reduces the feasible motions of the robot by *coordinating* the actuated degrees of freedom of Thumper, so that a lower-dimensional hybrid subsystem “emerges” from the robot’s closed-loop dynamics. This lower-dimensional hybrid subsystem governs the existence and stability properties of distinguished periodic orbits that correspond to running motions of interest on Thumper.

More specifically, to achieve the control objectives, the feedback law exploits the hybrid nature of the system by introducing control action on two levels; see Fig. 6.1. On the first

¹As opposed to *reduction-by-design*, in which constraints are imposed mechanically on the system resulting in symmetries and synergies, which reduce the dimensionality of the control problem. An example of this reduction paradigm is the design of the bipeds Max and Denise, see [112, Chap. 5, 6], in which the torso is *mechanically* constrained at an upright posture through a hip bisecting mechanism.

level, continuous-time feedback laws Γ_μ^c are employed in each of the continuous phases indexed by $\mu \in \mathcal{M}$, a finite index set. This stage introduces a set of parameters α_μ and β_μ , and its purpose is to create an invariant and attractive surface $\mathcal{Z}_{(\alpha_\mu, \beta_\mu)}$ embedded in the state space \mathcal{X}_μ of the corresponding continuous phase $\mu \in \mathcal{M}$. The role of the parameters α_μ and β_μ will become apparent in Section 6.2.

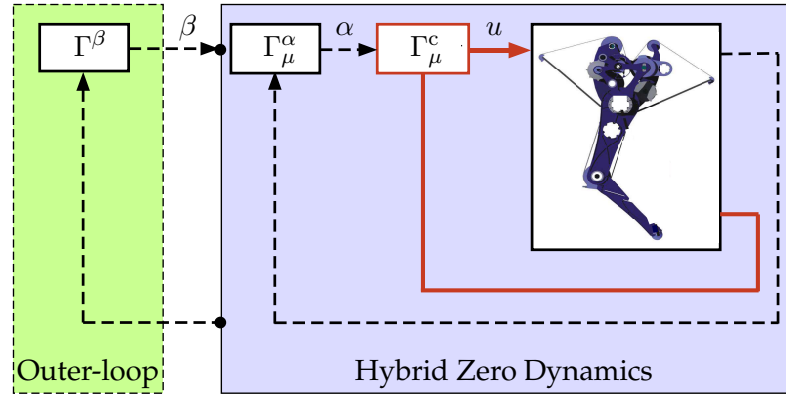


Figure 6.1: Feedback diagram presenting the basic structure of the controller. Continuous lines represent signals in continuous time; dashed lines represent signals in discrete time. The control laws Γ_μ^c and Γ_μ^α are intended to create a well defined hybrid zero dynamics (HZD), while the controller Γ^β ensures that the resulting HZD is exponentially stable.

On the second level, event-based updates of the parameters α_μ and β_μ are performed at transitions between continuous phases. The division of the parameters introduced in the continuous-time phases into two arrays, namely, α_μ and β_μ , follows the structure of the event-based parameter update law, which is organized in an inner/outer-loop architecture. The inner-loop controller Γ_μ^α properly updates the parameters α_μ to ensure that the initial condition x_μ^+ of the corresponding continuous phase lies on the surface $\mathcal{Z}_{(\alpha_\mu, \beta_\mu)}$, i.e., $x_\mu^+ \in \mathcal{Z}_{(\alpha_\mu, \beta_\mu)}$. Intuitively, updating α_μ “deforms” the surface $\mathcal{Z}_{(\alpha_\mu, \beta_\mu)}$ so that it includes the corresponding “entry” conditions. This inner-loop controller leads to the creation of a reduced-order hybrid subsystem governing the stability properties of the full-order model of Thumper, i.e., the *Hybrid Zero Dynamics* (HZD). Finally, the outer-loop controller Γ^β completes the control design by updating the parameters $\beta = \{\beta_\mu\}_{\mu \in \mathcal{M}}$ so that the resulting HZD is exponentially stable. Intuitively, updating the parameters β_μ is equivalent to locally deforming the surface $\mathcal{Z}_{(\alpha_\mu, \beta_\mu)}$ in a manner affecting the “exit” conditions for the

corresponding continuous phase $\mu \in \mathcal{M}$.

In the remaining sections of this chapter, the procedure described above will be made mathematically precise using the results in [81] and [109]. Sections 6.3, 6.4 and 6.5 particularize these ideas through explicit constructions of a set of feedback laws Γ_{μ}^c , Γ_{μ}^{α} and Γ^{β} that are organized according to Fig. 6.1 and achieve the control objectives resulting in (locally) exponentially stable running motions on Thumper. Before continuing with the design of the controllers, Section 6.2 presents a set of virtual holonomic constraints that encode the desired specifications.

6.2 Feedback Objectives: Designing Virtual Holonomic Constraints

In this section, the feedback objectives are described in detail. A set of virtual holonomic constraints is devised, which, when enforced on the dynamics of Thumper through zeroing properly selected output functions, guarantees that the objectives are achieved, resulting in periodic running motions on Thumper.

6.2.1 Stance Phase Virtual Holonomic Constraints

The purpose of the continuous-time control action during the stance phase is twofold. First, it ensures that the torso remains upright throughout stance and, in addition, that it enters the flight phase with *suitable* initial conditions. Second, the controller regulates the energy stored in the leg spring so that a desired hopping height is maintained.

In more detail, to the dynamics

$$\dot{x}_s = f_s(x_s) + g_s(x_s)u \quad (6.1)$$

of the stance phase associate the output

$$y_s = h_s(q_s, \alpha_s, \beta_s) := q_{c,s} - h_s^d(\theta(q_s), \alpha_s, \beta_s), \quad (6.2)$$

where $q_{c,s}$ contains the *controlled* variables, which are selected to be the torso orientation q_{Tor} and the motor position q_{mLS} , i.e. $q_{c,s} = (q_{\text{Tor}}, q_{\text{mLS}})'$. In (6.2), h_s^d represents the desired

evolution q_{Tor}^d and q_{mLS}^d of q_{Tor} and q_{mLS} , respectively. It corresponds to a spline that is parameterized with respect to the strictly monotonic (increasing) quantity θ representing the angle formed by the line connecting the toe with the hip relative to the ground, i.e.,

$$\theta(q_s) := -\frac{3\pi}{2} + q_{\text{LA}} + q_{\text{Tor}}. \quad (6.3)$$

Roughly speaking, θ is used to replace time in parameterizing the motion of Thumper in stance. Finally, the parameter arrays α_s and β_s in (6.2) include polynomial coefficients, and they will be detailed below.

Figure 6.2 illustrates the general shape of the commanded constraints on q_{Tor} and q_{mLS} . The commanded constraint for q_{Tor} is composed by a “transient” part, whose purpose is to drive—in a smooth way—the torso angle from its initial value², q_{Tor}^{s+} , to a desired final one, q_{Tor}^{s-} , in anticipation of liftoff. The transient stage is followed by a part during which q_{Tor} is kept constant and equal to q_{Tor}^{s-} so that switching to flight occurs with favorable initial conditions. In particular, commanding zero pitch velocity in the late stage of the stance phase ensures that the angular momentum associated with the torso is small when the system switches to flight, so that excessive pitching during flight is eliminated.

The transition part will be parameterized using a sixth order Beziér polynomial spanning a period from the beginning of the stance phase, $\theta_{\text{Tor}}^{\min} = \theta^{\min}$, until the angle θ reaches a “settling” value denoted by $\beta_{s,\text{set}}$, i.e., $\theta = \theta_{\text{Tor}}^{\max} = \beta_{s,\text{set}}$. Mathematically,

$$h_{s,1}^d(\theta(q_s)) := \begin{cases} \sum_{k=0}^6 b_k(s_{\text{Tor}}) \alpha_{s,(k,1)}, & 0 \leq s_{\text{Tor}} \leq 1 \\ \beta_{s,\text{Tor}}, & s_{\text{Tor}} > 1, \end{cases} \quad (6.4)$$

where the dependence of $h_{s,1}^d$ on α_s and β_s was suppressed. The coefficients b_k are given by

$$b_k(s) := \frac{M!}{k! (M-k)!} s^k (1-s)^{M-k}, \quad (6.5)$$

²Notation: The superscript “s+” denotes a value at the beginning of stance; “s-” denotes a value at the end of stance. Similar convention is adopted for flight.

for $M = 6$, and the normalized independent variable is computed by

$$s_{\text{Tor}} := \frac{\theta - \theta_{\text{Tor}}^{\min}}{\theta_{\text{Tor}}^{\max} - \theta_{\text{Tor}}^{\min}} = \frac{\theta - \theta_{\text{Tor}}^{\min}}{\beta_{\text{s,set}} - \theta_{\text{Tor}}^{\min}}. \quad (6.6)$$

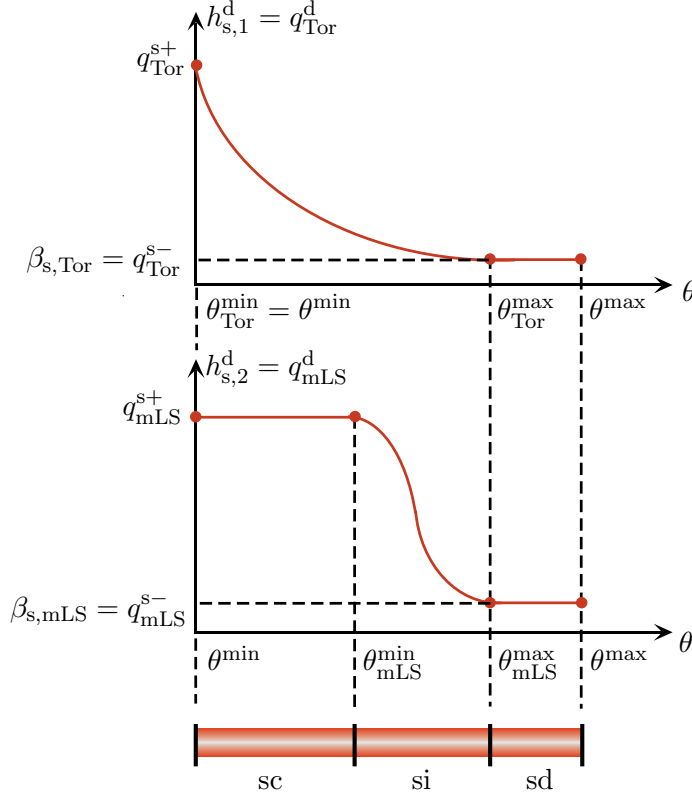


Figure 6.2: The general shape of the stance phase commanded constraints. Note that $\theta_{\text{Tor}}^{\max} = \theta_{\text{mLS}}^{\max} = \beta_{\text{s,set}}$ to avoid the introduction of an additional stance subphase.

On the other hand, as shown in Fig. 6.2, the desired evolution of the motor position q_{mLS} is as follows. First, the motorshaft is kept at a constant angle q_{mLS}^{s+} until $\theta = \theta_{\text{mLS}}^{\min}$, the point at which the spring is maximally compressed. This ensures that energy is stored in the spring without the actuator performing unnecessary negative work on the leg. When maximum compression is reached, the actuator injects (or removes) energy through compressing (or decompressing) the spring by rapidly repositioning the motorshaft at a new desired position, q_{mLS}^{s-} , which depends on the amount of energy that is required to maintain hopping. Then, the motorshaft is kept at this position until liftoff occurs.

Similarly to the torso angle, the transient period from $\theta_{\text{mLS}}^{\min}$ to $\theta_{\text{mLS}}^{\max}$ will be parameterized using a sixth order Beziér polynomial. Hence, the mathematical description of the

constraint $h_{d,2}$ for the motorshaft position q_{mLS} is

$$h_{s,2}^d(\theta(q_s)) := \begin{cases} \alpha_{s,(-1,2)}, & s_{\text{mLS}} < 0 \\ \sum_{k=0}^6 b_k(s_{\text{mLS}})\alpha_{s,(k,2)}, & 0 \leq s_{\text{mLS}} \leq 1 \\ \beta_{s,\text{mLS}}, & s_{\text{mLS}} > 1, \end{cases} \quad (6.7)$$

where the dependence of $h_{s,2}^d$ on α_s and β_s was suppressed, b_k is given by (6.5) using $M = 6$, and

$$s_{\text{mLS}} := \frac{\theta - \theta_{\text{mLS}}^{\min}}{\theta_{\text{mLS}}^{\max} - \theta_{\text{mLS}}^{\min}} = \frac{\theta - \theta_{\text{mLS}}^{\min}}{\beta_{s,\text{set}} - \theta_{\text{mLS}}^{\min}} \quad (6.8)$$

is the corresponding normalized independent variable. Note that in the definition of s_{mLS} , $\theta_{\text{mLS}}^{\max}$ is taken to be equal to the $\theta_{\text{Tor}}^{\max}$, which is equal to the parameter $\beta_{s,\text{set}}$. This is done to avoid the introduction of additional subphases in the stance phase.

This procedure introduces a number of parameters, namely, the coefficients of the polynomials used to describe the various regions of (6.4) and (6.7). It should be emphasized that not all the parameters participating in the definitions of the constraints (6.4) and (6.7) are available for event-based control. Indeed, to avoid discontinuities in the commanded torques, the polynomial coefficients must satisfy certain requirements, which guarantee that the constraints (6.4) and (6.7) are C^2 functions of s_{Tor} and s_{mLS} , respectively, thus, reducing the number of free coefficients. According to the properties of Beziér polynomials listed in [109, p. 139], imposing the relation

$$\alpha_{s,(0,2)} = \alpha_{s,(1,2)} = \alpha_{s,(2,2)} = \alpha_{s,(-1,2)}, \quad (6.9)$$

ensures that (6.4) is C^2 at $s_{\text{mLS}} = 0$, slaving $\{\alpha_{s,(0,2)}, \alpha_{s,(1,2)}, \alpha_{s,(2,2)}\}$ and leaving $\alpha_{s,(-1,2)}$ free for control. Similarly, imposing the relations

$$\begin{aligned} \alpha_{s,(4,1)} &= \alpha_{s,(5,1)} = \alpha_{s,(6,1)} = \beta_{s,\text{Tor}}, \\ \alpha_{s,(4,2)} &= \alpha_{s,(5,2)} = \alpha_{s,(6,2)} = \beta_{s,\text{mLS}}, \end{aligned} \quad (6.10)$$

ensures that (6.4) and (6.7) are C^2 at $s_{\text{Tor}} = 1$ and $s_{\text{mLS}} = 1$, respectively. These relations

slave $\{\alpha_{s,(4,1)}, \alpha_{s,(5,1)}, \alpha_{s,(6,1)}\}$ and $\{\alpha_{s,(4,2)}, \alpha_{s,(5,2)}, \alpha_{s,(6,2)}\}$ and leave $\beta_{s,\text{Tor}}$ and $\beta_{s,\text{mLS}}$ free for control. As a result, the parameters that are available for event-based control are

$$\alpha_s := \{\alpha_{s,(0,1)}, \alpha_{s,(1,1)}, \alpha_{s,(2,1)}, \alpha_{s,(3,1)}, \theta_{\text{Tor}}^{\min}, \alpha_{s,(-1,2)}, \alpha_{s,(3,2)}, \theta_{\text{mLS}}^{\min}\}, \quad (6.11)$$

and

$$\beta_s := \{\beta_{s,\text{Tor}}, \beta_{s,\text{mLS}}, \beta_{s,\text{set}}\}, \quad (6.12)$$

respectively. Before continuing with the design of the virtual holonomic constraints for the flight phase a few remarks are in order.

Remark 6.1. The coefficients $\beta_{s,\text{Tor}}$ and $\beta_{s,\text{mLS}}$ represent the values of the torso pitch angle and the motorshaft position prior to liftoff, i.e., q_{Tor}^{s-} and q_{mLS}^{s-} , respectively; see Fig. 6.2. Adjusting $\beta_{s,\text{Tor}}$ determines the posture of the torso as the robot enters the flight phase, while adjusting $\beta_{s,\text{mLS}}$ determines how much energy is injected or removed from the leg spring during the stance phase so that the hopping height is regulated at the desired value. Finally, the coefficient $\beta_{s,\text{set}}$ corresponds to the duration of the “transient” period for the evolution of the constraints. As shown in Fig. 6.2, adjusting $\beta_{s,\text{set}}$ determines the duration of the portion of the stance phase over which the momentum associated with the torso angle is removed and energy is injected in the spring. Updating these parameters provides a powerful control input for the stabilization of Thumper, as will be detailed in Section 6.4.2. ◁

Remark 6.2. Enforcing the constraints (6.4) and (6.7) organizes the stance phase into three subphases, namely, stance-compression, stance-injection, and stance-decompression, which will be denoted by the indices “sc”, “si” and “sd,” respectively; see Fig. 6.2. These additional phases, can be utilized to update some of the stance phase parameters α_s not only at the beginning of the stance phase, but also at transitions from one subphase to the next. This feature will be used in Sections 6.4.1 and 6.5.1 to update certain parameters from the array α_s in order to ensure that the hybrid zero dynamics is well defined. ◁

6.2.2 Flight Phase Virtual Holonomic Constraints

The purpose of the continuous-time controller during the flight phase is to place the leg at a proper configuration in anticipation of touchdown. In more detail, to the continuous dynamics

$$\dot{x}_f = f_f(x_f) + g_f(x_f)u \quad (6.13)$$

of the flight phase associate the output

$$y_f = h_f(q_f, \alpha_f, \beta_f) := q_{c,f} - h_f^d(\ell(q_f), \alpha_f, \beta_f), \quad (6.14)$$

where the vector $q_{c,f}$ contains the *controlled* variables. In selecting $q_{c,f}$ note that, as was recognized by Raibert, [91, Chapter 2], and others, e.g., [8], [101], [100], the position of the foot as it touches the ground at the end of flight has a strong influence on the ensuing stance phase, thereby providing an effective means for controlling forward speed; see also Fig. 6.3. Moreover, when placing the leg, toe stubbing and excessive pitching of the torso should be avoided. These objectives can be achieved through commanding properly designed virtual constraints on the horizontal distance between the toe and the COM and on the leg-shape angle, $(p_{\text{toe}}^h - x_{\text{cm}})$ and q_{LS} , respectively, i.e., $q_{c,f} = (p_{\text{toe}}^h - x_{\text{cm}}, q_{\text{LS}})'$.

In (6.14), h_f^d corresponds to the desired evolution of $q_{c,f}$, which depends on the parameters α_f and β_f , and is parameterized with respect to the strictly monotonic quantity ℓ . The variable ℓ corresponds to the horizontal distance traveled by the COM during flight,

$$\ell(q_f) := x_{\text{cm}} - x_{\text{cm}}^{\text{f}+}, \quad (6.15)$$

where $x_{\text{cm}}^{\text{f}+}$ is the position of the COM at the beginning of the flight phase. The desired evolution of the controlled variables in flight will be parameterized using sixth order Beziér polynomials, i.e.

$$h_f^d(\ell(q_f)) := \begin{bmatrix} \sum_{k=0}^5 b_k(s_f) \alpha_{f,(k,1)} + b_6(s_f) \beta_f \\ \sum_{k=0}^6 b_k(s_f) \alpha_{f,(k,2)} \end{bmatrix}, \quad (6.16)$$

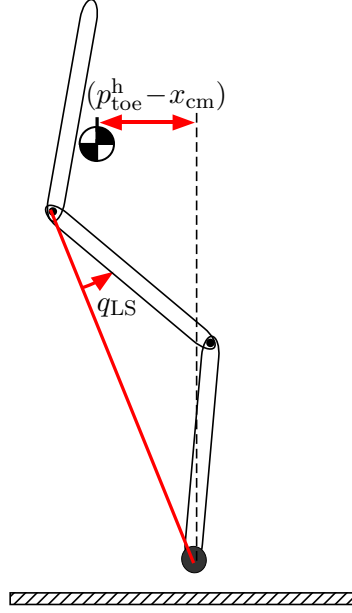


Figure 6.3: Controlled variables in the flight phase. The horizontal position of the toe relative to the COM, $(p_{\text{toe}}^h - x_{\text{cm}})$, corresponds to Raibert's touchdown angle controller. The leg-shape angle, q_{LS} determines leg length.

where the coefficients b_k are computed by (6.5), and

$$s_f := \frac{\ell - \ell^{\min}}{\ell^{\max} - \ell^{\min}} \quad (6.17)$$

is the normalized independent variable; the dependence of h_f^d on α_f and β_f has been suppressed. At the beginning of the flight phase $x_{\text{cm}} = x_{\text{cm}}^{f+}$, which in view of (6.15) implies that $\ell^{\min} = 0$; hence, ℓ^{\min} is not a parameter available for event-based control.

As in the stance phase, this procedure introduces a number of parameters that are available for event-based (discrete-time) control, and correspond to the coefficients of the polynomials defining h_f^d , which are grouped in the array

$$\alpha_f := \{\alpha_{f,(0,1)}, \dots, \alpha_{f,(5,1)}, \alpha_{f,(0,2)}, \dots, \alpha_{f,(6,2)}, \ell^{\max}\}.$$

It should be noted here that in Section 6.5.1 the flight parameter array will be refined so that it includes *only* those parameters that actually participate in the event-based control action. Abusing notation, the resulting parameter array will also be denoted by α_f ; see (6.68) of Section 6.5.1.

Remark 6.3. In order to explain why the coefficient of the highest order monomial of $h_{f,1}^d$ is denoted by β_f instead of $\alpha_{f,(6,1)}$ in (6.16), note that, by properties of the Beziér polynomials, see [109, p. 139], $h_{f,1}^d(\ell^{\max}) = \beta_f$. Hence, the coefficient β_f corresponds to the position of the toe relative to the COM just prior to touchdown, i.e. $(p_{\text{toe}}^h - x_{\text{cm}})^{f-}$, and it provides a powerful control input for regulating the forward speed. As a result, following the control diagram of Fig. 6.1, β_f will be updated in the outer-loop discrete controller to achieve stability of the hybrid zero dynamics, and not in the inner-loop controller like the rest of the coefficients grouped in α_f . ◁

6.3 Continuous-time Control of Thumper

The purpose of the continuous-time control action is to impose the virtual holonomic constraints designed in Section 6.2 on the dynamics of Thumper through its actuators. This is equivalent to zeroing the parameterized outputs (6.2) and (6.14) associated with the stance and flight phase dynamics. In this section, continuous-time control laws will be designed within the Isidori-Byrnes zero dynamics framework, [57, Sections 4.3 and 6.1], which achieve the objective of zeroing the outputs (6.2) and (6.14), thus asymptotically imposing the virtual holonomic constraints of the previous section.

6.3.1 Continuous-time Phases in the Closed-loop Thumper

As was mentioned in Section 6.2, enforcing the constraints (6.4) and (6.7) organizes the stance phase into the three subphases stance-compression, stance-injection, and stance-decompression, denoted by “sc”, “si” and “sd,” respectively. These subphases are present as separate phases only in the closed-loop system.

As a result of the continuous-time control action, a running gait in Thumper is composed by four phases, the three subphases of stance and the flight phase. Let $\mathcal{M} = \{\text{sc}, \text{si}, \text{sd}, \text{f}\}$ be the finite index set containing the indices of the continuous-time phases. In this work, we restrict our attention to running gaits, in which the continuous phases succeed each other according to the pattern shown in Fig. 6.4. As suggested by Fig. 6.4, a convenient way to capture the evolution of the hybrid dynamics of Thumper in discrete

time, i.e., the succession of the various phases, is to consider the set $\mathcal{G}_4 = \{0, 1, 2, 3\}$ under the operation $\oplus : \mathcal{G}_4 \times \mathcal{G}_4 \rightarrow \mathcal{G}_4$ defined by the rule

$$i \oplus j = \begin{cases} i + j & i + j < 4 \\ i + j - 4 & i + j \geq 4 \end{cases}, \quad (6.18)$$

where $+$ corresponds to standard integer addition. Then, (\mathcal{G}_4, \oplus) is a finite abelian group³, which is isomorphic to the group of integers under addition modulo 4. Hence, following standard notation, the symbol \mathbb{Z}_4 will be adopted instead of \mathcal{G}_4 .

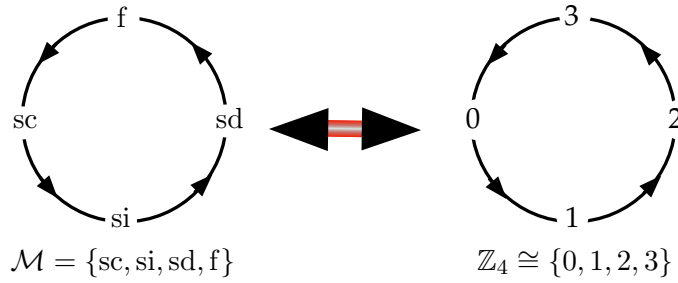


Figure 6.4: Succession of the phases $\mathcal{M} = \{sc, si, sd, f\}$ of the dynamics of Thumper in closed loop with the continuous-time controllers during running, and the correspondence with the cyclic group $\mathbb{Z}_4 \cong \{0, 1, 2, 3\}$.

As indicated in Fig. 6.4, the group \mathbb{Z}_4 reflects the cyclicity⁴ that underlies the composition of the continuous flows of each subphase to result in the hybrid flow that represents running in Thumper, and it can be put to bijective correspondence with the index set \mathcal{M} through the enumeration map $\nu : \mathbb{Z}_4 \rightarrow \mathcal{M}$ defined by

$$\nu(\kappa) := \begin{cases} sc, & \kappa = 0 \\ si, & \kappa = 1 \\ sd, & \kappa = 2 \\ f, & \kappa = 3 \end{cases}. \quad (6.19)$$

The dynamics in each phase $\nu(\kappa) \in \mathcal{M}$, $\kappa \in \mathbb{Z}_4$, evolves in a state space $TQ_{\nu(\kappa)}$ param-

³The identity element of \mathcal{G}_4 is $0 \in \mathcal{G}_4$ and the inverse of $i \in \mathcal{G}_4$ is $4 - i \in \mathcal{G}_4$.

⁴In fact, \mathbb{Z}_4 is a cyclic group since every element in it can be written as a finite composition of $1 \in \mathbb{Z}_4$ and its inverse; equivalently, the group can be *generated* by 1.

eterized by the states $x_{\nu(\kappa)} \in TQ_{\nu(\kappa)}$ ⁵, and is governed by vector fields, which depend on parameters that correspond to the coefficients of the polynomials used to realize the constraints of Section 6.2. In particular, the closed-loop dynamics in the flight phase depends on (α_f, β_f) , while the closed-loop dynamics in the stance-compression, stance-injection and stance-decompression phases depend on $(\alpha_{sc}, \beta_{sc})$, $(\alpha_{si}, \beta_{si})$, and $(\alpha_{sd}, \beta_{sd})$, respectively. The arrays α_{sc} , α_{si} , α_{sd} and α_f will be defined in Section 6.5.1 below, where details on the inner-loop event-based parameter update laws are provided. Finally, the arrays β_{sc} , β_{si} and β_{sd} take values in the sets \mathcal{B}_{sc} , \mathcal{B}_{si} and \mathcal{B}_{sd} , respectively, and they contain parameters that are entries of β_s , namely,

$$\begin{aligned}\beta_{sc} &:= \{\beta_{s,\text{Tor}}, \beta_{s,\text{set}}\}, \\ \beta_{si} &:= \{\beta_{s,\text{mLS}}, \beta_{s,\text{set}}\}, \\ \beta_{sd} &:= \{\beta_{s,\text{Tor}}, \beta_{s,\text{mLS}}\},\end{aligned}\tag{6.20}$$

and $\beta_f \in \mathcal{B}_f$. The meaning of β_{sc} , β_{si} and β_{sd} has been explained in Remark 6.1, and the role of β_f has been explained in Remark 6.3.

6.3.2 Enforcing the Virtual Holonomic Constraints

In Section 6.2, and for each $\kappa \in \mathbb{Z}_4$, an output function

$$y_{\nu(\kappa)} := h_{\nu(\kappa)}(q_{\nu(\kappa)}, \alpha_{\nu(\kappa)}, \beta_{\nu(\kappa)})\tag{6.21}$$

has been associated with the continuous dynamics

$$\dot{x}_{\nu(\kappa)} = f_{\nu(\kappa)}(x_{\nu(\kappa)}) + g_{\nu(\kappa)}(x_{\nu(\kappa)})u\tag{6.22}$$

⁵Note that the dynamics in the stance-compression, stance-injection, and stance-decompression phases evolve in TQ_s , i.e., the tangent bundle over the stance phase configuration manifold Q_s defined by (5.37). Hence, $TQ_{sc} = TQ_{si} = TQ_{sd} = TQ_s$, and they can all be parameterized by the same coordinates x_s . However, in order to emphasize the different closed-loop dynamics governing the behavior of Thumper in each of the stance subphases, the distinction will be made and different indexes will be used to identify them.

of the phase $\nu(\kappa) = \mu \in \mathcal{M}$, where ν is the enumeration map defined by (6.19). For given values of $\alpha_{\nu(\kappa)}$ and $\beta_{\nu(\kappa)}$, differentiating (6.21) twice with respect to time results in

$$\frac{d^2 y_{\nu(\kappa)}}{dt^2} = L_{f_{\nu(\kappa)}}^2 h_{\nu(\kappa)}(x_{\nu(\kappa)}, \alpha_{\nu(\kappa)}, \beta_{\nu(\kappa)}) + L_{g_{\nu(\kappa)}} L_{f_{\nu(\kappa)}} h_{\nu(\kappa)}(q_{\nu(\kappa)}, \alpha_{\nu(\kappa)}, \beta_{\nu(\kappa)}) u, \quad (6.23)$$

where $L_{g_{\nu(\kappa)}} L_{f_{\nu(\kappa)}} h_{\nu(\kappa)}(q_{\nu(\kappa)}, \alpha_{\nu(\kappa)}, \beta_{\nu(\kappa)})$ is the decoupling matrix. Under the condition that the decoupling matrix is invertible,

$$u^*(x_{\nu(\kappa)}, \alpha_{\nu(\kappa)}, \beta_{\nu(\kappa)}) := - \left(L_{g_{\nu(\kappa)}} L_{f_{\nu(\kappa)}} h_{\nu(\kappa)}(q_{\nu(\kappa)}, \alpha_{\nu(\kappa)}, \beta_{\nu(\kappa)}) \right)^{-1} L_{f_{\nu(\kappa)}}^2 h_{\nu(\kappa)}(x_{\nu(\kappa)}, \alpha_{\nu(\kappa)}, \beta_{\nu(\kappa)}), \quad (6.24)$$

is the unique control input that renders the surface

$$\mathcal{Z}_{(\alpha_{\nu(\kappa)}, \beta_{\nu(\kappa)})} = \left\{ x_{\nu(\kappa)} \in \mathcal{X}_{\nu(\kappa)} \mid \begin{aligned} h_{\nu(\kappa)}(q_{\nu(\kappa)}, \alpha_{\nu(\kappa)}, \beta_{\nu(\kappa)}) &= 0, \\ L_{f_{\nu(\kappa)}} h_{\nu(\kappa)}(x_{\nu(\kappa)}, \alpha_{\nu(\kappa)}, \beta_{\nu(\kappa)}) &= 0 \end{aligned} \right\} \quad (6.25)$$

invariant under the flow of the closed-loop dynamics; that is, for every $z \in \mathcal{Z}_{(\alpha_{\nu(\kappa)}, \beta_{\nu(\kappa)})}$,

$$f^*(z, \alpha_{\nu(\kappa)}, \beta_{\nu(\kappa)}) := f_{\nu(\kappa)}(z) + g_{\nu(\kappa)}(z) u^*(z, \alpha_{\nu(\kappa)}, \beta_{\nu(\kappa)}) \in T_z \mathcal{Z}_{(\alpha_{\nu(\kappa)}, \beta_{\nu(\kappa)})}. \quad (6.26)$$

Essentially, imposing the (virtual) holonomic constraints by zeroing the corresponding outputs reduces the dimension of the system by restricting its dynamics on the surface $\mathcal{Z}_{(\alpha_{\nu(\kappa)}, \beta_{\nu(\kappa)})}$ embedded in the corresponding continuous-time state space $\mathcal{X}_{\nu(\kappa)}$. Following standard terminology, the surface $\mathcal{Z}_{(\alpha_{\nu(\kappa)}, \beta_{\nu(\kappa)})}$ is called the *zero dynamics manifold*, and

$$\dot{z} = f^*|_{\mathcal{Z}_{(\alpha_{\nu(\kappa)}, \beta_{\nu(\kappa)})}}(z, \alpha_{\nu(\kappa)}, \beta_{\nu(\kappa)}) \quad (6.27)$$

is the corresponding *zero dynamics*. To establish *attractivity* of $\mathcal{Z}_{(\alpha_{\nu(\kappa)}, \beta_{\nu(\kappa)})}$, the input (6.24) is modified as

$$u = \Gamma_{\nu(\kappa)}^c(x_{\nu(\kappa)}, \alpha_{\nu(\kappa)}, \beta_{\nu(\kappa)}) := \left(L_{g_{\nu(\kappa)}} L_{f_{\nu(\kappa)}} h_{\nu(\kappa)}(q_{\nu(\kappa)}, \alpha_{\nu(\kappa)}, \beta_{\nu(\kappa)}) \right)^{-1} \left[v(y_{\nu(\kappa)}, \dot{y}_{\nu(\kappa)}, \epsilon) - L_{f_{\nu(\kappa)}}^2 h_{\nu(\kappa)}(x_{\nu(\kappa)}, \alpha_{\nu(\kappa)}, \beta_{\nu(\kappa)}) \right], \quad (6.28)$$

where

$$v(y_{\nu(\kappa)}, \dot{y}_{\nu(\kappa)}, \epsilon) := -\frac{1}{\epsilon^2} K_P y_{\nu(\kappa)} - \frac{1}{\epsilon} K_V \dot{y}_{\nu(\kappa)}, \quad (6.29)$$

and K_P, K_V are appropriately chosen gain matrices, and $\epsilon > 0$. Under the continuous-time feedback laws $\Gamma_{\nu(\kappa)}^c$, constructed for each phase $\nu(\kappa) = \mu \in \mathcal{M}$, the closed-loop dynamics becomes

$$\dot{x}_{\nu(\kappa)} = f_{\nu(\kappa), \text{cl}}(x_{\nu(\kappa)}, \alpha_{\nu(\kappa)}, \beta_{\nu(\kappa)}), \quad (6.30)$$

where

$$f_{\nu(\kappa), \text{cl}}(x_{\nu(\kappa)}, \alpha_{\nu(\kappa)}, \beta_{\nu(\kappa)}) := f_{\nu(\kappa)}(x_{\nu(\kappa)}) + g_{\nu(\kappa)}(x_{\nu(\kappa)}) \Gamma_{\nu(\kappa)}^c(x_{\nu(\kappa)}, \alpha_{\nu(\kappa)}, \beta_{\nu(\kappa)}), \quad (6.31)$$

whose solutions converge to the invariant surface $\mathcal{Z}_{(\alpha_{\nu(\kappa)}, \beta_{\nu(\kappa)})}$ exponentially fast at a rate that depends on ϵ . In other words, the controller ensures that the virtual holonomic constraints, which are given by (6.21) in the form of outputs that are zeroed by the control action, are (asymptotically) imposed on Thumper, thus restricting its dynamics in each phase on the corresponding lower-dimensional surface $\mathcal{Z}_{(\alpha_{\nu(\kappa)}, \beta_{\nu(\kappa)})}$.

6.4 Event-based Control of Thumper: General Considerations

As was mentioned in Section 6.3, enforcing the outputs (6.2) and (6.14), introduces a set of parameters in the resulting closed-loop system. The dependence on these parameters is evident in (6.30), and provides the possibility of a discrete feedback element—the *parameter update law*—which, when designed properly, can ensure invariance of the surfaces $\mathcal{Z}_{(\alpha_{\nu(\kappa)}, \beta_{\nu(\kappa)})}$ and stability of the system. In this section, some general considerations, which will enable the synthesis of event-base inner/outer loop control laws according to the control architecture briefly described in Section 6.1, are discussed. The details of the

particular event-based parameter update laws for Thumper are left to Section 6.5 below.

Before continuing with the specifics of the inner/outer loop controller design, the system is brought to a form that exposes its hybrid nature. According to Section 6.3.1, each $\kappa \in \mathbb{Z}_4$ corresponds to a continuous-time phase $\mu \in \mathcal{M}$ via the correspondence $\mu = \nu(\kappa)$ given by (6.19). Then, the dynamics of Thumper in closed loop with the continuous control laws $\Gamma_{\nu(\kappa)}^c$ designed in Section 6.3.2 is captured by concatenating the solutions of the *parameter-dependent* hybrid systems

$$\Sigma_{\nu(\kappa)}^{(\alpha, \beta)} : \left\{ \begin{array}{l} x_{\nu(\kappa)} \in TQ_{\nu(\kappa)}, \alpha_{\nu(\kappa)} \in \mathcal{A}_{\nu(\kappa)}, \beta_{\nu(\kappa)} \in \mathcal{B}_{\nu(\kappa)} \\ \dot{x}_{\nu(\kappa)} = f_{\nu(\kappa), \text{cl}}(x_{\nu(\kappa)}, \alpha_{\nu(\kappa)}, \beta_{\nu(\kappa)}) \\ \mathcal{S}_{\nu(\kappa) \rightarrow \nu(\kappa \oplus 1)} = \{(x_{\nu(\kappa)}, \beta_{\nu(\kappa)}) \in TQ_{\nu(\kappa)} \times \mathcal{B}_{\nu(\kappa)} \mid H_{\nu(\kappa) \rightarrow \nu(\kappa \oplus 1)}(x_{\nu(\kappa)}, \beta_{\nu(\kappa)}) = 0\} \\ x_{\nu(\kappa \oplus 1)}^+ = \Delta_{\nu(\kappa) \rightarrow \nu(\kappa \oplus 1)}(x_{\nu(\kappa)}^-) \end{array} \right.$$

where the operation “ \oplus ” corresponds to integer addition modulo 4—see (6.18)—and reflects the sequence according to which the systems $\Sigma_{\nu(\kappa)}^{(\alpha, \beta)}$ are composed to form the hybrid dynamics of Thumper in running. The various ingredients forming the hybrid systems $\Sigma_{\nu(\kappa)}^{(\alpha, \beta)}$ are provided below.

- $TQ_{\nu(\kappa)}$ is the state-space where the closed-loop dynamics of the phase $\nu(\kappa)$ evolves;
- $\mathcal{A}_{\nu(\kappa)}, \mathcal{B}_{\nu(\kappa)}$ are sets from which the parameters $\alpha_{\nu(\kappa)}$ and $\beta_{\nu(\kappa)}$ are drawn;
- $f_{\nu(\kappa), \text{cl}}$ is the parameter-dependent⁶ vector field of (6.30) determining the closed-loop dynamics on $TQ_{\nu(\kappa)}$;
- $\mathcal{S}_{\nu(\kappa) \rightarrow \nu(\kappa \oplus 1)}$ denotes the corresponding switching surface (guard), whose crossing signifies transition from the phase $\nu(\kappa) \in \mathcal{M}$ to the phase $\nu(\kappa \oplus 1) \in \mathcal{M}$. The guards are defined as zero level sets of associated threshold functions $H_{\nu(\kappa) \rightarrow \nu(\kappa \oplus 1)} :$

⁶Note that, in some phases, the vector field $f_{\nu(\kappa), \text{cl}}$ may not depend on both $\alpha_{\nu(\kappa)}$ and $\beta_{\nu(\kappa)}$. For instance, when $\nu(\kappa) = \text{sd}$, the vector field $f_{\text{sd}, \text{cl}}$ does not depend on any α parameters.

$TQ_{\nu(\kappa)} \times \mathcal{B}_{\nu(\kappa)} \rightarrow \mathbb{R}$, which are given below,

$$\begin{aligned}
H_{f \rightarrow sc}(x_f) &:= p_{\text{toe}}^v, \\
H_{sc \rightarrow si}(x_{sc}) &:= \dot{\theta}_{\text{B}_{\text{spring}}}, \\
H_{si \rightarrow sd}(x_{si}, \beta_{si}) &:= \theta - \beta_{s,\text{set}}, \\
H_{sd \rightarrow f}(x_{sd}) &:= \theta_{\text{B}_{\text{spring}}},
\end{aligned} \tag{6.32}$$

where p_{toe}^v is the vertical distance of the toe from the ground, $\theta_{\text{B}_{\text{spring}}}$ is the spring deflection and $\dot{\theta}_{\text{B}_{\text{spring}}}$ the corresponding rate, θ is the angle defined by (6.3), and $\beta_{s,\text{set}}$ is the parameter determining termination of the stance-injection phase;

- $\Delta_{\nu(\kappa) \rightarrow \nu(\kappa \oplus 1)} : \mathcal{S}_{\nu(\kappa) \rightarrow \nu(\kappa \oplus 1)} \rightarrow TQ_{\nu(\kappa \oplus 1)}$ is the corresponding reset map, providing the initial conditions for the ensuing phase $\nu(\kappa \oplus 1) \in \mathcal{M}$. Below are the reset maps for the various phases

$$\begin{aligned}
\Delta_{f \rightarrow sc} &:= \Delta_{f \rightarrow s}, \\
\Delta_{sc \rightarrow si} &:= \text{id}_{TQ_{sc}}, \\
\Delta_{si \rightarrow sd} &:= \text{id}_{TQ_{si}}, \\
\Delta_{sd \rightarrow f} &:= \Delta_{s \rightarrow f},
\end{aligned} \tag{6.33}$$

where the maps $\Delta_{f \rightarrow s}$ and $\Delta_{s \rightarrow f}$ are the flight-to-stance and the stance-to-flight reset maps defined in Sections 5.3.4 and 5.3.5 of Chapter V by (5.62) and (5.77), respectively, and $\text{id}_{TQ_{\nu(\kappa)}}$ is the identity map on $TQ_{\nu(\kappa)}$.

In the remarks that follow, some properties relative to the transitions from one phase to the next and the associated reset maps specific to Thumper are listed. These properties are important in developing controllers for Thumper.

Remark 6.4. Careful inspection of (6.32) reveals that *only* the transition from stance-injection to stance-decompression governed by $H_{si \rightarrow sd}$ depends explicitly on the β_{si} parameters⁷, namely, $\beta_{s,\text{set}}$. It should be emphasized that the rest of the switching conditions, and in particular, the flight-to-stance-compression surface, depend *explicitly* on the states, and

⁷This case is similar to the ASLIP, in which the flight-to-stance surface depends explicitly on the touchdown angle α_f , due to the assumption of the massless legs in the ASLIP. Note that in Thumper the β parameters play a role similar to the touchdown angle α_f of the ASLIP.

only *implicitly* on the parameters. ◁

Remark 6.5. According to the definition of $H_{\text{sd} \rightarrow \text{f}}$, see (6.32), switching from stance to flight in the closed-loop system is assumed to occur when the spring obtains its natural length. This assumption is a consequence of Thumper’s powertrain, in which the spring in series with the leg-shape motor is *unilateral* in the sense that it compresses, but does not extend beyond its nominal rest length. Instead, once the spring reaches its rest length, the position of the leg-shape motor, q_{mLS} , and the leg-shape angle, q_{LS} , are rigidly connected (i.e. no longer through a compliant element); see Fig. 5.1 and Section 5.2 for details on how this is achieved. This feature provides an advantage in initiating liftoff during hopping, because at liftoff the leg-shape motor does not “fight” the spring that is trying to extend due to the non-zero mass of the shin. Hence, switching from stance to flight becomes a control decision. The advantage of this assumption is that the introduction of additional phases is avoided. ◁

Remark 6.6. It is evident from (6.33) that the reset maps depend only on the states. As a result, no explicit dependence of the initial conditions of the ensuing phase on the parameters is present. This is true for all transitions. ◁

6.4.1 Inner-loop Event-based Control for Invariance

At the beginning of each continuous phase $\nu(\kappa) \in \mathcal{M}$, the parameters $\alpha_{\nu(\kappa)}$ can be updated to achieve invariance in the hybrid setting. The procedure leaves the parameters $\beta_{\nu(\kappa)}$ unaffected: $\beta_{\nu(\kappa)}$ do not participate in the inner-loop controller design. Hence, for the purposes of this section, it is sufficient to group the β -parameters in a single array $\beta := (\beta'_s, \beta'_f)' \in \mathcal{B}_s \times \mathcal{B}_f =: \mathcal{B}$, whose values will be updated by the outer-loop event-base controller; details on the outer-loop controller will be provided in Section 6.4.2.

6.4.1.1 Inner-loop Controller Objectives

Suppose that the parameters $\beta \in \mathcal{B}$ are given and let $x_{\nu(\kappa)}^- \in \mathcal{S}_{\nu(\kappa) \rightarrow \nu(\kappa \oplus 1)}$ be the exit conditions of the phase $\nu(\kappa) \in \mathcal{M}$. Then, extending invariance in the hybrid setting is accomplished by updating the parameters $\alpha_{\nu(\kappa \oplus 1)}$ of the ensuing phase $\nu(\kappa \oplus 1) \in \mathcal{M}$ to

a new value $\alpha_{\nu(\kappa\oplus 1)}^+$ so that the surface $\mathcal{Z}_{(\alpha_{\nu(\kappa\oplus 1)}^+, \beta)}$ is locally “deformed” to include the corresponding initial condition $x_{\nu(\kappa\oplus 1)}^+ = \Delta_{\nu(\kappa) \rightarrow \nu(\kappa\oplus 1)} \left(x_{\nu(\kappa)}^- \right)$, i.e. $x_{\nu(\kappa\oplus 1)}^+ \in \mathcal{Z}_{(\alpha_{\nu(\kappa\oplus 1)}^+, \beta)}$. As shown in Fig. 6.5, this is achieved through the parameter update law

$$\Gamma_{\nu(\kappa\oplus 1)}^\alpha : \Delta_{\nu(\kappa) \rightarrow \nu(\kappa\oplus 1)} \left(\mathcal{S}_{\nu(\kappa) \rightarrow \nu(\kappa\oplus 1)} \right) \times \mathcal{B} \rightarrow \mathcal{A}_{\nu(\kappa\oplus 1)} \quad (6.34)$$

given by the rule

$$\begin{aligned} \alpha_{\nu(\kappa\oplus 1)}^+ &:= \Gamma_{\nu(\kappa\oplus 1)}^\alpha \left(x_{\nu(\kappa\oplus 1)}^+, \beta \right) \\ &= \Gamma_{\nu(\kappa\oplus 1)}^\alpha \left(\Delta_{\nu(\kappa) \rightarrow \nu(\kappa\oplus 1)} \left(x_{\nu(\kappa)}^- \right), \beta \right), \end{aligned} \quad (6.35)$$

where $\Delta_{\nu(\kappa) \rightarrow \nu(\kappa\oplus 1)} \left(\mathcal{S}_{\nu(\kappa) \rightarrow \nu(\kappa\oplus 1)} \right) \subset \mathcal{X}_{\nu(\kappa\oplus 1)}$ is the image of the surface $\mathcal{S}_{\nu(\kappa) \rightarrow \nu(\kappa\oplus 1)} \subset \mathcal{X}_{\nu(\kappa)}$ under the reset map $\Delta_{\nu(\kappa) \rightarrow \nu(\kappa\oplus 1)}$.

Remark 6.7. Essentially, for each $\nu(\kappa) \in \mathcal{M}$, $\alpha_{\nu(\kappa)}$ is updated so that it affects only the *entry* conditions to the continuous phase $\nu(\kappa)$; the updated values leave the *exit* conditions unaffected. Note here that the exit conditions depend partly on β , which will be updated via the outer loop in order to achieve stability, as will be discussed in Section 6.4.2. \triangleleft

6.4.1.2 Parameterized Hybrid Extensions in Closed-loop with Inner-loop Controllers

To capture the effect of the parameters $\alpha_{\nu(\kappa)}$ in the *hybrid* dynamics of the system, the tool of *parameterized hybrid extensions*, which has been introduced in [83] and [81, Chapter 8], will be used. In particular, the hybrid systems $\Sigma_{\nu(\kappa)}^{(\alpha, \beta)}$ will be reformulated so that the parameters in the arrays $\alpha_{\nu(\kappa)}$ are part of the state vector of the corresponding phase—it should be emphasized that *only* the parameters that are updated by the inner-loop controller participate in the extended state vector.

Consider the extended state space $\mathcal{X}_{\nu(\kappa)}^e := TQ_{\nu(\kappa)} \times \mathcal{A}_{\nu(\kappa)}$ and let $x_{\nu(\kappa)}^e := (x'_{\nu(\kappa)}, \alpha'_{\nu(\kappa)})' \in \mathcal{X}_{\nu(\kappa)}^e$ be the extended state vector, which includes the corresponding $\alpha_{\nu(\kappa)}$ parameters only. The parameters in β do not contribute to the inner-loop controller design, and hence they are not part of the extended system; their role will be clarified in Section 6.4.2. Then, the extended dynamics of the phase $\nu(\kappa) \in \mathcal{M}$ in closed loop with the corresponding

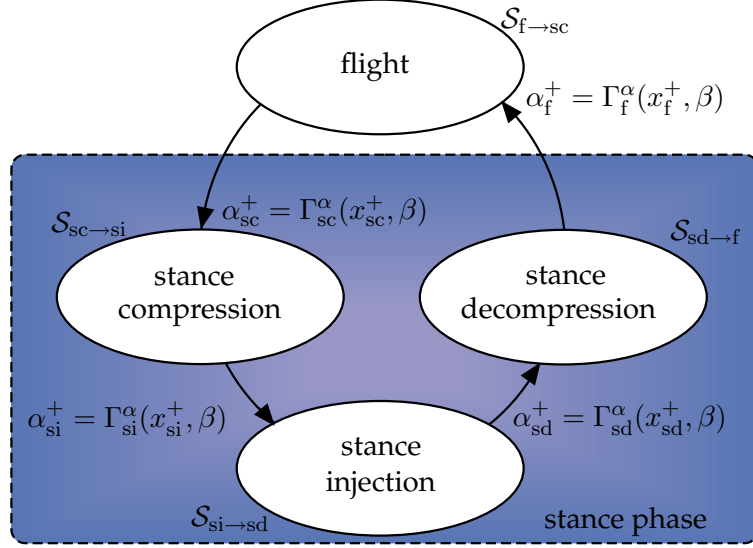


Figure 6.5: Inner-loop event-based control laws $\Gamma_{\nu(\kappa)}^\alpha$ for achieving invariance of the surfaces $\mathcal{Z}_{(\alpha_{\nu(\kappa)}, \beta_{\nu(\kappa)})}$, $\nu(\kappa) \in \mathcal{M}$. These controllers, in combination with the continuous-time control action (6.28), result in a well defined hybrid zero dynamics, which will be rendered exponentially stable via the outer-loop controller of Section 6.4.2; see Fig. 6.6. The symbols α_{sc}^+ , α_{si}^+ , α_{sd}^+ represent updated values of the parameter arrays α_{sc} , α_{si} , α_{sd} , respectively, at the beginning of the corresponding stance subphases.

continuous-time feedback law $\Gamma_{\nu(\kappa)}^c$ becomes

$$f_{\nu(\kappa),cl}^e(x_{\nu(\kappa)}^e, \beta) = \begin{bmatrix} f_{\nu(\kappa),cl}(x_{\nu(\kappa)}, \alpha_{\nu(\kappa)}, \beta) \\ 0 \end{bmatrix}, \quad (6.36)$$

in which the trivial dynamics $\dot{\alpha}_{\nu(\kappa)} = 0$ has been incorporated and $\beta = (\beta'_s, \beta'_f)' \in \mathcal{B}$. Let $H_{\nu(\kappa) \rightarrow \nu(\kappa \oplus 1)}^e : \mathcal{X}_{\nu(\kappa)}^e \times \mathcal{B} \rightarrow \mathbb{R}$ denote the (extended) threshold function whose zeroing defines the surface

$$\mathcal{S}_{\nu(\kappa) \rightarrow \nu(\kappa \oplus 1)}^e := \left\{ (x_{\nu(\kappa)}^e, \beta) \in \mathcal{X}_{\nu(\kappa)}^e \times \mathcal{B} \mid H_{\nu(\kappa) \rightarrow \nu(\kappa \oplus 1)}^e(x_{\nu(\kappa)}^e, \beta) = 0 \right\} \quad (6.37)$$

signifying switching from the phase $\nu(\kappa)$ to the ensuing phase $\nu(\kappa \oplus 1)$. The functions $H_{\nu(\kappa) \rightarrow \nu(\kappa \oplus 1)}^e$ are trivial extensions of the threshold functions $H_{\nu(\kappa) \rightarrow \nu(\kappa \oplus 1)}$ defined by (6.32), since *none* of these maps depends explicitly on the corresponding parameters $\alpha_{\nu(\kappa)}$. In fact, as was mentioned in Remark 6.4, the switching surfaces not only are independent of $\alpha_{\nu(\kappa)}$,

but also independent of β with the exception of $\mathcal{S}_{\text{si} \rightarrow \text{sd}}^e$ which depends explicitly on the parameters β_{si} . The extended reset map $\Delta_{\nu(\kappa) \rightarrow \nu(\kappa \oplus 1)}^e : \mathcal{S}_{\nu(\kappa) \rightarrow \nu(\kappa \oplus 1)}^e \times \mathcal{B} \rightarrow \mathcal{X}_{\nu(\kappa \oplus 1)}^e$ can then be given by the rule

$$\Delta_{\nu(\kappa) \rightarrow \nu(\kappa \oplus 1)}^e \left(x_{\nu(\kappa)}^-, \beta \right) := \begin{bmatrix} \Delta_{\nu(\kappa) \rightarrow \nu(\kappa \oplus 1)}(x_{\nu(\kappa)}^-) \\ \Gamma_{\nu(\kappa \oplus 1)}^\alpha \left(\Delta_{\nu(\kappa) \rightarrow \nu(\kappa \oplus 1)}(x_{\nu(\kappa)}^-), \beta \right) \end{bmatrix}, \quad (6.38)$$

where the reset maps $\Delta_{\nu(\kappa) \rightarrow \nu(\kappa \oplus 1)}$ are defined by (6.33). From (6.38), the dependence of the extended reset map $\Delta_{\nu(\kappa) \rightarrow \nu(\kappa \oplus 1)}^e$ on the corresponding inner-loop parameter update control law $\Gamma_{\nu(\kappa \oplus 1)}^\alpha$ is explicit.

Remark 6.8. By the right-hand side of (6.38) it is clear that the map $\Delta_{\nu(\kappa) \rightarrow \nu(\kappa \oplus 1)}^e$ depends *only* on the exit states $x_{\nu(\kappa)}^-$ of the previous phase and on β . As a result, the updated value $\alpha_{\nu(\kappa \oplus 1)}^+$ is independent of $\alpha_{\nu(\kappa)}$. To emphasize this property, the dependence of the map $\Delta_{\nu(\kappa) \rightarrow \nu(\kappa \oplus 1)}^e$ on the reduced state $x_{\nu(\kappa)}^-$ explicitly appears in (6.38). \triangleleft

Given these definitions, the deadbeat hybrid extension of $\Sigma_{\nu(\kappa)}^{(\alpha, \beta)}$ is given by

$$\left(\Sigma_{\nu(\kappa)}^\beta \right)^e : \begin{cases} x_{\nu(\kappa)}^e \in \mathcal{X}_{\nu(\kappa)}^e, \beta \in \mathcal{B} \\ \dot{x}_{\nu(\kappa)}^e = f_{\nu(\kappa), \text{cl}}^e(x_{\nu(\kappa)}^e, \beta) \\ \mathcal{S}_{\nu(\kappa) \rightarrow \nu(\kappa \oplus 1)}^e := \left\{ (x_{\nu(\kappa)}^e, \beta) \in \mathcal{X}_{\nu(\kappa)}^e \times \mathcal{B} \mid H_{\nu(\kappa) \rightarrow \nu(\kappa \oplus 1)}^e(x_{\nu(\kappa)}^e, \beta) = 0 \right\} \\ (x^e)_{\nu(\kappa \oplus 1)}^+ = \Delta_{\nu(\kappa) \rightarrow \nu(\kappa \oplus 1)}^e(x_{\nu(\kappa)}^-, \beta) \end{cases}$$

which, through the inclusion of the parameters $\alpha_{\nu(\kappa)}$ in the state vector $x_{\nu(\kappa)}^e$ of the continuous part of the system, exposes their role in the hybrid dynamics of Thumper.

Next, the concept of a *flow map* associated with each of the hybrid extensions $\left(\Sigma_{\nu(\kappa)}^\beta \right)^e$ is discussed. The flow maps will be useful in bringing the system to the form of a system with impulse effects, which will facilitate the design of the outer-loop control law in the following section. Roughly, the flow map associated with $\left(\Sigma_{\nu(\kappa)}^\beta \right)^e$ is a map taking the entry conditions $(x^e)_{\nu(\kappa)}^+$ of phase $\nu(\kappa)$ to the corresponding exit conditions $(x^e)_{\nu(\kappa)}^-$ given the values of the parameters β . More precisely, let $\phi_{\nu(\kappa), \text{cl}}^e : [0, +\infty) \times \mathcal{X}_{\nu(\kappa)}^e \times \mathcal{B} \rightarrow \mathcal{X}_{\nu(\kappa)}^e$ denote the flow generated by the closed-loop (extended) vector field $f_{\nu(\kappa), \text{cl}}^e$ of the contin-

uous phase $\nu(\kappa) \in \mathcal{M}$. Define the time-to-switching function $T_{\nu(\kappa)} : \mathcal{X}_{\nu(\kappa)}^e \times \mathcal{B} \rightarrow \mathbb{R} \cup \{\infty\}$ by the rule

$$T_{\nu(\kappa)} \left(x_{\nu(\kappa),0}^e, \beta \right) := \begin{cases} \inf \left\{ t \in [0, +\infty) \mid \phi_{\nu(\kappa),\text{cl}}^e \left(t, x_{\nu(\kappa),0}^e, \beta \right) \in \mathcal{S}_{\nu(\kappa) \rightarrow \nu(\kappa \oplus 1)}^e \right\}, \\ \text{if } \exists t \text{ such that } \phi_{\nu(\kappa),\text{cl}}^e \left(t, x_{\nu(\kappa),0}^e, \beta \right) \in \mathcal{S}_{\nu(\kappa) \rightarrow \nu(\kappa \oplus 1)}^e \\ \infty, \text{ otherwise.} \end{cases} \quad (6.39)$$

The flow map⁸ $F_{\nu(\kappa)}^e : \mathcal{X}_{\nu(\kappa)}^e \times \mathcal{B} \rightarrow \mathcal{S}_{\nu(\kappa) \rightarrow \nu(\kappa \oplus 1)}^e$ for the (extended) dynamics of the phase $\nu(\kappa) \in \mathcal{M}$ can then be defined by the rule

$$F_{\nu(\kappa)}^e \left(x_{\nu(\kappa),0}^e, \beta \right) := \phi_{\nu(\kappa),\text{cl}}^e \left(T_{\nu(\kappa)} \left(x_{\nu(\kappa),0}^e, \beta \right), x_{\nu(\kappa),0}^e, \beta \right). \quad (6.40)$$

The notion of the flow map can be used to define an overall stance flow map, taking the initial (entry) conditions of the stance-compression phase $(x_{\text{sc}}^e)^+ \in \mathcal{X}_{\text{sc}}^e$, i.e., the touchdown state, together with $\beta \in \mathcal{B}$, to the final (exit) conditions of the stance-decompression phase $(x_{\text{sd}}^e)^- \in \mathcal{X}_{\text{sd}}^e$, i.e., the liftoff state. Hence, the (extended) stance flow map $F_s^e : \mathcal{X}_{\text{sc}}^e \times \mathcal{B} \rightarrow \mathcal{S}_{\text{sd} \rightarrow \text{f}}^e$ can be defined by properly composing the individual flow maps of the three subphases of the stance phase, and is given by the rule

$$\begin{aligned} (x_{\text{sd}}^e)^- &= F_s^e \left((x_{\text{sc}}^e)^+, \beta \right) \\ &:= F_{\text{sd}}^e \left(\Delta_{\text{si} \rightarrow \text{sd}}^e \left(F_{\text{si}}^e \left(\Delta_{\text{sc} \rightarrow \text{si}}^e \left(F_{\text{sc}}^e \left((x_{\text{sc}}^e)^+, \beta \right), \beta \right), \beta \right), \beta \right), \beta \right). \end{aligned} \quad (6.41)$$

Note that the dependence of F_s^e on β corresponds to dependence on β_s only, since the individual stance flow maps do not depend on β_f . However, this distinction is not necessary for the design of the outer-loop controllers and it will be dropped. It is remarked here that the map F_s^e includes the effects of both the continuous-time and the event-based inner-loop control actions.

⁸The definition of a flow map presupposes the existence of a time instant t such that $\phi_{\nu(\kappa)}^e(t, x_{\nu(\kappa),0}^e, \beta) \in \mathcal{S}_{\nu(\kappa) \rightarrow \nu(\kappa \oplus 1)}^e$. The case where no such time instant exists does not correspond to periodic running motions.

6.4.2 Outer-loop Event-based Control for Stability

A critical aspect of the dynamics of Thumper in closed-loop with the continuous-time and inner-loop event-based controllers, $\Gamma_{\nu(\kappa)}^c$ and $\Gamma_{\nu(\kappa)}^\alpha$, respectively, is its dependence on the parameter array $\beta := \{\beta_s, \beta_f\} \in \mathcal{B}$, which can be selected according to an outer-loop event-based feedback law Γ^β , as shown in Fig. 6.1.

6.4.2.1 Outer-loop Controller Objectives

The purpose of Γ^β is to (locally) exponentially stabilize a desired periodic orbit representing running in Thumper. Let $x_f^- \in \mathcal{S}_{f \rightarrow sc}$ be the exit conditions of the flight phase. Then, exponential stability can be ensured by updating the parameters β to a new value β^+ based on feedback from x_f^- so that all the eigenvalues of the linearization of the Poincaré map associated with the desired running gait are within the unit disc. This will be achieved through properly designing the outer-loop event-based parameter update law $\Gamma^\beta : \mathcal{S}_{f \rightarrow sc} \rightarrow \mathcal{B}$, given by the rule

$$\beta^+ = \Gamma^\beta(x_f^-). \quad (6.42)$$

6.4.2.2 A System with Impulse Effects for Designing the Outer-loop Controller

In what follows, the hybrid systems $\left(\Sigma_{\nu(\kappa)}^\beta\right)^e$ will be brought to a suitable form, which will facilitate the design of the outer-loop controller Γ^β . As a matter of fact, under the influence of continuous-time and the inner-loop event-based controllers, the system can be transformed into the form⁹

$$\Sigma^\beta : \begin{cases} \dot{x}_f^e = f_{f,cl}^e(x_f^e, \beta), & x_f^- \notin \mathcal{S}_{f \rightarrow sc}, \beta \in \mathcal{B} \\ (x_f^e)^+ = \Delta_{cl}^e(x_f^-, \beta), & x_f^- \in \mathcal{S}_{f \rightarrow sc}, \beta \in \mathcal{B}, \end{cases} \quad (6.43)$$

⁹Note that since the system Σ^β evolves in the extended flight state space \mathcal{X}_f^e with its continuous flow interrupted by the switching surface $\mathcal{S}_{f \rightarrow sc}^e$, it would be proper to have the discrete part be dependent on the extended state vector $(x_f^e)^-$, and not on the reduced state vector x_f^- , as in (6.43), i.e.,

$$\Sigma^\beta : \begin{cases} \dot{x}_f^e = f_{f,cl}^e(x_f^e, \beta), & (x_f^e)^- \notin \mathcal{S}_{f \rightarrow sc}^e, \beta \in \mathcal{B} \\ (x_f^e)^+ = \Delta_{cl}^e((x_f^e)^-, \beta), & (x_f^e)^- \in \mathcal{S}_{f \rightarrow sc}^e, \beta \in \mathcal{B}. \end{cases}$$

The form of (6.43) highlights the fact that switching is triggered by the reduced state vector x_f^- , i.e., it does not depend explicitly on the parameters α_f , as was mentioned in Remarks 6.4, 6.6 and 6.8.

which corresponds to a parameter-dependent system with impulse effects; see Fig. 6.6. To achieve this transformation, the extended stance flow map defined by (6.41) is important.

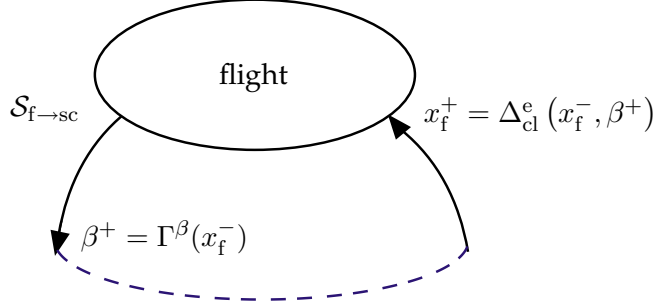


Figure 6.6: Thumper's dynamics represented as a system with impulse effects. The outer-loop event-based control achieves stability of the system.

The system Σ^β given by (6.43) evolves in continuous time in the extended flight state space \mathcal{X}_f^e according to the closed-loop extended flight vector field $f_{f,cl}^e$, defined by

$$f_{f,cl}^e(x_f^e, \beta) = \begin{bmatrix} f_{f,cl}(x_f, \alpha_f, \beta) \\ 0 \end{bmatrix}, \quad (6.44)$$

until the associated flow pierces the switching surface $\mathcal{S}_{f \to sc}^e := \{x_f^e \in \mathcal{X}_f^e \mid H_{f \to sc}^e(x_f^e) = 0\}$, which, as was mentioned in Remark 6.4, *does not* depend explicitly on the parameters α_f and β . Subsequently, the extended flight state is reset to a new initial condition according to the extended reset map $\Delta_{cl}^e : \mathcal{S}_{f \to sc}^e \times \mathcal{B} \rightarrow \mathcal{X}_f^e$ given by the rule

$$\Delta_{cl}^e(x_f^-, \beta) := \begin{bmatrix} \Delta_{cl}(x_f^-, \beta) \\ \Gamma_f^\alpha(\Delta_{cl}(x_f^-, \beta), \beta) \end{bmatrix}, \quad (6.45)$$

where Γ_f^α is the inner-loop parameter update controller for the flight phase defined by (6.34) for $\kappa = 2$, and the map $\Delta_{cl} : \mathcal{S}_{f \to sc} \times \mathcal{B} \rightarrow TQ_f$ is defined by the rule

$$\Delta_{cl}(x_f^-, \beta) := \Delta_{sd \to f}(\pi_{sd}(F_s^e(\Delta_{f \to sc}^e(x_f^-, \beta), \beta))), \quad (6.46)$$

and it provides the initial states $x_f^+ \in TQ_f$ for the reduced —not the extended— flight phase. In (6.46), $\Delta_{f \to sc}^e$ is the extended flight-to-stance-compression map defined by (6.38),

and the maps F_s^e and $\Delta_{sd \rightarrow f}$ correspond to the (extended) stance flow map defined by (6.41) and the (reduced) stance-decompression-to-flight transition map given by (6.33), respectively. Finally, the map $\pi_{sd} : \mathcal{X}_{sd} = TQ_{sd} \times \mathcal{A}_{sd} \rightarrow TQ_{sd}$, given by the rule $x_{sd}^e = (x'_{sd}, \alpha'_{sd})' \mapsto x_{sd}$ is the natural projection of the extended state to its first component corresponding to the reduced state vector.

As was mentioned above, the switching surface $\mathcal{S}_{f \rightarrow sc}^e \subset \mathcal{X}_f^e = TQ_f \times \mathcal{A}_f$ does *not* depend on the values of the parameters α_f . Neither does it depend on the parameters β ; it corresponds to the ground surface containing all the states compatible with the constraint $p_{toe}^v(x_f) = 0$, where p_{toe}^v is the vertical distance between the toe and the ground. Selecting the Poincaré section to be the ground surface $\mathcal{S}_{f \rightarrow sc}$, the (parameter-dependent) Poincaré map $\mathcal{P} : \mathcal{S}_{f \rightarrow sc} \times \mathcal{B} \rightarrow \mathcal{S}_{f \rightarrow sc}$ associated with the system with impulse effects Σ^β of (6.43) can be defined by

$$\mathcal{P}(x_f^-, \beta) := \pi_f \circ \phi_{f, cl}^e(\Delta_{cl}^e(x_f^-, \beta), T_f(\Delta_{cl}^e(x_f^-, \beta), \beta)), \quad (6.47)$$

where the map $\pi_f : \mathcal{X}_f = TQ_f \times \mathcal{A}_f \rightarrow TQ_f$, is the natural projection given by the rule $x_f^e = (x'_f, \alpha'_f)' \mapsto x_f$, $\phi_{f, cl}^e$ is the flow of the extended flight closed-loop vector field, Δ_{cl}^e is the (extended) flight reset map defined by (6.45), and T_f is the time-to-touchdown map defined by (6.39) for $\kappa = 3$.

The return map \mathcal{P} depends smoothly on x_f^- and on β and it gives rise to the discrete-time control system

$$x_f^-[k+1] = \mathcal{P}(x_f^-[k], \beta[k]), \quad (6.48)$$

where $x_f^-[k]$ is the state just prior to k -th touchdown and the parameter β is an input available for event-based control. In Thumper, we are interested in periodic running orbits, which can be represented by period-one fixed points of the return map \mathcal{P} , that is, points which satisfy

$$x_f^-[k+1] = x_f^-[k] \Leftrightarrow x_f^-[k] = \mathcal{P}(x_f^-[k], \beta[k]). \quad (6.49)$$

Such solutions of (6.49) will be denoted by \bar{x}_f^- and the corresponding input by $\bar{\beta}$, and they represent equilibrium points of the discrete-time time-invariant (6.48).

Linearizing (6.48) about the equilibrium conditions \bar{x}_f^- and $\bar{\beta}$ gives the discrete-time linear-time-invariant control system

$$\delta x_f^- [k + 1] = \left(\frac{\partial \mathcal{P}}{\partial x_f^-} \right) \Big|_{(x_f^- = \bar{x}_f^-, \beta = \bar{\beta})} \delta x_f^- [k] + \left(\frac{\partial \mathcal{P}}{\partial \beta} \right) \Big|_{(x_f^- = \bar{x}_f^-, \beta = \bar{\beta})} \delta \beta [k], \quad (6.50)$$

where $\delta x_f^- = x_f^- - \bar{x}_f^-$ and $\delta \beta = \beta - \bar{\beta}$. In Section 6.5.2, a controller will be devised for $\delta \beta$, so that the eigenvalues of the Jacobian matrix $\left(\frac{\partial \mathcal{P}}{\partial x_f^-} \right) \Big|_{(x_f^- = \bar{x}_f^-, \beta = \bar{\beta})}$ are all within the unit disc, thus ensuring (local) exponential stability of the system.

6.5 Event-based Control of Thumper: Details

In this section, the general considerations of Section 6.4 are particularized to design inner and outer-loop event-based parameter update laws suitable for stabilizing running in Thumper. The inner-loop parameter update laws, which will be proposed in Section 6.5.1 below, result in a well-defined hybrid zero dynamics, which is then rendered (locally) exponentially stable by the outer-loop controller of Section 6.5.2. The control-laws designed below are tested in simulation in Section 6.7.

6.5.1 Inner-loop Event-based Control for Invariance

In what follows, specific rules for updating the parameters $\alpha_{\nu(\kappa)}$ will be devised, so that, at the beginning of each continuous-time phase, the initial condition lies on the corresponding zero dynamics surface $\mathcal{Z}_{(\alpha_{\nu(\kappa)}, \beta_{\nu(\kappa)})}$. In some phases, not all the parameters participating in the definitions of the corresponding constraints of Section 6.2 are needed to achieve the objective. In other phases, it may be that there are not enough parameters to ensure invariance. In this section, the arrays $\alpha_{\nu(\kappa)}$ containing the parameters that are relevant to the control action—that is, the parameters that are necessary to be updated—are first defined for each phase $\nu(\kappa)$. Then, update laws for these parameters that achieve the objectives are derived.

6.5.1.1 Stance-compression phase coefficients

When the surface $\mathcal{S}_{f \rightarrow sc} = \mathcal{S}_{f \rightarrow s}$ is crossed, switching from flight to stance occurs and the stance-compression phase is initiated. At this point, given $\beta_{sc} \in \mathcal{B}_{sc}$, a number of the stance parameters α_s can be updated so that the initial state lies on the stance-compression zero dynamics manifold. However, this condition cannot be guaranteed only through updates of parameters participating in α_s as was defined by (6.11). Indeed, if $\dot{q}_{mLS} \neq 0$ at the beginning of the stance-compression phase, there is no available coefficient in $h_{s,2}^d$ in (6.7) that can be updated to match the non-zero velocity. To ensure that the condition $x_{sc}^+ \in \mathcal{Z}_{(\alpha_{sc}^+, \beta_{sc})}$ is satisfied, additional parameters are required. Following the procedure in [25], to introduce these additional parameters the output for the stance-compression phase is modified to be

$$\begin{aligned} y_{sc} &:= h_{sc}(q_{sc}, \alpha_{sc}, \beta_{sc}) \\ &:= h_s(q_s, \alpha_s, \beta_s) - h_{corr}(\theta(q_{sc}), \alpha_{corr}), \end{aligned} \quad (6.51)$$

where the term h_s corresponds to the part of the stance constraint (6.2), which is enforced during stance-compression. This part depends only on coefficients that are entries of the α_s given by (6.11). The correction term h_{corr} affects only the evolution of the desired q_{mLS} and is given by

$$h_{corr}(\theta(q_{sc}), \alpha_{corr}) = \begin{bmatrix} 0 \\ h_{corr}^{mLS}(\theta(q_{sc}), \alpha_{corr}) \end{bmatrix}, \quad (6.52)$$

where h_{corr}^{mLS} is selected to be a fourth order correction polynomial

$$h_{corr}^{mLS}(\theta(q_{sc}), \alpha_{corr}) = \sum_{k=0}^4 \alpha_{corr,k} s_{corr}^k(\theta(q_{sc})), \quad (6.53)$$

intended to drive the error between q_{mLS} and its desired value to zero, so that the evolution of q_{mLS} is smoothly joined to the original constraint shown in Fig. 6.2 by the middle of the compression phase. In (6.53),

$$s_{corr} = \frac{\theta - \bar{\theta}^{\min}}{\bar{\theta}_{mLS}^{\min} - \bar{\theta}^{\min}}, \quad (6.54)$$

where $\bar{\theta}^{\min}$ and $\bar{\theta}_{\text{mLS}}^{\min}$ denote the values of θ at the beginning and at the end of the stance-compression phase of the nominal orbit, respectively.

This procedure introduces a number of additional coefficients α_{corr} , which, together with some of the entries of the array α_s given by (6.11), define the parameters α_{sc} , namely

$$\alpha_{\text{sc}} := \{\alpha_{s,(0,1)}, \alpha_{s,(1,1)}, \theta_{\text{Tor}}^{\min}, \alpha_{\text{corr},0}, \dots, \alpha_{\text{corr},4}\}, \quad (6.55)$$

that are available in the stance-compression phase and can be used to achieve the feedback objectives. Note that the array (6.55) does not contain all the parameters that can affect the stance-compression dynamics; it contains only those parameters that will be updated through the inner-loop controller.

As a result of the inclusion of the correction polynomial, the input/output dynamics of (6.23) for the stance-compression phase becomes

$$\frac{d^2 y_{\text{sc}}}{dt^2} = L_{f_{\text{sc}}}^2 h_{\text{sc}}(x_{\text{sc}}, \alpha_{\text{sc}}, \beta_{\text{sc}}) + L_{g_{\text{sc}}} L_{f_{\text{sc}}} h_{\text{sc}}(q_{\text{sc}}, \alpha_{\text{sc}}, \beta_{\text{sc}})u, \quad (6.56)$$

in which,

$$\begin{aligned} L_{f_{\text{sc}}}^2 h_{\text{sc}} &:= L_{f_{\text{sc}}}^2 h_s \\ &- \left(\frac{\partial^2 h_{\text{corr}}^{\text{mLS}}}{\partial s_{\text{corr}}^2} \left[\frac{\partial s_{\text{corr}}}{\partial q_{\text{sc}}} \dot{q}_{\text{sc}} \right]^2 + \frac{\partial h_{\text{corr}}^{\text{mLS}}}{\partial s_{\text{corr}}} \frac{\partial s_{\text{corr}}}{\partial q_{\text{sc}}} D_s^{-1} (-C_s \dot{q}_{\text{sc}} - G_s) \right), \end{aligned} \quad (6.57)$$

and

$$L_{g_{\text{sc}}} L_{f_{\text{sc}}} h_{\text{sc}} := L_{g_{\text{sc}}} L_{f_{\text{sc}}} h_s - \frac{\partial h_{\text{corr}}^{\text{mLS}}}{\partial s_{\text{corr}}} \frac{\partial s_{\text{corr}}}{\partial q_{\text{sc}}} D_s^{-1} B_s, \quad (6.58)$$

where the dependence of $L_{f_{\text{sc}}}^2 h_{\text{sc}}$ and $L_{g_{\text{sc}}} L_{f_{\text{sc}}} h_{\text{sc}}$ on x_{sc} , α_{sc} and β_{sc} has been suppressed.

To formulate the inner-loop parameter-update law $\Gamma_{\text{sc}}^\alpha$, let $q_{\text{LA}}^{\text{sc}+}$ and $q_{\text{Tor}}^{\text{sc}+}$ be the values of the leg angle and torso pitch angle at the beginning of the stance-compression phase, respectively. Note that these values correspond to touchdown, i.e., they are identical to $q_{\text{LA}}^{\text{s}+}$ and $q_{\text{Tor}}^{\text{s}+}$. Then, $\theta_{\text{Tor}}^{\min}$ can be computed using (6.3) resulting in $s_{\text{Tor}} = 0$ at the beginning

of stance-compression phase, i.e.,

$$\theta_{\text{Tor}}^{\min} = -\frac{3\pi}{2} + q_{\text{LA}}^{\text{sc}+} + q_{\text{Tor}}^{\text{sc}+}. \quad (6.59)$$

Given $\beta_{\text{s,set}}$ so that $\theta_{\text{Tor}}^{\max} = \beta_{\text{s,set}}$ and with $\theta_{\text{Tor}}^{\min}$ specified at touchdown by (6.59), setting

$$\begin{aligned} \alpha_{\text{s,(0,1)}}^+ &= q_{\text{Tor}}^{\text{sc}+}, \\ \alpha_{\text{s,(1,1)}}^+ &= q_{\text{Tor}}^{\text{sc}+} + \frac{1}{M \dot{s}_{\text{Tor}}^{\text{sc}+}} \dot{q}_{\text{Tor}}^{\text{sc}+}, \end{aligned} \quad (6.60)$$

where $M = 6$ and $\dot{q}_{\text{Tor}}^{\text{sc}+}$ is the value of the torso pitch velocity at the beginning of the stance phase, ensures that the zero dynamics manifold includes the landing conditions on the pitch.

To complete the design of $\Gamma_{\text{sc}}^\alpha$, the coefficients α_{corr} of the correction polynomial are updated based on the initial conditions of stance-compression by solving the system

$$A_{\text{corr}} \alpha_{\text{corr}}^+ = e_{\text{mLS}} \Rightarrow \alpha_{\text{corr}}^+ = A_{\text{corr}}^{-1} e_{\text{mLS}}, \quad (6.61)$$

where $e_{\text{mLS}} = [q_{\text{mLS}}^{\text{sc}+} - \bar{\alpha}_{\text{s}(-1,2)} \dot{q}_{\text{mLS}}^{\text{sc}+} \ 0 \ 0 \ 0]'$, $\bar{\alpha}_{\text{s}(-1,2)}$ is the nominal value of q_{mLS} at touch-down, and

$$A_{\text{corr}} = \begin{bmatrix} 1 & s_{\text{corr}}^{\text{in}} & (s_{\text{corr}}^{\text{in}})^2 & (s_{\text{corr}}^{\text{in}})^3 & (s_{\text{corr}}^{\text{in}})^4 \\ 0 & 1 & 2s_{\text{corr}}^{\text{in}} & 3(s_{\text{corr}}^{\text{in}})^2 & 4(s_{\text{corr}}^{\text{in}})^3 \\ 1 & s_{\text{corr}}^{\text{fin}} & (s_{\text{corr}}^{\text{fin}})^2 & (s_{\text{corr}}^{\text{fin}})^3 & (s_{\text{corr}}^{\text{fin}})^4 \\ 0 & 1 & 2s_{\text{corr}}^{\text{fin}} & 3(s_{\text{corr}}^{\text{fin}})^2 & 4(s_{\text{corr}}^{\text{fin}})^3 \\ 0 & 0 & 2 & 6s_{\text{corr}}^{\text{fin}} & 12(s_{\text{corr}}^{\text{fin}})^2 \end{bmatrix}, \quad (6.62)$$

where $s_{\text{corr}}^{\text{in}}$ and $s_{\text{corr}}^{\text{fin}}$ are computed by (6.54) using the values $\theta = \theta^{\text{sc}+}$ and

$$\theta = \theta^{\text{sc}+} + 0.5 (\bar{\theta}_{\text{mLS}}^{\min} - \bar{\theta}^{\min}), \quad (6.63)$$

respectively. This procedure for computing the coefficients α_{corr} of the correction polynomial guarantees that the error is driven to zero in a *smooth* way by the middle of the

stance-compression phase. In other words, for any initial error in the q_{mLS} , the virtual constraint $h_{\text{s},2}^{\text{d}}$ in (6.7) is exactly satisfied by the end of the compression part of the stance phase.

The update law (6.61) for the coefficients of the correction polynomial, together with (6.59) and (6.60) provide explicit formulas for the design of the update law $\Gamma_{\text{sc}}^{\alpha}$.

6.5.1.2 Stance-injection phase coefficients

When the surface $\mathcal{S}_{\text{sc} \rightarrow \text{si}}$ is crossed, transition from stance-compression to stance-injection occurs. This allows for updating some of the parameters in α_{s} to ensure that the initial conditions lie on the corresponding zero dynamics manifold. To meet this requirement, no additional parameters are needed; therefore, no correction polynomials will be used. The output associated with the stance-injection phase is

$$y_{\text{si}} := h_{\text{si}}(q_{\text{si}}, \alpha_{\text{si}}, \beta_{\text{si}}) := h_{\text{s}}(q_{\text{s}}, \alpha_{\text{s}}, \beta_{\text{s}}), \quad (6.64)$$

where the term h_{s} corresponds to the part of the stance constraint (6.2), which is enforced during stance-injection. In (6.64), the only parameter participating in α_{si} is $\theta_{\text{mLS}}^{\text{min}}$, i.e.,

$$\alpha_{\text{si}} := \{ \theta_{\text{mLS}}^{\text{min}} \}, \quad (6.65)$$

and will be updated by $\Gamma_{\text{si}}^{\alpha}$ as follows. Let $q_{\text{LA}}^{\text{si}+}$, and $q_{\text{Tor}}^{\text{si}+}$ be the values of the leg and torso angles at the beginning of the stance-injection phase respectively. Then, $\theta_{\text{mLS}}^{\text{min}}$ can be computed by

$$\theta_{\text{mLS}}^{\text{min}} = -\frac{3\pi}{2} + q_{\text{LA}}^{\text{si}+} + q_{\text{Tor}}^{\text{si}+}. \quad (6.66)$$

Remark 6.9. Note that the correction polynomial (6.53), which is part of the modified constraint (6.51) enforced in the stance-compression phase, ensures that for any initial error in q_{mLS} and \dot{q}_{mLS} , the (nominal) virtual constraint $h_{\text{s},2}^{\text{d}}$ in (6.7) is *exactly* satisfied by the end of the compression part of the stance phase. In other words, $q_{\text{mLS}}^{\text{sc}-} = q_{\text{mLS}}^{\text{si}+} = \bar{\alpha}_{\text{s},(-1,2)}$, the nominal value of the motorshaft position throughout stance-compression, and $\dot{q}_{\text{mLS}}^{\text{si}+} = \ddot{q}_{\text{mLS}}^{\text{si}+} = 0$, so that the requirement for the C^2 smoothness of the desired q_{mLS} constraint

imposed on $\{\alpha_{s,(0,2)}, \alpha_{s,(1,2)}, \alpha_{s,(2,2)}\}$ by (6.9) is satisfied without any further updates. \triangleleft

Remark 6.10. No updates in the coefficients of the polynomial describing the desired evolution of q_{Tor} are needed at the beginning of the stance-injection phase. Leaving these coefficients at their values in the stance-compression phase, not only ensures C^2 smoothness in the torso angle constraint, but also ensures that the initial conditions $(q_{\text{Tor}}^{\text{si}+}, \dot{q}_{\text{Tor}}^{\text{si}+})$ belong in the surface $\mathcal{Z}_{(\alpha_{\text{si}}^+, \beta)}$. \triangleleft

6.5.1.3 Stance-decompression phase coefficients

When the surface $\mathcal{S}_{\text{si} \rightarrow \text{sd}}$ is crossed, transition from stance-injection to stance-decompression occurs. The output associated with the stance-decompression phase is

$$y_{\text{sd}} := h_{\text{sd}}(q_{\text{sd}}, \alpha_{\text{sd}}, \beta_{\text{sd}}) := h_{\text{s}}(q_{\text{s}}, \alpha_{\text{s}}, \beta_{\text{s}}), \quad (6.67)$$

where the term h_{s} corresponds to the part of the stance constraint (6.2), which is enforced during stance-decompression. This part of the stance constraints is independent of the parameters α_{s} ; hence, $\alpha_{\text{sd}} = \emptyset$, and no updates take place during the transition from the stance-injection to the stance-decompression phase.

6.5.1.4 Flight phase coefficients

When the surface $\mathcal{S}_{\text{sd} \rightarrow \text{f}}$ is crossed, transition from stance-decompression to flight occurs. The output associated with the flight phase is given by (6.14), in which the parameters α_{f} , which will be updated by $\Gamma_{\text{f}}^{\alpha}$ are

$$\alpha_{\text{f}} := \{\alpha_{\text{f},(0,1)}, \alpha_{\text{f},(1,1)}, \alpha_{\text{f},(0,2)}, \alpha_{\text{f},(1,2)}\}. \quad (6.68)$$

It is emphasized once more that α_{f} does not include all the parameters on which the flight dynamics depends; it only includes those that will be updated to achieve $x_{\text{f}}^+ \in \mathcal{Z}_{(\alpha_{\text{f}}^+, \beta)}$.

Let $x_{\text{cm}}^{\text{f}+}$ be the value of horizontal position of the COM and $\dot{x}_{\text{cm}}^{\text{f}+}$ the corresponding velocity at the beginning of the flight phase. Then, if $(p_{\text{toe}}^{\text{h}})^{\text{f}+}$ and $(\dot{p}_{\text{toe}}^{\text{h}})^{\text{f}+}$ are the horizontal position and velocity of the toe, and in view of the properties of the Beziér polynomials

listed in [109, p. 139], the coefficients $\alpha_{f,(0,1)}$ and $\alpha_{f,(1,1)}$ are updated using

$$\begin{aligned}\alpha_{f,(0,1)} &= (p_{\text{toe}}^h)^{f+} - x_{\text{cm}}^{f+}, \\ \alpha_{f,(1,1)} &= \left[(p_{\text{toe}}^h)^{f+} - x_{\text{cm}}^{f+} \right] + \frac{1}{M\dot{s}_f^+} \left[(\dot{p}_{\text{toe}}^h)^{f+} - \dot{x}_{\text{cm}}^{f+} \right].\end{aligned}\tag{6.69}$$

Similarly, if q_{LS}^{f+} and \dot{q}_{LS}^{f+} denote the values of the leg-shape angle and its rate, then the coefficients $\alpha_{f,(0,2)}$ and $\alpha_{f,(1,2)}$ will be updated by

$$\begin{aligned}\alpha_{f,(0,2)} &= q_{\text{LS}}^{f+}, \\ \alpha_{f,(1,2)} &= q_{\text{LS}}^{f+} + \frac{1}{M\dot{s}_f^+} \dot{q}_{\text{LS}}^{f+},\end{aligned}\tag{6.70}$$

where in both (6.69) and (6.70), $M = 6$. The update laws (6.69) and (6.70) provide explicit formulas for the design of the update law Γ_f^α , completing the inner-loop controller design.

Remark 6.11. Note that (6.15) results in $\ell^{\min} = 0$, hence, $s_f = 0$ always at the beginning of the flight phase, so that there is no need to update ℓ^{\min} at transitions from stance to flight. Moreover, the parameter ℓ^{\max} is left unchanged from the inner-loop controller, and is selected to be equal to its nominal value resulting to $s_f \neq 1$ just prior to touchdown when the system does not evolve on the limit cycle. \triangleleft

6.5.2 Outer-loop Event-based Control for Stability

The system with impulse effects Σ^β defined by (6.43), exposes the dependence of the dynamics of Thumper in closed loop with the continuous-time and the inner-loop event-based control laws, $\Gamma_{\nu(\kappa)}^c$ and $\Gamma_{\nu(\kappa)}^\alpha$, respectively, on the parameters β , which can be used to stabilize periodic running motions, as was explained in Section 6.4.2. Recall here that such periodic motions can be represented by fixed-points of the return map \mathcal{P} defined by (6.48). As was explained in Section 6.4.2, this procedure gives rise to a discrete-time time-invariant control system, in which the parameter β corresponds to an input available for event-based control.

One possibility for the outer-loop event-based parameter update law Γ^β is to use Raibert-style controllers. Indeed, according to Remark 6.1, the parameter $\beta_{s,\text{mLS}}$ determines the

amount of energy that is injected by the leg actuator to maintain hopping. This parameter could be updated at transitions from flight to stance based on feedback from the total hopping energy of the system —alternatively, based on feedback from the hopping height— in a simple PD control fashion as suggested by Raibert in [91, Chapter 6]. Moreover, according to Remark 6.3, the parameter β_f plays a role analogous to that of the touchdown angle, which can be updated based on feedback from the horizontal speed, as in Raibert’s touchdown controller detailed in [91, Chapter 2].

Instead of using Raibert-type control arguments, an LQR controller for updating all the parameters β except $\beta_{s,\text{set}}$ will be derived in this section. This controller ensures (local) exponential stability of the running orbit. First, the parameter $\beta_{s,\text{set}}$ will be fixed based on feedback from the state prior to touchdown, x_f^- , so that the duration of the “transient” part of the desired evolution of q_{Tor} shown in Fig. 6.2 is 70% of the nominal duration of the total stance phase. Specifically, if $\bar{\theta}^{\min}$ and $\bar{\theta}^{\max}$ denote the nominal, i.e., fixed-point, values of θ at the beginning and end of the entire –not only the compression part– stance phase, respectively, then we select

$$\theta_{\text{Tor}}^{\max} = \theta_{\text{Tor}}^{\min} + 0.7 (\bar{\theta}^{\max} - \bar{\theta}^{\min}). \quad (6.71)$$

By $\Gamma_{\text{sc}}^\alpha$, the parameter $\theta_{\text{Tor}}^{\min}$ is given by (6.59), which is repeated here for convenience

$$\theta_{\text{Tor}}^{\min} = -\frac{3\pi}{2} + q_{\text{LA}}^{\text{sc}+} + q_{\text{Tor}}^{\text{sc}+},$$

and since the configuration variables remain invariant under the flight-to-stance impact map, i.e., $q_{\text{LA}}^{\text{f}-} = q_{\text{LA}}^{\text{sc}+}$ and $q_{\text{Tor}}^{\text{f}-} = q_{\text{Tor}}^{\text{sc}+}$, the rule for updating $\beta_{s,\text{set}}$ is

$$\beta_{s,\text{set}}^+ = \left[-\frac{3\pi}{2} + 0.7 (\bar{\theta}^{\max} - \bar{\theta}^{\min}) \right] + q_{\text{LA}}^{\text{f}-} + q_{\text{Tor}}^{\text{f}-}, \quad (6.72)$$

The remaining three parameters, namely, $\beta_{s,\text{Tor}}$, $\beta_{s,\text{mLS}}$ and β_f , are grouped to one array, β_{LQR} , whose value is updated through the use of discrete LQR techniques according to

$$\beta_{\text{LQR}}^+ = \bar{\beta}_{\text{LQR}} + K (x_f^- - \bar{x}_f^-), \quad (6.73)$$

where \bar{x}_f^- is the nominal value of the state just prior to k -th touchdown, and $\bar{\beta}_{\text{LQR}}$ the nominal value of the parameters β_{LQR} . The LQR is designed based on the linearization (6.50) of the return map \mathcal{P} about a fixed point $(\bar{x}_f^-, \bar{\beta})$, which is repeated below

$$\delta x_f^- [k + 1] = \left(\frac{\partial \mathcal{P}}{\partial x_f^-} \right) \Big|_{(x_f^- = \bar{x}_f^-, \beta = \bar{\beta})} \delta x_f^- [k] + \left(\frac{\partial \mathcal{P}}{\partial \beta_{\text{LQR}}} \right) \Big|_{(x_f^- = \bar{x}_f^-, \beta = \bar{\beta})} \delta \beta_{\text{LQR}} [k].$$

Combining (6.72) and (6.73), the outer-loop event-base parameter update law Γ^β is given by

$$\beta^+ = \Gamma^\beta(x_f^-) := K_1 + K_2 x_f^- \quad (6.74)$$

where $\beta := [\beta_{\text{s,set}}, \beta'_{\text{LQR}}]'$ and

$$K_1 = \begin{bmatrix} -\frac{3\pi}{2} + 0.7(\bar{\theta}^{\max} - \bar{\theta}^{\min}) \\ \bar{\beta}_{\text{LQR}} - K \bar{x}_f^- \end{bmatrix} \quad (6.75)$$

and

$$K_2 = \begin{bmatrix} 1 & 0 & 0 & 1 & 0 & 0 & 0 & 0 \\ & & & & K & & & \end{bmatrix} \quad (6.76)$$

The feedback controller (6.74) guarantees that all the eigenvalues of the linearization (6.50) of the Poincaré map (6.48) are within the unit disc, and completes the control design.

6.6 Nominal Running Orbits through Optimization

Consider the hybrid dynamics of the Thumper in closed-loop with the continuous-time and event-based feedback controllers $\Gamma_{\nu(\kappa)}^c$ and $(\Gamma_{\nu(\kappa)}^\alpha, \Gamma^\beta)$ developed in Section 6.3 and in Sections 6.4 and 6.5, respectively. The problem of finding a periodic motion for the closed-loop system can be cast as a constrained minimization problem according to the procedure of [109, Chapter 6]. This procedure results in a fixed point \bar{x}_f^- of the Poincaré return map (6.48), and in the nominal values $\bar{\alpha}$ and $\bar{\beta}$ of the parameters.

In particular, to the closed-loop hybrid dynamics of Thumper associate the cost func-

tion

$$\mathcal{I}(\alpha, \beta) = \frac{1}{x_{\text{cm}}^{\text{f}-} - x_{\text{cm}}^{\text{f}+}} \int_0^{T_s + T_f} (u_1^2(t) + u_2^2(t)) dt, \quad (6.77)$$

where $x_{\text{cm}}^{\text{f}-}$ and $x_{\text{cm}}^{\text{f}+}$ represent the horizontal position of the COM at the beginning and end of the flight phase, and T_s and T_f are the stance and flight duration, respectively¹⁰. Append to (6.77) the equality constraint

$$x_f^- - \mathcal{P}(x_f^-, \alpha, \beta) = 0, \quad (6.78)$$

so that the nominal orbit is periodic. Then, the problem of finding a fixed point of the closed-loop Poincaré map (6.48) and the corresponding nominal values $\bar{\alpha}$ and $\bar{\beta}$ of the coefficients α and β , respectively, reduces to a constrained minimization problem, which can be (numerically) solved using MATLAB's `fmincon`. One can also include other constraints that correspond to additional gait requirements. For instance, the following criteria could be included in the optimization in the form of equality and inequality constraints:

- the vertical ground reaction force component is nonnegative, so that the unilateral nature of the toe/ground interaction is respected;
- the ratio of the horizontal over the vertical ground reaction force components does not exceed the value of the static friction coefficient, which is assumed to be 0.7, i.e., the friction cone constraint is respected;
- the required control inputs are within the capabilities of the motors;
- the ground clearance achieved during flight exceeds the minimum value of 4 cm;
- the peak-to-peak amplitude of the torso pitch oscillation is kept small;
- the forward running speed is above 1.2. m/s.

Using this procedure a nominal running orbit is computed. Figure 6.7 shows the virtual holonomic constraints defined by (6.4) and (6.7) for the stance, and by (6.16) for the flight phase. Two steps corresponding to a periodic running motion of Thumper are presented

¹⁰Note that multiplying the performance index (6.77) by the factor $1/(x_{\text{cm}}^{\text{f}-} - x_{\text{cm}}^{\text{f}+})$ results in discarding solutions where no flight phase is present.

showing cyclicity. The general shape of the constraints in stance resembles that of Fig. 6.2, and as mentioned in Section 6.2, it reflects our desire to make effective use of the spring while stabilizing the torso to a desired upright posture and ensuring that excessive pitching is not present in flight. Figure 6.8 shows the evolution of the variables s_{Tor} and s_{mLS} , computed by (6.6), (6.8), respectively, which are used to parameterize the stance virtual holonomic constraints.

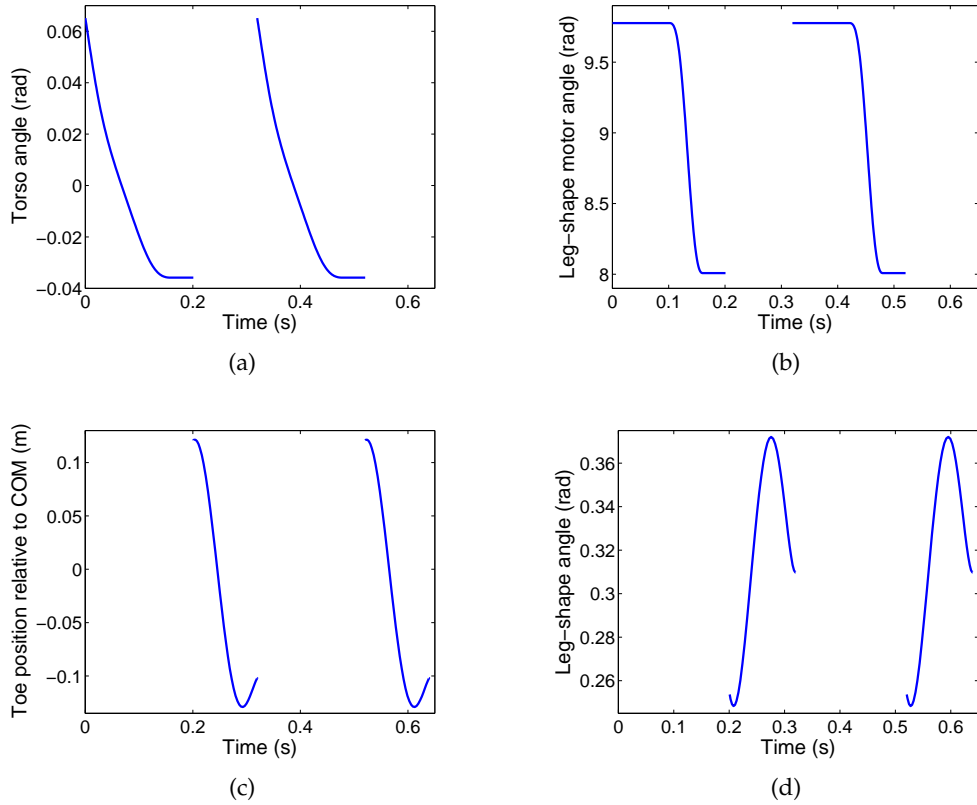


Figure 6.7: Virtual constraints during nominal motion. **Top:** Stance phase torso angle, (a), and leg-shape motor position, (b), constraints given by (6.4) and (6.7), respectively. Compare with Fig. 6.2. **Bottom:** Flight phase toe horizontal position relative to the COM, (c), and leg-shape angle uniquely determining virtual leg length, (d).

Figure 6.9 shows the spring deflection and the associated spring force. As can be seen, when the maximum deflection is reached during the stance-compression phase, the leg-shape actuator performs work on the spring by rapidly repositioning the motorshaft, thus, further increasing the deflection so that additional elastic energy is stored to compensate for losses. Note that according to $S_{\text{sd} \rightarrow \text{f}}$, the stance phase is terminated when the spring

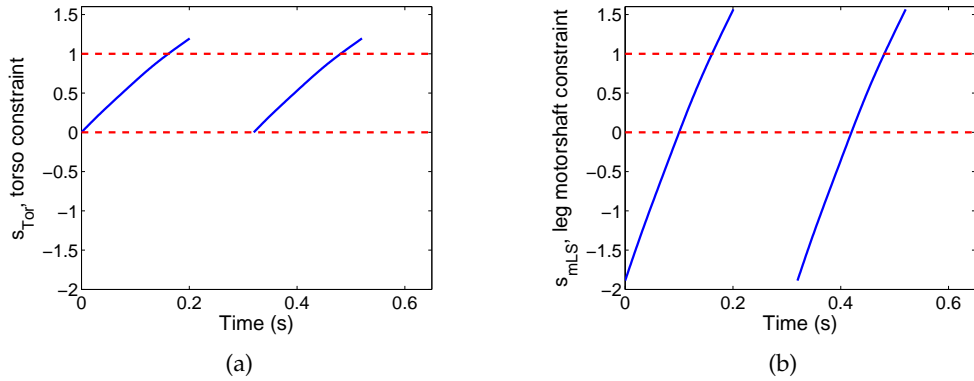


Figure 6.8: Evolution of the independent parameters s_{Tor} in (a), and s_{mLS} in (b), corresponding to the constraints of the stance phase.

deflection becomes zero. At this point, the vertical component of the ground reaction force also becomes zero; see Fig. 6.10.

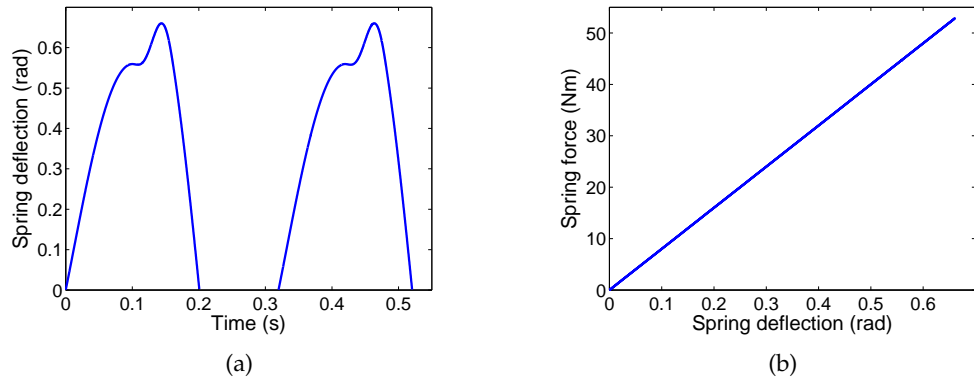


Figure 6.9: Spring deflection, (a), and spring force versus spring deflection, (b).

It should be emphasized that the virtual constraints of Fig. 6.7 induce a nominal running motion in Thumper, which respects all the constraints as Fig. 6.10 and 6.11 demonstrate. In particular, the ground reaction forces respect the friction cone constraints and the unilateral nature of the toe/ground interaction, while, at the same time, the input torques are within the capabilities of the actuators.

In fact, as Fig. 6.10 shows the vertical ground reaction is always positive indicating that the actuators do not produce torques that result in the leg “pulling” the ground. Furthermore, the ratio $|F_{\text{toe}}^T|/F_{\text{toe}}^N$ of the horizontal over the vertical component of the ground reaction force stays below the value of the average static friction coefficient, which is as-

sumed to be equal to 0.7; hence, the toe/ground contact can be modeled as a frictionless pin joint, as Hypothesis HGT3) of Chapter V demands.

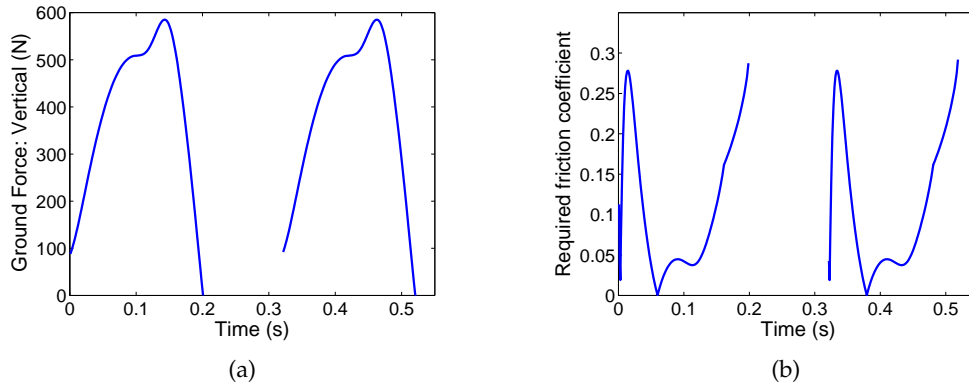


Figure 6.10: Vertical component of the ground reaction force, (a), and minimum required friction coefficient computed by $|F_{toe}^T|/F_{toe}^N$, (b).

Finally, Fig. 6.11 illustrates that the actuator torques required to impose the constraints of Fig. 6.7 on the dynamics of Thumper are within the motor capabilities. Indeed, according to data from the manufacturer, the maximum torque for the leg-angle motor is 32.781Nm, and for the leg-shape motor is 62.130Nm, while the required torques according to Fig. 6.11 never exceed 15Nm for the leg-angle motor and 22Nm for the leg-shape motor.

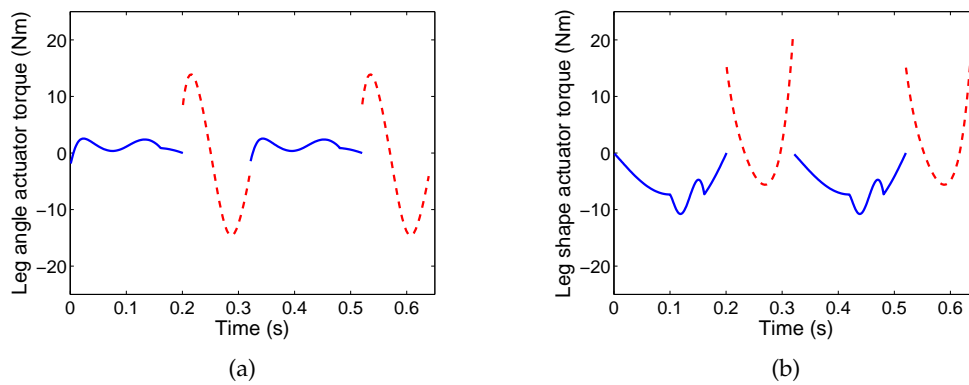


Figure 6.11: Actuator inputs corresponding to the nominal gait presented in Fig. 6.7. Dashed lines correspond to flight phase inputs. Both torques are well within the capabilities of the actuators.

6.7 Evaluation of the Controller in Simulation

Given the nominal running orbit computed in Section 6.6, the gain matrix K that participates in the design of the outer-loop controller Γ^β of Section 6.5.2 can be computed by MATLAB's command "dlqr". Indeed, using the linearization (6.50) of the Poincaré map \mathcal{P} given by (6.47) about the fixed point computed in Section 6.6, the gain matrix K is found to be

$$K = \begin{bmatrix} 0.47 & -0.30 & 0.58 & 0.04 & 0.04 & 0.08 & -0.41 & -0.07 \\ 7.01 & -0.46 & 7.75 & -0.35 & -0.54 & -0.66 & 1.07 & 2.03 \\ 0.44 & -0.19 & 0.51 & 0.01 & 0.01 & 0.02 & -0.15 & 0.01 \end{bmatrix}. \quad (6.79)$$

Then, under the influence of the continuous-time and the event-based control laws of Sections 6.3 and 6.5, the closed-loop eigenvalues are computed to be

$$\lambda_{cl} = \begin{bmatrix} 0.79 & -0.09 & -0.09 & 0.01 & 0 & 0 & 0 & 0 \end{bmatrix}. \quad (6.80)$$

To illustrate the orbit's local stability, the state prior to touchdown is perturbed away from the fixed point \bar{x}_f^- . An initial error of +2 deg is introduced on each angle and an error of +10deg/s and +0.1m/s on each angular velocity and on the velocity of the COM, respectively, i.e.,

$$\delta x_f^- = \begin{bmatrix} 2\frac{\pi}{180} & 2\frac{\pi}{180} & 2\frac{\pi}{180} & 0 & 0 & 10\frac{\pi}{180} & 10\frac{\pi}{180} & 10\frac{\pi}{180} & 0.1 & 0.1 \end{bmatrix}. \quad (6.81)$$

Figure 6.12 shows the evolution of the errors in the torso angle and horizontal velocity in discrete time demonstrating convergence to zero. Figure 6.13 presents the constraints imposed on torso angle and leg-shape motorshaft position during the stance phase. It is interesting to note how the event-based controller manipulates the shape of the imposed constraints. For instance, observe in Fig. 6.13(b) how the shape of the constraint is deformed by the correction polynomial, so that the initial conditions of the stance-compression phase belong in the corresponding zero dynamics surface. Most importantly, note how the outer-loop controller updates the coefficient $\beta_{s,mLS}$, corresponding to the motorshaft position

prior to liftoff, q_{mLS}^{s-} , in order to manipulate the energy stored at the spring. A similar action takes place in updating the torso angle $\beta_{s,Tor}$ at liftoff, as is evident from Fig. 6.13(a).

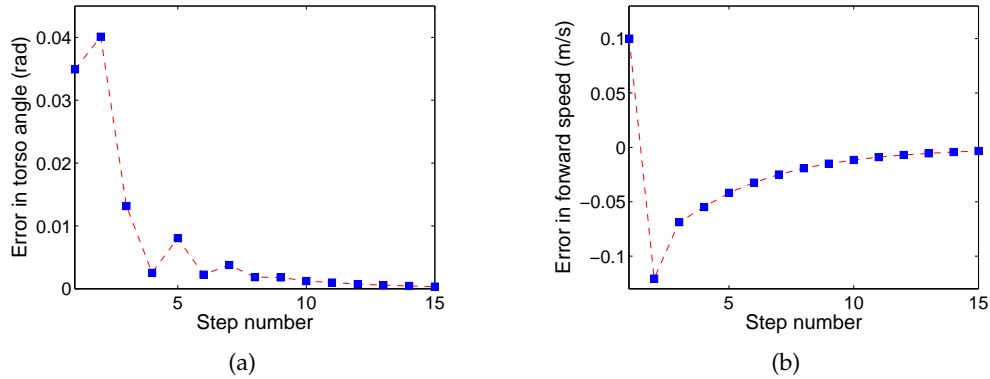


Figure 6.12: Discrete errors in pitch angle and forward speed showing convergence to zero. The norm of the maximum eigenvalue is 0.79; see (6.80).

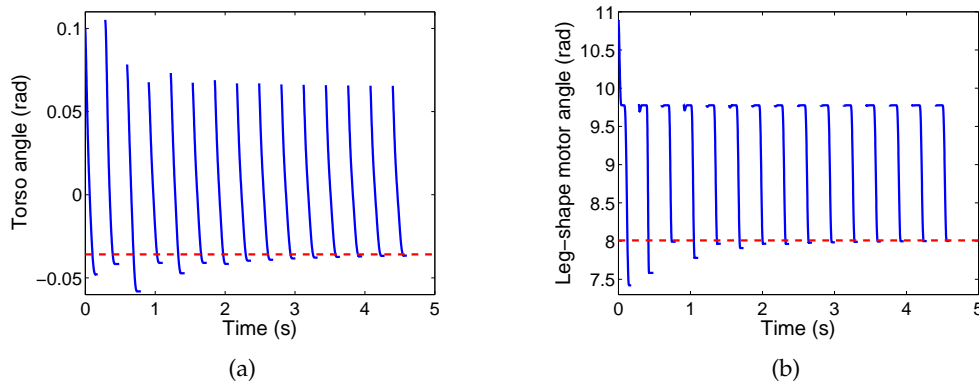


Figure 6.13: Stance phase virtual constraints during recovery from a perturbation: torso angle, (a), and leg-shape motor position, (b). Dashed line represents nominal liftoff values: The outer-loop controller adjusts the liftoff values for the torso angle and the motor position (corresponding to energy input) to ensure convergence to the nominal orbit.

Figure 6.14 shows the corresponding evolution of the torso pitch angle and spring deflection. As can be seen from Fig. 6.14(a) the peak-to-peak amplitude of the pitch oscillation is approximately 10deg demonstrating that the controller is successful in ensuring that the resulting pitch motion does not exhibit excessive pitching. Careful inspection of Fig. 6.14(b) reveals that sometimes liftoff occurs when the spring deflection is not zero. This corresponds to the case where transition from flight to stance is triggered by the ver-

tical component of the ground reaction force becoming zero, while the spring is still compressed. In the results presented in this section, the stance to flight transition is assumed to occur when either the spring deflection becomes zero or the vertical component of the ground reaction force becomes zero. This modification ensures that the vertical component of the ground reaction forces is positive throughout the gait implying that the commanded torques do not result in the leg “pulling” the ground, as is demonstrated in Fig. 6.15(a). It is implicitly assumed that, when liftoff occurs with the spring compressed, the corresponding elastic energy is dissipated into heat in the actuator. Figure 6.15(b) presents the ratio $|F_{\text{toe}}^T|/F_{\text{toe}}^N$, which, excluding the very initial and final part of the stance phase, is bounded above from 0.7 meaning that no slippage between the toe and the ground occurs.

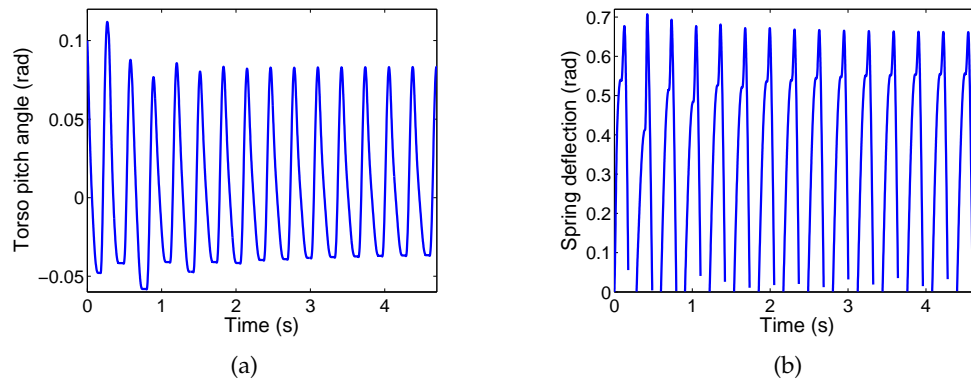


Figure 6.14: Torso pitch angle, (a), and spring deflection, (b), during convergence to the nominal orbit. Note that no excessive pitching is observed.

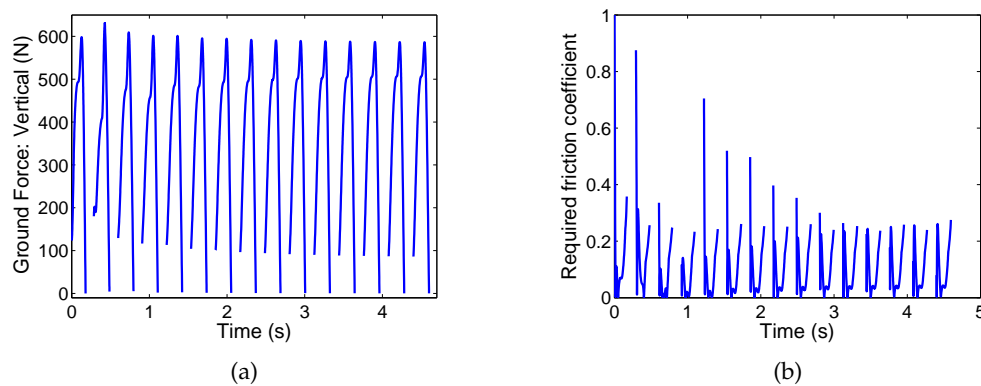


Figure 6.15: Vertical component of the ground reaction force, (a), and minimum required friction coefficient computed by $|F_{\text{toe}}^T|/F_{\text{toe}}^N$, (b).

Finally, Fig. 6.16 shows the corresponding input torques, which are both within the capabilities of the leg-angle and leg-shape motors.

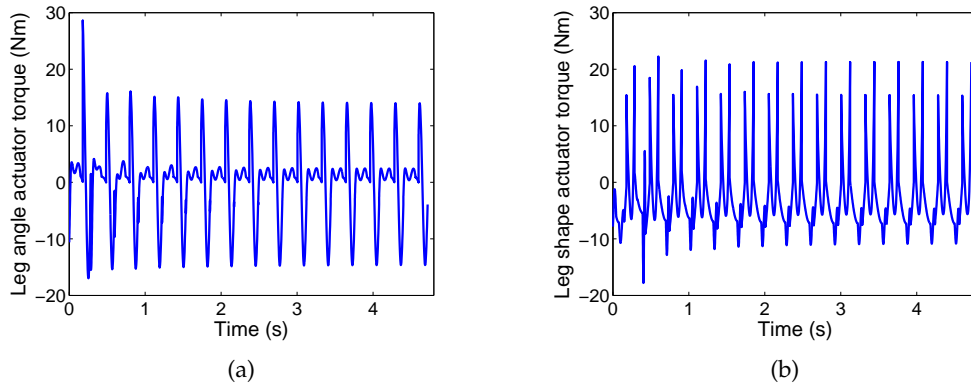


Figure 6.16: Actuator torques: Leg-angle, (a), and leg-shape, (b), motors, showing that the required input torques are within the capabilities of the motors.

CHAPTER VII

Concluding Remarks and Future Work

The work presented in this thesis bridges the gap between “empirical” control approaches for dynamically stable *compliant* running robots and rigorous controller synthesis procedures. The ground-breaking work of Marc Raibert in the 1980’s and early 1990’s offered a set of intuitive rules for the control of running, and dominated the field of dynamically stable legged locomotion. Analytically tractable investigations of the success of Raibert’s controllers for compliant legged systems are largely limited to simplified models, such as the Spring Loaded Inverted Pendulum (SLIP). These simplified models do not constitute faithful representations of legged robots, and thus their value in synthesizing prescriptive control procedures for these robots is limited. As a result, there was a need for a methodology that combines *realistic* models with *tractable* stability analysis to design feedback controllers that work *in concert* with compliance to produce efficient natural-like running motions. This thesis developed such a methodology for monopedal robots.

7.1 Summary of New Contributions

The *terminus a quo* of this research was the running experiments performed on the bipedal robot RABBIT —see [84]— in which running was successfully initiated, but not sustained. Through these experiments, it became apparent that modifications to the robot structure to include compliant elements would be necessary for realizing running. This observation prompted the design and construction of the monopedal robot Thumper, which is the subject of this work. The existence of compliant elements in the structure of Thumper

called for nontrivial extensions of the hybrid zero dynamics (HZD) controller design framework, originally proposed in [110] and further detailed in [109]. In particular, the presence of compliance posed an additional requirement: the control law had to guarantee that the compliant element in the open-loop dynamics of Thumper would dominate the behavior of the closed-loop system. In other words, the feedback action should *preserve* the compliant nature of the system. Achieving this additional requirement was at the core of this thesis.

To address this issue, a standing hypothesis in the modeling and control of running was first examined. Namely, it has been conjectured that when animals (and robots) run, they coordinate their limbs so that a lower-dimensional compliant system, the Spring Loaded Inverted Pendulum (SLIP), governs the observed behavior; see [100] and references therein. Along the same vein, Chapters III and IV “translated” this conjecture into precise mathematical terms, and developed a rigorous procedure, through which the actuated degrees of freedom of a model that constitutes a more faithful representation of Thumper were coordinated so that the SLIP governed its behavior.

In particular, to bridge the gap between the SLIP and Thumper, the *Asymmetric Spring Loaded Inverted Pendulum (ASLIP)*, an extension of the SLIP that includes nontrivial torso pitch dynamics — a mode of Thumper’s motion not captured by point-mass hoppers such as the SLIP — was proposed in Chapter III. The ASLIP is envisioned as a “building block” toward the construction of controllers for more elaborate models that constitute realistic representations of legged robots such as Thumper. Chapter IV proposed a control law for the ASLIP that realized the SLIP as its target dynamics in a rigorous sense. A feedback control law, termed the *SLIP embedding controller*, was devised that coordinates the actuated degrees of freedom of the ASLIP so that the SLIP “emerged” from the closed-loop system as its hybrid zero dynamics, thereby governing the existence and stability properties of running orbits in the ASLIP.

An immediate consequence of this result is that the SLIP is rendered directly relevant to the control of a more elaborate model, such as the ASLIP, thereby allowing for a large body of controller results available for the SLIP to be applicable in stabilizing the ASLIP. Most importantly, the control law design is suggestive of how feedback could be used *in concert*

with the compliant dynamics of the system to stabilize running motions on Thumper. The key idea was to design the control law so that the corresponding hybrid zero dynamics is a two degree-of-freedom *compliant* dynamical system. Indeed, in Chapter IV, it was deduced through comparisons of the SLIP embedding controller with a rigid target model controller creating a one-degree-of-freedom non-compliant subsystem, that the underlying compliant nature of the SLIP enhances performance through significantly improving the transient response and reducing actuator effort.

The results in Chapter IV should be viewed as a preliminary step toward the control of Thumper. This task was undertaken in Chapters V and VI, in which a stabilizing feedback control law for running was developed. Chapter V provided a mathematical model for the dynamics of Thumper in running and highlighted the relation with the ASLIP. Similarly to the structure of the ASLIP, the robot is composed of a heavy torso, on which a relatively light leg is mounted so that the hip joint is displaced from the torso COM. On the other hand, the robot's leg is not prismatic and, despite the fact that it is relatively light with respect to the torso, its mass cannot be assumed zero as was the case in the ASLIP. Furthermore, Thumper features a novel compliant powertrain, which introduces nontrivial dynamics in transferring the control inputs from the actuators to the robot's structure.

Despite these morphological differences between the ASLIP and Thumper, the proposed feedback law for Thumper heavily relied on control ideas developed in the context of the ASLIP. As described in Chapter VI, the control law was developed within the hybrid zero dynamics framework, and it creates a lower-dimensional hybrid subsystem determining the stability properties of periodic motions of the full model of Thumper. This was achieved through the proper design of a set of virtual holonomic constraints that were asymptotically imposed on Thumper's dynamics through its actuators. The resulting control law achieved the dual objectives of working harmoniously with the system's compliant dynamics and inducing provably exponentially stable running motions, while all relevant physical constraints were respected. It is anticipated that these properties will render this controller synthesis method an attractive alternative to traditional heuristic approaches by avoiding laborious trial-and-error procedures during experimental implementation.

7.2 Perspectives on Future Work

The most natural next step of the results presented in this thesis is the experimental implementation of the compliant hybrid zero dynamics controller developed in Chapter VI on Thumper. A number of issues need to be resolved before this goal can be achieved. First, extensive parameter identification experiments need to be conducted so that the various parameters associated with the inertia properties of the transmission system and the robot's limbs can be reasonably well approximated. These experiments are currently in progress. With these parameters in hand, extensive testing of the controller of Chapter VI in more accurate simulation environments that include modeling aspects such as physically realistic ground contact models and actuator dynamics, will be required before experimental implementation. In addition, the development of transition controllers that initiate and maintain running over a range of forward velocities, including hopping on the spot, will greatly facilitate the experiments on Thumper.

A major extension of the work in this thesis is the development of controllers for bipedal running and their implementation on the robotic biped MABEL. The controller for Thumper developed in Chapter VI suggests how to use splines to effectively control MABEL without “fighting” the spring during the stance phase. However, MABEL is a much heavier robot than Thumper—as a matter of fact, it weights twice as much as Thumper—thus placing more stringent requirements on exploiting the natural dynamics of the robot, and in particular compliance. On the other hand, MABEL exhibits different flight dynamics from Thumper. Indeed, the existence of the second leg can be used to limit the net effect of leg motion on the pitch dynamics during the flight phase due to conservation of the total angular momentum about the center of mass—a possibility which is not present in the monopedal Thumper.

Finally, the development of control laws for running in Thumper—and in the future in MABEL—requires nontrivial extensions of the theory of hybrid zero dynamics in the presence of event-based parameter update laws. For instance, including the touchdown angle as an input available for event-based control, as was done in Thumper, results in a parameter-dependent switching surface of the system with impulse effects on which

part of the event-based parameter update law is designed. This situation is not explicitly addressed in the existing theory of hybrid parameter extensions as was developed in [81]. In this work, the reduced switching surface being invariant under the parameter update law is a necessary condition for the validity of the reduced-order stability test.

In summary, there is still a long research path to follow until the experimental evaluation of our feedback controller synthesis framework for the design of provably stable control prescriptions that work together with the natural dynamics of the system in inducing running motions on compliant mechanisms such as Thumper and MABEL. It is anticipated that the results presented in thesis constitute an important step in this direction.

APPENDICES

APPENDIX A

Details on The Rigid Target Controller

This appendix complements Section 4.5 of Chapter IV, and provides details on how to design Γ_c , Γ_s and Γ_f . To ease implementation, it is favorable to use Bézier polynomials. Let q_u^{\min} and q_u^{\max} be the (known) min and max values of the angle q_u of the leg with respect to the ground during the *nominal* stance motion, and define $s = (q_u - q_u^{\min}) / (q_u^{\max} - q_u^{\min}) \in [0, 1]$. Then, the desired leg length parameterized by a Bézier polynomial is given by

$$l_d(s) = \sum_{j=0}^M \left[\frac{M!}{j!(M-j)!} s^j (1-s)^{M-j} \right] \alpha_j, \quad (\text{A.1})$$

where the coefficients α_j satisfy the following properties,

$$l_d(0) = \alpha_0, \quad l_d(1) = \alpha_M, \quad (\text{A.2})$$

$$\left. \frac{\partial l_d(s)}{\partial s} \right|_{s=0} = M(\alpha_1 - \alpha_0), \quad \left. \frac{\partial l_d(s)}{\partial s} \right|_{s=1} = M(\alpha_M - \alpha_{M-1}). \quad (\text{A.3})$$

In the simulations of Section 4.6, $M = 6$, while the constant polynomial $\theta_d = \alpha_7$ is selected for the desired pitch angle.

The properties (A.2) and (A.3) are exactly those required to ensure conditions (i) and (ii) of Section 4.1.2. Suppose that $x_s^- \in \hat{\mathcal{S}}_{s \rightarrow f} \cap \mathcal{Z}_{\alpha_s}$ and $\alpha_f = (l^{\text{td}}, \varphi^{\text{td}})$ is a given set of flight parameters (specified by the outer-loop feedback law Γ_f). To ensure that the state at touchdown belongs in the zero dynamics surface, i.e. $x_s^+ = \Delta(x_s^-, \alpha_f) \in \mathcal{Z}_{\alpha_s}$, it is sufficient

to update the two first coefficients α_0 and α_1 according to

$$\alpha_0^+ = l^+ \quad \alpha_1^+ = \frac{\dot{l}^+}{M\dot{s}} + \alpha_0^+. \quad (\text{A.4})$$

Leaving the rest of the coefficients unchanged (i.e. equal to their nominal values), ensures that $\hat{\mathcal{S}}_{s \rightarrow f} \cap \mathcal{Z}_{\alpha_s^+} = \hat{\mathcal{S}}_{s \rightarrow f} \cap \mathcal{Z}_{\alpha_s}$, which is the surface $\hat{\mathcal{S}}_{s \rightarrow f} \cap \mathcal{Z}_{\diamond}$ in Section 4.1.2. Equation (A.4) provides a rule for updating α_s . The pitch angle polynomial need not be updated due to the trivial pitch dynamics in flight.

APPENDIX B

Details on the Transmission Mechanism

Figure B.1 provides a schematic of the cable drive layout of the transmission mechanism actuating the leg of Thumper; see Table B.1 for the meaning of the various symbols. Before describing the way the differentials are combined to form the transmission mechanism of Thumper, we provide a brief description of how each differential works. As can be seen in Fig. B.1, each of the differentials of the transmission is composed of three pulleys A, B and C, and an internal unobserved idler D. Its purpose is to deliver the same amount of torque to pulleys A and B regardless of the speed at which the A and B rotate. More specifically, if the positive direction is the same for each pulley, then the torques τ_A and τ_B of A and B respectively are always the same, i.e.

$$\tau_A = \tau_B. \tag{B.1}$$

Similarly, based on the kinematics of the mechanism, the angular velocities $\omega_A, \omega_B, \omega_C, \omega_D$ at which the pulleys rotate satisfy the following relations

$$\begin{aligned} \omega_A r_A + \omega_B r_B &= (r_A + r_B) \omega_C, \\ \omega_A r_A - \omega_B r_B &= (r_A + r_B) \omega_D, \end{aligned} \tag{B.2}$$

where r_A, r_B, r_C, r_D correspond to the radii of the pulleys.

The kinematics of the transmission involves eighteen variables: twelve describing the

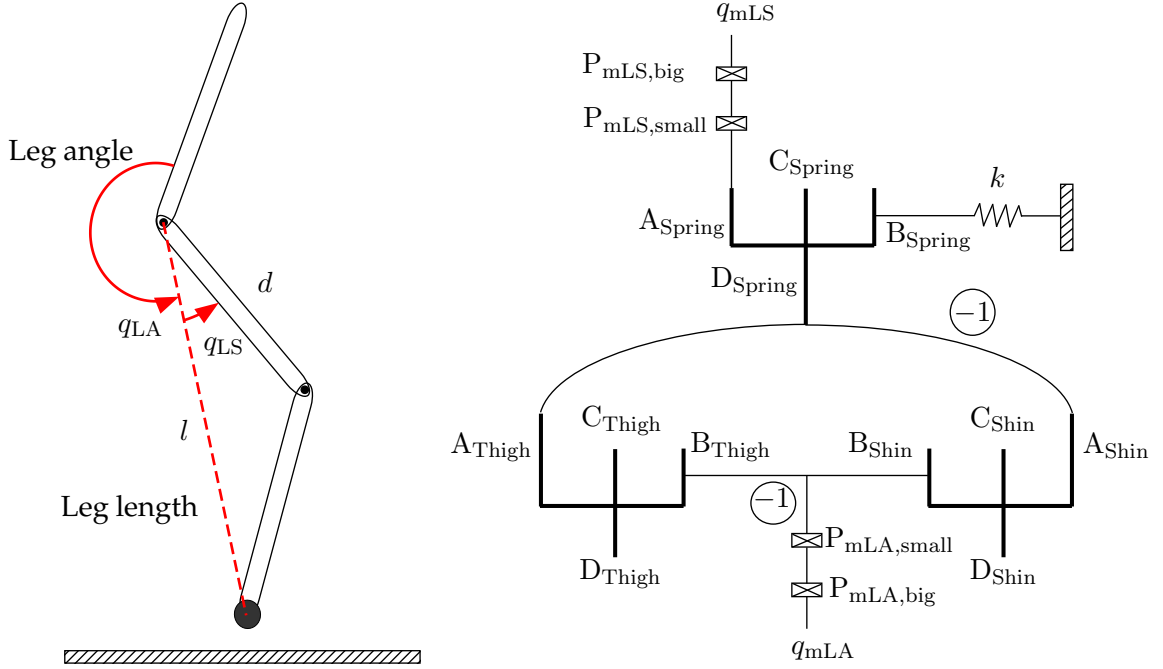


Figure B.1: **Left:** Basic robot configuration. **Right:** Conceptual diagram showing the placement of the three differentials (solid black lines) in the transmission system with the names of each pulley. The “-1” means that direction is inverted. B

Table B.1: Transmission system nomenclature.

Symbol	Meaning
r, θ, ω	Radius, angle and angular rate of a pulley
$\{A_{Thigh}, B_{Thigh}, C_{Thigh}, D_{Thigh}\}$	Indices for pulleys of thigh differential
$\{A_{Shin}, B_{Shin}, C_{Shin}, D_{Shin}\}$	Indices for pulleys of shin differential
$\{A_{Spring}, B_{Spring}, C_{Spring}, D_{Spring}\}$	Indices for pulleys of spring differential
$\{P_{mLS,big}, P_{mLS,small}\}$	Stepdown pulleys connecting the leg shape motor
$\{P_{mLA,big}, P_{mLA,small}\}$	Stepdown pulleys connecting the leg angle motor
$\{q_{mLS}, q_{mLA}\}$	Angular positions for leg shape and leg angle motor
$\{q_{LS}, q_{LA}\}$	Leg shape and leg angle

positions of each of the pulleys of the three differentials, two for the scaling (stepdown) pulleys connecting the motorshafts with the differentials, two for the motorshaft positions, and, finally, two corresponding to the leg angle and the leg shape variables, namely

$$\{\theta_{A_i}, \theta_{B_i}, \theta_{C_i}, \theta_{D_i}\}, \quad i \in \{\text{Thigh}, \text{Shin}, \text{Spring}\},$$

$$\theta_{P_{mLA,small}}, \theta_{P_{mLS,small}}, q_{mLA}, q_{mLS}, q_{LA}, q_{LS}.$$

Among those variables there exist fifteen constraint equations: six refer to the constituting relations of the differentials and nine to their interconnections according to Fig. B.1. These constraints are given below in terms of velocities so that they can be used to compute the kinetic energy associated with the transmission.

Thigh differential:

$$\begin{aligned}\omega_{A_{\text{Thigh}}} r_{A_{\text{Thigh}}} + \omega_{B_{\text{Thigh}}} r_{B_{\text{Thigh}}} - (r_{A_{\text{Thigh}}} + r_{B_{\text{Thigh}}}) \omega_{C_{\text{Thigh}}} &= 0 \\ \omega_{A_{\text{Thigh}}} - \omega_{B_{\text{Thigh}}} + r_{D_{\text{Thigh}}} \left(\frac{1}{r_{A_{\text{Thigh}}}} + \frac{1}{r_{B_{\text{Thigh}}}} \right) \omega_{D_{\text{Thigh}}} &= 0\end{aligned}$$

Shin differential:

$$\begin{aligned}\omega_{A_{\text{Shin}}} r_{A_{\text{Shin}}} + \omega_{B_{\text{Shin}}} r_{B_{\text{Shin}}} - (r_{A_{\text{Shin}}} + r_{B_{\text{Shin}}}) \omega_{C_{\text{Shin}}} &= 0 \\ \omega_{A_{\text{Shin}}} - \omega_{B_{\text{Shin}}} + r_{D_{\text{Shin}}} \left(\frac{1}{r_{A_{\text{Shin}}}} + \frac{1}{r_{B_{\text{Shin}}}} \right) \omega_{D_{\text{Shin}}} &= 0\end{aligned}$$

Spring differential:

$$\begin{aligned}\omega_{A_{\text{Spring}}} r_{A_{\text{Spring}}} + \omega_{B_{\text{Spring}}} r_{B_{\text{Spring}}} - (r_{A_{\text{Spring}}} + r_{B_{\text{Spring}}}) \omega_{C_{\text{Spring}}} &= 0 \\ \omega_{A_{\text{Spring}}} - \omega_{B_{\text{Spring}}} + r_{D_{\text{Spring}}} \left(\frac{1}{r_{A_{\text{Spring}}}} + \frac{1}{r_{B_{\text{Spring}}}} \right) \omega_{D_{\text{Spring}}} &= 0\end{aligned}$$

Interconnection constraints:

$$\begin{aligned}\omega_{B_{\text{Thigh}}} - \omega_{B_{\text{Shin}}} &= 0 \\ r_{C_{\text{Spring}}} \omega_{C_{\text{Spring}}} + r_{A_{\text{Shin}}} \omega_{A_{\text{Shin}}} &= 0 \\ r_{C_{\text{Spring}}} \omega_{C_{\text{Spring}}} - r_{A_{\text{Thigh}}} \omega_{A_{\text{Thigh}}} &= 0 \\ r_{P_{mLA,small}} \omega_{P_{mLA,small}} + r_{B_{\text{Thigh}}} \omega_{B_{\text{Thigh}}} &= 0 \\ r_{mLA} q_{mLA} - r_{P_{mLA,big}} \omega_{P_{mLA,big}} &= 0 \\ r_{P_{mLS,small}} \omega_{P_{mLS,small}} - r_{A_{\text{Spring}}} \omega_{A_{\text{Spring}}} &= 0 \\ r_{mLS} q_{mLS} - r_{P_{mLS,big}} \omega_{P_{mLS,big}} &= 0\end{aligned}$$

$$q_{LS} + \frac{\omega_{C_{\text{Shin}}} - \omega_{C_{\text{Thigh}}}}{2} = 0$$

$$q_{LA} - \frac{\omega_{C_{\text{Shin}}} + \omega_{C_{\text{Thigh}}}}{2} = 0$$

The constraints above form a system of fifteen equations with eighteen unknowns. As a result, there will be three independent variables, which completely determine the configuration of all the pulleys in the transmission system. In accordance to the configuration variables selected to describe the linkage configuration, let $q^{\text{tr}} := (q_{LA}, q_{LS}, q_{mLS})' \in Q^{\text{tr}}$, a simply connected subset of \mathbb{S}^3 , be the configuration variables for the transmission system. Similarly, the angular rates of each of the pulleys in the transmission system can be determined as a function of $\dot{q}^{\text{tr}} := (\dot{q}_{LA}, \dot{q}_{LS}, \dot{q}_{mLS})$ by solving the system of constraints given above.

Next, the kinetic energy associated with the transmission system is calculated. For convenience, let $\mathcal{I} := \{\text{Thigh}, \text{Shin}, \text{Spring}\}$ be a finite index set containing indices corresponding to the thigh, shin and spring differentials, respectively. Then, by Hypothesis HMT4) of Chapter V, the kinetic energy $\mathcal{K}^{\text{tr}} : TQ^{\text{tr}} \rightarrow \mathbb{R}$ of the transmission computed in coordinates is given by

$$\begin{aligned} \mathcal{K}^{\text{tr}}(q_{\text{tr}}, \dot{q}_{\text{tr}}) &= \sum_{i \in \mathcal{I}} \left(\frac{1}{2} J_{A_i} \omega_{A_i}^2 + \frac{1}{2} J_{B_i} \omega_{B_i}^2 + \frac{1}{2} J_{C_i} \omega_{C_i}^2 + \frac{1}{2} J_{D_i} \omega_{D_i}^2 \right) \\ &\quad + \frac{1}{2} J_{P_{mLS, \text{big}}} \omega_{P_{mLS, \text{big}}}^2 + \frac{1}{2} J_{P_{mLA, \text{big}}} \omega_{P_{mLA, \text{big}}}^2 \\ &\quad + \frac{1}{2} J_{mLS} \dot{q}_{mLS}^2 + \frac{1}{2} J_{mLA} \dot{q}_{mLA}^2. \end{aligned} \tag{B.3}$$

BIBLIOGRAPHY

BIBLIOGRAPHY

- [1] M. Ahmadi, "Stable control of a one-legged robot exploiting passive dynamic," Ph.D. dissertation, McGill University, Montreal, QC, Canada, May 1998.
- [2] M. Ahmadi and M. Buehler, "Stable control of a simulated one-legged running robot with hip and leg compliance," *IEEE Transactions on Robotics and Automation*, vol. 13, no. 1, pp. 96–104, Feb. 1997.
- [3] —, "Control passive dynamic running experiment with the ARL Monopod II," *IEEE Transactions on Robotics*, vol. 22, no. 5, pp. 974–986, Oct. 2006.
- [4] R. Alexander, "Walking and running," *American Scientist*, vol. 72, pp. 348–354, 1984.
- [5] —, *Elastic mechanisms in animal movement*. Cambridge: Cambridge University Press, 1988.
- [6] —, "A model of bipedal locomotion on compliant legs," *Phil. Trans. R. Soc. Lond. B.*, vol. 338, pp. 189–98, 1992.
- [7] —, "Walking lessons from robots," *Biologist*, vol. 52, no. 5, pp. 277–281, October 2005.
- [8] R. Altendorfer, D. E. Koditschek, and P. Holmes, "Stability analysis of legged locomotion models by symmetry-factored return maps," *International Journal of Robotics Research*, vol. 23, no. 10-11, pp. 979–999, Oct. 2004.
- [9] A. D. Ames and R. D. Gregg, "Stably extending two-dimensional bipedal walking to three," in *Proceedings of the American Control Conference*, New York, U.S.A., Jul. 2007, pp. 2848–2854.
- [10] A. D. Ames, R. D. Gregg, E. D. B. Wendel, and S. Sastry, "On the geometric reduction of controlled three-dimensional bipedal robotic walkers," in *Proceedings of the 3rd IFAC Workshop on Lagrangian and Hamiltonian Methods for Nonlinear Control*, Nagoya, Japan, Jul. 2006.
- [11] R. Blickhan, "The spring-mass model for running and hopping," *Journal of Biomechanics*, vol. 22, no. 11-12, pp. 1217–1227, 1989.
- [12] R. Blickhan and R. J. Full, "Locomotion energetics of the ghost crab. II. Mechanics of the center of mass during walking and running," *Journal of Experimental Biology*, vol. 130, pp. 155–174, 1987.
- [13] —, "Similarity in multi-legged locomotion: bouncing like a monopode," *Journal of Comparative Physiology A*, vol. 173, pp. 509–517, 1993.

- [14] A. M. Bloch, *Nonholonomic Mechanics and Control*, ser. *Inderdisciplinary Applied Mathematics*. New York: Springer, 2003, vol. 24.
- [15] W. M. Boothby, *An Introduction to Differentiable Manifolds and Riemannian Geometry*, 2nd ed. New York: Academic Press, 1975.
- [16] J. Brown, H. and G. Zeglin, "The bow-leg hopping robot," in *Proceedings of the International Conference on Robotics and Automation*, Leuven, Belgium, May 1998, pp. 781–786.
- [17] M. Buehler, "Dynamic locomotion with one, four and six-legged robots," *Journal of the Robotics Society of Japan*, vol. 20, no. 3, pp. 15–20, 2002.
- [18] M. Bühler, D. Koditschek, and P. Kindlmann, "A family of robot control strategies for intermittent dynamics environments," *IEEE Control Systems Magazine*, vol. 10, no. 2, pp. 16–22, Feb. 1990.
- [19] F. Bullo and A. D. Lewis, *Geometric Control of Mechanical Systems*, ser. *Texts in Applied Mathematics*. New York: Springer, 2005, vol. 49.
- [20] G. A. Cavagna and M. Kaneko, "Mechanical work and efficiency in level walking and running," *Journal of Physiology*, vol. 268, pp. 467–481, 1977.
- [21] G. A. Cavagna, H. Thys, and A. Zamboni, "The sources of external work in level walking and running," *Journal of Physiology*, vol. 262, pp. 639–657, 1976.
- [22] G. A. Cavagna, N. C. Heglund, and R. C. Taylor, "Mechanical work in terrestrial locomotion: Two basic mechanisms for minimizing energy expenditure," *American Journal of Physiology*, vol. 233, no. 5, pp. R243–R261, 1977.
- [23] N. Cherouvim and E. Papadopoulos, "Single actuator control analysis of a planar 3DOF hopping robot," in *Robotics: Science and Systems I*, S. Thrun, G. Sukhatme, and S. Schaal, Eds. MIT Press, 2005, pp. 145–152.
- [24] C. Chevallereau, G. Abba, Y. Aoustin, F. Plestan, E. R. Westervelt, C. Canudas, and J. W. Grizzle, "RABBIT: a testbed for advanced control theory," *IEEE Control Systems Magazine*, vol. 23, no. 5, pp. 57–79, Oct. 2003.
- [25] C. Chevallereau, J. W. Grizzle, and C.-L. Shih, "Asymptotically stable walking of a five-link underactuated 3D bipedal robot," *IEEE Transactions on Robotics*, to appear.
- [26] C. Chevallereau, E. R. Westervelt, and J. W. Grizzle, "Asymptotically stable running for a five-link, four-actuator, planar bipedal robot," *International Journal of Robotics Research*, vol. 24, no. 6, pp. 431–464, Jun. 2005.
- [27] S. H. Collins, A. Ruina, R. Tedrake, and M. Wisse, "Efficient bipedal robots based on passive-dynamic walkers," *Science*, vol. 307, pp. 1082–85, 2005.
- [28] M. Di Benedetto and J. W. Grizzle, "Asymptotic model matching for nonlinear systems," *IEEE Transactions on Automatic Control*, vol. 39, no. 8, pp. 1539–1550, 1994.
- [29] M. Dickinson, C. Farley, R. Full, M. Koehel, R. Kram, and S. Lehman, "How animals move: An integrative view," *Science*, vol. 288, pp. 100–6, Apr. 2000.

- [30] J. M. Donelan, R. Kram, and A. D. Kuo, "Simultaneous positive and negative mechanical work in human walking," *Journal of Biomechanics*, vol. 35, pp. 117–124, 2002.
- [31] C. François and C. Samson, "Running with constant energy," in *Proceedings of the IEEE International Conference on Robotics and Automation*, vol. 1, San Diego, U.S.A., May 1994, pp. 131–136.
- [32] —, "A new approach to the control of the planar one-legged hopper," *International Journal of Robotics Research*, vol. 17, no. 11, pp. 1150–1166, Jan. 1998.
- [33] R. Full and D. E. Koditschek, "Templates and anchors: Neuromechanical hypotheses of legged locomotion on land," *Journal of Experimental Biology*, vol. 202, pp. 3325–3332, Dec. 1999.
- [34] R. J. Full, "Mechanics and energetics of terrestrial locomotion: Biped to polypeds," in *Energy Transformations in Cells and Animals*, W. Wieser and E. Gnaiger, Eds. Stuttgart - New York: Georg Thieme Verlag, 1989, pp. 175–182.
- [35] R. J. Full, K. Autumn, J. I. Chung, and A. A., "Rapid negotiation of rough terrain by the death-head cockroach," *American Zoologist*, vol. 38, p. 81A, 1998.
- [36] R. J. Full and C. T. Farley, "Musculoskeletal dynamics in rhythmic systems: A comparative approach to legged locomotion," in *Biomechanics and Neural Control of Movement*, J. M. Winters and P. E. Crago, Eds. New York: Springer-Verlag, 1999, pp. 192–203.
- [37] R. J. Full, T. Kubow, J. Schmitt, P. Holmes, and D. Koditschek, "Quantifying dynamic stability and maneuverability in legged locomotion," *Integrative and Comparative Biology*, vol. 42, p. 149157, 2002.
- [38] G. Gabrielli and T. von Kármán, "What price speed?" *Mechanical Engineering*, vol. 72, no. 10, pp. 775–781, 1950.
- [39] M. Garcia, A. Chatterjee, and A. Ruina, "Efficiency, speed, and scaling of two-dimensional passive-dynamic walking," *Dynamics and Stability of Systems*, vol. 15, no. 2, pp. 75–99, Jun. 2000.
- [40] M. Garcia, A. Chatterjee, A. Ruina, and M. Coleman, "The simplest walking model: Stability, complexity, and scaling," *ASME Journal of Biomechanical Engineering*, vol. 120, no. 2, pp. 281–8, Apr. 1998.
- [41] H. Geyer, A. Seyfarth, and R. Blickhan, "Compliant leg behaviour explains basic dynamics of walking and running," *Proceedings of The Royal Society B*, vol. 273, pp. 2861–2867, 2006.
- [42] R. M. Ghigliazza, R. Altendorfer, P. Holmes, and D. E. Koditschek, "A simply stabilized running model," *SIAM Journal of Applied Dynamical Systems*, vol. 2, no. 2, pp. 187–218, May 2003.
- [43] P. Gregorio, M. Ahmadi, and M. Buehler, "Design, control, and energetics of an electrically actuated legged robot," *IEEE Transactions on Systems, Man and Cybernetics*, vol. 27, no. 4, pp. 626–634, Aug. 1997.

- [44] P. Gregorio, M. Ahmadi, and B. M., "Design, control and energetics of an electrically actuated legged robot," *IEEE Transactions on Systems, Man and Cybernetics-Part B: Cybernetics*, vol. 27, no. 4, pp. 626–634, 1997.
- [45] J. W. Grizzle, "Papers on biped robots," <http://www.eecs.umich.edu/~grizzle/papers/robotics.html>, retrieved on 2 December 2008.
- [46] J. W. Grizzle, G. Abba, and F. Plestan, "Asymptotically stable walking for biped robots: Analysis via systems with impulse effects," *IEEE Transactions on Automatic Control*, vol. 46, no. 1, pp. 51–64, Jan. 2001.
- [47] J. W. Grizzle, J. W. Hurst, B. Morris, H.-W. Park, and S. Koushil, "MABEL, a new robotic bipedal walker and runner," in *American Control Conference*, 2008, submitted.
- [48] W. M. Haddad, V. Chellaboina, and S. G. Nersesov, *Impulsive and Hybrid Dynamical Systems*, ser. Applied Mathematics. Princeton, NJ: Princeton University Press, 2006.
- [49] P. Holmes, R. J. Full, D. Koditschek, and J. Guckenheimer, "The dynamics of legged locomotion: Models, analyses, and challenges," *SIAM Review*, vol. 48, no. 2, pp. 207–304, May 2006.
- [50] Y. Hürmüzlü and D. B. Marghitu, "Rigid body collisions of planar kinematic chains with multiple contact points," *International Journal of Robotics Research*, vol. 13, no. 1, pp. 82–92, 1994.
- [51] J. W. Hurst, "The role and implementation of compliance in legged locomotion," Ph.D. dissertation, The Robotics Institute, Carnegie Mellon University, 2008.
- [52] J. W. Hurst, J. E. Chestnutt, and A. A. Rizzi, "Design and philosophy of the BiMASC, a highly dynamic biped," in *Proceedings of the IEEE International Conference of Robotics and Automation*, Roma, Italy, Apr. 2007, pp. 1863–1868.
- [53] J. W. Hurst and A. Rizzi, "Series compliance for an efficient running gait," *IEEE Robotics and Automation Magazine*, vol. 15, no. 3, pp. 42–51, Sep. 2008.
- [54] S. H. Hyon and T. Mita, "Development of a biologically inspired hopping robot - "Kenken"," in *Proceedings of the IEEE International Conference of Robotics and Automation*, Washington DC, U.S.A., 2002, pp. 3984–3991.
- [55] S.-H. Hyon and T. Emura, "Symmetric walking control: Invariance and global stability," in *Proceedings of the IEEE International Conference on Robotics and Automation*, Barcelona, Spain, 2005, pp. 1455–1462.
- [56] —, "Energy-preserving control of a passive one-legged running robot," *Advanced Robotics*, vol. 18, no. 4, pp. 357–381, May 2004.
- [57] A. Isidori, *Nonlinear Control Systems*, 3rd ed. Berlin: Springer-Verlag, 1995.
- [58] H. K. Khalil, *Nonlinear Systems*, 3rd ed. Upper Saddle River, NJ: Prentice Hall, 2002.
- [59] D. Koditschek, R. Full, and M. Buehler, "Mechanical aspects of legged locomotion control," *Arthropod Structure and Development*, vol. 33, pp. 251–272, 2004.

- [60] D. E. Koditschek and M. Bühler, "Analysis of a simplified hopping robot," *International Journal of Robotics Research*, vol. 10, no. 6, pp. 587–605, Dec. 1991.
- [61] M. Krstic, I. Kanellakopoulos, and P. Kokotovic, *Nonlinear and Adaptive Control Design*. New York: John Wiley & Sons, 1995.
- [62] T. M. Kubow and R. J. Full, "The role of the mechanical system in control: a hypothesis of self-stabilization in hexapedal runners," *Philosophical Transactions of the Royal Society of London, Series B Biological Sciences*, vol. 354, pp. 849–862, 1999.
- [63] A. D. Kuo, "A simple model of bipedal walking predicts the preferred speed-step length relationship," *Journal of Biomechanical Engineering*, vol. 123, pp. 264–9, 2001.
- [64] —, "Energetics of actively powered locomotion using the simplest walking model," *Journal of Biomechanical Engineering*, vol. 124, no. 1, pp. 113–20, 2002.
- [65] —, "Choosing your steps carefully: Trade-offs between economy and versatility in dynamic walking bipedal robots," *IEEE Robotics and Automation Magazine*, vol. 14, no. 2, pp. 18–29, June 2007.
- [66] —, "The six determinants of gait and the inverted pendulum analogy: A dynamic walking perspective," *Human Movement Science*, vol. 26, pp. 617–656, 2007.
- [67] A. Kuo, J. M. Donelan, and A. Ruina, "Energetic consequences of walking like an inverted pendulum: Step-to-step transitions," *Exercise and Sport Sciences Reviews*, vol. 33, pp. 88–97, 2005.
- [68] R. Margaria, *Biomechanics and Energetics of Muscular Exercise*. Oxford University Press, 1976.
- [69] T. McGeer, "Stability and control of two-dimensional biped walking," Center for Systems Science, Simon Fraser University, Burnaby, B.C., Canada V5A 1S6, Tech. Rep. 1, 1988.
- [70] —, "Passive dynamic walking," *International Journal of Robotics Research*, vol. 9, no. 2, pp. 62–82, Apr. 1990.
- [71] —, "Passive walking with knees," in *Proc. of the 1990 IEEE International Conference on Robotics and Automation, Cincinnati, OH*, vol. 3, May 1990, pp. 1640–1645.
- [72] R. M'Closkey and J. Burdick, "Periodic motions of a hopping robot with vertical and forward motion," *International Journal of Robotics Research*, vol. 12, no. 3, pp. 197–218, Jun. 1993.
- [73] T. A. McMahon, *Muscles, Reflexes, and Locomotion*. Princeton University Press, 1984.
- [74] —, "The role of compliance in mammalian running gaits," *Journal of Experimental Biology*, vol. 115, pp. 263–282, 1985.
- [75] T. A. McMahon and G. C. Cheng, "The Mechanics of Running: Hoes does Stiffness Couple with Speed?" *Journal of Biomechanics*, vol. 23 (suppl. 1), pp. 65–78, 1990.
- [76] T. A. McMahon, G. Valiant, and E. C. Frederick, "Groucho running," *Journal of Applied Physiology*, vol. 62, no. 6, pp. 2326–37, Jun. 1987.

- [77] H. Miura and I. Shimoyama, "Dynamic walking of a biped," *International Journal of Robotics Research*, vol. 3, no. 2, pp. 60–74, 1984.
- [78] S. Mochon and T. A. McMachon, "Ballistic walking," *Journal of Biomechanics*, vol. 13, no. 1, pp. 49–57, 1980.
- [79] S. Mochon and T. A. McMachon, "Ballistic walking: an improved model," *Mathematical Biosciences*, vol. 52, pp. 241–60, 1980.
- [80] K. D. Mombaur, R. W. Longman, H. G. Bock, and J. P. Schlöder, "Stable one-legged hopping without feedback and with a point foot," in *Proceeding of the IEEE International Conference on Robotic and Authomation*, Washington DC, U.S.A., May 2002, pp. 3978–3983.
- [81] B. Morris, "Stabilizing highly dynamic locomotion in planar bipedal robots with dimension reducing control," Ph.D. dissertation, University of Michigan, 2008.
- [82] B. Morris and J. W. Grizzle, "A restricted Poincaré map for determining exponentially stable periodic orbits in systems with impulse effects: Application to bipedal robots," in *Proceedings of the IEEE International Conference on Decision and Control*, Seville, Spain, Dec. 2005, pp. 4199–4206.
- [83] —, "Hybrid invariance in bipedal robots with series compliant actuators," in *Proceedings of the IEEE International Conference on Decision and Control*, San Diego, USA, Dec. 2006, pp. 4793–4800.
- [84] B. Morris, E. R. Westervelt, C. Chevallereau, G. Buche, and J. W. Grizzle, "Achieving bipedal running with RABBIT: Six steps toward infinity," in *Fast Motions Symposium on Biomechanics and Robotics*, ser. Lecture Notes in Control and Information Sciences, K. Mombaur and M. Dheil, Eds. Heidelberg, Germany: Springer-Verlag, 2006, pp. 277 – 297.
- [85] R. M. Murray, Z. Li, and S. Sastry, *A Mathematical Introduction to Robotic Manipulation*. CRC Press, 1994.
- [86] J. Nakanishi, T. Fukuda, and D. E. Koditschek, "A brachiating robot controller," *IEEE Transactions on Robotics and Automation*, vol. 16, no. 2, pp. 109–123, Apr. 2000.
- [87] I. Poulakakis, E. G. Papadopoulos, and M. Buehler, "On the stability of the passive dynamics of quadrupedal running with a bounding gait," *International Journal of Robotics Research*, vol. 25, no. 7, pp. 669–687, July 2006.
- [88] M. Raibert, "Trotting, pacing and bounding by a quadruped robot," *Journal of Biomechanics*, vol. 23, Suppl. 1, pp. 79–98, 1990.
- [89] M. Raibert and J. Brown, H., "Experiments in balance with a 2d one-legged hopping machine," *ASME Journal of Dynamic Systems Measurement, and Control*, vol. 106, pp. 75–81, 1984.
- [90] M. H. Raibert, "Hopping in legged systems—modeling and simulation for the two-dimensional one-legged case," *IEEE Transactions on Systems, Man and Cybernetics*, vol. 14, no. 3, pp. 451–63, Jun. 1984.

- [91] ———, *Legged Robots that Balance*. Cambridge, MA: MIT Press, 1986.
- [92] M. H. Raibert, M. Chepponis, and J. Brown, H., "Running on four legs as though they were one," *IEEE Transactions on Robotics and Automation*, vol. RA-2, no. 2, pp. 70–82, Jun. 1986.
- [93] R. Ringrose, "Self-stabilizing running," in *Proc. of the 1997 IEEE International Conference on Robotics and Automation, Albuquerque, NM, 1997*, pp. 487–93.
- [94] U. Saranli and D. Koditschek, "Template based control of hexapedal running," in *Proceedings of the IEEE International Conference on Robotics and Automation*, vol. 1, Taipei, Taiwan, Sep. 2003, pp. 1374–1379.
- [95] U. Saranli, W. Schwind, and D. E. Koditschek, "Toward the control of a multi-jointed, monopod runner," in *Proceedings of the IEEE International Conference on Robotics and Automation*, vol. 3, Leuven, Belgium, May 1998, pp. 2676–2682.
- [96] A. Sayyad, B. Seth, and P. Seshu, "Single-legged hopping robotics research," *Robotica*, vol. 25, pp. 587–613, 2007.
- [97] F. Sheck, *Mechanics. From Newton's Laws to Deterministic Chaos*, 3rd ed. Berlin: Springer-Verlag, 1999.
- [98] J. Schmitt and P. Holmes, "Mechanical models for insect locomotion: Dynamics and stability in the horizontal plane i. theory," *Biological Cybernetics*, vol. 83, pp. 501–515, 2000.
- [99] W. Schwind and D. Koditschek, "Approximating the stance map of a 2-dof monopod runner," *Journal of Nonlinear Science*, vol. 10, pp. 533–568, 2000.
- [100] W. J. Schwind, "Spring loaded inverted pendulum running: A plant model," Ph.D. dissertation, University of Michigan, 1998.
- [101] W. J. Schwind and D. E. Koditschek, "Control of forward velocity for a simplified planar hopping robot," in *Proceedings of the IEEE International Conference of Robotics and Automation*, vol. 1, Nagoya, Japan, May 1995, pp. 691–696.
- [102] ———, "Characterization of monopod equilibrium gaits," in *IEEE Int. Conf. on Rob. and Aut.*, Albuquerque, New Mexico, Apr. 1997.
- [103] J. E. Seipel and P. Holmes, "Running in three dimensions: Analysis of a point-mass sprung-leg model," *International Journal of Robotics Research*, vol. 24, no. 8, pp. 657–674, Aug. 2005.
- [104] A. Seyfarth, H. Geyer, M. Gunther, and R. Blickhan, "A movement criterion for running," *Journal of Biomechanics*, vol. 35, no. 5, pp. 649–55, May 2002.
- [105] A. Seyfarth, H. Geyer, and H. Herr, "Swing leg retraction: A simple control model for stable running," *Journal of Experimental Biology*, vol. 206, pp. 2547–2555, 2003.
- [106] M. W. Spong, S. Hutchinson, and M. Vidyasagar, *Robot Modeling and Control*. New York: John Wiley & Sons, 2006.

- [107] M. Spong and F. Bullo, "Controlled symetries and passive walking," *IEEE Transactions on Automatic Control*, vol. 50, no. 7, pp. 1025–1031, July 2003.
- [108] A. Vakakis, J. Burdick, and T. Caughey, "An "interesting" strange attractor in the dynamics of a hopping robot," *International Journal of Robotics Research*, vol. 10, no. 6, pp. 606–618, Dec. 1991.
- [109] E. R. Westervelt, J. W. Grizzle, C. Chevallereau, J. H. Choi, and B. Morris, *Feedback Control of Dynamic Bipedal Robot Locomotion*. Taylor & Francis/CRC Press, 2007.
- [110] E. R. Westervelt, J. W. Grizzle, and D. E. Koditschek, "Hybrid zero dynamics of planar biped walkers," *IEEE Transactions on Automatic Control*, vol. 48, no. 1, pp. 42–56, Jan. 2003.
- [111] M. Wisse, A. L. Schwab, R. Q. van der Linde, and F. C. T. van der Helm, "How to keep from falling forward: Elementary swing leg action for passive dynamic walkers," *IEEE Transactions on Robotics*, vol. 21, no. 3, pp. 393–401, 2005.
- [112] M. Wisse and R. Q. van der Linde, *Delft Pneumatic Biped*, ser. Springer Tracts in Advanced Robotics, B. Siciliano, O. Khatib, and F. Groen, Eds. Berlin Heidelberg: Springer-Verlag, 2007, vol. 34.
- [113] H. Ye, A. N. Michel, and L. Hou, "Stability theory for hybrid dynamical systems," *IEEE Transactions of Automatic Control*, vol. 43, no. 4, pp. 461–474, April 1998.